DOCUMENT 158-80
(Formerly 130-80)

DATA REDUCTION AND COMPUTER GROUP

DATA REDUCTION AND ANALYSIS TECHNIQUES FOR MISS-DISTANCE DETERMINATION (MDD) AND SCORING SYSTEMS

WHITE SANDS MISSILE RANGE
KWAJALEIN MISSILE RANGE
YUMA PROVING GROUND
DUGWAY PROVING GROUND
ELECTRONIC PROVING GROUND

ATLANTIC FLEET WEAPONS TRAINING FACILITY
NAVAL AIR WARFARE CENTER WEAPONS DIVISION
NAVAL AIR WARFARE CENTER AIRCRAFT DIVISION
NAVAL UNDERSEA WARFARE CENTER DIVISION NEWPORT

30TH SPACE WING
45TH SPACE WING
AIR FORCE FLIGHT TEST CENTER
AIR FORCE DEVELOPMENT TEST CENTER
AIR FORCE WEAPONS AND TACTICS CENTER
DETACHMENT 2, SPACE AND MISSILE SYSTEMS CENTER

DOCUMENT 158-80

DATA REDUCTION AND ANALYSIS TECHNIQUES FOR MISS-DISTANCE DETERMINATION (MDD) AND SCORING SYSTEMS

DATA REDUCTION AND COMPUTING GROUP
RANGE COMMANDERS COUNCIL

SEPTEMBER 1980

Published by

SECRETARIAT
RANGE COMMANDERS COUNCIL
WHITE SANDS MISSILE RANGE,
NEW MEXICO 88002

FOREWORD

This document supersedes RCC Document 130-75, *Data Reduction and Analysis Techniques for Miss-Distance Indicator (MDI) and Impact Scoring Systems*. Although portions of the latter document have been retained in this new publication, several sections have been added and some material which previously appeared in the original document has been deleted. As a result, the scope of Document 130-80 has been expanded to include all Miss-Distance Determination (MDD) Scoring Systems. However, the discussion of scoring systems in this document is restricted to those systems which measure weapon accuracy. Consequently, the effects of weapon accuracy on lethality or vulnerability are not addressed.

The views, opinions and/or findings contained in this report are those of the author(s) of each section and should not be construed as an official Department of Defense position, policy or decision, unless so designated by other official documentation. Users of this publication are encouraged to recommend changes and submit comments for its improvement. Comments should be keyed to the specific page, paragraph and line of the text in which the change is recommended. Reasons must be provided for each comment to ensure understanding and complete evaluation. Comments should be submitted to: Secretariat, Range Commanders Council, STEWS-SA-R, White Sands Missile Range, NM 88002, ATTN: Chairman, Data Reduction & Computing Group.

This document was prepared by DR&CG members representing the following organizations:

Pacific Missile Test Center
National Aviation Facilities Experimental Center
US Army Operational Test and Evaluation Agency
Western Space and Missile Center
Air Force Flight Test Center
Armament Division
Sandia Laboratories
Eastern Space and Missile Center
Naval Air Test Center
White Sands Missile Range
Kwajalein Missile Range

TABLE OF CONTENTS

PAGE

CHAPTER 2

PREFACE

The purpose of this document is to describe, under a single cover, the data reduction techniques, advantages, disadvantages, accuracies, cost estimates, and reliability factors associated with the various types of miss-distance determination (MDD), miss-distance indicator (MDI), and scoring systems in use at the various ranges.

All ranges are engaged in the collection and reduction of test data for the purpose of evaluating various types of systems, either under development or requiring improvement. Normally, one of the end products resulting from system evaluation is miss-distance measurement or impact scoring. Various methods are employed to reduce data to generate these end products. In some cases, the data reduction techniques are involved and complicated. In others, the techniques are simple and straightforward or not required at all (as in the case of completely automated MDI and scoring systems).

Although the MDD, MDI and scoring systems currently in use are many and varied, they can be classified into the following three categories:

a. Atmospheric or Space MDD/MDI/Scoring Systems
b. Ground Impact MDD/MDI/Scoring Systems
c. Ocean MDD/MDI/Scoring Systems

Each of these categories can be further divided into three or more of the following systems:

a. Optical
b. Electromagnetic or radar
c. Radiation
d. Acoustic
e. Seismic
f. Survey

Hopefully, this document will provide the reader with sufficient information and references on state-of-the-art MDD/MDI and scoring systems to allow selection of the most appropriate techniques available for optimum data reduction. This in turn, will result in a higher quality data product and thereby, benefit both the ranges and the range users.

CHAPTER 1

1.1 ATMOSPHERIC OR SPACE MISS-DISTANCE DETERMINATION/MISS-DISTANCE INDICATOR (MDD/MDI) SCORING SYSTEMS

1.1.1 General

Atmospheric or space miss-distance determination (MDD) typically involves finding the distance between the point of closest approach of two moving objects; one object defined as a target and the second defined as an interceptor. Generally, the word "target" refers to a drone or a reentry vehicle (RV) and the word "interceptor" to a missile or a projectile.

1.1.2 Methods

Methods for determining the atmospheric miss distance are divided into the following three categories:

a. Optical systems. Typically, optical systems use cameras and pictures to determine miss distance. The systems are either airborne or ground located, and the resulting pictures can contain either one or both of the objects.

b. Electromagnetic systems. Electromagnetic systems make use of radars located either onboard the target, the interceptor, or both and ground-located radars to calculate miss distance.

c. Radiation systems. The radiation systems include only the onboard Photon Miss-Distance Indicator (MDI) System which typically involves the use of radioactive tags placed on the missile and radiation detectors or counters on the target. Miss distance is determined through application of the inverse square relationship of intensity to distance.

1.2 DRONE CAMERA SCORING WITH TIME CORRELATION

1.2.1 General Description

a. When two or more drone cameras are used to compute miss distance, the procedure required for data reduction is somewhat less complicated if there is time correlation between the cameras. Time correlation is usually effected through the use of timing marks on the film from each camera. When correlation is available, the problem of determining the distance to the target at any instant in time for which data is available is reduced to simple triangulation. The trajectory of the target is determined by computing the position of the weapon with respect to the target at as many points as desired. The point of closest approach is determined by fitting a three-dimensional (3-D) polynomial to the position data and determining the minimum distance between the fitted curve and the target.

b. Since one of the most important systems using this setup is the firing error indication (FEI) camera scoring system, much of the discussion which follows uses the approach employed in data reduction for that system. However, variations are given when the author feels that a different approach would give better results.

1.2.2 Math Model

a. A typical installation of the FEI scoring system shown in figures 1.2-1 and 1.2-2 consists of a pod mounted on each wing of an airplane. Each pod contains two high-speed cameras; one looking up, the other looking down. When the weapon is above the plane of the wings, it is recorded on the upper two cameras; below the plane of the wings, the lower two; and when near the plane of the wings, by either set of cameras. The solution given applies to data read from either pair of cameras when it is recognized that one case is just the mirror image of the other. The equations given are for the case in which the upper cameras are used.

b. The geometry of the setup described is shown in figure 1.2-3. The angle of depression is defined as the angle between the vertical axis of the camera and the line of sight to the target. The bearing angle is defined as the angle between the longitudinal axis of the target aircraft (direction of flight) and the projection of the line of sight to the target into the plane of the cameras. The angles of bearing and depression of the weapon are determined for the film images from each camera. The reading of this film is facilitated by projecting the developed images onto a grid which has been properly oriented as shown in figure 1.2-4. The concentric circles are lines of equal depression and the rays are lines of equal bearing.

c. Figures 1.2-5, 1.2-6 and 1.2-7 depict the geometry in 3-D space (the horizontal geometry and the vertical geometry, respectively).

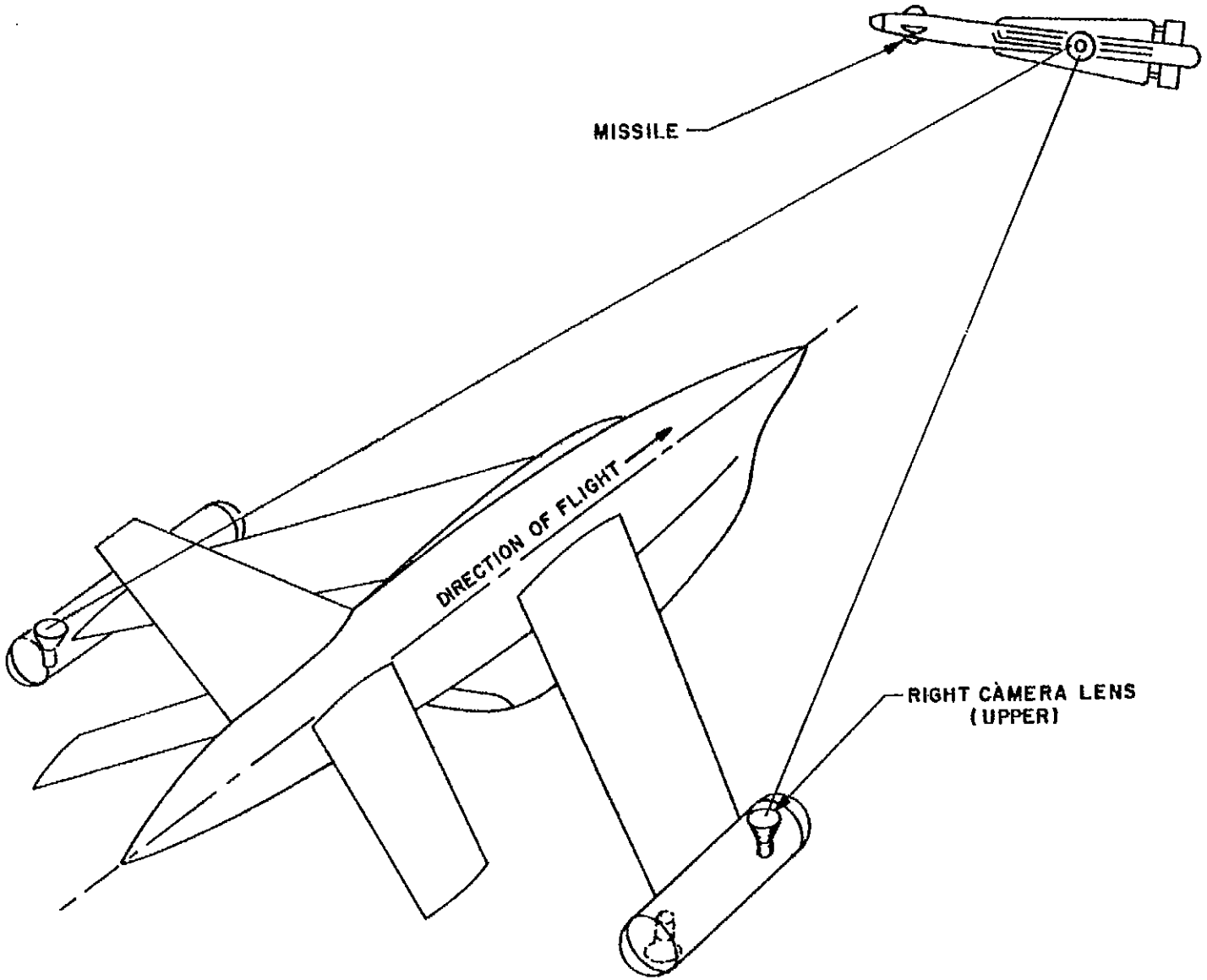

Figure 1.2-1 FEI scoring system on BQM-34A.

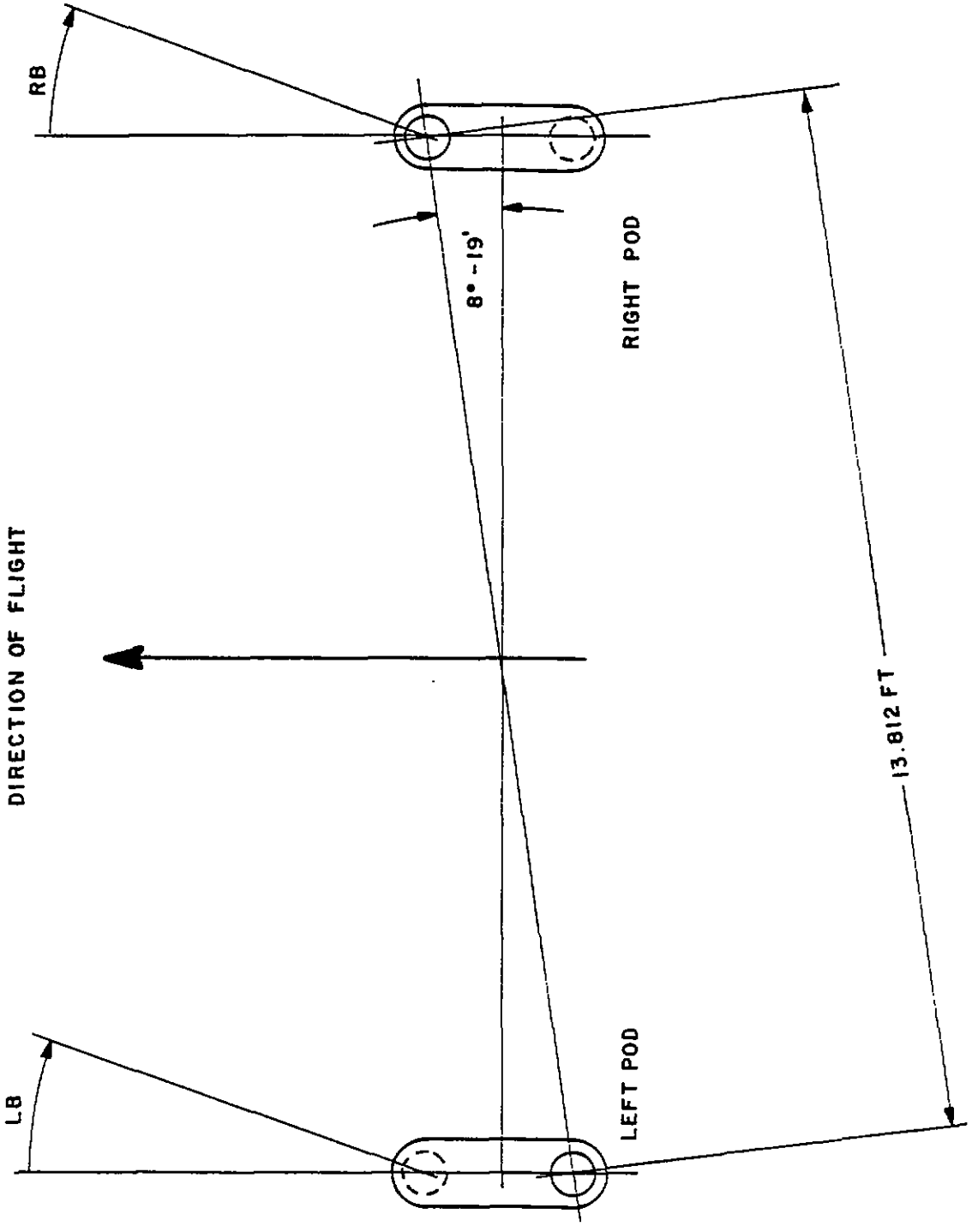

Figure 1.2-2 Plan view of FEI system on BQM-34A.

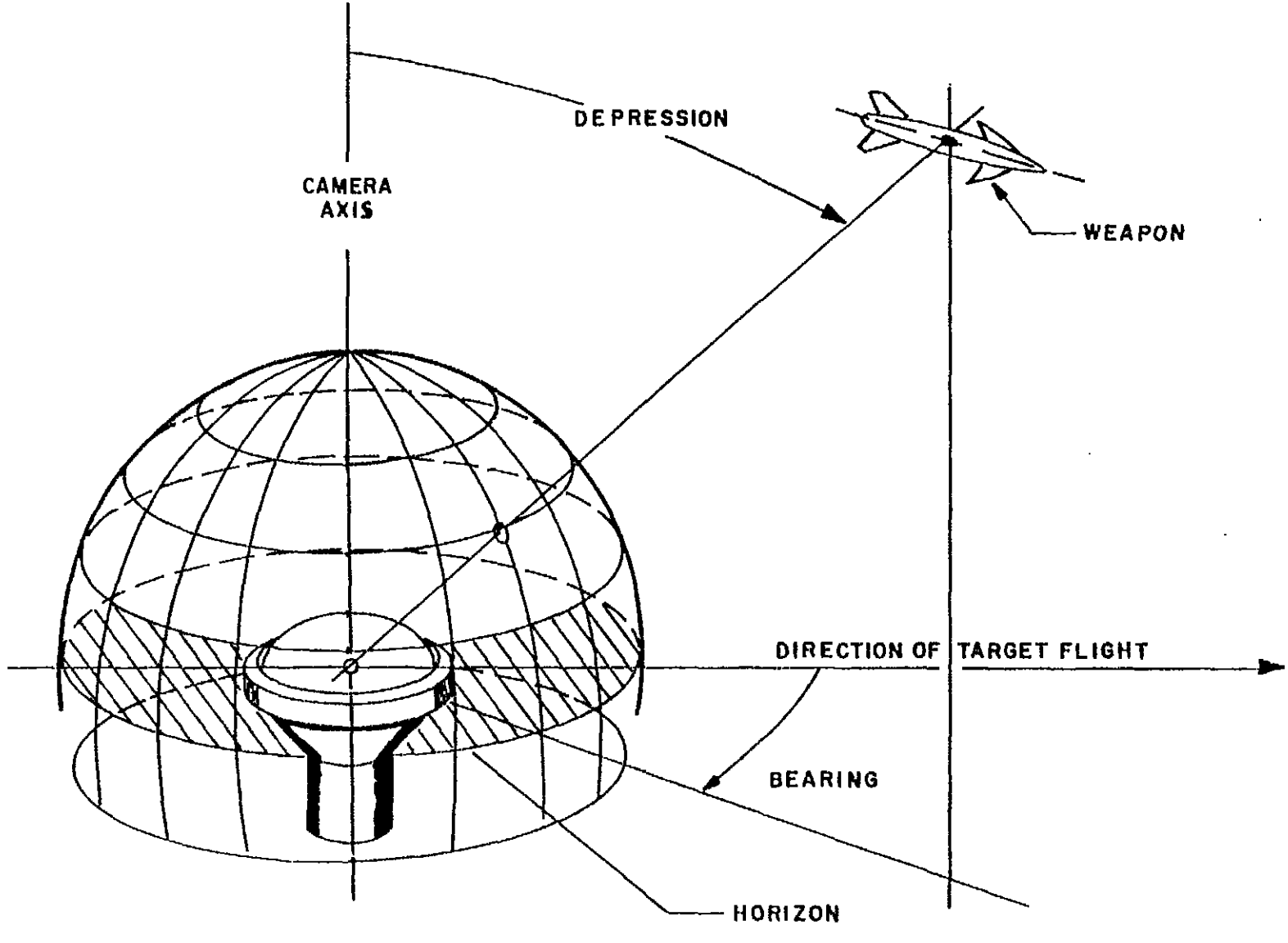

Figure 1.2-3 View from camera to weapon.

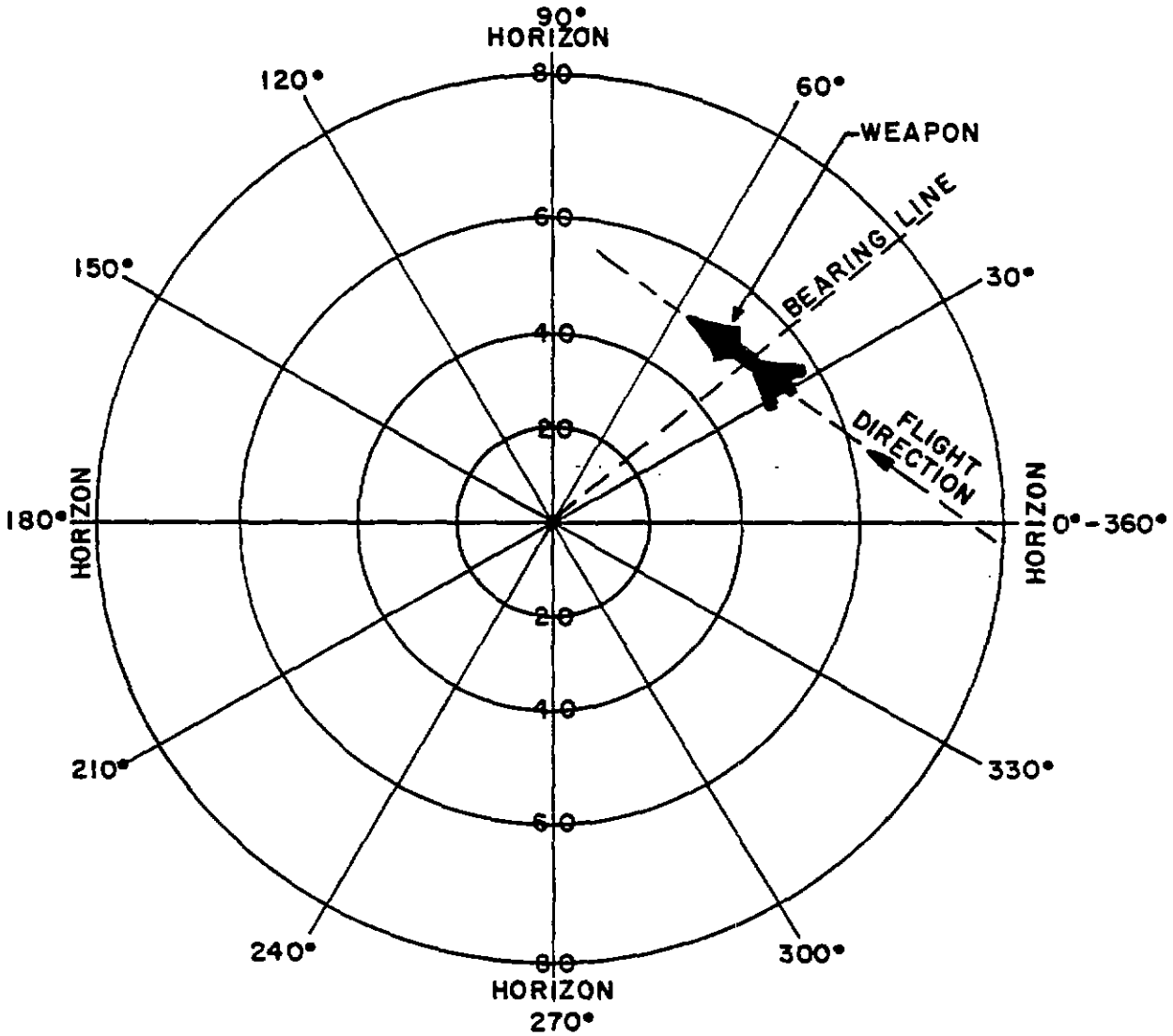

Figure 1.2-4 View recorded by camera with grid lines superimposed.

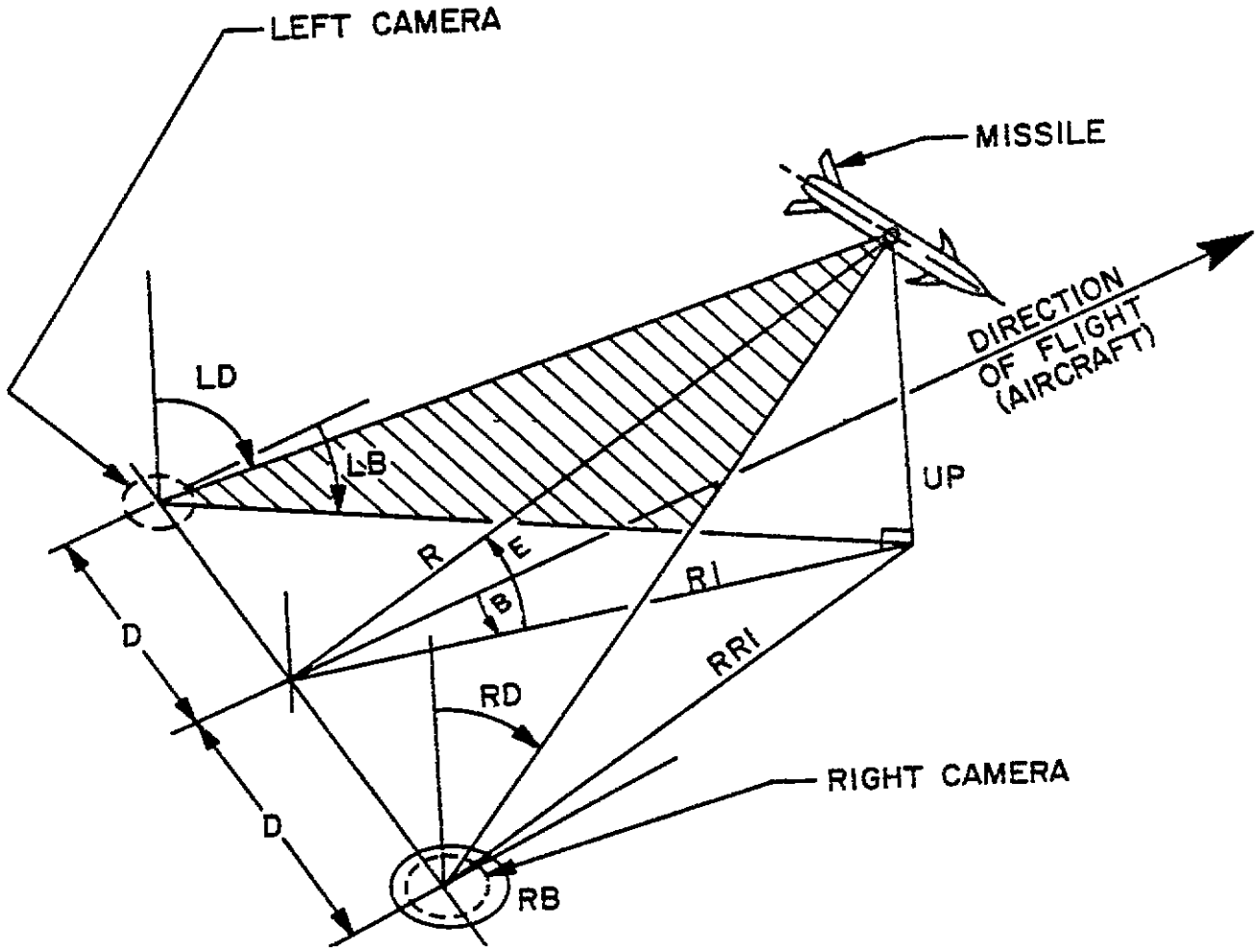

Figure 1.2-5 Model of the FEI problem.

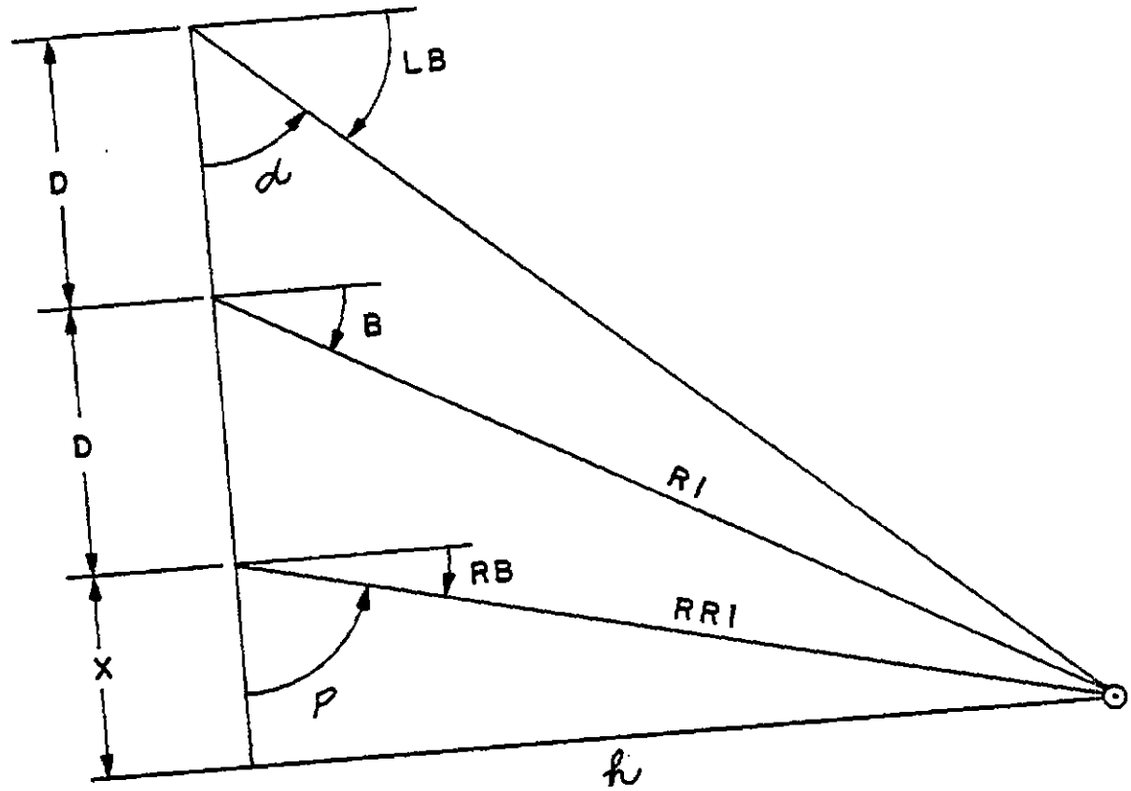

Figure 1.2-6 Horizontal problem.

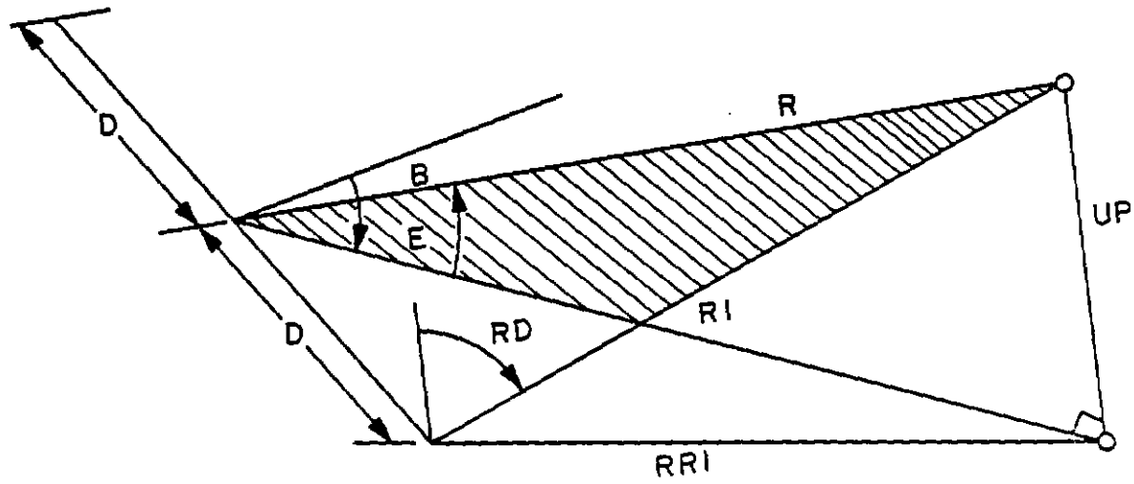

Figure 1.2-7 Elevation problem.

In these figures, the measured angles are as follows: left-depression (LD) angle, left-bearing (LB) angle, right-depression (RD) angle, and right-bearing (RB) angle. Here the origin is assumed to lie halfway between the cameras on a line through them. Defined distances are as follows: the horizontal projection of the range from the right-hand camera to the missile (RR1), the horizontal projection of the range from the origin to the missile (R1), the vertical distance from the plane of the cameras to the missile (UP), and the distance between the cameras (2D). Figure 1.2-6 shows X and h.

d. The quantities of interest are R, E and B (the range elevation and bearing of the missile in a coordinate system located at the origin). Using plane trigonometry, the following results are easily obtained relating these quantities to the raw measured angles:

$$B=\tan^{-1}\left[\frac{\sin (LB+RB)}{2 \cos LB \cos RB}\right] \quad (1)$$

$$E=\tan^{-1}\left[\frac{(\cos B \cot RD)}{\cos RB}\right] \quad (2)$$

$$R=2D\left[\frac{(\cos LB \cos RB)}{\cos B \cos E \sin (LB-RB)}\right] \quad (3)$$

e. In actual FEI installations, the line between the two cameras is not perpendicular to the principal axis of the airplane. This non-orthagonality is taken into account by a rotation. The equations above break down for LB=90° and 270°, RB=90° and 270°, RD=0°. However, this problem is solved by reducing data just before and just after these conditions occur.

f. Equations (1), (2) and (3) represent the solution to the problem of determining the position of the missile with respect to the aircraft.

g. The XYZ coordinates of the missile with respect to the aircraft are determined from the following equations:

$$R_1=R \cos E \quad (4)$$

$$X=R_1 \cos B \quad (5)$$

$$Y=-R_1 \sin B \tag{6}$$

$$Z=R \sin E \tag{7}$$

h. The missile trajectory and the point of closest approach are determined by fitting a 3-D curve to XYZ data about the data point closest to the aircraft. The equations used to represent the trajectory are as follows:

$$X=X \tag{8}$$

$$Y=\sum_{i=0}^{N} a_i x^i \tag{9}$$

$$Z=\sum_{i=0}^{N} b_i x^i \tag{10}$$

where N represents the degree of the polynomial used in fitting the data. In the past, a fourth-degree curve has been fitted to the five data points closest to the airplane. Because of the tendency of such a curve to follow noise and, hence, induce erroneous peaks, some feel that a lower degree curve and possibly more data points should be used. If this approach is used, the a_i and b_i are determined by the well-known method of least squares.

i. Once the a_i and b_i are obtained, X, Y and Z can be determined at any point on the curve over the span of the data points. The point of closest approach is determined by requiring that the function

$$R=(X^2+Y^2+Z^2)^{\frac{1}{2}} \tag{11}$$

be a minimum over the span of data points used in the curve fit. A necessary condition for the minimum is that

$$\frac{dR}{dX}=0 \tag{12}$$

since R can be written as a function of X only.

When equations (8), (9) and (10) are substituted into equation (11) and the partial with respect to X is taken and set equal to zero, a 2N-first-degree polynomial is obtained. By solving for the zeroes of this polynomial and picking the zero which falls in the range of the data span, the desired minimum is obtained. Letting Xm, Ym and Zm be the X, Y and Z when this minimum occurs, the range, Rm; bearing, Bm; and elevation, Em; at this minimum are as follows:

$$Rm=(Xm^2+Ym^2+Zm^2)^{\frac{1}{2}} \quad (13)$$

$$Em=\sin^{-1}(Zm/Rm) \quad (14)$$

$$Bm=\cos^{-1}(Xm/Rm \cos Em) \quad (15)$$

1.2.3 Accuracy

The following accuracy figures apply when this technique is used to compute miss distance:

Miss Distance	Error
>100 ft	Completely erroneous
25-100 ft	10-15 percent or 3.75 ft, whichever is larger
<25 ft	15 percent or 3 ft, whichever is larger

The above accuracies depend upon the cut angle between the rays formed by the two cameras and target and the distance between the cameras and target.

1.2.4 Advantage

If time correlation is available, this method gives better results than those obtained by techniques required when time correlation is not available.

1.2.5 Disadvantage

This method cannot be used if time correlation is poor or nonexistent.

BIBLIOGRAPHY

Duval, G. *Computerized Data Reduction for the FEI Scoring System.* Report No. NADC-AM-7035, Warminister, Pennsylvania: Naval Air Development Center, October 1970.

1.3 DRONE CAMERA SCORING WITHOUT TIME CORRELATION

1.3.1 General Description

a. One system used in missile testing consists of two or more motion picture cameras mounted on a target drone aircraft without time correlation between the cameras. From the film recorded when the missile appears in view of the cameras, the elevation and azimuth in the film coordinate system of the missile can be determined. Therefore, a plane consisting of a set of rays from the camera to the missile can be associated with each camera. Because there is no time correlation between the cameras, the trajectory of the missile cannot be determined by triangulation as is done in time correlated systems. Instead, the trajectory is established by using two cameras at a time and by determining the intersection of the planes established by the two cameras. In this manner, the miss distance can be determined.

b. The coordinate system used in this analysis is an inverted right-hand system oriented along the principal axis of the aircraft with the origin at the center of gravity. The usual convention is followed having positive X along the nose axis, positive Z down, and positive Y along the right wing.

c. The coordinate system (X', Y', Z') of the camera is also an inverted right-hand system with its origin at (X_0, Y_0, Z_0) of the aircraft and $+X'$ in the direction the camera is pointing. Figure 1.3-1 illustrates the geometry of the problem.

1.3.2 Math Model

a. A matrix, M, is developed for rotating from the camera system into the aircraft system using the azimuth-, elevation- and tilt-pointing angles of the camera.

b. Direction cosines of each ray in the camera system are established from the elevation and azimuth of the missile in the film system.

c. Direction cosines of those rays are rotated using M into the aircraft system.

d. Direction cosines of vectors A and B, which are nearest to the planes established by cameras 1 and 2 respectively, are determined (see figure 1.3-2). This is accomplished with the following reasoning:

1. For the ideal case, the unknown direction cosines could be determined by taking the cross product of two of the rays in the plane. Because the directions of the rays are determined from measured data with errors and the assumption that the rays form a plane is only an approximation, a least-squares criterion is used to determine the direction cosines for A and B.

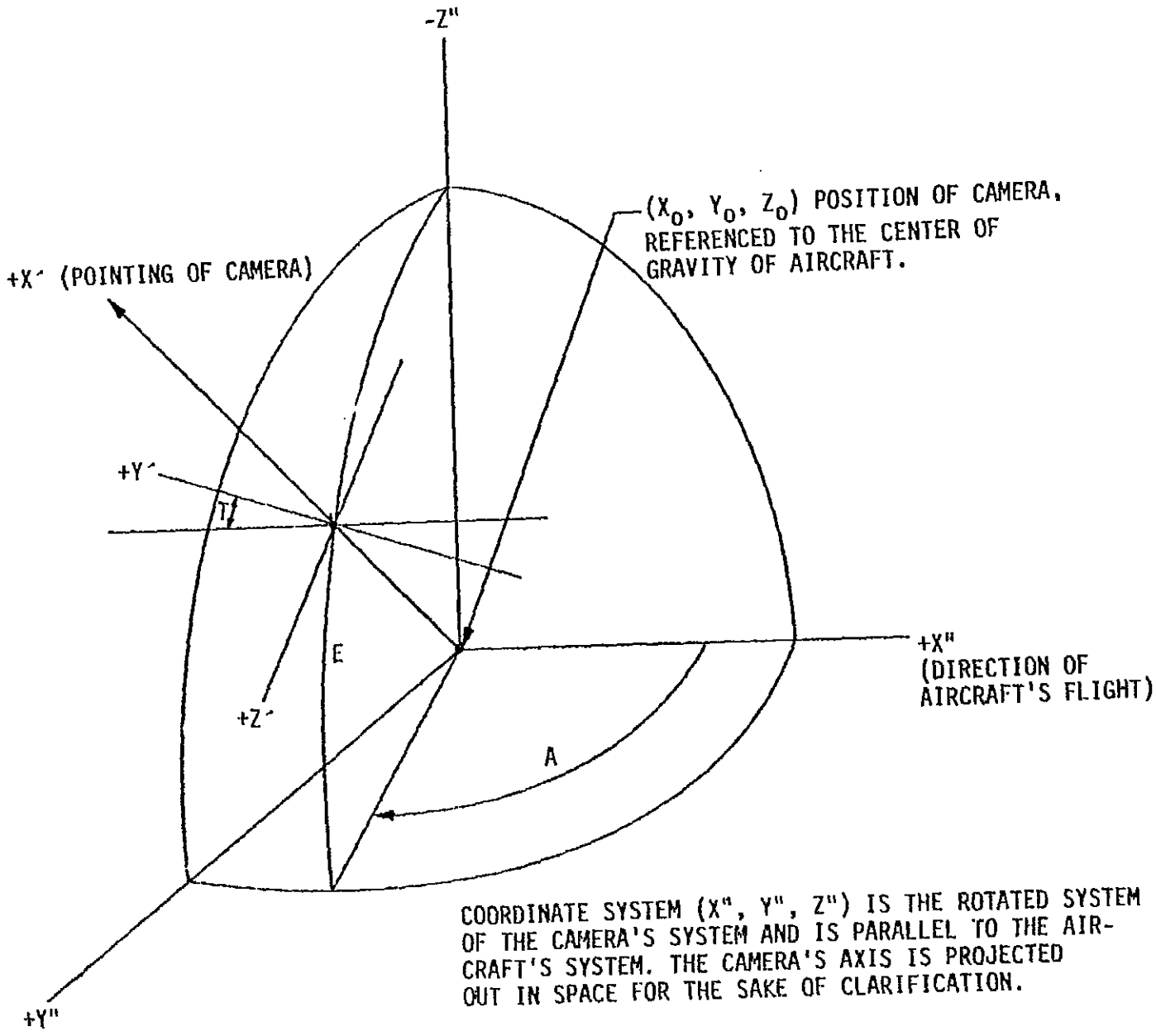

Figure 1.3-1 Coordinate system geometry.

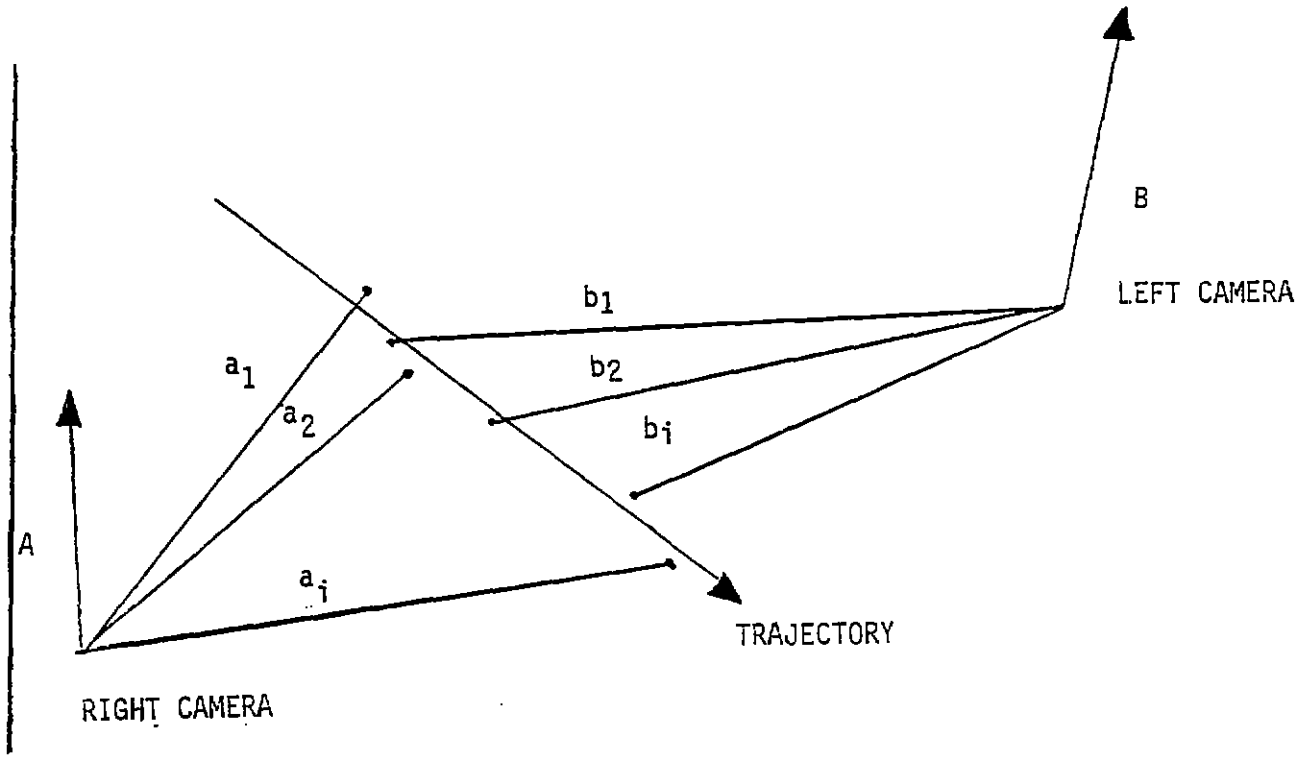

Figure 1.3-2 Direction cosines of vectors A and B.

2. Therefore, the cost function to be minimized is the sum of the squares of the dot product of all rays associated with each camera and the unknown perpendicular to the rays. The constraint which must be taken into account is that the sum of the squares of the unknown direction cosines equal one. Hence, the constraint must be added to the cost function and unknown Lagrange multipliers introduced. The setting of this gradient equal to zero results in two 3x3 eigenvalue problems in which the smallest roots to the third-degree characteristic equations give the unknown Lagrange multipliers. Once the Lagrange multipliers are determined, the unknown direction cosines are solved for giving the direction A and B. The cross product of A and B yields the direction cosines of the trajectories. Once the direction cosines are determined, the closest point to this trajectory is determined from the direction cosines of A, B and the trajectory and the positions of the two cameras being used with respect to the origin. The mathematical details and equations are contained in PMTC Technical Note No. 3285-503.[1]

1.3.3 Accuracy

Data is usually less accurate than time correlated data.

1.3.4 Advantage

The main advantage of this method of computing miss distance is that no time correlation is required between cameras on the drone aircraft.

1.3.5 Disadvantage

The algorithm assumes trajectory is a straight line.

REFERENCE

1. T. Magaoay. *DROCAM.* Technical Note No. 3285-503 (Point Mugu, California: Pacific Missile Test Center, April 1964).

1.4 WHITE SANDS MISSILE RANGE (WSMR) TRACKING CAMERAS - TWO OBJECTS IN SAME FRAME

1.4.1 Description

a. Assume that two or more tracking cameras have recorded an intercept test and that each instrument obtains a film record, with timing, containing both the missile and target in the same film frame. If the position and velocity of one of the objects is known, the position of the second object can be computed using the measured separation of the objects recorded on the film, the surveyed locations of the tracking cameras, and the optical characteristics of the tracking cameras and film reading machine. When the position of the second object is found, the miss distance relative to one of the objects is determined by subtracting the like position components of one object from the like position components of the other object. From a series of such observations and computations, a set of data that describes the position of both the missile and the target and, consequently, the relative data or miss distance is produced. This set of data can be smoothed and differentiated, with respect to time, to compute the component closing velocities of the missile with respect to the target. This information, in turn, can be used to determine the time of minimum approach (TMA) between the missile and target. The position of the missile and target can be extrapolated to the TMA and their differences taken to yield the minimum approach distance.

b. The geometry used in this discussion is presently in use at WSMR. The positions of all the tracking cameras and launchers are known in both the Geodetic Coordinate System and the White Sands Cartesian System (WSCS). The position of the known object is in the Launcher Coordinate System (LTS). Two more coordinate systems are necessary; the Station Coordinate System (STP) and the Camera Coordinate System (CCS). A description of each follows:

1. The Geodetic Coordinate System assumes that the earth is a spheroid of revolution. This system defines points on the earth's surface in terms of two angles, λ and ϕ. Latitude (ϕ) is the angle at which the normal to the spheroid at the point in question makes with the equatorial plane. Longitude (λ) is the angle between the plane of the geodetic meridian at the point and the plane of an initial meridian through Greenwich, England, and defined as longitude 0°. The origin of the system is the initial meridian or longitude 0° and the geodetic equator or latitude 0°.

2. The WSCS is a left-hand orthogonal system defined by the ordered triple (N, E, P). The NE-plane is tangent to the Clark Spheroid of 1866 at the intersection of latitude 33°05' and longitude 106°20'. The N-axis is positive northward, the E-axis is positive eastward, and the P-axis is perpendicular to the NE-plane and positive upward. The origin has arbitrarily been assigned a value in feet of 500,000; 500,000; 0. Therefore, all instrumentation locations on the range will have positive values in the NE-plane.

3. The LTP System is a left-hand orthogonal system defined by the ordered triple (X, Y, Z). The XY-plane is tangent to the earth at the launcher, which is the origin. The X-axis is positive along the azimuth of fire, the Y-axis is perpendicular to the X-axis and positive in the left-hand sense, while the Z-axis is perpendicular to the XY-plane and positive up. Most of the data at WSMR is computed and presented in this coordinate system.

4. The CCS is a left-hand orthogonal system defined by the ordered triple (A, B, C). The A-axis lies along the optical center of the lens. The BC-plane lies in the film plane of the camera perpendicular to the A-axis with the C-axis positive toward the top of the film frame parallel to the frame sides, and with the B-axis positive toward the side of the film frame in a left-hand sense. The origin is the center of the film frame and is considered to be coincident with the STP.

5. The STP System is a left-hand orthogonal system defined by the ordered triple (U, V, W). The UV-plane is tangent to the earth at the station, which is the origin. The U-axis is positive in the direction of true north. The V-axis is positive east, while the W-axis is positive up. (The vector from missile to target is depicted in figure 1.4-1.)

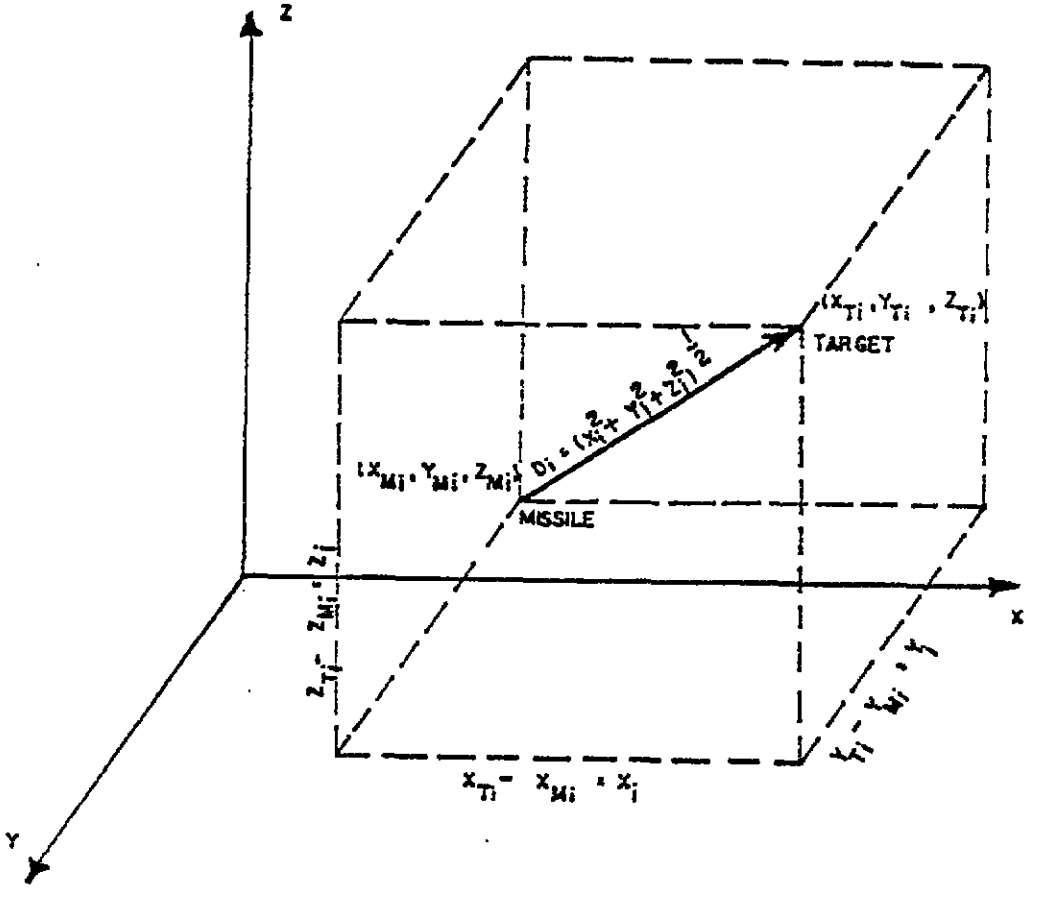

Figure 1.4-1 Graphical representation of miss-distance vector.

1.4.2 Math Model

a. Assuming that the target position and velocity are known in the LTP System, this subparagraph provides the necessary steps to determine the missile position in the same system. Since the observations made from each of the stations are in different coordinate systems, it is necessary to develop the transformations to relate all the observations in the LTP System.

b. The geodetic coordinates of the WSCS origin and those of the launcher are used to compute the rotation matrix to transform the WSCS station coordinates into the LTP System.

$$\begin{bmatrix} X_{Si} \\ Y_{Si} \\ Z_{Si} \end{bmatrix} = T_L \begin{bmatrix} N_{Si}-N_L \\ E_{Si}-E_L \\ P_{Si}-P_L \end{bmatrix} \qquad (1)$$

where:

X_{Si}, Y_{Si}, Z_{Si}=Coordinates of the ith station with respect to the launcher

N_{Si}, E_{Si}, P_{Si} and N_L, E_L, P_L=WSCS coordinates, respectively, of the ith station and the launcher.

$$T_L = \begin{bmatrix} t_{11} & t_{12} & t_{13} \\ t_{21} & t_{22} & t_{23} \\ t_{31} & t_{32} & t_{33} \end{bmatrix} = \text{Rotation matrix from WSCS to LTP System}$$

$$t_{11} = \sin\phi_0 \sin\phi_L \cos\alpha_L \cos(\lambda_0-\lambda_L) + \cos\phi_0 \cos\phi_L \cos\alpha_L + \sin\phi_0 \sin\alpha_L \sin(\lambda_0-\lambda_L)$$

$$t_{12} = -\sin\phi_L \cos\alpha_L \sin(\lambda_0-\lambda_L) + \sin\alpha_L \cos(\lambda_0-\lambda_L)$$

$$t_{13}=-\cos\phi_0 \sin\phi_L \cos\alpha_L \cos(\lambda_0-\lambda_L) + \sin\phi_0 \cos\phi_L \cos\alpha_L - \cos\phi_0 \sin\alpha_L \sin(\lambda_0-\lambda_L)$$

$$t_{21}=-\sin\phi_0 \sin\phi_L \sin\alpha_L \cos(\lambda_0-\lambda_L) - \cos\phi_0 \cos\phi_L \sin\alpha_L + \sin\phi_0 \cos\alpha_L \sin(\lambda_0-\lambda_L)$$

$$t_{22}=\sin\phi_L \sin\alpha_L \sin(\lambda_0-\lambda_L) + \cos\alpha_L \cos(\lambda_0-\lambda_L)$$

$$t_{23}=\cos\phi_0 \sin\phi_L \sin\alpha_L \cos(\lambda_0-\lambda_L) - \sin\phi_0 \cos\phi_L \sin\alpha_L - \cos\phi_0 \cos\alpha_L \sin(\lambda_0-\lambda_L)$$

$$t_{31}=-\sin\phi_0 \cos\phi_L \cos(\lambda_0-\lambda_L) + \cos\phi_0 \sin\phi_L$$

$$t_{32}=\cos\phi_L \sin(\lambda_0-\lambda_L)$$

$$t_{33}=\cos\phi_0 \cos\phi_L \cos(\lambda_0-\lambda_L) + \sin\phi_0 \sin\phi_L$$

α_L=Azimuth of fire with respect to true north

ϕ_0=Geodetic latitude of WSCS origin

=33°05'

λ_0=Geodetic longitude of WSCS origin

=106°20'

ϕ_L=Geodetic latitude of launcher

λ_L=Geodetic longitude of launcher

The position of the target, which is known in the LTP System, can now be found in each of the STP Systems (one for each camera station) by the following transformation:

$$\begin{bmatrix} U_{Ti} \\ V_{Ti} \\ W_{Ti} \end{bmatrix} = M_i \begin{bmatrix} X_t - X_{Si} \\ Y_t - Y_{Si} \\ Z_t - Z_{Si} \end{bmatrix} \qquad (2)$$

where:

U_{Ti}, V_{Ti}, W_{Ti}=Coordinates of the target with respect to the ith station in the ith STP System.

X_T, Y_T, Z_T =Target coordinates in the LTP System

X_{Si}, Y_{Si}, Z_{Si}=Coordinates of the ith station in the LTP System

$$M_i = \begin{bmatrix} m_{11} & m_{12} & m_{13} \\ m_{21} & m_{22} & m_{23} \\ m_{31} & m_{32} & m_{33} \end{bmatrix}$$ Rotation matrix =from LTP System to STP System

$$m_{11} = \sin\phi_i \sin\phi_L \cos\alpha_L \cos(\lambda_i - \lambda_L) + \cos\phi_i \cos\phi_L \cos\alpha_L + \sin\phi_i \sin\alpha_L \sin(\lambda_i - \lambda_L)$$

$$m_{12} = -\sin\phi_L \cos\alpha_L \sin(\lambda_i - \lambda_L) + \sin\alpha_L \cos(\lambda_i - \lambda_L)$$

$$m_{13} = -\cos\phi_i \sin\phi_L \cos\alpha_L \cos(\lambda_i - \lambda_L) + \sin\phi_i \cos\phi_L \cos\alpha_L - \cos\phi_i \sin\alpha_L \sin(\lambda_i - \lambda_L)$$

$$m_{21} = -\sin\phi_i \sin\phi_L \sin\alpha_L \cos(\lambda_i - \lambda_L) - \cos\phi_i \cos\phi_L \sin\alpha_L + \sin\phi_i \cos\alpha_L \sin(\lambda_i - \lambda_L)$$

$$m_{22} = \sin\phi_L \sin\alpha_L \sin(\lambda_i - \lambda_L) + \cos\alpha_L \cos(\lambda_i - \lambda_L)$$

$$m_{23}=\cos\phi_i \sin\phi_L \sin\alpha_L \cos(\lambda_i-\lambda_L) - \sin\phi_i \cos\phi_L \sin\alpha_L - \cos\phi_i \cos\alpha_L \sin(\lambda_i-\lambda_L)$$

$$m_{31}=-\sin\phi_i \cos\phi_L \cos(\lambda_i-\lambda_L) + \cos\phi_i \sin\phi_L$$

$$m_{32}=\cos\phi_L \sin(\lambda_i-\lambda_L)$$

$$m_{33}=\cos\phi_i \cos\phi_L \cos(\lambda_i-\lambda_L) + \sin\phi_i \sin\phi_L$$

ϕ_i=Geodetic latitude of ith station

λ_i=Geodetic longitude of ith station

ϕ_L=Geodetic latitude of launcher

λ_L=Geodetic longitude of launcher

α_L=Azimuth of fire with respect to true north

The azimuth and elevation of the target is now found in each of STP systems.

$$\alpha_{Ti}=\tan^{-1}(V_{Ti}/U_{Ti})$$
$$\varepsilon_{Ti}=\tan^{-1}\left[W_{Ti}/(U_{Ti}^2+V_{Ti}^2)^{\frac{1}{2}}\right] \qquad (3)$$

where:

α_{Ti}=Azimuth of target with respect to ith station in the ith STP System

ε_{Ti}=Elevation of target with respect to ith station in ith STP System

U_{Ti}, V_{Ti}, W_{Ti} as found in equation (2)

The direction cosines of the lines of sight from each of the stations to the missile can now be found and rotated into each of the STP Systems.

The direction cosines of the lines of sight to the missile are found in each of the CCSs. First from:

$$\cos a_{Mi}=A/(A^2+B^2+C^2)^{\frac{1}{2}}$$
$$\cos b_{Mi}=B/(A^2+B^2+C^2)^{\frac{1}{2}} \qquad (4)$$
$$\cos c_{Mi}=C/(A^2+B^2+C^2)^{\frac{1}{2}}$$

where:

$\cos a_{Mi}$, $\cos b_{Mi}$, $\cos c_{Mi}$=Direction cosines of the line of sight from the ith CCS to the missile.

A=Focal length of camera in machine counts

B=Horizontal distance on film from target to missile in machine counts

C=Vertical distance on film from target to missile in machine counts

NOTE

When reading the film, the machine is zeroed on the target; that is, the origin of the ABC system is in the image of the target.

The direction cosines found in equation (4) are rotated into the respective STP System. Since the optical axis of the camera is oriented on the target, the rotation is through the azimuth and elevation angles in equation (3).

$$\begin{bmatrix} \cos u_{Mi} \\ \cos v_{Mi} \\ \cos w_{Mi} \end{bmatrix} = C_i \begin{bmatrix} \cos a_{Mi} \\ \cos b_{Mi} \\ \cos c_{Mi} \end{bmatrix} \qquad (5)$$

where: $\cos u_{Mi}$, $\cos v_{Mi}$, $\cos w_{Mi}$ are direction cosines of the line of sight from the ith station to the missile in the ith STP System. Cos a_{Mi}, $\cos b_{Mi}$, $\cos c_{Mi}$ as in equation (4).

$$C_i = \begin{bmatrix} c_{11} & c_{12} & c_{13} \\ c_{21} & c_{22} & c_{23} \\ c_{31} & c_{32} & c_{33} \end{bmatrix}$$ = Rotation matrix from ith CCS to ith STP System

$c_{11} = \cos \alpha_{Ti} \cos \varepsilon_{Ti}$

$c_{12} = -\sin \alpha_{Ti}$

$c_{13} = -\cos \alpha_{Ti} \sin \varepsilon_{Ti}$

$c_{21} = \sin \alpha_{Ti} \cos \varepsilon_{Ti}$

$c_{22} = \cos \alpha_{Ti}$

$c_{23} = -\sin \alpha_{Ti} \sin \varepsilon_{Ti}$

$c_{31} = \sin \varepsilon_{Ti}$

$c_{32} = 0$

$c_{33} = \cos \varepsilon_{Ti}$

α_{Ti}, ε_{Ti} are found in equation (3)

An additional rotation of the direction cosines found in equation (5) will yield the direction cosines of the line of sight from each station to the missile in the LTP System. The inverse of the matrix found in equation (2) will accomplish this rotation; and since the matrix is orthogonal, the inverse is the transponse.

$$\begin{bmatrix} \cos x_{Mi} \\ \cos y_{Mi} \\ \cos z_{Mi} \end{bmatrix} = M_i^T \begin{bmatrix} \cos u_{Mi} \\ \cos v_{Mi} \\ \cos w_{Mi} \end{bmatrix} \qquad (6)$$

where:

$\cos x_{Mi}$, $\cos y_{Mi}$, $\cos z_{Mi}$ are direction cosines of line of sight from ith station to the missile in the LTP System. Thus, $\cos u_{Mi}$, $\cos v_{Mi}$, and $\cos w_{Mi}$ are as in equation (5). Mi^T=Transpose of matrix in equation (2).

Enough information is now available to find the missile position in the LTP System using a combination of any two of the stations. Ideally, the lines of sight from the stations should intersect at the point in space occupied by the missile. In practice, this is never the case, and a least-squares solution is used to minimize the perpendicular distance between the lines of sight. A solution for each station used is the result.

$$
\begin{aligned}
X_{Mi} &= R_i \cos x_{Mi} + X_{Si} \\
Y_{Mi} &= R_i \cos y_{Mi} + Y_{Si} \\
Z_{Mi} &= R_i \cos z_{Mi} + Z_{Si} \\
X_{Mj} &= R_j \cos x_{Mj} + X_{Sj} \\
Y_{Mj} &= R_j \cos y_{Mj} + Y_{Sj} \\
Z_{Mj} &= R_j \cos z_{Mj} + Z_{Sj}
\end{aligned}
\qquad (7)
$$

where:

X_{Mi}, Y_{Mi}, Z_{Mi} and X_{Mj}, Y_{Mj}, Z_{Mj}=Coordinates of the missile using the ith and jth stations, respectively.

X_{Si}, Y_{Si}, Z_{Si} and X_{Xj}, Y_{Sj}, Z_{Sj}=Station coordinates in the LTP System found in equation (1).

$\cos x_{Mi}$, $\cos y_{Mi}$, $\cos z_{Mi}$, and $\cos x_{Mj}$, $\cos z_{Mj}$, $\cos z_{Mj}$ are found in equation (6).

R_i and R_j are the ranges from the ith and jth stations to the missile found from:

$$
\begin{aligned}
R_i &= (L_j K - L_i)/(K^2 - 1) \\
R_j &= (-L_i K + L_j)/(K^2 - 1)
\end{aligned}
\qquad (8)
$$

where:

$$L_i=(X_{Sj}-X_{Si})\cos x_{Mi}+(Y_{Sj}-Y_{Si})\cos y_{Mi}+(Z_{Sj}-Z_{Si})\cos z_{Mi}$$

$$L_j=(X_{Sj}-X_{Si})\cos x_{Mj}+(Y_{Sj}-Y_{Si})\cos y_{Mj}+(Z_{Sj}-Z_{Si})\cos z_{Mj}$$

$$K=\cos x_{Mi}\cos x_{Mj}+\cos y_{Mi}\cos y_{Mj}+\cos z_{Mi}\cos z_{Mj}$$

The two solutions in equation (8) are averaged to yield the missile position for the two stations used.

$$X_{Mt}=(X_{Mi}+X_{Mj})/2$$

$$Y_{Mt}=(Y_{Mi}+Y_{Mj})/2 \qquad (9)$$

$$Z_{Mt}=(Z_{Mi}+Z_{Mj})/2$$

The solution found in equation (9) above is known as the Two-Station Bodwell Solution and is used as the trial solution for the Davis Solution. The Davis Solution determines a best estimate of the missile position, using the data from all the available stations. This method is a least-squares solution that determines a change in the trial solution so that the sum of the squares of the angular residuals of the stations used in the solution is a minimum. The angular residuals are defined as the difference in the azimuth and elevation angles of the missile as observed from the station and the corresponding azimuth and elevation angles as computed from the trial solution found in equation (9).

The least-squares solution for determining the change in the trial solution is found by solving the following set of normal equations:

$$a_{11}\Delta X_{Mt}+a_{12}\Delta Y_{Mt}+a_{13}\Delta Z_{Mt}=d_1$$

$$a_{21}\Delta X_{Mt}+a_{22}\Delta Y_{Mt}+a_{23}\Delta Z_{Mt}=d_2 \qquad (10)$$

$$a_{31}\Delta X_{Mt}+a_{32}\Delta Y_{Mt}+a_{33}\Delta Z_{Mt}=d_3$$

where:

ΔX_{Mt}, ΔY_{Mt}, ΔZ_{Mt}=Values to be added to the trial solution to minimize the squares of the residual angles

$$a_{11}=\Sigma\left[(P_iA_{i1})^2+E_{i1}^2\right]$$

$$a_{12}=\Sigma(P_i^2A_{i1}A_{i2}+E_{i1}E_{i2})$$

$$a_{13}=\Sigma(P_i^2A_{i1}A_{i3}+E_{i1}E_{i3})$$

$$a_{21}=\Sigma(P_i^2A_{i2}A_{i1}+E_{i2}E_{i1})$$

$$a_{22}=\Sigma\left[(P_iA_{i2})^2+E_{i2}^2\right]$$

$$a_{23}=\Sigma(P_i^2A_{i2}A_{i3}+E_{i2}E_{i3})$$

$$a_{31}=\Sigma(P_i^2A_{i3}A_{i1}+E_{i3}E_{i1})$$

$$a_{32}=\Sigma(P_i^2A_{i3}A_{i2}+E_{i3}E_{i2})$$

$$a_{33}=\Sigma\left[(P_iA_{i3})^2+E_{i3}^2\right]$$

$$d_1=\Sigma\left[P_iA_{i1}\cos\ \varepsilon_{Ti}(\alpha_{0i}-\alpha_{Ti})+E_{i1}(\varepsilon_{0i}-\varepsilon_{Ti})\right]$$

$$d_2=\Sigma\left[P_iA_{i2}\cos\ \varepsilon_{Ti}(\alpha_{0i}-\alpha_{Ti})+E_{i2}(\varepsilon_{0i}-\varepsilon_{Ti})\right]$$

$$d_3=\Sigma\left[P_iA_{i3}\cos\ \varepsilon_{Ti}(\alpha_{0i}-\alpha_{Ti})+E_{i3}(\varepsilon_{0i}-\varepsilon_{Ti})\right]$$

All summations from i=1 to N where N is the number of stations used in the solution.

$$A_{i1}=\partial\alpha_{Ti}/\partial X_{Mt}$$

$$A_{i2}=\partial\alpha_{Ti}/\partial Y_{Mt}$$

$$A_{i3}=\partial\alpha_{Ti}/\partial Z_{Mt}$$

$$E_{i1}=\partial\varepsilon_{Ti}/\partial X_{Mt}$$

$$E_{i2}=\partial\varepsilon_{Ti}/\partial Y_{Mt}$$

$$E_{i3}=\partial\varepsilon_{Ti}/\partial Z_{Mt}$$

$$\alpha_{Ti}=\tan^{-1}\left[(Y_{Mt}-Y_{Si})/(X_{Mt}-X_{Si})\right]$$

$$\varepsilon_{Ti}=\tan^{-1}\left\{\left[(Z_{Mt}-Z_{Si})/\left[(X_{Mt}-X_{Si})^2+(Y_{Mt}-Y_{Si})^2\right]^{\frac{1}{2}}\right\}\right.$$

$P_i=\cos\ \varepsilon_{Ti}$=square root of the weight assigned the azimuth residual

$$\left.\begin{aligned}\alpha_{0i}&=\tan^{-1}(\cos\ y_{Mi}/\cos\ x_{Mi})\\ \varepsilon_{0i}&=\sin^{-1}(\cos\ z_{Mi})\end{aligned}\right\}\ \text{From equation (6)}$$

then

$$A_{i1}=-(Y_{Mt}-Y_{Si})/\left[(X_{Mt}-X_{Si})^2+(Y_{Mt}-Y_{Si})^2\right]$$

$$A_{i2}=(X_{Mt}-X_{Si})/\left[(X_{Mt}-X_{Si})^2+(Y_{Mt}-Y_{Si})^2\right]$$

$$A_{i3}=0$$

$$E_{i1}=\left[-(X_{Mt}-X_{Si})(Z_{Mt}-Z_{Si})\right]/\left\{\left[(X_{Mt}-X_{Si})^2+(Y_{Mt}-Y_{Si})^2\right]\left[+(Z_{Mt}-Z_{Si})^2\right]\left[(X_{Mt}-X_{Si})^2+(Y_{Mt}-Y_{Si})^2\right]^{1/2}\right\}$$

$$E_{i2}=\left[-(Y_{Mt}-Y_{Si})\ (Z_{Mt}-Z_{Si})\right]/\left\{\left[(X_{Mt}-X_{Si})^2+(Y_{Mt}-Y_{Si})^2+(Z_{Mt}-Z_{Si})^2\right]\left[(X_{Mt}-X_{Si})^2+(Y_{Mt}-Y_{Si})^2\right]^{1/2}\right\}$$

$$E_{i3}=\left[(X_{Mt}-X_{Si})^2+(Y_{Mt}-Y_{Si})^2\right]^{1/2}/\left[(X_{Mt}-X_{Si})^2+(Y_{Mt}-Y_{Si})^2+(Z_{Mt}-Z_{Si})^2\right]$$

where: X_{Mt}, Y_{Mt}, Z_{Mt}, and X_{Si}, Y_{Si}, Z_{Si}, are found in equations (9) and (11), respectively.

The set of normal equations in equation (10) can be solved for ΔX_{Mt}, ΔY_{Mt} and ΔZ_{Mt} using any convenient method. When Cramer's Rule for determinants is used, the solution is:

$$\Delta X_{Mt}=D_1/D_0$$

$$\Delta Y_{Mt}=D_2/D_0 \qquad (11)$$

$$\Delta Z_{Mt}=D_3/D_0$$

where:

the elements of D_0, D_1, D_2, D_3 are found from equation (10).

$$D_0=\begin{vmatrix} a_{11} & a_{12} & a_{13} \\ a_{21} & a_{22} & a_{23} \\ a_{31} & a_{32} & a_{33} \end{vmatrix}=\text{The Least-Squares Determinant}$$

$$D_1=\begin{vmatrix} d_1 & a_{12} & a_{13} \\ d_2 & a_{22} & a_{23} \\ d_3 & a_{32} & a_{33} \end{vmatrix}$$

$$D_2=\begin{vmatrix} a_{11} & d_1 & a_{13} \\ a_{21} & d_2 & a_{23} \\ a_{23} & d_3 & a_{33} \end{vmatrix}$$

$$D_3=\begin{vmatrix} a_{11} & a_{12} & d_1 \\ a_{21} & a_{22} & d_2 \\ a_{31} & a_{32} & d_3 \end{vmatrix}$$

The position estimate of the missile now becomes:

$$\begin{aligned} X_m &= X_{Mt}+\Delta X_{Mt} \\ Y_m &= Y_{Mt}+\Delta Y_{Mt} \\ Z_m &= Z_{Mt}+\Delta Z_{Mt} \end{aligned} \qquad (12)$$

The component error estimates are computed at the 1σ or 68.27-percent confidence level using the least-squares determinant, the angular residuals, and the appropriate value for the student t statistic.

$$\begin{aligned} E_X &= (J_{11}\sigma_A^2/D_0)^{\frac{1}{2}}S_n \\ E_y &= (J_{22}\sigma_A^2/D_0)^{\frac{1}{2}}S_n \\ E_Z &= (J_{33}\sigma_A^2/D_0)^{\frac{1}{2}}S_n \end{aligned} \qquad (13)$$

where:

E_X, E_y, E_Z=Error estimates in the missile position at the 68.27-percent confidence level

J_{11}, J_{22}, J_{33}=Cofactors of the a_{11}, a_{22}, a_{33} elements, respectively, of the least-squares determinant found in equation (11).

$$\sigma_A=\left\{\sum_{i=1}^{N}\left[(r_{\alpha i}\cos\varepsilon_i)^2+r_{\varepsilon i}^2\right]/(2N-3)\right\}^{1/2}$$

=Standard deviation of the angular residuals found in equation (10)

$r_{\alpha i}=(\alpha_{oi}-\alpha_{ti})$=Azimuth residual from ith station

$r_{\varepsilon i}=(\varepsilon_{oi}-\varepsilon_{ti})$=Elevation residual from ith station

ε_i=Elevation of missile with respect to ith station as computed from trial solution

N=Number of stations used in solution

S_n=Student t values for n degrees of freedom at 68.27-percent confidence level

n=2N-3=Degrees of freedom in system

By applying the previous part of this discussion to the entire series of observations, a set of unsmoothed data describing the missile trajectory is produced. This set of data is now smoothed and differentiated with respect to time, using a least-squares moving arc technique that fits a second-degree curve to P consecutive position points and evaluates the curve at the midpoint. The midpoint is advanced one point at a time until the entire set of data is smoothed. The equations shown below are for the X coordinate with the Y and Z coordinates exactly the same after replacing X with Y or Z.

$$XS_{Mi}=g_{oi}$$
$$VX_{Mi}=g_{1i}/\Delta T \qquad (14)$$
$$AX_{Mi}=2g_{2i}/\Delta T^2$$

where:

XS_{Mi}, VS_{Mi}, AX_{Mi}=Smoothed position, velocity and acceleration, respectively, of the missile at the ith time in the set of smoothed position data

ΔT=Time interval between observations

and:

g_{0i}, g_{1i}, g_{2i} are found from:

$$\begin{bmatrix} g_{0i} \\ g_{1i} \\ g_{2i} \end{bmatrix} = H \cdot \begin{bmatrix} \Sigma X_{Mj} \\ \Sigma X_{Mj}(j-p) \\ \Sigma X_{Mj}(j-p)^2 \end{bmatrix} \begin{matrix} \text{Summations} \\ \text{from} \\ j=k \text{ to } m \end{matrix}$$

where:

g_{0i}, g_{1i}, g_{2i}=Coefficients of the normal equations for the least-squares curve fitted to the data.

X_{Mj}, Y_{Mj}, Z_{Mj}=Position coordinates of the missile at the jth time in the set of unsmoothed position data found in equation (12)

NOTE

Replace X_{Mj} with Y_{Mj} or Z_{Mj} when solving for YS_{Mi} or ZS_{Mi}

P=Number of points used for the curve fit (must be odd and ≥ 3)

N=Number of points of unsmoothed data

Q=Number of points of smoothed data=N-(P-1)

k=1, 2, ..., Q

m=k+(P-1)

i=1, 2, ..., Q

p=Midpoint of odd smoothing interval=k+(P-1)/2

and:

$$H=\begin{bmatrix} h_{11} & h_{12} & h_{13} \\ h_{21} & h_{22} & h_{23} \\ h_{31} & h_{32} & h_{33} \end{bmatrix}$$

$$h_{11}=3(3P^2-7)/[4P(P^2-4)]$$

$$h_{12}=0$$

$$h_{13}=-15/P(P^2-4)$$

$$h_{21}=0$$

$$h_{22}=12/P(P^2-1)$$

$$h_{23}=0$$

$$h_{31}=-15/P(P^2-4)$$

$$h_{32}=0$$

$$h_{33}=[12/P(P^2-1)]\,[15/(P^2-4)]$$

The smoothed missile position data can now be combined with the known target data to yield the relative or miss-distance data for the ith time point.

$$\begin{aligned} XR_i&=(XS_{Mi}-X_{Ti})\\ YR_i&=(YS_{Mi}-Y_{Ti})\\ ZR_i&=(ZS_{Mi}-Z_{Ti})\\ MD_i&=(XR_i^2+YR_i^2+ZR_i^2)^{1/2} \end{aligned} \qquad (15)$$

where:

XR_i, YR_i, ZR_i=Relative coordinates of the missile with respect to the target

XS_{Mi}, YS_{Mi}, ZS_{Mi} as computed in equation (14)

X_{Ti}, Y_{Ti}, Z_{Ti}=Target coordinates known from another source

MD_i=Total distance between missile and target

The error estimates for the total miss distance at the ith time is found from:

$$EMD_i=\frac{(XR_i^2E_{xi}^2+YR_i^2E_{yi}^2+ZR_i^2E_{zi}^2)^{1/2}}{MD_i} \qquad (16)$$

where:

EMD_i=Error estimate for total miss distance

XR_i, YR_i, ZR_i and E_{xi}, E_{yi}, E_{zi} as in equations (15) and (13), respectively.

The relative velocities at the ith time are found in the same manner.

$$VXR_i=(VX_{Mi}-VX_{Ti})$$
$$VYR_i=(VY_{Mi}-VY_{Ti}) \qquad (17)$$
$$VZR_i=(VZ_{Mi}-VZ_{Ti})$$
$$VTR_i=(VXR_i^2+VYR_i^2+VZR_i^2)^{\frac{1}{2}}$$

where:

VXR_i, VYR_i, VZR_i=Relative velocities of the missile with respect to the target

VX_{Mi}, VY_{Mi}, VZ_{Mi}=Components of missile velocity as found in equation (14)

VX_{Ti}, VY_{Ti}, VZ_{Ti}=Components of target velocity known from another source

VRT_i=Total relative or closing velocity between missile and target

The time of minimum approach (TMA) between missile and target is now found.

$$TMA=t_c-\left[(XR_cVXR_c+YR_cVYR_c+ZR_cVZR_c)/(VXR_c^2+VYR_c^2+VZR_c)\right] \qquad (18)$$

where:

TMA=Time of minimum approach

t_c=Time of closest apparent approach determined by the smallest miss distance (MD_i) computed in equation (15)

XR_c, YR_c, ZR_c and VXR_c, VYR_c, VZR_c are the relative position and velocity data corresponding to time t_c and computed from equations (15) and (17).

The relative position of missile and target can now be extrapolated to the TMA to determine the closest approach between missile and target.

$$XR_{min}=XR_c+VXR_c(TMA-t_c)$$
$$YR_{min}=YR_c+VYR_c(TMA-t_c) \qquad (19)$$
$$ZR_{min}=ZR_c+VZR_c(TMA-t_c)$$
$$MD_{min}=(XR^2_{min}+YR^2_{min}+ZR^2_{min})^{1/2}$$

where:

XR_{min}, YR_{min}, ZR_{min}=Relative components of the missile with respect to the target at TMA

MD_{min}=Total miss distance at TMA

All other variables as in equation (18).

1.4.3 Accuracy

The accuracy of the miss-distance method described in this report depends largely on the following factors:

a. The geometrical relationship of the tracking cameras with respect to intercept. Accuracy suffers as the azimuth angle between any two lines of sight from the tracking cameras to intercept approaches 180°. The azimuth angle also becomes unreliable as the elevation angle approaches 90° and is undefined at this point.

b. Distance from tracking cameras to intercept. When these distances exceed 50,000 ft, other methods of miss distance should be investigated. When the distances are in the 5,000-ft range, the error estimates of missile position are usually within 1.5 ft.

c. Image quality of film and timing. The quality of the film image determines whether a discernible point can be read on either the target or missile. At WSMR, the film is normally read from the center of the target image to the tail of the missile image. Errors in timing can result in degrading the quality of the data, often rendering it useless.

1. The WSMR Quality Assurance Office publishes statistics on the average angular error and the average position data error for telescopes used in miss-distance reductions. The latest figures available show the average azimuth and elevation errors to be 25 and 16 seconds, respectively, and the position data error to be 3.43 ft.

2. WSMR is currently attempting to increase the precision of this miss-distance method by taking multiple readings of the film records and statistically editing this data to produce a best estimate of the true reading.

1.4.4 Advantages

a. As this method is used at WSMR, only one point of target position data is needed at a time near minimum approach. The point is then extrapolated throughout the time interval covered by the tracking cameras. The known position can be obtained from optical, radar, DOVAP, or any other source. Furthermore, since this point is used to compute the azimuth and elevation angles with respect to each station, no new error is introduced as would be the case if each instrument were observing and measuring these azimuth and elevation angles independently.

b. The film from the tracking cameras can be read more rapidly, since only the timing and the distance between the target and the missile is read for each frame.

c. The film records can be used for other purposes such as event time determination and also serve as a permanent visual record of the test.

1.4.5 Disadvantages

a. The missile and target must both be in the field of view of the tracking camera with the position of one of the objects known.

b. Reasonably good weather with no obscuring clouds is required to obtain data by this method.

c. The distance between the recording stations and intercept is limited by the resolving ability of the optical systems involved.

d. Night tests require light sources on both objects in the field of view.

1.4.6 Cost

When furnished in conjunction with other optical reductions, the charge to range users in FY 80 was $241.00; however, this method, as implemented at WSMR, uses telescope tracking cameras which do not record azimuth and elevation. These cameras were installed for recording event time history information. This method increases the usefulness of the

tracking telescopes without additional expense. Also, the film is read on the same machines used to read the film from cinetheodolites that obtain position data.

1.4.7 Reliability

No statistics are available for the telescope coverage of miss distance alone. The overall reliability of telescopes used for all purposes was set at 92 percent for the latest quarter available at WSMR. Reliability, as defined by the WSMR Quality Assurance Office, is the percent of assigned operations on which no failure occurred.

BIBLIOGRAPHY

1. Byers, Blaine E. *Intercept, A Program for Computing Miss Distance from Optical Input Parameters.* Technical Report No. 33, White Sands Missile Range, New Mexico: Analysis and Computation Division, Data Reduction Branch, Optical Section, January, 1972.

2. Comstock, Darold W.; Wright, Madeleine H.; and Tipton, Virginia B. *Handbook of Data Reduction Methods.* White Sands Missile Range, New Mexico: NR-A, Data Reduction Branch, Third Printing, 1 March 1969.

3. Davis, R. C. *Techniques for the Statistical Analysis of Cinetheodolite Data.* NAVORD Report 1299. Inyokern, California: NOTS 369, United States Naval Ordnance Test Station, 22 March 1951.

4. Page, Woodrow W. *Some Mathematical Techniques Used in Reduction of Tracking Data.* Internal Memorandum 38, White Sands Missile Range, New Mexico: Analysis and Computation Directorate, NR-A, Evaluation Division, January 1967.

5. Starkweather, F. T. *Special Report for Computation of Minimum Miss Distance.* White Sands Missile Range, New Mexico: Data Analysis Section, South Range Branch, DRD, IRM, 25 August 1959.

1.5 WSMR TRACKING CAMERAS - SINGLE OBJECT ON FILM FRAME

1.5.1 General Description and Math Model

a. This miss-distance program computes time histories of parameters associated with the line-of-sight vector between two objects in an arbitrary 3-D coordinate system. One or both of the objects may be in motion.

b. The inputs to this miss-distance program, when both objects are in motion, are mutual time histories of the rectangular space coordinates of both objects. (As a matter of convenience, one object will be called the "missile" and the other will be called the "target.")

c. When both missile and target are in motion, the time points of each must be correlated for the parameters to be computed at corresponding time points. To do this, the program computes a probable time constant between uninterpolated data samples:

$$\Delta t = 1/s$$

where: s is the sampling rate.

An allowable tolerance for testing target missile times for equality is computed: $E = .1\Delta t$. (Time points will be accepted as mutual if they agree within $.1\Delta t$.) Miss-distance data is correlated when mutual time points exist. The missile and target must also be in the same coordinate system for the computed parameters to be meaningful. The rotation matrix and translation constants from a translation and rotation (T&R) program are made available to the miss-distance program.

d. Uninterpolated component missile-to-target distance for every time, T, for which missile and target data are available is computed from:

$$X_i = X_{Ti} - X_{Mi}$$

$$Y_i = Y_{Ti} - Y_{Mi}$$

$$Z_i = Z_{Ti} - Z_{Mi}$$ (See Figure 1.5-1)

The total missile-to-target distance is derived from the distance formula:

$$D_i = (X_i^2 + Y_i^2 + Z_i^2)^{1/2}$$

The interpolated components of missile-to-target distance are then computed from:

$$X_j = A_{x_0} + A_{x_1} T_j + A_{x_2} T_j^2$$

$$Y_j = A_{y_0} + A_{y_1} T_j + A_{y_2} T_j^2$$

$$Z_j = A_{z_0} + A_{z_1} T_j + A_{z_2} T_j^2$$

The total missile-to-target distance is computed from:

$$D_j = (X_j^2 + Y_j^2 + Z_j^2)^{\frac{1}{2}}$$

The scaled time points, T_j, are converted to the correct test for output. Missile-to-target velocities, accelerations and other derivative data are computed in the same method as when both objects are in the same frame (see section 1.4).

1.5.2 Advantages

The advantages of having one object per frame as opposed to having both objects in the same frame are:

a. more points may be computed

b. any two systems (not necessarily optic) may be used

c. better geometry.

1.5.3 Disadvantages

The disadvantages realized by utilizing the one object per frame method are:

a. precision is poorer than that obtained when both objects are in the same frame

b. time correlation problems exist

c. more stations required.

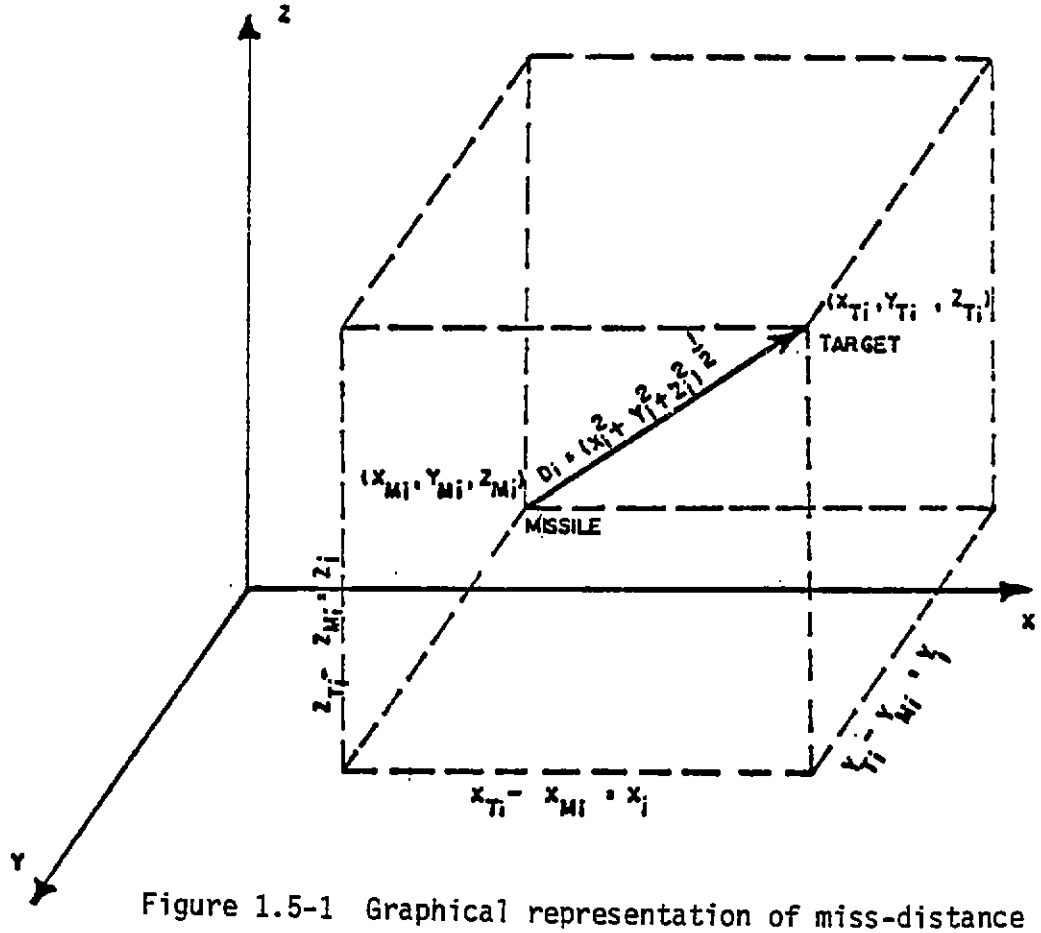

Figure 1.5-1 Graphical representation of miss-distance vector.

1.5.4 Reliability

Reliability is about the same as that attained in the method used when both objects are in the same frame (see section 1.4).

1.5.5 Applicable Programs

All applicable programs relative to this method of determining miss distance may be obtained from Analysis and Computation Division, ATTN: STEWS-NR-A, White Sands Missile Range, New Mexico 88002.

1.6 KWAJALEIN MISSILE RANGE (KMR) MISS-DISTANCE MEASUREMENTS (MDM) - TWO OBJECTS IN A SINGLE FRAME

1.6.1 General Description and Geometry

a. The sensor system currently used for collection of optical metric data at Kwajalein Missile Range (KMR) is composed of four Recording Automatic Digital Optical Trackers (RADOTs)] and five SUPERADOTs strategically located on the Kwajalein Atoll for optimal coverage and to obtain a high degree of accuracy. It is with these sensor systems that optical MDM is obtained.

b. In processing mission data to determine the optical MDM, data from each sensor are used in a Bodwell Solution[2] to determine the position of the interceptor. The separation distance is found by using the position of the interceptor as a reference; that is to say, the distance from the interceptor to the target vehicle is calculated using the azimuth and elevation differences measured on a single frame of data from each optical sensor. This calculation finds the position of the target vehicle relative to the interceptor so that the angles formed between the line joining the optical sensor and the target vehicle and the line between the optical sensor and the estimated position of the target vehicle are minimized for all sensors in a least-squares sense.[3] This interactive process of refining the estimated position of the target vehicle through successive approximation leads to an optimal estimate for MDM.

1.6.2 Input Data

Data are processed to ensure precision and accuracy in MDM. A brief summary of the data gathering procedures is presented prior to discussion of MDM.

1.6.3 Selection of Optical Sensor Coverage and Frame Rates

Optical sensors which have recorded the interceptor and the target vehicle in the same data frame are selected on the following basis:

a. Good geometry. Colocated stations will not provide optimal triangulation.

b. Sensors with the longest focal length lenses (254 cm to 600 cm) provide the best resolution.

c. Fastest nominal frame rates.

1.6.4 Data Digitizing Equipment

The data digitizing equipment (both for film and video data) has three components which can affect MDM accuracy - the projection system,

the cursors and the encoder. Measurements of the nonlinearities and nonorthogonalities of the data digitizing equipment are made by projecting a calibrated grid and measuring the grid coordinate. These measurements are also used to determine the vertical and horizontal scale factors.

1.6.5 Timing

In MDM, timing is of initial importance, particularly for ICBM intercepts. Times from the individual optical sensors are determined to 0.1 ms. After time alignment and data processing, the overall timing accuracy for MDM is ±0.1 ms (one standard deviation).

1.6.6 Math Model

a. Miss distance in the X, Y, and Z direction is represented by a vector. The separation can be expressed as a function of time:

$$\text{Separation}=f(t)=X_t^2+Y_t^2+Z_t^2 \qquad (1)$$

where:

X_t, Y_t, and Z_t are the X, Y, and Z components at time t.

To find the time of minimum separation, the derivative of f(t) in equation (1) is set equal to zero and solved for t; considering two time points, t_i and t_{i-1}, are connected by a straight line where:

$$X_t=M_x t+b_x$$

$$Y_t=M_y t+b_y$$

$$Z_t=M_z t+b_z$$

Solving for M_x, M_y, and M_z where $\Delta t=t_i-t_{i-1}$.

$$M_x=(X_i-X_{i-1})/\Delta t=m_x$$

$$M_y=(Y_i-Y_{i-1})/\Delta t=m_y$$

$$M_z=(Z_i-Z_{i-1})/\Delta t=m_z$$

Solving for b_x, b_y, b_z

$$b_x=X_i-m_x t_i$$

$$b_y=Y_i-m_y t_i$$

$$b_z=Z_i-m_z t_i$$

Substituting the values of X, Y, and Z and taking the derivative with respect to time t

$$\text{Separation}=\sqrt{(m_x t+b_x)^2+(m_y t+b_y)^2+(m_z t+b_z)^2}$$

$$f'(t)=t(m_x^2+m_y^2+m_z^2)+m_x b_x+m_y b_y+m_z b_z$$

To find the time of minimum separation,

$$t(m_x^2+m_y^2+m_z^2)=-(m_x b_x+m_y b_y+m_z b_z)$$

$$t_{min}=\frac{-(m_x b_x+m_y b_y+m_z b_z)}{m_x^2+m_y^2+m_z^2}$$

Using the time of minimum separation and solving for the X, Y, and Z miss distance components:

$$X_{min}=m_x t_{min}+b_z$$

$$Y_{min}=m_y t_{min}+b_y$$

$$Z_{min}=m_z t_{min}+b_z$$

$$\text{Minimum Separation}=\sqrt{X_{min}^2+Y_{min}^2+Z_{min}^2}$$

b. Figure 1.6-1 is an illustration of the graphic presentation of miss distance data that is reported. Tabular listings of X, Y and Z components are also listed as a function of time.

c. If a specific time is known, such as a specific burst time, the X, Y and Z components are, at that time, considered the miss distance. The terms "miss distance" and "minimum separation" are not synonymous.

1.6.7 Accuracy

MDM accuracy for this mode is very good. Since it is dependent on geometry, each case must be examined individually. In general, accuracies of 1 m or less out to slant ranges of 50 km are typical.

1.6.8 Actual Data and Case Example

Miss distance measurements for KMR have been provided for reentry ICBMs and locally launched SPRINT missiles. Miss distance reports have been published by Kentron International, Inc., for missions conducted at KMR through 1974.

1.6.9 Advantages

One advantage of recording two objects in a single frame for MDM is that the measurements are made relative to each other. Therefore, the effect of sensor systematic errors is eliminated.

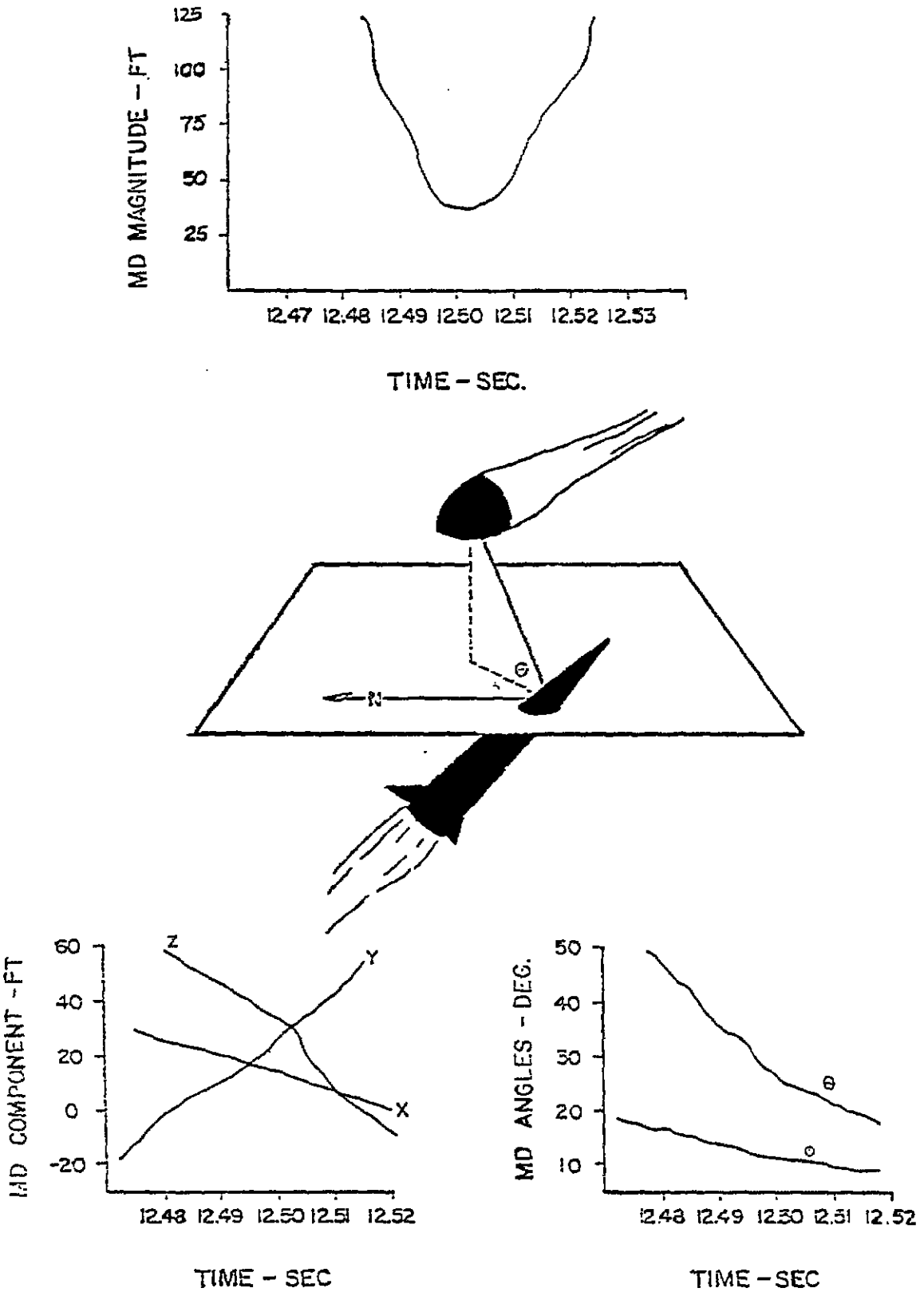

Figure 1.6-1 Graphic presentation of miss-distance data.

b. Since MDM is a vector, it provides magnitude and direction of miss.

1.6.10 Disadvantage

The objects must both be photographed within the same frame. This necessitates that both objects be visible.

1.6.11 Cost

Data reduction is a minimal cost. Data acquisition costs include operator, recording medium (film or video tape), and film processing for the number of sensors required.

1.6.12 Reliability - Checkout

MDM is highly weather dependent and is also a function of slant range and types of vehicles.

1.6.13 Applicable Programs

KMR has provided optical MDM for the SAFEGUARD ABM System for actual SPRINT launches against incoming ICBMs.

REFERENCES

1. J. F. Nicola, "RADOT - A New System for Optical Range Instrumentation," *12th SPIE Technical Symposium* (February-March 1968).

2. C. A. Bodwell, *A Least Squares Solution for the Cinetheodolite Problem.* MTHT-138: (Inyokern, California: Naval Ordnance Test Station, 12 December 1951).

3. R. C. Davis, *Techniques for the Statistical Analysis of Cinetheodolite Data.* NAVORD Report No. 1299 (Inyokern, California: Naval Ordnance Test Station, 22 March 1951).

1.7 KMR MISS-DISTANCE ESTIMATION - GENERAL METHOD

1.7.1 General Description and Geometry

a. KMR has radar and optical sensors, including three C-band tracking radars, three SUPERADOTs, four RADOTs, and six ballistic cameras. In order to obtain MDM data on the intercept of multiple target vehicles, these sensors are divided into two groups - one group is assigned to track the interceptor and the other group is assigned to track the targets.

b. Generally, it is desired that all objects appear within the same frame of film. The method for estimating MDM for that case is discussed in section 1.6. However, it is possible that a large separation distance may occur and simultaneous coverage of two objects in a single frame cannot be achieved.

c. When this situation occurs, MDM must be derived from analysis of the individual trajectories obtained from the two groups of sensors. How this is accomplished will be addressed briefly in this section.

1.7.2 Math Model

a. As stated above, the approach to obtain MDM for the general case is embodied in the estimation of individual trajectories. The multisensor trajectories are estimated using a nonlinear weighted least-squares technique.

b. The method utilized by KMR involves the estimation of the individual trajectories and differencing them directly.

1.7.3 Accuracy

The trajectory uncertainty varies depending upon the quantity and type of sensor data in the solution and sensor geometry. From previous experience, the trajectory estimation uncertainty with good coverage at an altitude of 120 km (slant range$\sim$300 km) is approximately 1 to 2 m. The uncertainty in the MDM for two separate trajectories of this kind would be 2 to 3 m.

1.7.4 Actual Data

The case of a single object in each frame has not been encountered by KMR; that is, there have always been sufficient data with multiple objects in a single frame to allow determination of MDM.

1.7.5 Advantages

This method does not depend upon the field of view of the cameras since each object is independently tracked. Separate tracking assignments for the sensors increase the probability of obtaining MDM in the case of a large miss.

1.7.6 Disadvantages

In this method, the position uncertainty of each object must be considered. The MDM uncertainty is almost totally dependent on the individual trajectory estimates. In contrast, when the multiple objects are recorded in a single frame, this effect is minimal.

1.7.7 Cost

There are no cost figures available for this method.

1.7.8 Reliability

Based on past performances of trajectory data acquisition as a standard, this is a very reliable method of obtaining MDM.

1.7.9 Applicable Programs

KMR has provided MDM for the SAFEGUARD ABM System for actual SPRINT launches against incoming ICBMs.

1.8 KMR IMPACT MISS DISTANCE

1.8.1 General Description and Geometry

The impact location is determined by a nonlinear least-squares estimate from sensor measurements of the vehicle impact. The sensors include two splash detection radars, telemetry sensors and the hydro-acoustic impact timing system. In addition, the multisensor trajectory estimate (when available) is propagated to impact and used with the other impact sensor data.

1.8.2 Accuracy

The impact estimate uncertainty is dependent upon the quantity and type of sensor data in the solution. From previous experience, the impact estimation uncertainty with good coverage is approximately 2 to 3 m.

1.8.3 Actual Data

Impact miss distance data have been routinely provided for reentry vehicles for the past 7 years.

1.8.4 Cost

No cost figures are available.

1.8.5 Reliability

Based on past performance of impact miss distance as a standard, this is a very reliable method.

1.8.6 Applicable Programs

KMR currently provides miss distance for reentry vehicles for MMII, MMIII and the ABRES programs.

1.9 COOPERATIVE DOPPLER DRQ-4

1.9.1 General Description

The DRQ-4 Cooperative Doppler System uses a transponder in the target which receives the missile telemetry signal, mixes it with a local oscillator, and transmits the difference frequency to the ground station. The ground station is composed of a dual receiving system which receives the signal from the transponder and the direct signal from the missile transmitter. The signals from both receivers are mixed together and the difference frequency is mixed with a local oscillator on the ground which produces a difference frequency in the range of IRIG B and G which is suitable for recording on magnetic tape (see figure 1.9-1).

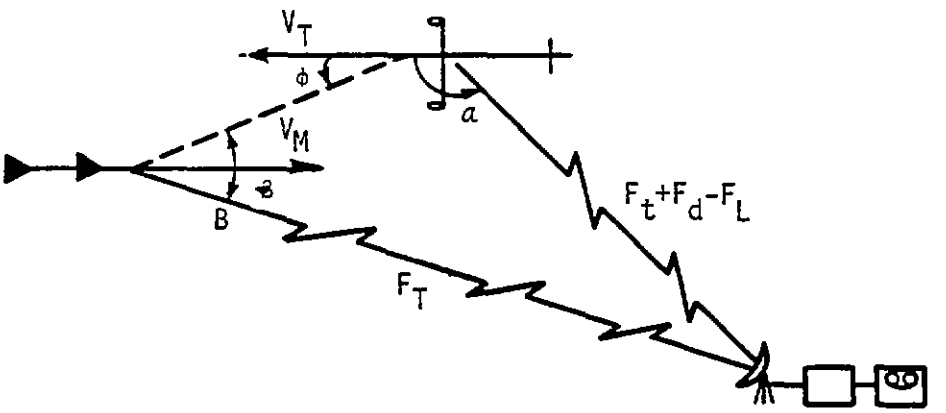

Figure 1.9-1 DRQ-4 cooperative doppler system.

1.9.2 Math Model

The frequency received at the target is:

$$F_R=F_T+(V_M/\lambda)\cos\theta+(V_T/\lambda)\cos\phi=F_t+F_d \qquad (1)$$

where:

F_T=Transmitted frequency

V_M=Missile velocity

θ=Angle between the missile velocity vector and the line of sight to the target

V_T=Target velocity

ϕ=Angle between the target velocity vector and the line of sight to the missile

F_d=Doppler frequency

The frequency received by ground receiver 1 is:

$$F_{R1}=F_T+F_d+(V_T/\lambda_1)\cos\alpha-F_{L1} \quad (2)$$

where:

λ_1=Wavelength of the transponder signal

F_{L1}=Frequency of the local oscillator in the transponder

α=Angle between the target velocity vector and the line connecting the target with the ground receiving antenna

The frequency received by ground receiver 2 is:

$$F_{R2}=F_t+(V_M/\lambda)\cos\beta \quad (3)$$

where:

β=Angle between the missile velocity vector and the line connecting the target with the ground receiving antenna

The frequency recorded is:

$$F_o=F_{R1}-F_{R2}-F_{L2}=F_t+(V_M/\lambda)\cos\theta+(V_T/\lambda)\cos\phi+(V_T/\lambda_1)$$

$$\cos\alpha-F_{L1}-F_t-(V_M/\lambda)\cos\beta-F_{L2}$$

or

$$F_o=V_M/\lambda\cos\theta+(V_T/\lambda)\cos\phi+V_T/\lambda_1\cos\alpha-F_{L1}-F_{L2}-(V_M/\lambda)\cos\beta \quad (4)$$

where F_{L2} is the frequency of the local oscillator in the ground station.

If V_T is considered to be only the velocity component parallel to the missile velocity vector , $\theta=\phi$.

For most operations, the distance from the ground station to the intercept point is much greater than the distance travelled by the missile and target during the short intercept period. We can assume $(V_T/\lambda_1)\cos\alpha-(V_M/\lambda)$. $\cos\beta$=k a constant.

Equation (4) now becomes:

$$F_o=\left(\frac{V_M+V_T}{\lambda}\right)\cos\theta+K+F_{L1}-F_{L2} \tag{5}$$

$$F_o=\frac{V_o\cos\theta}{\lambda}+C \tag{6}$$

where:

V_o=Missile velocity relative to the target

C=Sum of all constant terms

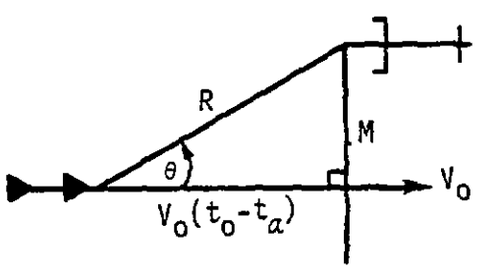

Figure 1.9-2 Missile velocity vector.

From figure 1.9-2 (7)

$$\cos\theta=\frac{V_o(t_o-t)}{\sqrt{V_o^2(t_o-t)^2+M^2}}$$

and solving equation (6) for cos θ yields:

$$\cos\theta=\frac{\lambda F_o}{V_o}-\frac{\lambda C}{V_o} \tag{8}$$

So that

$$\frac{\lambda F_o}{V_o} = \frac{V_o(t_o-t)}{\sqrt{V_o^2(t_o-t)^2+M^2}} + \frac{\lambda C}{V_o}$$

and

$$F_o = \frac{V_o^2(t_o-t)}{\sqrt{V_o^2(t_o-t)^2+M^2}} + C \qquad (9)$$

Taking the derivative of equation (9) with respect to time yields:

$$\dot{F}_o = \frac{-V_o^2\sqrt{V_o^2(t_o-t)^2+M^2}+V_o^2(t_o-t)\left(V_o^2(t_o-t^2)+M^2\right)^{\frac{1}{2}}V_o^2(t_o-t)}{\lambda\sqrt{V_o^2(t_o-t)^2+M^2}}$$

or

$$\dot{F}_o = \frac{-V_o^2\left[V_o^2(t_o-t)^2+M^2\right]+V_o^4(t_o-t)^2}{\lambda\left[V_o^2(t_o-t)^2+M^2\right]^{3/2}} \qquad (10)$$

Expanding equation (10) gives:

$$\dot{F}_o = \frac{-V_o^2M^2}{\lambda\left[V_o^2(t_o-t)^2+M^2\right]^{3/2}} \qquad (11)$$

The maximum value of $\dot{F}_o$ occurs at $t=t_o$

$$\dot{F}_o(max) = \frac{-V_o^2M^2}{\lambda M^3} = \frac{-V_o^2}{\lambda M}$$

therefore:

$$M = \frac{-V_o^2}{\lambda \dot{F}_d(max)} \qquad (12)$$

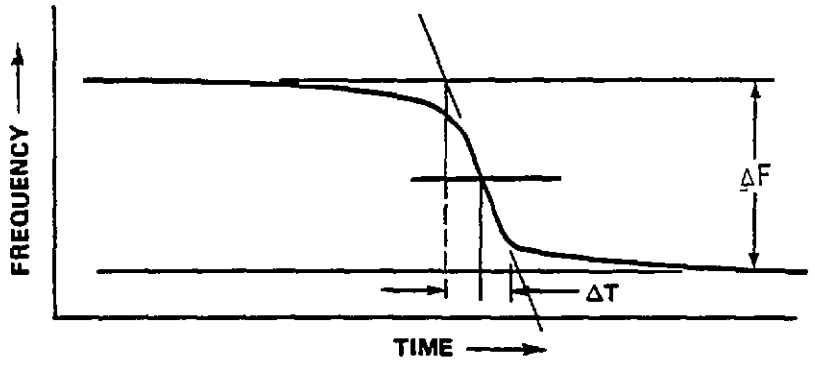

Figure 1.9-3 Intercept time.

Examination of figure 1.9-3 will show that:

$\theta \rightarrow 0°$ when $T << T_o$ and

$\theta \rightarrow 180°$ when $T >> T_o$

So that prior to intercept, using equation (6)

$$F_o \rightarrow \frac{V_o}{\lambda} + C = F_o(\max) \tag{13}$$

and after intercept

$$F_o \rightarrow -\frac{V_o}{\lambda} + C = F_o(\min) \tag{14}$$

Subtracting equation (14) from equation (13) yields:

$$F_o(\max) - F_o(\min) = \frac{V_o}{\lambda} + \frac{V_o}{\lambda} = \frac{2V_o}{\lambda} = \Delta F$$

or

$$V_o = \frac{\lambda \Delta F}{2} \tag{15}$$

Substituting in equation (12) gives

$$M = \frac{\lambda \Delta F^2}{4F_0(max)} \qquad (16)$$

an equation that is independent of any constant frequency shifts.

1.9.3 Data Reduction Procedures

a. Quick-Look Reduction

1. The doppler signal from the ground station is recorded on magnetic tape and passed through an IRIG-B and G discriminator onto an oscillograph recorder where it is displayed along with IRIG-B time at 16 in/s. Using a straight edge, draw a pair of parallel lines on the oscillograph through the asymptotes of the curve. The distance between the two lines is measured against the frequency calibration on the front of the oscillograph to convert it to frequency. This measurement is recorded as ΔF. Next, a line is drawn tangent to the curve at the point of steepest slope and extended until it crosses the two lines which were previously drawn. Perpendicular lines are drawn from the points of intersection of the lines to the IRIG-B time code. The distance between these two lines is read off of the time code and recorded as ΔT. Using ΔT and ΔF and knowing the wavelength of the missile telemetry transmitter, the miss distance and relative velocity can be calculated and

$$V_0 = \frac{\lambda \Delta F}{2} \text{ and } M = \frac{\lambda \Delta F \Delta T}{4} = \frac{V_0 \Delta T}{2} \qquad (17)$$

2. Intercept time is the midpoint between the intersection of the two vertical lines and the time code signal.

b. Digital Reduction

1. The recorded doppler signal is digitized in the same manner as an ordinary FM signal with the output calibrated in frequency using the discriminator calibrations. In this procedure as well as the quick-look procedure described above, be careful not to overfilter the data since this would distort the slope of the curve at intercept and cause an error in the miss distance.

2. For the balance of the reduction see PMR Technical Note Number 3284-483, May 1965, written by C. Thomas.

1.9.4 Accuracy

The accuracy of the cooperative doppler is not known precisely since it is difficult to perform a controlled test. However, for tests in which both the cooperative doppler and photon MDI were used, the two systems produced equivalent results which indicated an accuracy of within ±5 ft.

1.9.5 Advantages

a. The cooperative doppler data is very easy to reduce by both manual and digital methods.

b. The range of the system is dependent only on the signal power of the missile telemetry transmitter and the threshold limitation of the transponder.

c. No special hardware is necessary for data reduction.

d. Quick-look miss distance can be computed within 10 min after a test.

1.9.6 Disadvantages

a. A special ground station receiver is required.

b. The system cannot be tested during flight to be certain that it is operating. If no signal is received, it is not certain whether the missile was out of the range of the transponder or the system malfunctioned.

c. The transmitter power used on missiles since the change to S-band frequencies has caused problems in receiving adequate signal strength at the transponder for the system to be reliable.

d. The system can only be used for missiles equipped with transmitters.

e. The signal must be received for some time before and after intercept to determine miss distance, making it unusable for surface targets.

BIBLIOGRAPHY

1. *Bidops MDI - Doppler Scoring of Projectiles.* Army Missile Command Document RM-TM-65-35, Ref. USAF Document ATL-TR-66-15.

2. G. C. Dewey Corporation. *MDI - Doppler Scoring of Projectiles.* Army Missile Command Document TR-TM-65-20.

3. Giannini Corporation. *MDI - Radiation Method of Scoring Missiles.* WSMR Data Analysis Memo DAM-64-10. White Sands Missile Range, New Mexico, 27 July 1964.

4. *IGOR, Interpolation of Missile Trajectory Determined from Optical Recording, A Survey of Miss-Distance Methods.* Technical Publication HR2, White Sands Missile Range, New Mexico: Data Analysis Directorate, April 1965.

5. *Matts MDI, Two Radar Tracking Sites.* USAF Document APGS-TR-GI-57.

6. *NADC MDI - Photographic POD System.* USM Report No. NADC-ED-L6343.

7. Thomas, C. "AN/USG-11" (Gives scaler miss distance and scaler velocity at a missile relative to a target.) *The Determination of Distance of Closest Approach from Doppler Frequency.* Technical Note 3284-483, Point Mugu, California: Pacific Missile Test Center, 1965.

1.10 DIGIDOPS AN/DSQ-24

1.10.1 General Description

a. The DIGIDOPS miss-distance indicator sensor, developed by Babcock Electronics Corporation, is a narrow-pulse, noncooperative radar system designed for installation in airborne target vehicles. The sensor emits a narrow pulse of RF energy which is reflected from any device that passes within 200 ft of the target vehicle. The reflected signal (echo) is received and compared in time to the transmitted pulse in 1 of 30 range gates. The range gate output, an analog voltage proportional to range, is transmitted to a ground receiving station where it is displayed on a stripchart in real time.

b. The sensor is capable of detecting miss distance in 5-ft zones between 0 and 100 ft and in 10-ft zones between 100 and 200 ft. The offensive device can have a relative velocity between 200 and 8,000 ft/s and a minimum radar cross section of 1 square foot. Other electrical and physical characteristics of the DIGIDOPS sensor are as follows:

Electrical

Transmitter

Frequency	1775 MHz
Power	3 W peak
Pulse width	10 ns
Pulse rise time	4 ns (maximum)
Pulse frequency	350 kHz

Receiver

Frequency	1775 MHz
Bandwidth	180 MHz
Sensitivity	-97 dBm

Physical

Dimensions

5.25-in diameter
13-in length

Weight

9 lb

1.10.2 Math Model and Data Reduction Technique

a. Normally, the miss distance is read directly from the strip chart recording that is taken in real time. Since there are 30 range gates in the DIGIDOPS sensor, there are 30 discrete miss distances that can be read directly from the strip chart. The strip chart has a staircase appearance as follows:

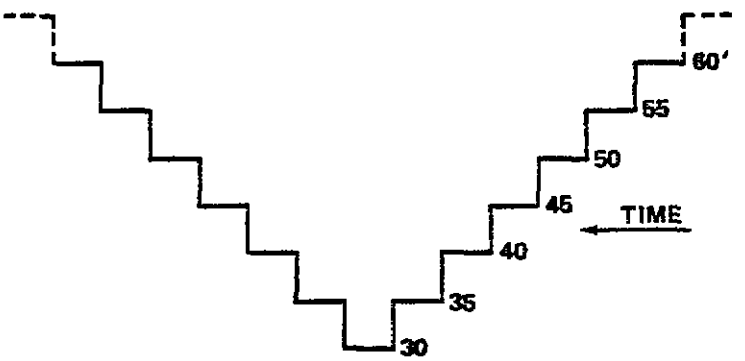

b. The lowest value is the direct-read miss distance. In this example, the miss distance is between 25 and 30 ft. Ten of the range gates are used for ranges 100 to 200 ft, with each range gate having a discrete difference of 10 ft. Within 100 ft, the remaining 20 gates are used with 5-ft discrete differences. Thus, within 100 ft, the miss distance can be read to the nearest 5 ft.

c. To obtain a miss-distance accuracy better than 5 ft, a least-squares fit of the data to a parabola is made. The time of each step change and the step value are manually read from the strip chart and put into a least-squares program in a programmable calculator. The program determines the best quadratic fit and the minimum point (point of closest approach).

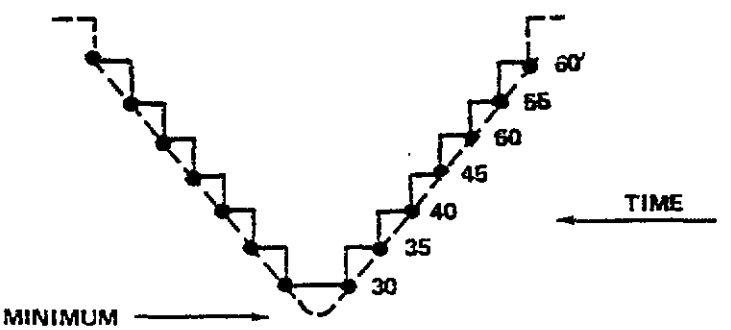

d. Both the direct-read method and the least-squares method are sometimes corrupted by the environmental noise that affects the doppler system and by the noise in the received telemetry signal. Telemetry noise causes indistinct discrete step changes on the strip chart and makes reading the step changes difficult, therefore, affecting the miss-distance solution. The environmental noise around some target vehicles degrades the performance of the range gates, specifically the very close-in gates. Therefore, all gates under 40 ft have been disconnected and the least-squares method used to determine miss distances under this 40-ft cutoff. In both least-squares examples shown, the computed miss distance is approximately 27 ft as compared to 30 ft for the direct-read method.

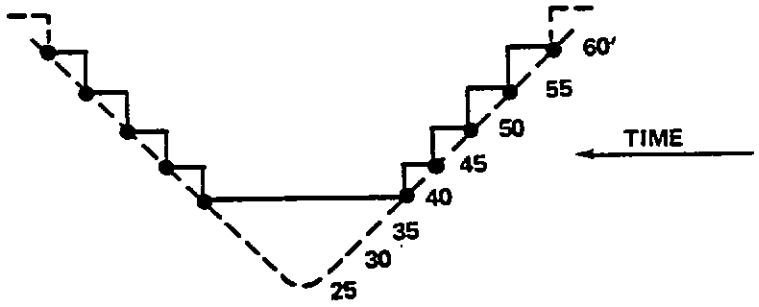

1.10.3 Accuracy

a. The DIGIDOPS was first tested for accuracy in a ground test and then in an airborne test. The ground test involved suspending the DIGIDOPS sensor on a wire between two poles and firing a 105-mm Howitzer projectile past the sensor at known miss distances. The 105-mm Howitzer was assumed accurate to ±0.5 ft. The errors in the direct-read method and the least-squares method were computed over 127 data samples (firings), taken over a 5-day period, using 3 of the DIGIDOPS sensors. The 2-sigma error for the direct-read method was 4.2 ft and the 2-sigma error for the least-squares method was 2.5 ft. Thus, the ground test accuracy of the DIGIDOPS is quoted at ±2.5 ft.

b. The airborne test was performed at WSMR using theodolites as the accuracy standard. Preliminary results indicate that the DIGIDOPS airborne accuracy is comparable to the quoted ±2.5 ft; however, the theodolite accuracy is near the quoted accuracy of the DIGIDOPS and, therefore, obtaining better accuracy figures is doubtful.

1.10.4 Advantages (When the DIGIDOPS is compared with other doppler systems in general.)

a. A common antenna is used for both transmit and receive, eliminating the need for isolation.

b. The operational scoring range is from 0 to 200 ft.

c. The pulse doppler system allows for "dead zones" to gate out some of the drone environmental noise.

d. Scoring data is easier to read and reduce.

1.10.5 Disadvantages

The DIGIDOPS system has not entirely removed all drone environmental noise.

1.10.6 Cost

Each DIGIDOPS sensor costs about $8,500; the airborne telemetry equipment is extra.

1.10.7 Reliability

The DIGIDOPS is reliable in the sense that it has rarely failed in testing. Although the environmental noise interference mentioned before is less than that of previous doppler systems, it still remains a problem.

1.10.8 Applicable Programs

The DIGIDOPS has been installed on BQM-34A Firebee drones and CQM-10B Bomarcs for testing of the AIM-series air-to-air missiles. The antennas for DIGIDOPS have been installed both in the nose and in the aft of the target vehicle. This provides for either forward scoring or rear scoring depending on the test requirements.

1.10.9 Point of Contact

475 Test Sq/TEU
Tyndall AFB, FL 32403
AUTOVON: 970-2271

1.11 THE INTERNAL MISSILE VIDEO DOPPLER SYSTEM

1.11.1 General Description

This system employs a target illuminator in the launch aircraft and two receivers in the missile. The launch aircraft illuminates the target with a narrow band CW RF signal. This signal is received directly by the missile rear receiver and the reflected signal is received by the missile front receiver. The signals from both receivers are mixed in the missile and the difference frequency is telemetered to ground stations.

1.11.2 Math Model

The frequency received by the missile rear receiver is:

$$X+V_L/\lambda-V_M/\lambda \tag{1}$$

where:

X=Transmitted frequency

V_L=Velocity of launch aircraft

V_M=Velocity of missile

λ=Wavelength of the transmitted signal

The frequency received by the missile rear receiver is:

$$X+V_L/\lambda+V_T/\lambda+(V_T/\lambda)\cos\theta+(V_M/\lambda)\cos\phi \tag{2}$$

where:

V_T=Target velocity component in the direction of the interceptor

V_M=Missile velocity

θ=Angle between the line of sight connecting the launch aircraft and target and the line of sight from target to missile

ϕ=Angle between the line of sight from missile to target and the missile velocity vector

At an intermediate point of the trajectory (figure 1.11-1), the angles θ and ϕ are approximately zero so the difference becomes:

$$f_{do}=X+V_L/\lambda+V_T/\lambda+V_T/\lambda+V_M/\lambda-X-V_L/\lambda+V_M/\lambda$$

or

$$f_{do}=\frac{2(V_T+V_M)}{\lambda}$$

where:

$V_T+V_M=V_0$ the velocity of the missile relative to the target.

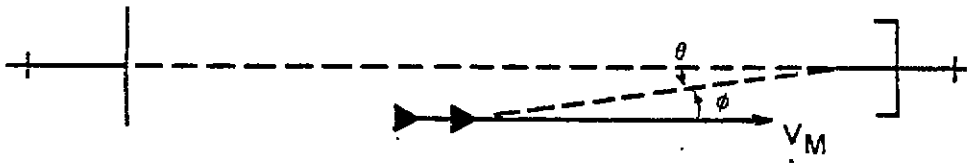

Figure 1.11-1 Point of trajectory.

When the missile approaches the target (figure 1.11-2) the two angles become approximately equal so the doppler frequency becomes:

$$f_{d1}=X+V_L/\lambda+V_T/\lambda+(V_T/\lambda)\cos\theta+(V_M/\lambda)\cos\theta-X-V_L/\lambda+V_M/\lambda$$

or

$$f_{d1}=\frac{(V_T+V_M)}{\lambda}(\cos\theta+1)=\frac{V_0(\cos\theta+1)}{\lambda}$$

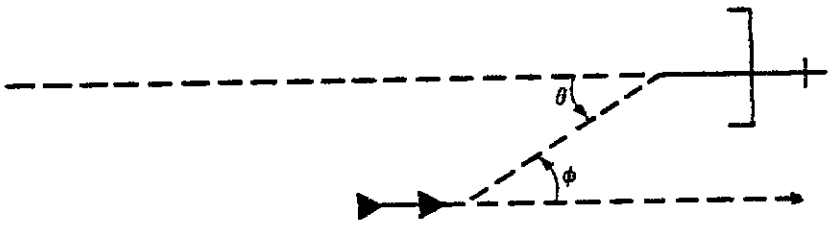

Figure 1.11-2 Missile/target approach.

1.11.3 Reduction Procedures

a. The doppler information is recorded on a magnetic tape at 60 in/s. This tape contains the difference or doppler frequency observed by the missile in a spectrum from near 0 to about 60 kHz. The tape is played back through a vibrolyzer which displays the spectrum in a 3-D type chart on which frequency is measured along the vertical scale and time is measured along the horizontal. The darkness of the chart is an indication of the relative signal power. The vibrolyzer has four frequency ranges or scales available, the highest being from 133 Hz to 13 kHz. Thus, to analyze the data the tape speed must be reduced to 15 in/s or 7.5 in/s in playback. The relationship between the doppler frequencies at two points on the missile trajectory as shown in figure 1.11-3 is:

$$\cot \theta_1 = \frac{a}{M}$$

$$\cot \theta_2 = \frac{b}{M}$$

$$\cot \theta_1 - \cot \theta_2 = \frac{a-b}{M}$$

$$M = \frac{a-b}{\cot \theta_1 - \cot \theta_2} = \frac{V_0 \Delta t}{\cot \theta_1 - \cot \theta_2}$$

$$\cos \theta_1 = \frac{2F_{d1}}{F_{d0}} - 1 \qquad \theta_1 = \arccos\left(\frac{2F_{d1}}{F_{d0}} - 1\right)$$

$$\cos \theta_2 = \frac{2F_{d2}}{F_{d0}} - 1 \qquad \theta_2 = \arccos\left(\frac{2F_{d2}}{F_{d0}} - 1\right)$$

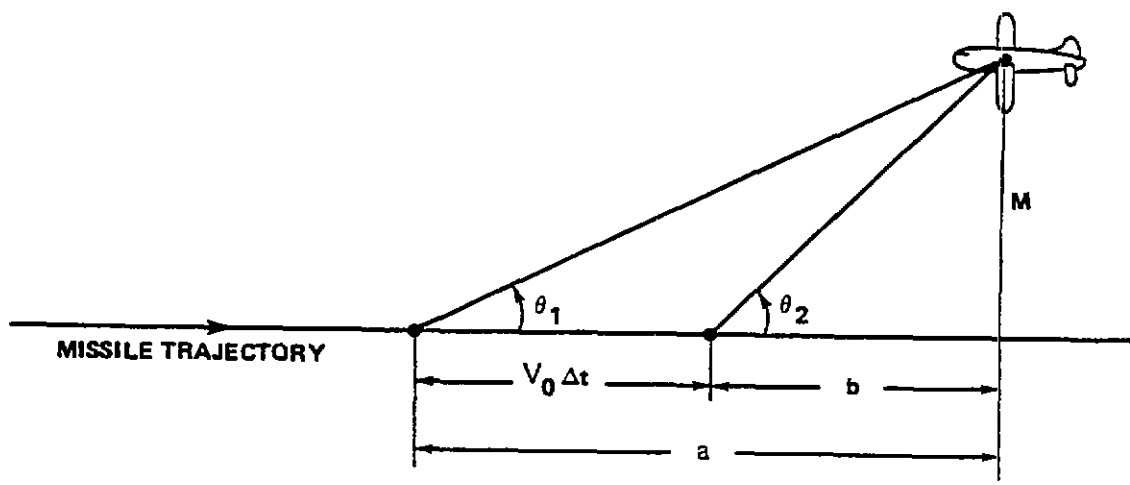

Figure 1.11-3 Relationship of doppler frequencies.

b. The sample record sketched in figure 1.11-4 is much simpler than the usual flight record. In general, the missile will see a doppler shift for each reflective surface it passes. When several curves are present, extreme care must be taken to avoid confusion. Since each curve is thick, a light pencil line drawn by hand will assist in recognizing individual curves. Keep penciled lines in the middle of the curve to avoid leading and trailing edges.

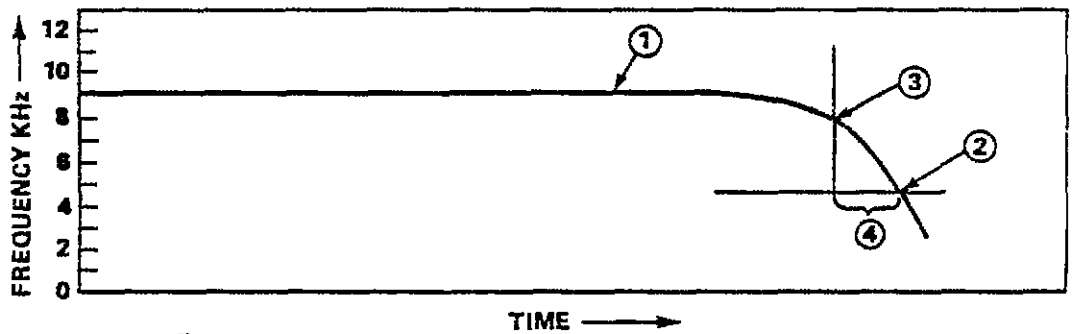

① F_{do}
② $\frac{1}{2}F_{do}$
③ F_{di}
④ Δt

Figure 1.11-4 Sample record.

$$V_o = \frac{F_{do}}{2\lambda}$$

$$\cos \theta_1 = \frac{2F_{d1}}{F_{do}} - 1$$

$$\cos \theta_2 = \frac{2F_{d2}}{F_{do}} - 1$$

$$M = \frac{V_o \Delta t}{\cot \theta_1 - \cot \theta_2}$$

c. On any given curve proceed as follows: read initial doppler frequency, F_{do}, at a convenient point on the curve prior to the start of the doppler shift (see figure 1.11-4), using the calibration strip on the end of the record. Compute $\frac{1}{2} F_{do}$ and draw in the $\frac{1}{2} F_{do}$ line. Next, select a point on the curve above the $\frac{1}{2} F_{do}$ line and draw a vertical line through this point down to intersect the $\frac{1}{2} F_{do}$ line. Read and

record the frequency at this point, F_{d1}, and the time between the points, Δt. Remember that F_{do} is equal to 1/n times the actual doppler frequency because of tape speed reduction. To correct the measured frequencies, multiply by the tape speed reduction factor n.

NOTE

In selecting the ½ F_{do} point for use in the computation, Θ_2 has become 90° and the cot Θ_2 term drops out of the miss-distance computation. Most reductions can be handled in this manner, but the formulas may be used with any two convenient points if the ½ F_{do} point is unreadable.

1.11.4 Accuracy

The accuracy of the system depends somewhat on the skill of the person doing the reduction and on the sharpness of the doppler trace, but repeatability is usually within 10 percent of the miss distance.

1.11.5 Advantages

a. No additional equipment is needed on the target.

b. The doppler signal is a byproduct of the missile guidance and fuzing system.

c. The miss distances to several surfaces can be computed.

d. The missile velocity relative to the target can be computed.

e. The ground equipment required is relatively inexpensive.

1.11.6 Disadvantages

a. The doppler signal is sometimes hard to delineate.

b. False dopplers are sometimes received from ground or water return.

c. The missile must be designed to incorporate the system.

d. The reduction must be performed manually.

1.12 GROUND TRACKING RADARS

1.12.1 General Description

Ground tracking radars provide spherical coordinate measurements, azimuth, A; elevation, E; and range, R; to each object being tracked. The spherical coordinates are transformed into a common Cartesian coordinate system (X, Y, Z) and the distance between the target and interceptor or missile at time, t, would be:

$$d_t = \sqrt{(X_{tT}-X_{tM})^2+(Y_{tT}-Y_{tM})^2+(Z_{tT}-Z_{tM})^2}$$

where:

(X_T, Y_T, Z_T)=Target position

(X_M, Y_M, Z_M)=Missile position

The miss distance between the points tracked by the two radars would be the point where d_t was minimum. The point can be estimated by first performing least-squares polynomial regression on (X_T-X_M), (Y_T-Y_M) and (Z_T-Z_M) then, finding t such that the quantity

$$d_t^2=(a_0+a_1t+a_2t^2)^2+(b_0+b_1t+b_2t^2)^2+(c_0+c_1t+c_2t^2)^2$$

is minimized. This is done by taking

$$\frac{\partial d_t^2}{\partial t}=0$$

and solving for t in terms of the polynomial coefficients.

1.12.2 Disadvantages

The use of ground tracking radars is not considered the best method for determining the vector miss distance between two objects. There are several reasons for this, but the most important reason is that the propagated radar errors are too large. For misses under 50 ft the propagated radar errors are usually larger than the magnitude of the miss distance itself. Another reason is that the vector miss distance is usually measured with respect to two tracking beacons and not the closest surface areas between the two objects. For example, beacons located on wing pods could be over two wingspans apart when in fact the opposite wing tips could almost touch. For these reasons, ground tracking radar data is usually not used for accurate, detailed, miss-distance analysis.

1.13 ONBOARD PHOTON MDI SYSTEMS

1.13.1 General Description

a. The Photon MDI System requires the use of radioactive tags placed on the missile and radiation detectors on the target to determine miss distance through application of the inverse square relationship of intensity to distance.

b. The main components of the radiation detector system are: scintillation detector, pulse-height discriminator and amplifier circuit, pulse code modulator (PCM) encoder, and voltage controlled oscillator (VCO) and line driver amplifier.

The scintillation detector produces an electrical pulse when penetrated by each gamma ray. The pulses pass through the pulse height discriminator, which improves signal-to-noise ratio (SNR) by removing low amplitude system noise. The pulses then enter the PCM encoder. The encoder divides the pulse rate by four and accumulates the result in a six-bit binary counter. Each millisecond the contents of the counter are encoded at millisecond intervals to produce an eight-bit serial binary word (two-bits sync and six-bits data) which then modulates the VCO. A line driver amplifier is provided to allow the VCO to modulate the target telemetry transmitter, usually located at some distance from the photon detector.

c. Calibration is accomplished by recording the detector signal on the magnetic tape while placing the missile radioactive tag at measured distances from the detector. The usual distances are 50, 30, 20, 15, 10, 6 and 4 ft.

1.13.2 Math Model

The pulse rate of the MDI detector is inversely proportional to the square of the distance, R, between the source and the detector, i.e.,

$$I=\frac{K}{R^2} \tag{1}$$

where K is a function of the radioactive source strength, detector efficiency and scintillation crystal size. The true theoretical equation for I is

$$I_d=\frac{I_0 EAe^{-\frac{\mu_0}{D_0}DR}}{4\pi R^2}+I_B \tag{2}$$

where:

I_d=Detected pulse rate

I_o=Gamma photons emitted per second from the radioactive source. (By physical law $I_o=(3.7\times10^7)$ NC where N is the average number of gamma photons emitted per nuclear disintegration, and C is the number of millicuries of activity in the source.)

E=Detector efficiency which is related to the density and thickness (gamma photon stopping ability) of the plastic scintillator, the efficiency of conversion to light of gamma photons, the efficiency of the photomultiplier (PM) tube to detect the light and convert it to electron flow, the gain of the PM tube, and the pulse height discriminator setting.

A=Effective cross-sectional area of the scintillator

R=Distance between source and scintillator

μ_o=Linear gamma photon absorption coefficient for air at standard temperature and pressure is a function of the gamma photon energy

D_o=Density of air at standard temperature and pressure

D=Density of air at the altitude of interest

I_B=Background pulse rate not originating from the desired source (noise, cosmic radiation, other radioactivity, etc.)

For a given radioactive source, the gamma photon emission, I, is a constant during a time interval which is small compared to the half life. The efficiency, E, is approximately constant for a given pulse height setting. The effective area, A, of the scintillator is constant for distances greater than several times the actual diameter of the scintillator. The μ_o and D_o are constants. The density of air, D, and the background radiation, I, are functions of altitude.

The previous equation of I can then be written as

$$I_d=\frac{Ke^{-\mu DR}}{R^2}+I_B \qquad (3)$$

where:

$$K=\frac{I_oEA}{4\pi}$$

$$\mu=\frac{\mu_o}{D_o}$$

I_B can be determined quite easily immediately before and/or after an intercept when the pulse rate due to the radioactive source was insignificant. The exponential term in equation (3) is the transmission factor of gamma photons in air. When the exponential term is assumed equal to unity, the fractional error in miss distance can be derived as

$$E_R = 1 - \left(\frac{e^{-\mu D_c R_c}}{e^{-\mu D_u R_u}} \right)^{\frac{1}{2}} = 1 - e^{\frac{\mu(D_u R_u - D_c R_c)}{2}} \qquad (4)$$

where the c subscripts refer to calibrations and the u subscripts refer to the operational conditions. This assumption allows an explicit equation of I_d.

1.13.3 Reduction Techniques

a. Manual Reduction

1. The signal is played back at reduced speed (4:1) from magnetic tape on to a high-speed oscillograph at 80 ips. Each frame's binary value is then decoded to give a time history of the detector's counts each millisecond during the intercept. IRIG-B timing is also displayed on the oscillograph to allow time correlation.

2. The data is plotted on graph paper with time in milliseconds on the abscissa and accumulated counts (total counts received from an arbitrary time, T=0, up to the present time) on the ordinate. The curve developed will resemble an arc tangent with the maximum slope corresponding to the maximum count rate which occurs at minimum range. Using a straightedge to draw a best straight line through the steepest part of the curve allows the maximum intensity, I_d, to be determined from the ordinate and abscissa values. Background intensity, I_b, is found by averaging several seconds of data at some time shortly before the intercept. True intensity, I_s, from the missile is then determined by $I_s = I_d - I_b$.

3. The calibration data is displayed on the oscillograph in a similar manner, and at least 200 frames are averaged to determine the intensity, I_c, at each distance. Calibration background intensity, I_{bc}, is averaged for several seconds. To determine the miss distance, the following equation is used:

$$\text{Miss Distance} = D\sqrt{\frac{(I_c - I_{bc})}{I_s}} \qquad (5)$$

where D is the calibration distance and I_c is the intensity at that distance. The calibration distance which most closely corresponds to the miss distance is used.

4. Special ground station equipment has been developed which allows a quick-look result to be determined within 1 min.

b. Digital Reduction. A computer program has been developed which will calculate miss distance from photon MDI data, but it is generally not used because manual reduction requires only about 30 min and has proved to be as accurate as computer reduction.

1.13.4 Accuracy

The system accuracy has been tested by firing high-velocity bullets past photon detectors. The results showed accuracies of +10 percent out to ranges of 50 ft and with velocities up to 5,000 ft/s.

1.13.5 Advantages

a. The detectors can be installed in wing-tip pods on larger targets giving nearly spherical coverage.

b. No additional TM transmitter is required.

c. Standard ground station equipment can be used for receiving and displaying the data.

d. The operational status of the detectors can be verified during flight by observing background radiation which is always present.

e. Three or more detectors can be used on larger targets to provide some missile trajectory information.

f. The detectors and radioactive tags are relatively inexpensive (detectors: $1,600 each and tags: $230 each) and have been adapted to a wide variety of targets and missiles. The following targets have been equipped with Photon MDI Systems: BQM-34A, BGM-34E, MQM-74C, AQM-37, CQM-10 (BOMARC), QT-33, QF-9, QF-86, QF-4, Septar MK35, and TDU-22. The following missiles have flown with photon tags: SPARROW III, SIDEWINDER, STANDARD, SHRIKE, PHOENIX, and CHAPARREL.

g. The system is simple to maintain and highly reliable. In over 300 missile launches, the Photon MDI System has been more than 95-percent effective in providing miss-distance results.

1.13.6 Disadvantages

a. Nuclear Regulatory Commission (NRC) licenses must be obtained for handling the radioactive tags.

b. NRC requirements limit the launch areas which may be used.

c. The radioactive tags cannot be installed on the missile until shortly before aircraft takeoff to minimize unnecessary radiation exposure to personnel.

d. The gamma radiation is subject to shielding effects if the path of the radiation encounters parts of the target vehicle before reaching the detector. This should be no problem if two wing-tip pods are used.

1.13.7 Special Uses

A wing-tip pod containing both camera and Photon MDI Systems has been developed. The advantages of this combined system are:

a. Real-time Photon MDI information for instant success/failure determination.

b. Vector intercept data when camera film has been recovered and analyzed.

c. Redundancy in case one system fails.

1.14 ELECTRO-OPTICAL VECTOR-SCORING SYSTEM (EOVSS)

1.14.1 General Description

An Electro-Optical Vector-Scoring System (EOVSS) consists of a target-mounted, pulsed, IR source arranged to scan the region in the vicinity of the target. When a missile intercepts the IR radiation, energy is returned to a detector on the target. If more than one scanned beam is employed, two vector scores result. These two points describe the final trajectory. The time interval between the two intercepts may be used to compute missile velocity. A simple scanning geometry, consisting of a cone and a plane, is shown in figure 1.14-1. A surface-target version of this same configuration is shown in figure 1.14-2. Depending upon the scenario, additional scan patterns may be appropriate.

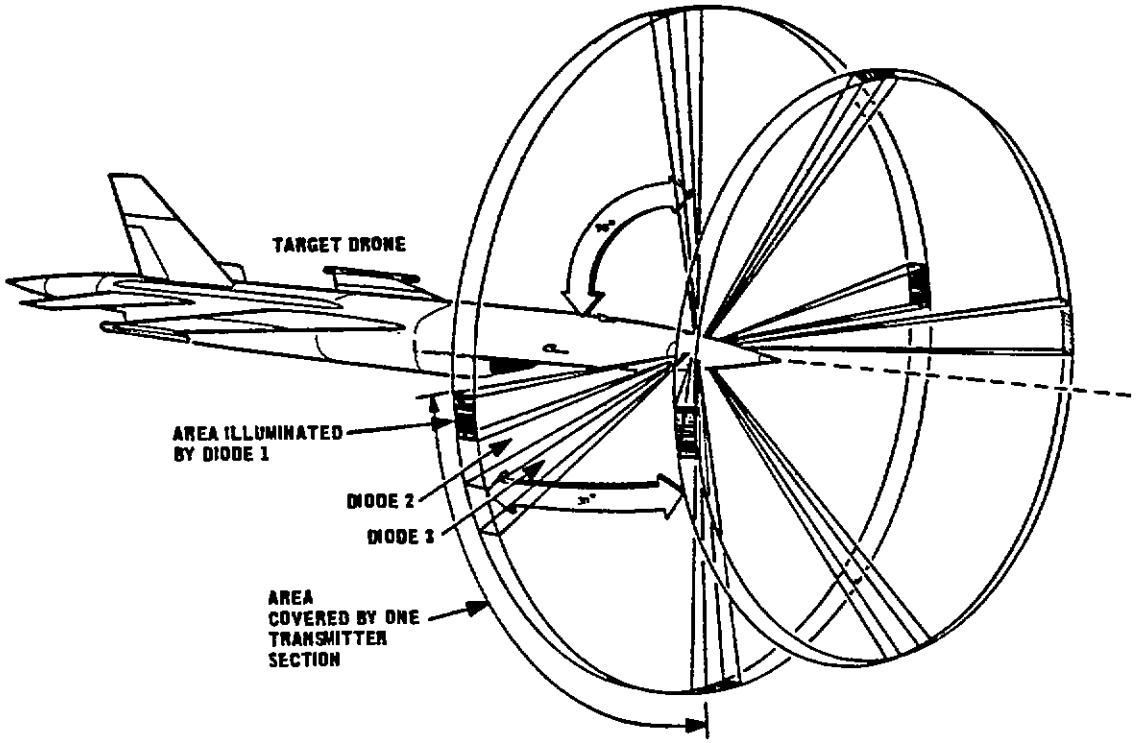

Figure 1.14-1 Beam geometry.

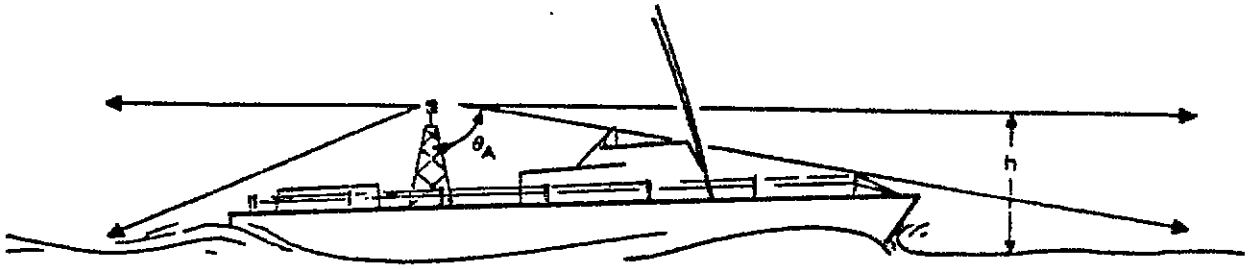

Figure 1.14-2 Shipboard vector scoring system.

1.14.2 Math Model

Using c for the speed of light, the time, t, for a transmitted pulse to travel m meters and return is

$$t=\frac{2m}{c} \tag{1}$$

The range, m, in meters is

$$m=\frac{ct}{2} \tag{2}$$

Typically, the beam is wider than the target in one dimension and, for the shorter ranges, narrower than the target in the other dimension.

This leads to an inverse third-power relationship between returned power range.

$$P(R)=\frac{P_X N_X N_r G\ A\ d}{\pi R^3 \theta_X} \tag{3}$$

where:

P(R)=Power impinging the diode as a function of range

P_X=Power output of a single diode

N_X=Transmitter optical efficiency

N_r=Receiver optical efficiency

G=Retroreflective surface gain (may be up to several hundred)

A=Effective receiver aperture; a function of the diode position in the fan beam. Consequently, $A=A_o \cos \alpha$; where A_o is the receiver aperture and α is the angle between the normal to the receiver and the line of sight to the projectile. For example, a projectile at beam edge $A=A_o \cos 45°$.

d=Width of the target

R=Range

O_x=Azimuth illumination angle (beam width) for a single diode

The term "target" in this section refers to the retroreflecting surface portion of the target, in this case 30 cm by 30 cm.

1.14.3 System Parameters

a. Feasibility models have been demonstrated for two techniques. One is a mechanical scan version employing a multispeed rotating mirror with approximately I° beams, and the other an all-electronic version with approximately I° by 10° beams where nine diodes are pulsed in succession to scan each 90° sector.

b. Other parameters which have been utilized or achieved include: maximum range 60 m; scan rate 8,000 m/s corresponding to a maximum intercept velocity of 2,438 m/s (8,000 ft/s); range precision for digital readout, ±1 m; angle precision, ±5°; and retroreflecting area on missile, 30 cm by 30 cm.

1.14.4 Accuracy

Range accuracy is dependent upon the precise determination of the difference between transmitted and received pulses--approximately 2 ns/ft. One feasibility model demonstrated precision of ±1 ft for most ranges. Another system, designed for a ±1-m digital readout, performed within these specifications so consistently as to strongly suggest a ±0.5-m potential. Azimuth angle precision of less than 2° is readily achieved with a mechanical scan; a ±5° precision is possible for the 0.5 by 10° digital all-electronic mechanization.

1.14.5 Advantages

The development program on EOVSS represented an effort to develop a short-range, low cost, reliable system providing real-time readout. The results indicate that these characteristics can be achieved. The advantages are:

a. Low cost

b. Angle and range data as a direct readout

c. Final trajectory and missile velocity available, if desired

d. Real-time readout compatible with any existing telemetry link

e. Minimum (passive) cooperation from missile (30 cm by 30 cm retroreflector surface) required.

f. Adaptable to packaging with flush apertures for minimum aerodynamic disturbance

g. Adaptable to air or surface targets.

1.14.6 Disadvantages

a. Passive cooperation of 30 cm by 30 cm retroreflection material required

b. Not currently feasible for ranges much in excess of 60 to 75 m

c. Light beam geometry consistency with intercept scenario needed; i.e., some applications may require more than two beams.

1.15 SOCIETE FRANCAISE D EQUIPMENTS POUR LA NAVIGATION AERIENNE (SFENA) MEASURER ACOUSTIQUE ESCARTES (MAE)-15 ACOUSTICAL BULLET SCORING SYSTEM

1.15.1 General Description

a. The Measurer Acoustique Escartes (MAE)-15 Acoustical Bullet Scoring System (acoustical miss-distance measuring equipment) is an integral part of the Secapem aerial tow target (see figure 1.15-1). The target system was manufactured as a joint venture by two French companies, the Secapem Company and the Societe Francaise D Equipments pour la Navigation Aerienne (SFENA). The system was introduced into the United States through the U. S. licensee, Teledyne-Brown Engineering of Huntsville, Alabama. Its primary use is for evaluation of air-to-air gunnery.

b. The MAE-15 consists of a microphone in the nose of the target, a radio transmitter, and a receiving station/display. The microphone converts the pressure disturbance due to bullet passage into an electrical signal proportional to the magnitude of that disturbance. The transmitter then sends a frequency shift key (FSK) modulation of the subcarrier to the receiver. The duration of the frequency shift is also proportional to the pressure disturbance. The receiver may be either ground based or installed in the tow aircraft. If the receiver is ground based, the carrier frequency is generally in the very high frequency (VHF) band. Fixed crystals currently exist for 138.8 MHz, 141.9 MHz, 146.7 MHz and 150.5 MHz. The airborne receiver is equipped to receive 1489.5 MHz (L-band). The target transmitter is changed to accommodate the desired type of receiver.

c. The MAE-15 operates on the principle that the pressure disturbance due to the shock wave of a passing supersonic bullet is a function of the bullet caliber, target altitude, target speed, and distance between the bullet trajectory and the microphone. Bullet caliber and target altitude are compensated for by manual adjustments to the receiver prior to gun fire; target speed is calibrated for a nominal 30 knots indicated airspeed (KIAS); deviations cause small errors. The remaining parameter, distance, is then directly translatable from the duration of the frequency shift.

d. The receivers have preset miss-distance scorers built into them. The ground receiver and display unit (figure 1.15-2) is equipped for three settings:

Caliber	Inner Radius	Outer Radius
20 mm	2 m	3 m
30 mm	3 m	4.5 m
30 mm	4 m	6 m

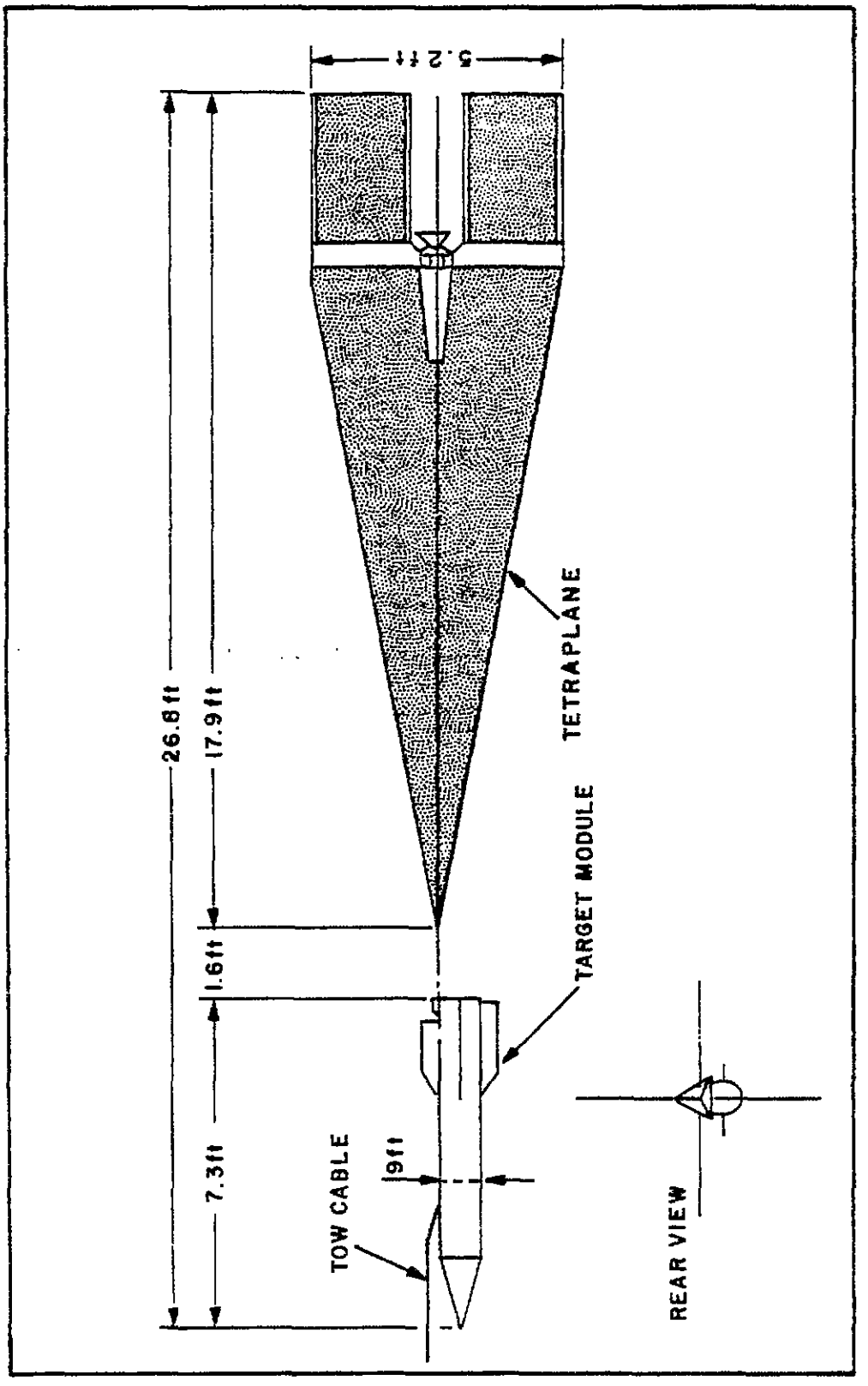

Figure 1.15-1 Secapem/SFENA MAE-15 target system.

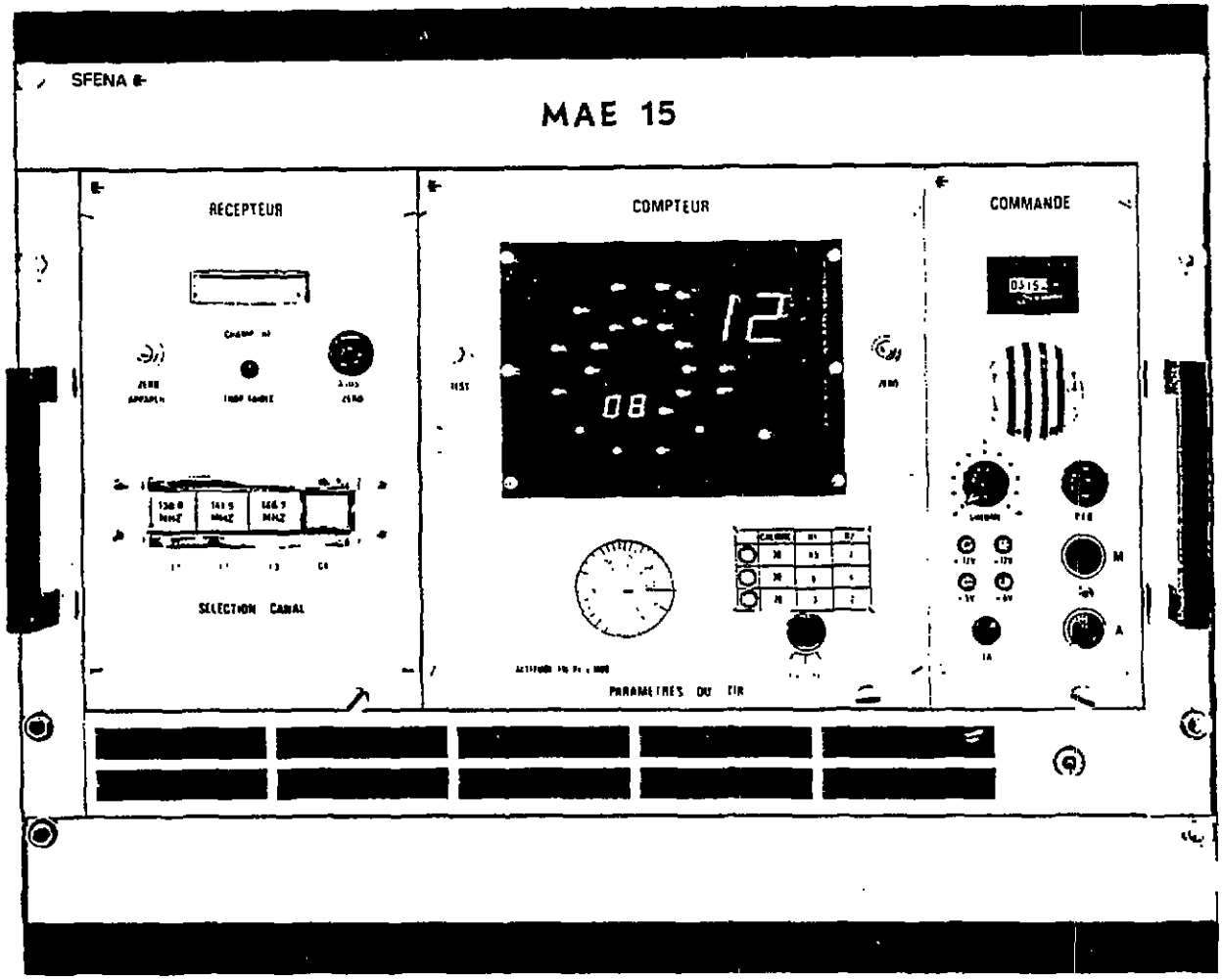

Figure 1.15-2 SFENA MAE-15 ground receiver and display unit.

The cockpit receiver and display unit (figure 1.15-3) has two settings:

Caliber	Inner Radius	Outer Radius
20 mm	2 m	3 m
20 mm	3 m	5 m

The duration of the received pulse is compared to predetermined durations based upon the radii selected. If the receiver pulse is longer than that preset for the outer radius, the display will accumulate one hit to the outer display (add one to whatever score was already displayed). If the receiver pulse is also longer than the preset value for the inner radius, the display will add one to the inner display. The miss distances scored are assumed to be radii of spheres centered on the microphone. (For further discussion, see subparagraph 1.15.5.)

e. Figure 1.15-4 shows the sequence of events for three possible bullets. Bullet number 1 passes approximately 2.5 m from the center of the scoring sphere. The pressure disturbance is of such a magnitude that an FSK pulse of 2.4 ms is generated. The pulse is received and demodulated with a ramp function for comparison with the preset values of 1.6 ms and 3.2 ms. As the ramp peak exceeds the 1.6-ms or 3-m value, a hit is added to the outer display. Bullet number 2 passes approximately 1 m from the center of the scoring sphere and generates a pulse duration of 4.1 ms. Since this exceeds both thresholds (1.6 ms and 3.2 ms), a hit is accumulated on the inner display as well as the outer. Bullet number 3 passes approximately 3.5 m from the scoring center generating a pulse duration of 0.9 ms, less than either threshold. Thus, no score is accumulated. Note that adjustment of the caliber, altitude and miss-distance range causes no physical adjustment of the sensor. Instead, the value of the comparator is adjusted to equal a certain change in pressure disturbance magnitude.

f. Although the scores displayed on the receiver provide near real-time feedback to the pilot and a limited amount of quantitative miss-distance information, more exact data are available within the receiving unit. By recording either the FSK pulse or the demodulated signal, radial miss distance can be determined for each bullet within the practical sensor limits of approximately 25 ft.

1.15.2 Math Model and Data Reduction

a. The data reduction method is derived using technical information gathered from French flight test operations (see figure 1.15-5). A nominal set of flight conditions was chosen which represents a base line for miss-distance calculations. These conditions were 350 KIAS and 20,000-ft target speed and altitude, respectively. Using regression analysis, minimizing the square of the miss-distance error, the miss-distance versus pulse-duration test data was approximated with an exponential:

$$\text{Miss Distance} = 6.465 \times e^{(-.307 \times \text{Pulse Duration})} \qquad (1)$$

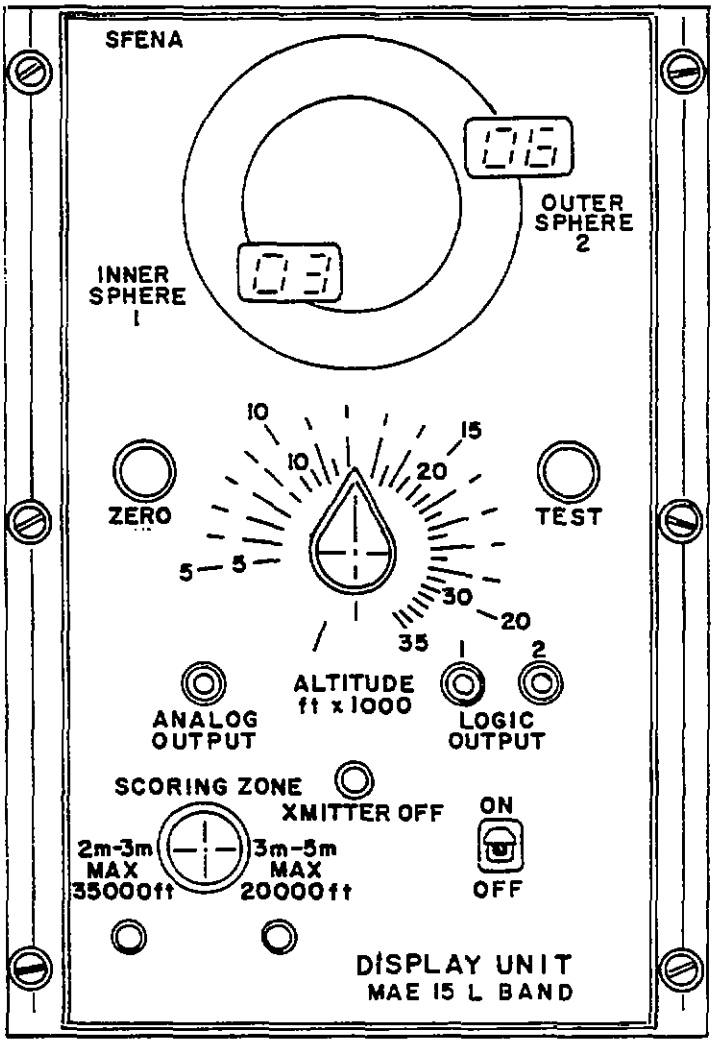

Figure 1.15.3 SFENA MAE-15 cockpit receiver and display unit.

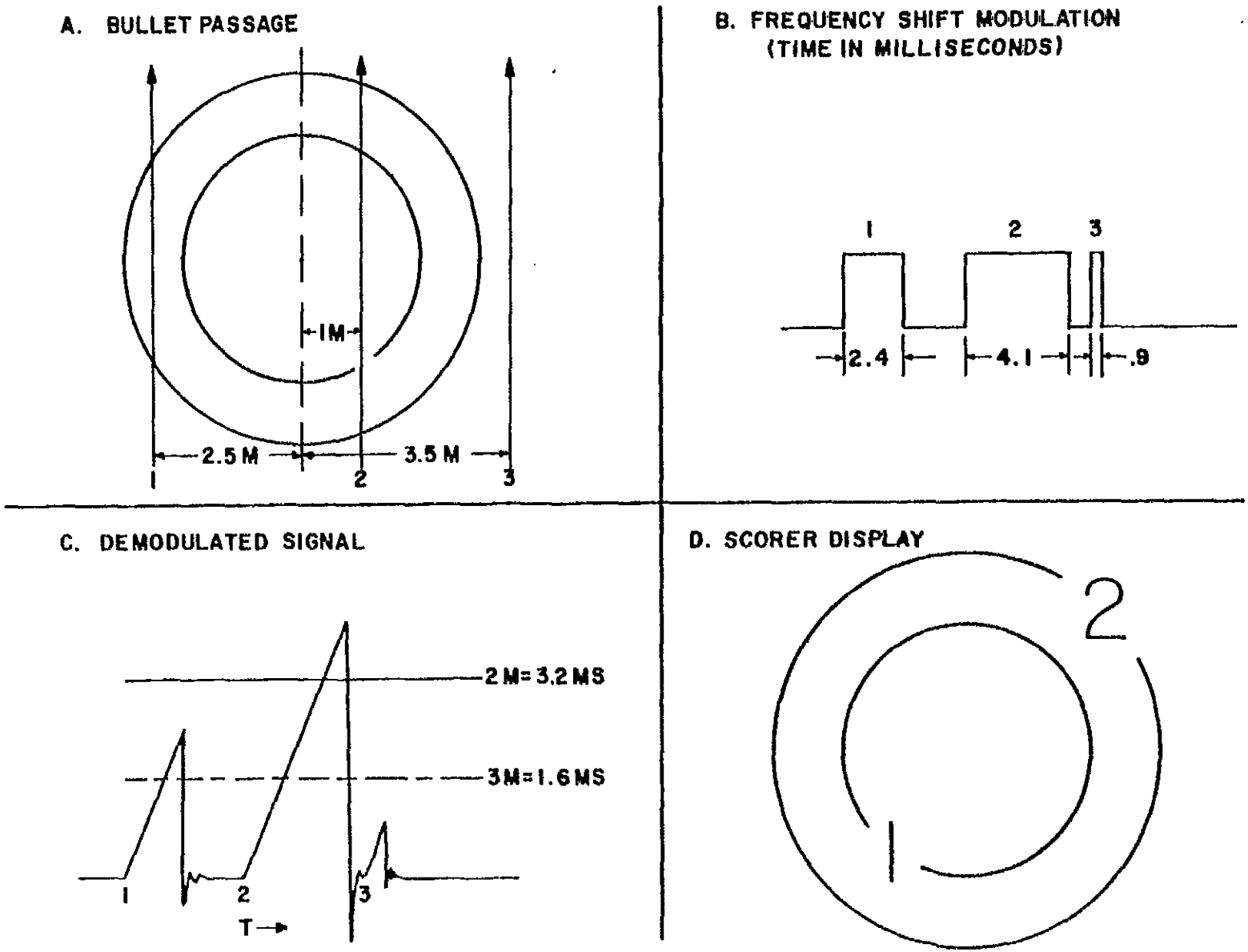

Figure 1.15-4 SFENA MAE-15 bullet scoring process.

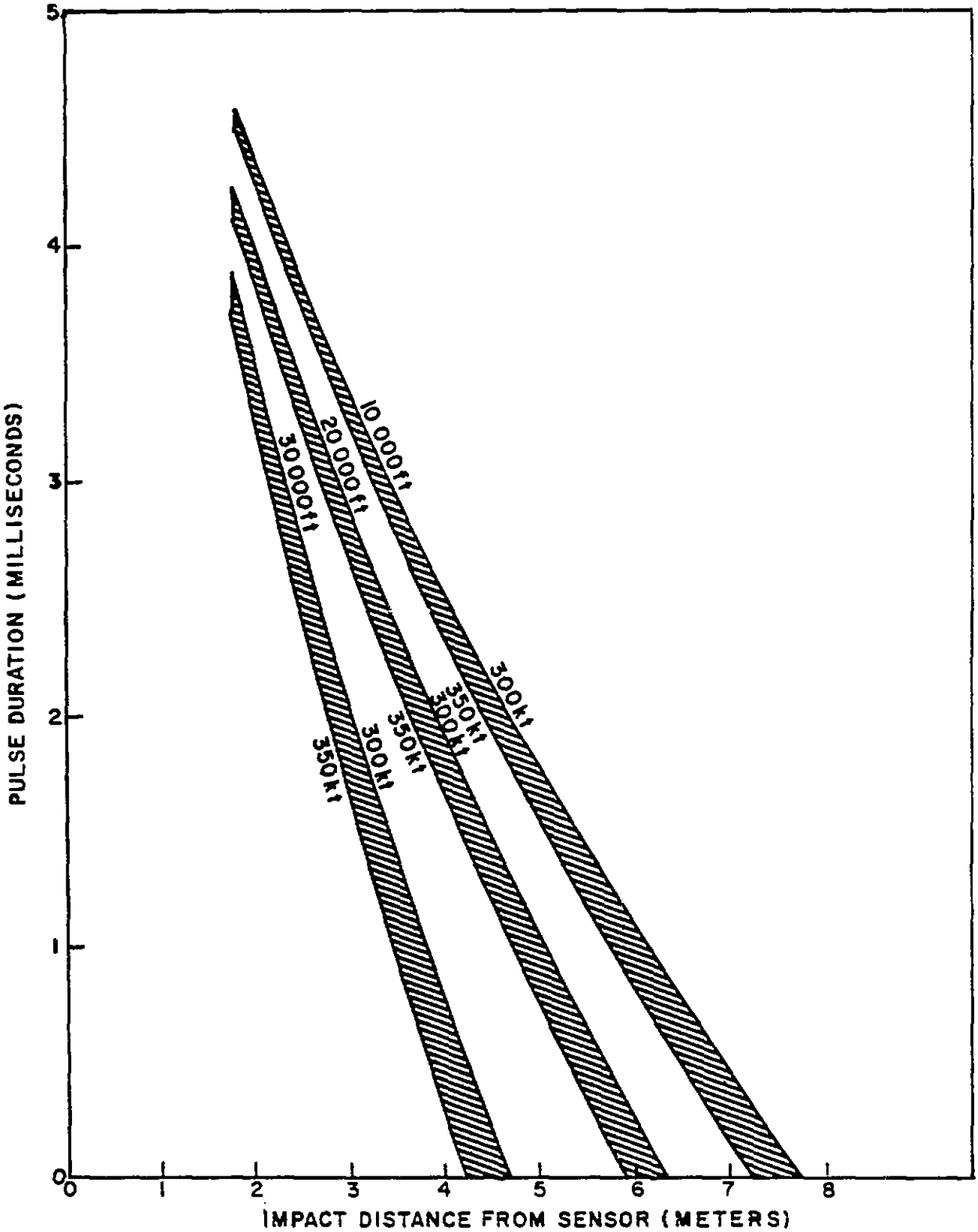

Figure 1.15-5 20-mm French flight test data.

b. Empirical adjustments were made for altitude and airspeed variations from the nominal. The resulting data reduction equation is

$$\text{Miss}=6.465\left\{\left[e^{(-.307PD)}\right]+\left[\frac{(0.5-0.1PD)(350-V)}{350}\right]+\left[\frac{(1.3-0.25PD)\ (20000-alt)}{10000}\right]\right\} \quad (2)$$

where:

MD=Miss distance in meters

PD=Pulse duration in milliseconds

V=Velocity in KIAS

alt=Pressure altitude in feet mean sea level

Table 1.15-I shows representative errors in miss distance using the data reduction equation.

c. To reduce the data, the pulse duration is measured either manually or by digitized output. The value for each pulse duration of a given gunnery pass is entered into a simple computer program, along with the target speed and pressure altitude for that pass. The calculated miss distances are then printed out in order of occurrence as well as in order of increasing miss distance. Average radial error and standard deviation are also computed.

1.15.3 Accuracies

a. The equation developed from the French data has an expected error of 0.1 m (1σ) based upon the representative values shown in table 1.15-I. This error is due to the inexact fit of the flight test results.

b. Manual reduction of the ramp values requires very close reading of the zero point and the peak. Data gathered and reduced in this manner can be expected to have an error of 0.05 m (1σ) due to reading errors.

c. There is a variance in the sensitivity of the scoring microphones. This variation is estimated to produce an error of 0.1 m (1σ).

d. All other errors within the MAE-15 System are negligible compared to those addressed above.

Table 1.15-I Comparison of Plotted and Computed Miss Distance

Pulse Duration (ms)	Target Altitude Ft (m.s.l.)	Target Speed (KIAS)	Miss Distance Figure 1.15-5 (m)	Miss Distance Equation (m)	Error (m)
1	10,000	300	6.22	6.21	-.01
2			4.66	4.60	-.06
3			3.88	3.33	-.05
4			2.34	2.30	-.04
1	10,000	350	5.73	5.81	+.08
2			4.33	4.30	-.03
3			3.21	3.13	-.08
4			2.25	2.20	-.05
1	20,000	300	5.09	5.16	+.07
2			3.89	3.80	+.09
3			2.86	2.78	+.08
4			1.97	2.00	+.03
1	20,000	350	4.73	4.76	+.03
2			3.62	3.50	+.12
3			2.64	2.58	+.06
4			1.85	1.90	+.05
1	30,000	300	3.82	4.11	+.29
2			3.05	3.00	+.05
3			2.36	2.23	-.13
4			1.72	1.70	-.02
1	30,000	350	3.47	3.71	+.24
2			2.78	2.70	-.08
3			2.13	2.03	-.10
4			1.62	1.60	-.02

e. The expected composite error due to all sources is:

$$\sqrt{(0.1)^2+(0.05)^2+(0.1)^2}=0.15 \text{ m} \quad (3)$$

or approximately 6 in. If the data is digitized, the reading error is removed and the total error is reduced to approximately 4 in.

f. The accuracy statement above is based upon the assumption that the data provided by French flight tests can be considered a truth model.

1.15.4 Advantages

a. The primary advantage of the MAE-15 is its capability of producing measurable miss-distance information, a capability which is currently unique in air-to-air gunnery scoring. In addition to miss distance, the time of closest approach can be recorded to verify bullet time of flight.

b. Other advantages are that the scoring field is spherical, thereby presenting a circular target from any aspect angle; and the sensor is recoverable and reusable with minor maintenance. Three flights can be expected with each sensor unit.

1.15.5 Disadvantages

a. Because both the sensor and the shock wave are acoustic in nature, the system is subject to an apparent shift of the scoring field. The shock wave of a passing bullet travels at the speed of sound and, as it travels through the air, the intensity of the pressure disturbance decreases. Thus, the shock wave caused by a bullet passing 5 ft behind the microphone must travel that 5 ft plus some distance equal to the speed of the target times the time to catch the microphone. The effect is as if the center of the scoring field was shifted forward proportional to the target Mach number. See figure 1.15-6 for a graphic representation of the position of the scoring field. This shift complicates use of the system. The pilot, for accurate score, must aim forward of the forebody. Time of flight verification must be adjusted for relative target motion to be accurate.

b. The system can be recovered after release in a soft ground area. Generally, the damage which occurs can be repaired; however, there exists a risk that the impact may cause irreparable damage.

c. The scoring rate is design limited to 9,000 shots per minute.

1.15.6 Cost

The cost of a Secapem/SFENA system is estimated at $3,500 per sortie on a continuous use basis.

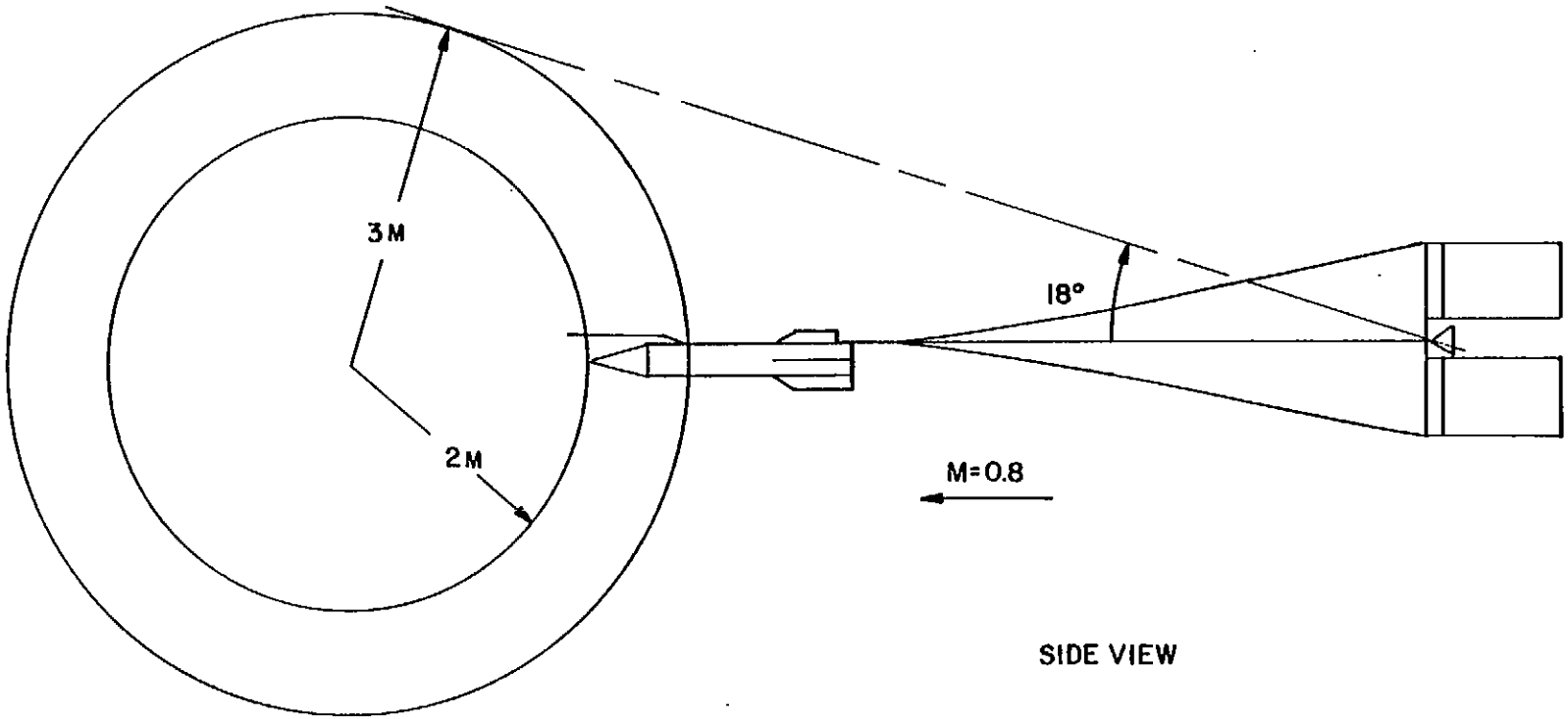

Figure 1.15-6 Position of scoring field relative to target.

1.15.7 Reliability/Survivability

a. The SFENA MAE-15 has been used on 52 aerial gunnery missions with only two flight failures for a reliability in excess of 96 percent.

b. The system has been irreparably damaged on two of the 50 successful missions giving a survivability rate of 96 percent.

c. The overall mission effectiveness rate for the system is greater than 92 percent.

1.16 AN/DSQ-37 MISS-DISTANCE INDICATOR (MDI)

1.16.1 General Description

The AN/DSQ-37 is a noncooperative (the object to be scored can be passive and requires no modification) scaler scoring system with a range of 75 ft capable of scoring projectiles the size of 3-in shells (1 ft^2 radar cross section) and larger at closing velocities up to 5,500 ft/s.

1.16.2 Objective

The AN/DSQ-37 was developed to meet the Navy's scoring requirements for most surface-to-air missile and gun shots and air-to-air missile launches.

1.16.3 Instrumentation Description

a. The airborne portion of the system consists of the receiver-transmitter (radar) unit, the doppler score detector/subcarrier mixer unit and the telemetry (TM) transmitter, all contained in a watertight enclosure measuring 4-1/2 x 6-3/4 x 13 in. The system requires 28 volts d.c., 1.6 amps, from the target vehicle's power source. Installation kits consisting of mounting brackets, antennas for the radar and TM, and coaxial cables are required to operate an MDI system in each target.

b. The receiver-transmitter radiates 100 ns pulses of RF at a frequency of 1775 MHz with a pulse repetition frequency (PRF) of 500 kHz. The RF pulses are doppler shifted when reflected from a moving projectile within 75 ft of the target (a timing circuit excludes return pulses from objects more than 75 ft away). The return pulses are mixed with the MDI's RF oscillator output to produce doppler cycles of 200 Hz to 20 kHz from which miss distance can be determined.

c. The doppler score detector unit senses an intercept by the amplitude and duration of output doppler cycles from the receiver-transmitter unit and produces a 0.5-s wide pulse when a score occurs. An automatic gain control (AGC) circuit is used to eliminate false scores caused by target generated noise.

1.16.4 Test Procedures

After installation of the target, the AN/DSQ-37 is tested with a hand-held doppler simulator. This device simulates a moving object by reflecting and frequency modulating the AN/DSQ-37 signal. The MDI continually monitors the reflected signal as the activated hand-held doppler simulator is moved by a test technician away from the target. The doppler output of this MDI diminishes to zero when the distance between the MDI and the hand-held doppler simulator is equal to or greater than 75 ft.

1.16.5 General Application

a. Data requirements. A standard two-band TM system is used (typically 1527.5 MHz) with IRIG bands H and 8 transmitting the two MDI signals. The TM system is normally radiating when the target vehicle is powered.

b. Data collection. The data is collected by a reciever with an IF bandwidth of 1.2 MHz with an output video bandwidth of 250 kHz and is recorded on magnetic tape for later reduction. When a shipboard portable MDI receiving station is used, the H-band data is first demodulated before recording on magnetic tape. The portable station also contains circuits to decode the 8-band VCO signal and a counter to display the number of scores that have occurred in real time.

c. Data reduction. The magnetic tape is played back at a reduced speed (8:1) and the demodulated H-band data (the doppler audio cycles) are recorded on oscillograph paper.

1.16.6 General Solution

a. Analysis technique. When an object approaches the target, no doppler cycles are produced until the range is less than 75 ft. As the object continues to approach, one cycle is produced each time the distance from object to target changes by 0.25 wavelength of the radar's 1775-MHz RF frequency which is 0.2772 ft. The maximum number of cycles that can be produced, if the miss distance equals 0, is 75 ft/0.2772 ft per cycle = 270 cycles. Note that an equal number of cycles will be produced as the range increases from 0 to 75 ft after the point of closest approach (PCA) has occurred. The center of the intercept can be identified, since the doppler frequency falls to 0 at the PCA.

b. Math model. If N = the number of cycles counted between the PCA and the 75-ft limit, the miss distance, MD, is calculated as follows:

$$MD=(270-N)Hz \times 0.2772\ ft/Hz$$

c. Computer program. Due to the simplicity of data reduction, no computer reduction is required.

1.16.7 Accuracy

When TM data is clean so all cycles can be counted, accuracy is +1 ft.

1.16.8 Advantages

a. The system is noncooperative; i.e., the object to be scored can be passive and requires no modification.

b. The data reduction is very simple.

c. A portable checkout/receiving station is all that is required to prepare the target and to receive and reduce miss-distance data.

1.16.9 Disadvantages

a. The target must be carefully installed to assure noise-free operation.

b. Data reduction personnel require training and experience to consistently interpret doppler cycle data.

1.16.10 Reliability/Availability/Maintainability

The AN/DSQ-37 is designed to meet Military Specifications and should be highly reliable. A limited number of systems and installation kits for the BQM-34S, MQM-74C and TDU-22 were available in FY 78. Larger numbers and additional target types were available in FY 79. Maintenance will be by system replacement only.

1.16.11 Cost

A typical installation, ready to fly, is $9k. A portable checkout/receiving station costs approximately $20k.

1.17 MISS-DISTANCE INDICATOR (MDI) SYSTEM

1.17.1 General

The Miss-Distance Indicator (MDI) System was developed for scoring surface-to-air weapons and proving near real-time miss-distance scores.

1.17.2 Objectives

The primary objective for the development of the MDI System was to score rapid fire weapon systems (which could not be scored by optics) with rounds as small as 20 mm and firing rates up to 3,600 rounds per minute and provide scores in near real time.

1.17.3 Instrumentation Description

The MDI System is comprised of a multihorn monopulse radar with an SPC-16/70 computer and associated peripheral equipment including a quick-look (miss-distance) CRT display, teletype, magnetic tape units, and a line printer. The MDI equipment is housed in a mobile trailer van. Operational characteristics are as follows:

Operating Frequency	9.6 to 9.9 GHz
Transmitter	
Peak Power	750/kW
Pulse Repetition Frequency	640/1230/2560 Hz
Pulse Width	30 ns
Receiver	
Bandwidth	40 MHz
Noise Figure	8 dB
Dynamic Range (Linear)	70 dB
Antenna	
Gain (small dish)/beamwidth	36 dB/2.5°
Gain (large dish)/beamwidth	42 dB/1.25°
Polarization	Linear - vertical
Tracking Range on 1 square meter	
Minimum	200 m
Maximum	20 km
Tracking Accuracy (corrected)	
Angle Data	1 mil
Range Data	5 m

1.17.4 Test Procedures

The only procedure required for test support is to site the MDI radar behind the weapon or launcher for optimum scoring. The system must be calibrated 1 hr prior to a firing. The target is tracked, and projectiles or missiles are detected in the scoring windows. Raw data is obtained on individual rounds and scoring is accomplished after the tests are completed.

1.17.5 General Applications

a. The MDI radar can score a wide class of surface-to-air rapid fire weapons and missiles fired at aerial targets. Measurements can be made on projectiles as small as 20 mm at rates of fire up to 3,600 rounds per minute. The MDI radar tracks in skin mode only and operates using a very simple concept. Data collection is obtained in the following manner. The target is null tracked like existing instrumentation radars. In addition, two range gates (windows) are slaved in proximity to the target-tracking gate for detecting projectiles in the vicinity of the target. Off-boresight monopulse measurements are made to determine the target displacement in its tracking gate and projectile displacements in the two windows. These displacement measurements are utilized with antenna encoder readings, tracking gate range and target-weapon geometry to compute the minimum miss-distance vector between the target and a detected projectile.

b. When MDI is operating as a scoring system, the target and projectile off-boresight monopulse measurements, the antenna encoder readings, and samples of the tracking gate range are recorded continuously on magnetic tape. This is referred to as the raw data tape. When the target is within weapon range, scoring data is recorded in an MDI file. One or more bursts of projectiles may be fired at the target on a given pass. The raw data thus obtained is used as an input to the deferred scoring programs in order to generate scoring.

1.17.6 General Solution

a. At the end of a firing test, an independent program, the Deferred Time Gun Scoring Computer Program (DEFT-G), generates accurate scoring results for each pass of the test. The MDI files on the raw data tape provide the input data for the DEFT-G program, which is strictly a nonreal-time data reduction computer program.

b. The DEFT-G program reads one MDI file at a time from the magnetic tape, smooths the target data, detects projectiles in the Window-1 and Window-2 data, computes the 3-D miss-distance vector for each detected projectile, and outputs the results to the line printer on a burst basis. These outputs may also be recorded on a magnetic tape called the history-data tape. The DEFT-G program can process an MDI pass of 100 rounds and print out the results in approximately 6 min from the time the computer commences reading the MDI file for that pass.

c. Output data includes pass identification and error summaries, gun firing time and muzzle velocity for each projectile by burst, smoothed target position and velocity data during engagement at selected rates, vector miss distance of each scored projectile in window 1 and/or window 2 with target position and speed and projectile speed at time of minimum miss, and statistical data for the burst. All data is correlated with test range IRIG time to within 1 ms, and all target output data is parallax corrected to the weapon location. The data is printed on the line printer and recorded at operator option on magnetic tape as history data. Special off-line processing is available through the WSMR computer facility (Univac 1108) using the MDI raw data tapes and history tapes. Target position, velocity and acceleration can be provided in any desired coordinate system. Any data contained in the tapes can be provided as a computer listing or on 7-track 0.5-inch magnetic tape.

1.17.7 Accuracy

a. 20-mm gun projectiles. Vector miss-distance scores from the MDI radar, when compared to optics-measured miss distance, verify an accuracy of ±1 m or 10 percent of the measured miss distance, whichever is greater.

b. Missiles. Vector miss-distance scores from the MDI compared to optics miss distance shows a vector miss-distance difference of ±1 m. The comparisons have been made on 15 TOW antitank missiles versus a QH-50 helicopter target, 7 STINGER missiles versus MQM-34 drones, and 2 ROLAND missiles versus MQM-34 drones.

1.17.8 Advantages

The principal advantages of the MDI system are the availability of scoring results minutes after completion of the test and the ability of the MDI to individually score small rounds of rapid fire defense weapon systems.

1.17.9 Disadvantages

Performance of the MDI system in support of scoring cannot be measured in terms of accuracy alone, although accuracy is of primary importance to the project. System limitations and mobility and safety constraints are factors which must be considered before effective support commitment of the MDI radar.

a. System scoring limitations. The maximum range that the MDI can score is 10 km because of software limitations, and the minimum scoring elevation from the radar is 47 mils in relatively flat terrain to avoid false alarms due to clutter. The MDI system will usually be sited behind the launcher so that the missile will cross the radar beam and be detected in the scoring windows. Positioning the radar behind the launcher poses safety problems since safety regulations usually require personnel evacuation of this area during firings against incoming drones.

b. Mobility. System mobility becomes a significant factor in general missile scoring support. It takes one working day for preparation of the system prior to moving it and one working day to set up the system for support. This lack of mobility makes it impossible to support more than one missile program at a time since different launchers are used for each program.

c. Safety. Safety constraints significantly reduce the number of scores that can be obtained during missile scoring. Positioning the radar behind the missile launcher usually places the system in the safety cone, and MDI personnel are evacuated on all tests with full-scale drones and on tests with subscale drone headings toward the launcher.

d. Adverse weather. The MDI is unable to score intercepts in rain or in heavy clouds because of reflected energy causing false alarms in the detection windows.

1.17.10 Reliability/Availability/Maintainability

The MDI System has performed reliably during test support. Maintenance is a problem because some components are inaccessible.

1.17.11 Cost

The preset operation and maintenance cost for MDI support offrange is $3,700 per week plus roundtrip transportation for the system. Rates for WSMR customers are $100 per hour.

1.17.12 Point of Contact

STEWS-NR-DR
White Sands Missile Range, NM 88002
AUTOVON: 258-1836

1.18 TELEVISION MISS-DISTANCE TECHNIQUE

1.18.1 General Description

Television has long been a tool for observing test item performance in real time. However, little has been done with television images, especially when velocities are too great for television to "stop" the motion. A mechanical shutter has been introduced between the lens and the imaging tube of a television camera to record short time-exposure images, thus minimizing movement during the picture-forming period. With this adaptation, it is now possible to "freeze" objects moving at high rates of speed and to make discrete measurements from these television pictures. The Naval Weapons Center has, with this adaptation, made it possible to obtain a TV miss-distance solution.

1.18.2 Objectives

The objectives of a TV miss-distance solution are to be able to determine, within reasonable accuracy and within a very short period of time, a vector miss distance between two items of interest.

1.18.3 Instrumentation Description

The instrumentation required to perform this task consists of at least two shuttered TV cameras, appropriate lenses, video time insertion generators, a video reader capable of eight-bit resolution (1 part in 256), a desk calculator that has at least the capability of an HP 9830, two video tape recorders, and two video disc recorders.

1.18.4 Test Procedures

Images from at least two shuttered TV cameras located near the intercept area are recorded on a video tape recorder and disc recorder. Time is mixed with these images so that the exposure of each field is known within ±1 ms. To perform a least-squares solution, at least five images that contain both objects within the same scene are required from each camera. A good geometrical relationship between cameras and intercept is required. When these images are played back on the disc recorders, an x, y reading of a point on the missile and a point on the target are entered, with a corresponding discrete time, into the calculator. The position of each camera, as well as the intercept coordinates in a local tangent plan coordinate system, are entered into the program along with the x,y readings. If there is a warhead action involved, the data cannot include the picture containing the warhead detonation or any data beyond that point. This limitation is also valid if the missile strikes the target.

1.18.5 General Application

a. Data requirements

1. Instrument locations in a local tangent plane system

2. Focal length and relative x, y readings from up to 5 instruments containing up to 10 frames with known times for each frame

3. Scale factors for x, y to account for measurement nonlinearities

4. Estimate of intercept position (approximate, but in same local tangent plane system)

b. Data collection

1. Intercept estimate from radar

2. x, y TV readings of center of frame, missile and target

3. Quantities entered into calculator

c. Data reduction. The relative trajectory is determined by a least-squares fit to a second-degree polynomial with respect to time. A more general program performs a least-squares fit of the trajectory to a polynomial of degress less than or equal to 5. Once the coefficients have been determined, the relative trajectory is output at equal intervals. Input times can be nonsynchronous but must be known to ±0.001 s.

1.18.6 General Solution

The 3-D least-squares curve-fitting technique is outlined in *An Introduction to Least-Squares Theory and Its Application to Data Reduction Problems*, by Dr. F. C. Reed, March 1956. This approach assumes the relative trajectory may be represented by a polynomial in time;

$$X=a_0+a_1t+a_2t^2+ \ldots$$

$$Y=b_0+b_1t+b_2t^2+ \ldots$$

$$Z=c_0+c_1t+c_2t^2+ \ldots$$

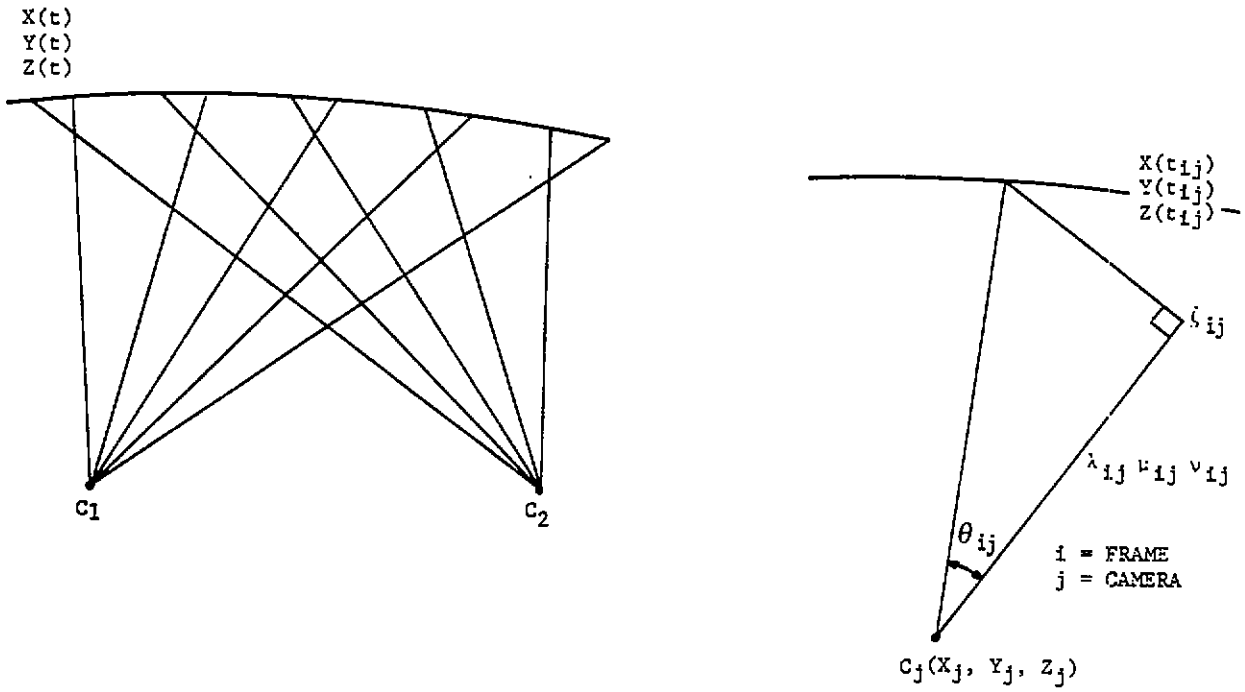

Figure 1-18-1 Trajectory visualization.

From these sketches one might visualize that the trajectory being sought is that which minimizes the sums of the squares of the ζ_{ij}'s (the distance from the lines of sight to this trajectory). The relation used is:

$$\zeta_{ij}^2=\sin^2\Theta_{ij}\left[\left[x(t_{ij})-X_j\right]^2+\left[y(t_{ij})-Y_j\right]^2+\left[Z(t_{ij})-Z_j\right]^2\right]$$

Finally:

$$\sum_{ij}\zeta^2=\sum_{ij}|\lambda_{ij},\ \mu_{ij}|^2+|\lambda_{ij},\ \nu_{ij}|^2+|\mu_{ij},\ \nu_{ij}|^2$$

where:

$$\lambda_{ij}=x(t_{ij})-X$$

$$\mu_{ij}=y(t_{ij})-Y$$

$$\nu_{ij}=z(t_{ij})-Z$$

is minimized. Stopping the polynomial at the second degree in each component, there is a system of nine equations with nine unknows (the coefficients, a_o, a_i, b_o, etc.). Matrix representation (see table 1.18-I) is simply, $AX=B$, $X=\bar{A}^{-1}B$, where X is the column vector of coefficients. The elements are not simple, since they are the results of sums of sums and products of the direction cosines, times and station coordinates for all available frames.

This solution is quite general in that it is not restricted to synchronous data. However, care should be taken to assure that the measurements are in the common coordinate system. The program on the HP 9830 is limited to this example (degree 2) with a maximum of 10 frames for 5 cameras.

1.18.7 Accuracy

As of this writing, very little data have been collected to evaluate the accuracy of the system under all conditions. Two sample solutions (film camera solutions versus TV camera solutions) indicate favorable comparison between the two systems:

Data from Film Cameras

	Downrange	Offrange	Elevation	Radial Miss
Round 1	-11 ft	-1 ft	-2 ft	11 ft
Round 2	0 ft	-2 ft	0 ft	2 ft

Data from TV Cameras

	Downrange	Offrange	Elevation	Radial Miss
Round 1	-11.1 ft	-1.5 ft	-3.6 ft	11.7 ft
Round 2	-1.9 ft	0.2 ft	-3.0 ft	3.5 ft

These data were collected from two air-to-air missile firings using two shuttered TV cameras.

1.18.8 Advantages

a. Data processed at low cost

b. Time saved by using TV images

c. Technique can be used with color as well as black and white TV.

1.18.9 Disadvantages

a. Sampling rate low

b. Measurements nonlinear

c. Measurements inaccurate

Table 1.18-I. MATRIX REPRESENTATION

$$
A=(9\times 9)\qquad
\begin{array}{|ccc|ccc|ccc|}
\hline
(\mu^2+\nu^2) & (\ )t & (\ )t^2 & (-\lambda\mu) & (\ )t & (\ )t^2 & (-\lambda\nu) & (\ )t & (\ )t^2 \\
(\ )t & (\ )t^2 & (\ )t^3 & (\ )t & (\ )t^2 & (\ )t^3 & (\ )t & (\ )t^2 & (\ )t^3 \\
(\ )t^2 & (\ )t^3 & (\ )t^4 & (\ )t^2 & (\ )t^3 & (\ )t^4 & (\ )t^2 & (\ )t^3 & (\ )t^4 \\
\hline
(-\lambda\mu) & (\ )t & (\ )t^2 & (\lambda^2+\nu^2) & (\ )t & (\ )t^2 & (-\mu\nu) & (\ )t & (\ )t^2 \\
(\ )t & (\ )t^2 & (\ )t^3 & (\ )t & (\ )t^2 & (\ )t^3 & (\ )t & (\ )t^2 & (\ )t^3 \\
(\ )t^2 & (\ )t^3 & (\ )t^4 & (\ )t^2 & (\ )t^3 & (\ )t^4 & (\ )t^2 & (\ )t^3 & (\ )t^4 \\
\hline
(-\lambda\nu) & (\ )t & (\ )t^2 & (-\mu\nu)t & (\ )t & (\ )t^2 & (\lambda^2+\mu^2) & (\ )t & (\ )t^2 \\
(\ )t & (\ )t^2 & (\ )t^3 & (\ )t & (\ )t^2 & (\ )t^3 & (\ )t & (\ )t^2 & (\ )t^3 \\
(\ )t^2 & (\ )t^3 & (\ )t^4 & (\ )t^2 & (\ )t^3 & (\ )t^4 & (\ )t^2 & (\ )t^3 & (\ )t^4 \\
\hline
\end{array}
$$

$$
B=(9\times 1)\qquad
\begin{array}{|c|}
\hline
\overset{\vee}{\Lambda}(\mu^2+\nu^2)t^\kappa-\Upsilon(\lambda\mu t^\kappa)-\overset{\vee}{Z}(\lambda\nu t^\kappa) \\
\Upsilon(\lambda^2+\nu^2)t_\kappa-\chi(\lambda\mu t^\kappa)-\overset{\vee}{Z}(\mu\nu t^\kappa) \\
\overset{\vee}{Z}(\lambda^2+\mu^2)t^\kappa-\chi(\lambda\nu t^\kappa)-\Upsilon(\mu\nu t^\kappa) \\
\hline
\end{array}
\qquad \kappa=0,1,2
$$

1.18.10 Reliability/Availability/Maintainability

The system has proved to be very reliable. By FY 79, four cameras will be mounted permanently on tracking mounts for gathering intercept data. The TV equipment is standard off-the-shelf 525-line RS-170 synch equipment commercially available.

1.18.11 Cost

The cost breakdown is as follows:

RCA camera 1005/Plumbicon®	$ 1,350.00
HP calculator	$ 4,900.00
Video disc recorder	$ 17,000.00
Video tape recorder	$ 2,000.00
Shutter assemby and electronics	$ 4,000.00
Time insertion generator (4 cameras)	$ 4,000.00
Video X, Y reader	$ 4,000.00

® Registered Trademark

1.18.12 Points of Contact

Naval Weapons Center, China Lake, CA 93555
Mechanical -- Code 6237, PH (714) 939-6389 (AV 437-6389)
Electronic -- Code 6231, PH (714) 939-6331 (AV 437-6331)
Data Reduction -- Code 6224, PH (714) 939-6441 (AV 437-6441)
Operation -- Code 6231, PH (714) 939-6346 (AV 437-6346)

1.19 GRAPHIC ATTITUDE DETERMINING SYSTEM (GADS)

1.19.1 General

The Graphic Attitude Determining System (GADS), which is a system for determining relative spatial position and attitude information of an aircraft store during release, can be used for miss-distance determination (MDD). Because target intercept is the reverse of a store separating from an aircraft and the final configuration for the GADS has not been determined for MDD, this section will describe the technique for separation studies. It will be left to the reader to translate this technique to MDD. The data required for MDD are recorded on 16-mm or 35-mm photographic movie film by cameras mounted on the target/aircraft--similar to the case for a store separating from an aircraft. The cameras may also be located on the ground, onboard a ship or on a chase aircraft. When the cameras are not located on the target, care must be taken to ensure that the image of the missile is of sufficient size.

1.19.2 Objectives

The GADS was designed to allow an operator with minimum training and skill to superimpose a computer-generated picture of a store in pseudo six degrees of freedom over a displayed film image. By knowing the parameters required to generate the computer picture, the position of the actual store at the time of release will be known.

1.19.3 Instrumentation Description

a. Computer group:

CPU-SEL 32/75, 128-kb memory
Disc storage - CDC 80 Mb
Magnetic tape - 9 track, 1600 b/in
Line printer - 64 character, 132 column, 300 lines/min
Operator's terminal - 30-c/s dot matrix printer, 128-character ASCII keyboard
Programmer's terminal - 240-c/s, 128-character ASCII CRT/keyboard

b. Console group:

Two film transport/projector/video camera assemblies - accepts standard 16-mm or 35-mm pin-registered film
Video display/mixer - mixes and displays 1,000-line video from film transports with 1,024 x 1, 024 raster computer-generated graphics
Computer model position control - XY joystick, Z joystick
Computer model attitude control - three axes (roll/pitch/yaw)

Control panel - video select/controls
Foot switch
Keyboard - 128-character ASCII keyboard

1.19.4 Test Procedures

Motion picture cameras (16-mm or 35-mm) are mounted on an aircraft to record the store as it is released and travels through the earliest part of its fall. Cameras are under pilot control and are run for a short time before release until store is out of field of view. Film is processed through normal procedures and delivered to the data reduction facility for assessment and reduction.

1.19.5 General Application

a. Data requirements. Reduction of data is dependent upon a software model of the store being dropped. This model is developed accurately from engineering drawings of the store. The attitude and position of the cameras must be determined.

b. Data collection. Cameras should have low-distortion lenses. Several high-speed cameras normally film each release, and the best is selected for reduction. A second film can be mounted and used to resolve questionable movements.

c. Data reduction. The film is mounted and positioned to show the store just prior to release, and this image is displayed. All position and attitude parameters of the store at rest are set equal to zero. The operator inputs the camera location and attitude with respect to the store. With this information plus the model of the store, the computer generates an image of the store on the display. The operator uses the position and attitude controls to superimpose the computer-generated image over the film image, thereby determining the exact camera position with respect to the store. The true camera location obtained is fixed, and the film is advanced past the release point. The operator again uses the controls to move the model and achieve superposition. Upon superimposing the two images, the operator depresses a foot switch to record the current orientation of the model and to advance the film. The data are later edited and smoothed to obtain the final data.

1.19.6 General Solution

a. Analysis techniques. Analysts need to review the results and the film as necessary to confirm answers.

b. Math model. The solution utilizes the trigonometric relationship between camera and store. The graphic image for most stores can be derived from a series of concentric circles of varying radii at measured distances along the store's longitudinal axis plus fixed points defining fins or other appendages.

1.19.7 Accuracy

Accuracy of 1 inch in position over a field of view of 25 ft is expected.

1.19.8 Advantages

As compared to presently existing photogrammetric techniques, the following advantages should be realized:

a. Saves time and money by not having to paint store with reference dots.

b. Saves labor costs and makes reduction of large quantities of data possible due to faster reduction times.

1.19.9 Disadvantage

The difficulty of modeling complex shapes may necessitate special software development for high-performance stores.

1.19.10 Reliability/Availability/Maintainability

To be determined.

1.19.11 Cost

The total cost of the GADS will be approximately $550k including in-house software development.

1.19.12 Points of Contact

Armament Division
Eglin Air Force Base, FL 32542
AD/KRES AUTOVON 872-5819
AD/KRBA AUTOVON 872-2298/2004

1.20 SURFACE MISS DISTANCE

1.20.1 General Description

a. Surface miss distance is an application of the WSMR system described in section 1.4, which computes the TMA and the minimum distance between the missile and the surface of the target aircraft. The input includes the TMA, position and velocity data at TMA obtained from the WSMR tracking cameras. All computations are done in the target/roll coordinate system which is defined as that left-handed Cartesian Coordinate System (CCS) obtained by rotating the primary coordinate system axes through the azimuth and elevation angles of the longitudinal axis of target and the roll angle of target. The X-axis is parallel to the longitudinal axis of the target (positive in the tail-to-nose direction). The longitudinal axis is usually approximated by the target total velocity vector. The Y-axis is positive in a direction parallel to the right wing of the aircraft. The Z-axis is positive above the aircraft. The technique used in the computations assumes that the shape of the wings and tail can be approximated by triangles and the fuselage by cylinders. These assumptions are correct if the target is an F102-A or similar aircraft.

b. This is the first version of the program. It makes use of two triangles (wing and tail) and three cyclinders (fuselage). The instrumentation description, test procedures, data collection, and data reduction are identical to those contained in section 1.4.

1.20.2 Input Data

a. The input required (position and velocity data at TMA) is obtained from the output of the WSMR Tracking Cameras - Two Objects in Same Frame MD (Program MSD123).

b. The target aircraft configuration is also required (see figures 1.20-1 and 1.20-2). For the first wing miss distance, the program requires the points W1 (X1, Y1, Z1) and W2 (X2, Y2, Z2), which define the edge of wing; the second miss distance needs points W3 and W4; and finally, the third miss distance needs W1 and W4. Likewise, on the first tail miss distance, input required is T1 and T2. Finally, T1 and T3 are used on the second tail miss distance.

c. The order of input (X1, Y1, Z1) and (X2, Y2, Z2) is very important. The wing miss distances required that $Y1 \geq Y2$. On the tail miss distance, the program requires that $Z1 \geq Z2$.

1.20.3 Math Model

a. The input to surface miss distance is target configuration (see figures 1.20-1 and 1.20-2) and TMA, position and velocity data in the target/roll coordinate system as obtained from program MSD123.

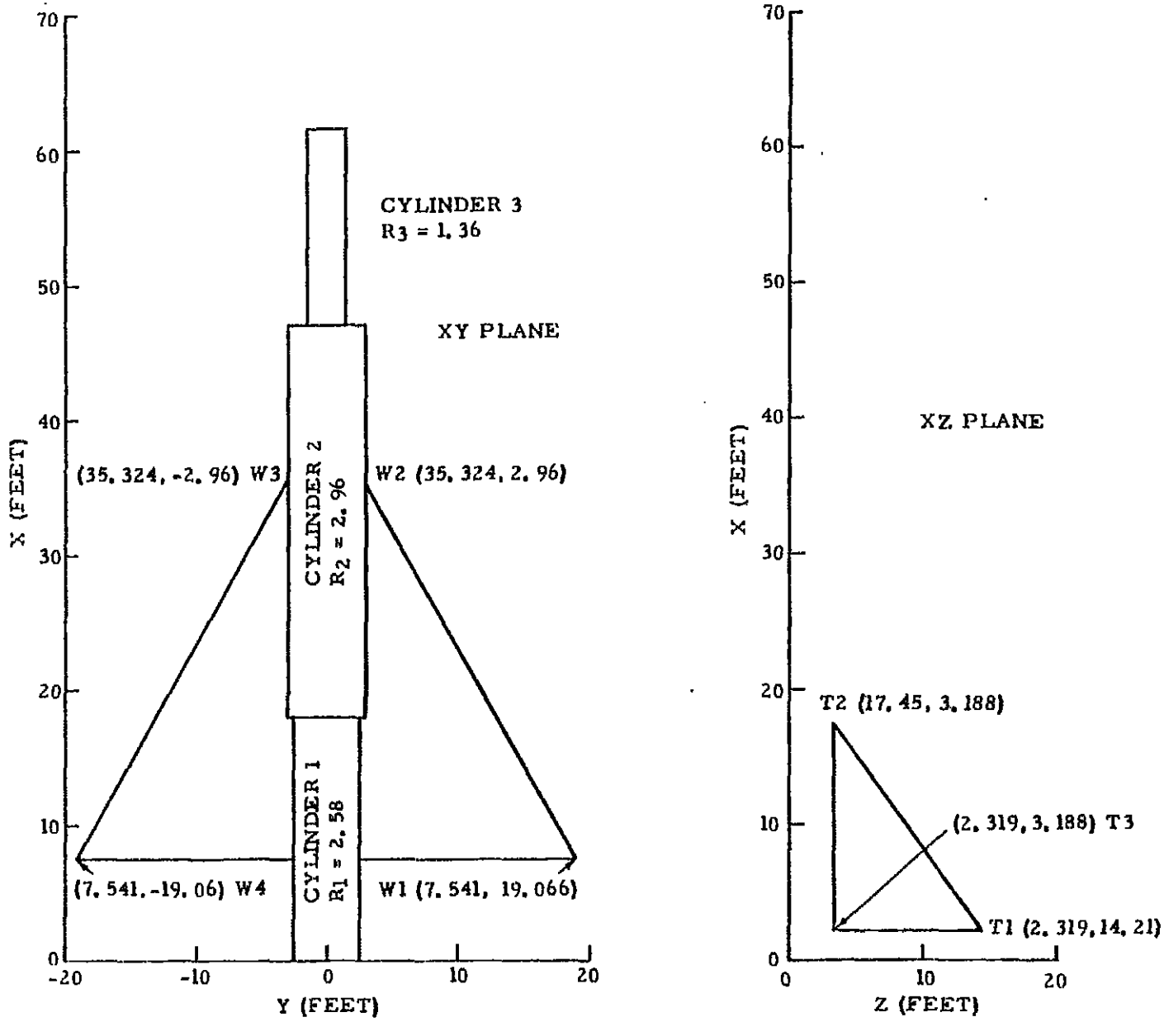

Figure 1.20-1 Target aircraft configuration (two dimensional).

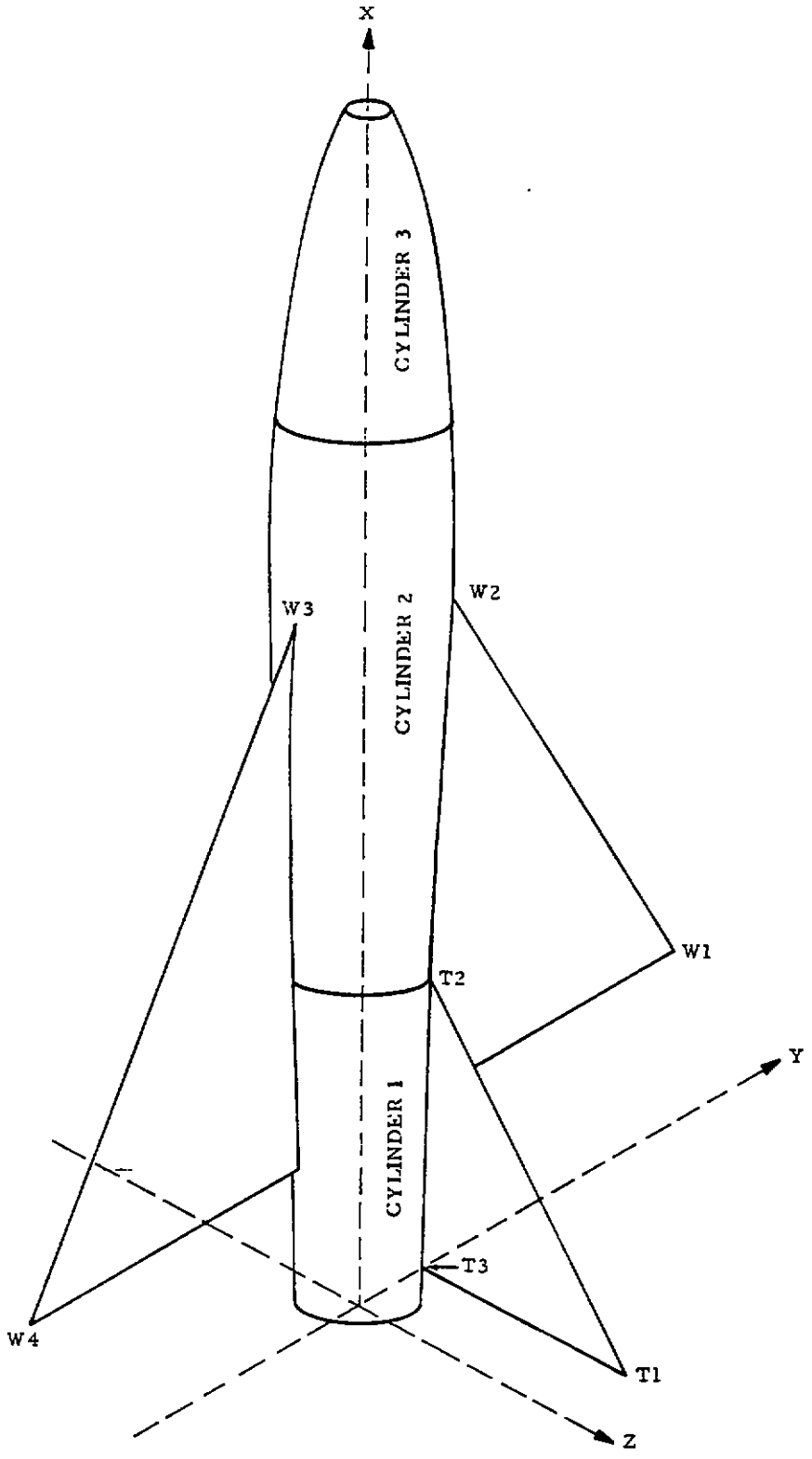

Figure 1.20-2 Target aircraft configuration (three dimensional).

b. Minimum miss to a triangle is determined by selecting successive points along the edge of the triangle and determining a minimum miss of the missile trajectory to each point. Using the coordinates (X1, Y1, Z1) and (X2, Y2, Z2) of the given edges that define the wings, successive TMAs and miss distances are computed at approximately 0.010 of a foot along the edge of the wing using

$$TMA_j = Tc - \left[XR \cdot VX + YR \cdot VY + ZR \cdot VZ\right] / \left[VX^2 + VY^2 + VZ^2\right]$$

where:

TMA_j=TMA to the jth location on edge of wing

T_c= Time of the smallest miss distance from MSD123

XR,YR,ZR,VX,VY,VZ=Relative position and velocity components of the missile with respect to wing edge at Tc.

After the TMA is established, the minimum miss distance is computed from the relative position data.

$$MD_j = \left\{\left[XR + VX(TMA_j - Tc)\right]^2 + \left[YR + VY(TMA_j - Tc)\right]^2 + \left[ZR + VZ(TMA_j - Tc)\right]^2\right\}^{\frac{1}{2}}$$

The smallest MD_j becomes the miss distance to the wing edge.

The identical procedure is applied to the two other edges on the wings and two edges on the tail. Thus far, there are five miss distances to these different surfaces.

By modeling the fuselage with cylinders, the fuselage miss distance can be computed. To do this, input the top and bottom coordinates (H_i and B_i) along the X-axis as well as the radius, R_i, of cylinders, where i ranges from 1 to as many cylinders as desired).

c. Minimum miss to a cylinder is determined by selecting successive points along the missile trajectory and determining a minimum miss to the cylinder from each point. The equations used are shown below. Compute these every 10 μs along the missile's trajectory.

1. MD_j occurs within cylinder (fuselage) height

   $$MD_j = (YR^2 + ZR^2)^{\frac{1}{2}} - R_i$$

2. MD_j occurs above cylinder height

   $$MD_j = \left\{\left[(YR^2 + ZR^2)^{\frac{1}{2}} - R_i\right]^2 + \left[XR - H_i\right]^2\right\}^{\frac{1}{2}}$$

3. MD_j occurs below cylinder height

$$MD_j=\left\{\left[(YR^2+ZR^2)^{1/2}-R_i\right]^2+\left[XR-B_i\right]^2\right\}^{1/2}$$

where:

XR, YR, ZR=Relative positions of missile in the target/roll coordinate system

H_i=Value assigned to top of the ith cylinder measured along X-axis

B_i=Value assigned to bottom of the ith cylinder measured along X-axis

R_i=Radius of the ith cylinder

The smallest MD_j becomes the miss distance to ith cylinder.

This identical procedure is applied to n cylinders. Thus, there are n miss distances to fuselage.

1.20.4 Output Data

The output data from the surface miss-distance program is shown in tables 1.20-I and 1.20-II. At the top of table 1.20-I the required input is printed. Next is printed the nearest approach information (surface TMA, surface miss distance, missile position at TMA, and the coordinates of closest target surface) to the wing edge defined by W1 and W2. Following this is the nearest approach information to W3 and W4, W1 and W4, T1 and T2, and T1 and T3. Table 1.20-II shows the nearest approaches to the fuselage segments. Described first is the fuselage segment (cylinder size, height and radius) and the nearest approach information to this surface. Following this, the nearest approach to cylinders 2 and 3 (fuselage segments 2 and 3) are shown. The analysts must now look at the magnitude of these eight nearest approaches and determine which is the smallest and call it the surface miss distance.

1.20.5 Accuracy

The accuracy of the method described in this section depends on the following:

a. All the factors mentioned in subparagraph 1.4.3

b. How well the triangles and cylinders approximate the true shape of the target aircraft.

Table 1.20-I SURFACE MISS DISTANCE

INPUT DATA

TMA= .150 X= -10.000 Y= 5.000 Z= 20.000 VX=-1000.000 VY= -100.000 VZ= 200.000

****

WING ENDPOINTS X1= 7.540 Y1= 19.070 Z1= .000 X2= 35.320 Y2= 2.960 Z2= .000

SURFACE TMA	SURFACE MISS-DISTANCE	MISSILE POSITIONS AT TMA X	Y	Z	COORDINATES OF CLOSEST SURFACE X_W	Y_W	W1 - W2 MD
.1077	12.184	32.322	9.232	11.536	30.354	5.840	

****

WING ENDPOINTS X1= 35.320 Y1= -2.960 Z1= .000 X2= 7.540 Y2=-19.070 Z2= .000

SURFACE TMA	SURFACE MISS-DISTANCE	MISSILE POSITIONS AT TMA X	Y	Z	COORDINATES OF CLOSEST SURFACE X_W	Y_W	W3 - W4 MD
.1038	16.577	36.213	9.621	10.757	35.320	-2.960	

****

WING ENDPOINTS X1= 7.540 Y1= 19.070 Z1= .000 X2= 7.540 Y2=-19.070 Z2= .000

SURFACE TMA	SURFACE MISS-DISTANCE	MISSILE POSITIONS AT TMA X	Y	Z	COORDINATES OF CLOSEST SURFACE X_W	Y_W	W1 - W4 MD
.1293	16.172	10.711	7.071	15.858	7.540	7.070	

****

TAIL ENDPOINTS X1= 2.320 Y1= .000 Z1= 14.210 X2= 17.456 Y2= .000 Z2= 3.190

SURFACE TMA	SURFACE MISS-DISTANCE	MISSILE POSITIONS AT TMA X	Y	Z	COORDINATES OF CLOSEST SURFACE X_W	Z_W	T1 - T2 MD
.1376	7.004	2.360	6.236	17.528	2.320	14.210	

****

TAIL ENDPOINTS X1= 2.320 Y1= .000 Z1= 14.210 X2= 2.320 Y2= .000 Z2= 3.190

SURFACE TMA	SURFACE MISS-DISTANCE	MISSILE POSITIONS AT TMA X	Y	Z	COORDINATES OF CLOSEST SURFACE X_W	Z_W	T1 - T3 MD
.1376	7.004	2.360	6.236	17.528	2.320	14.210	

Table 1.20-II SURFACE MISS DISTANCE

FUSELAGE TOP = 18.05 FUSELAGE BOTTOM= .00 RADIUS = 2.58

CYLINDER 1
MD

SURFACE TMA	SURFACE MISS-DISTANCE	MISSILE POSITIONS AT TMA X	Y	Z
.1203	13.682	19.737	7.974	14.053

****

FUSELAGE TOP = 40.95 FUSELAGE BOTTOM= 18.05 RADIUS = 2.96

CYLINDER 2
MD

SURFACE TMA	SURFACE MISS-DISTANCE	MISSILE POSITIONS AT TMA X	Y	Z
.0926	10.758	47.445	10.745	8.511

****

FUSELAGE TOP = 61.43 FUSELAGE BOTTOM= 46.95 RADIUS = 1.36

CYLINDER 3
MD

SURFACE TMA	SURFACE MISS-DISTANCE	MISSILE POSITIONS AT TMA X	Y	Z
.0800	12.056	60.005	12.000	5.999

****

1.20.6 Advantages and Disadvantages

All advantages and disadvantages of this method are the same as those mentioned in subparagraphs 1.4.4 and 1.4.5. An additional advantage is that the nearest miss from the tail of the missile to target surface can be obtained. (In the past, miss distance has usually been the nearest miss from tail of missile to tail of target.)

1.20.7 Reliability

Reliability factors are the same as those in subparagraph 1.4.7.

1.20.8 Cost

The cost associated with this technique is nominal since it uses the output of the method described in section 1.4. Thus, the only cost involved is the computer time needed to run this program, which is a function of the number of triangles and cylinders used in the solution. (Typical computer time expended when using two triangles and three cylinders on a UNIVAC 1108 is 45 s.)

1.20.9 Point of Contact

Analysis and Computation Division
White Sands Missile Range, NM 88002
PH (505) 678-2738
AUTOVON: 258-2738

CHAPTER 2

2.1 GROUND IMPACT MISS-DISTANCE DETERMINATION (MDD)/SCORING SYSTEMS

2.1.1 General

Ground impact scoring systems generally involve determining the X, Y coordinates of the single or multiple impacts of bombs, missiles, rockets, or small caliber items. Targets are horizontal on the ground plane, but for small caliber items, vertical targets may also be used.

2.1.2 Methods

Methods for determining the impact coordinates include techniques in the following categories:

a. Optical systems. Typically, optical systems use cameras and pictures to obtain scaled distance values to determine X, Y values. The systems are either airborne or ground located; tracking or fixed cameras may be used.

b. Electromagnetic systems. Electromagnetic sysems involve either radar or doppler-type radar located near the impact area.

c. Acoustic systems. Acoustic-systems use is primarily experimental for multiple or burst firing of small caliber items.

d. Seismic systems. Seismic systems use geophones to obtain ground shock wave data for single bombs or missiles.

e. Survey systems. Survey systems use nonphotographic optical techniques or standard distance measuring and other survey equipment for impact locations.

2.2 SHRIKE SCORING SYSTEM

2.2.1 General

The following input was extracted from PMR Technical Note No. 3284-1-65, *Miss Distance When Radar Data Are Not Present Near the Point of Interest*. This method may have additional general applications.

2.2.2 Description of the Problem and the Information Available

a. The missile is acquired by radar at a distance. Near the target, the vertical component of the missile trajectory is relatively important. The missile is lost by the radar at a certain altitude. Subsequent to this, the missile makes its closest approach to the target; then it impacts on the earth's surface. The coordinates of the impact point are measured. The time of impact, t, will be known.

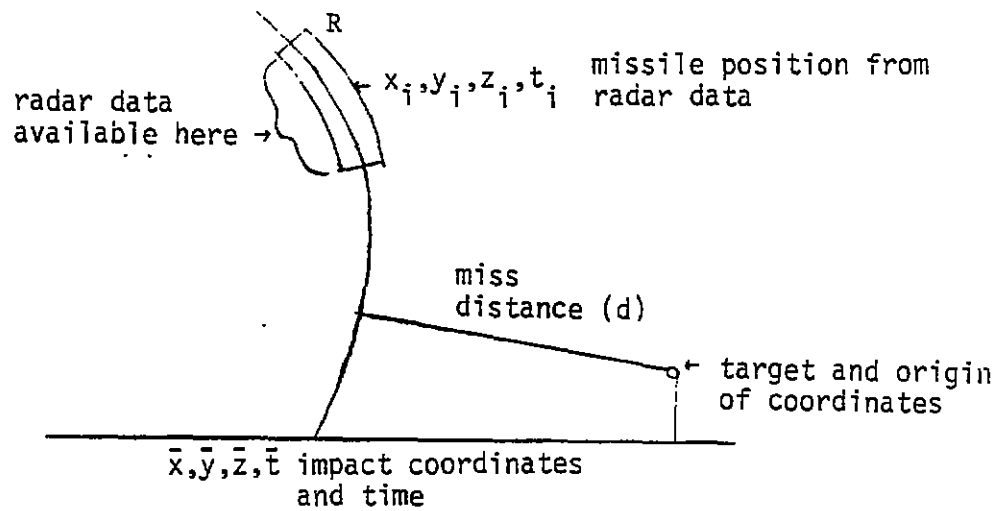

Figure 2.2-1 Impact information with radar data.

The nature of the information from the two different sources (radar and a system which gives independent information about the impact point, e.g., MILS) differs markedly. This fact governs the procedure suggested.

b. The impact coordinates are a single point of high relative accuracy. The radar data consists of a large number of points. Since radar is subject to bias, a constant error in the radar measurements is possible.

c. Any curve which is fit to the radar data will necessarily be in error by the amount of the bias. However, if the approximate trajectory is differentiated, the bias error is removed. Then, the relatively accurate impact coordinates may be used to obtain the trajectory by integrating backward with respect to time.

2.2.3 Determination of Miss Distance

The trajectory may be approximated by a least-squares fit of a polynomial to radar data from the region, R. A quadratic approximation will allow varying curvature. A higher degree polynomial is undesirable since the result is to be extrapolated. Then the biased approximate trajectory is:

$$\begin{aligned} x(t) &= c_{x2}t^2 + c_{x1}t + c_{x0} \\ y(t) &= c_{y2}t^2 + c_{y1}t + c_{y0} \\ z(t) &= c_{z2}t^2 + c_{z1}t + c_{z0} \end{aligned} \qquad (1)$$

where the coefficients have the usual least-square values.

The derivatives are:

$$\begin{aligned} \dot{x}(t) &= 2c_{x2}t + c_{x1} \\ \dot{y}(t) &= 2c_{y2}t + c_{y1} \\ \dot{z}(t) &= 2c_{z2}t + c_{z1} \end{aligned}$$

The trajectory with the bias eliminated is given by:

$$X(t) = \bar{x} + \int_{-\bar{t}}^{t} \left[2c_{x2}\lambda + c_{x1} \right] d\lambda$$

with analogous expressions for Y(t) and Z(t). If

$$\begin{aligned} K_x &= \bar{x} - c_{x1}\bar{t} - c_{x2}\bar{t}^2 \\ K_y &= \bar{y} - c_{y1}\bar{t} - c_{y2}\bar{t}^2 \\ K_z &= \bar{z} - c_{z1}\bar{t} - c_{z2}\bar{t}^2 \end{aligned}$$

then

$$X(t)=c_{x2}t^2+c_{x1}t+K_x$$

$$Y(t)=c_{y2}t^2+c_{y1}t+K_y \qquad (2)$$

$$Z(t)=c_{z2}t^2+c_{z1}t+K_z$$

The closest approach of the missile to the target occurs at t=t*. At this point:

$$\frac{d}{dt}(X^2(t)+Y^2(t)+Z^2(t))=0$$

This condition requires that:

$$X(t)\dot{x}(t)+Y(t)\dot{y}(t)+Z(t)\dot{z}(t)=0 \qquad (3)$$

This equation is a cubic and will have at least one real root. From the geometry of the problem, the real root, t*, will be very near $\bar{t}$ and there will be no other real root placed similarly. The usual case will be that $t^* < \bar{t}$; however, it is possible to visualize the case $t^* > t$. In the latter case, the point of closest approach will be the impact point. Since t* is near $\bar{t}$, Newton's method may be used to solve equation (3).

2.2.4 Accuracy of the Result

The bias error will have been removed from the radar signal by the use of the surveyed impact point. The remaining errors will be centered around zero. Also, there will be an error in the surveyed impact point which is independent of, and uncorrelated with, the radar errors.

If σ_d^2 is the variance of this result,

then

$$\sigma_d^2=\left(\frac{x}{d}\right)^2\sigma_x^2+\left(\frac{y}{d}\right)^2\sigma_y^2+\left(\frac{z}{d}\right)^2\sigma_z^2$$

and

$$\sigma_d^2<\sigma_x^2+\sigma_y^2+\sigma_z^2,$$

while

$$\sigma_x^2=\sigma_{x0}^2+\sigma_{xR}^2, \text{ etc.}$$

where: σ_{x0}^2 is the variance in the x component of the impact point measurement and σ_{xR2} is the variance in the x component of the calculated miss distance due to noise in the radar signal. This is fundamentally influenced by the fact that the trajectory out to the region in which the data are given was extrapolated.

By letting x*(t), etc., denote the actual trajectory, and x(t), etc., denote the calculated trajectory, so that ε_d, the error in d*, may be separated into tangential and normal components, ε_T and ε_N.

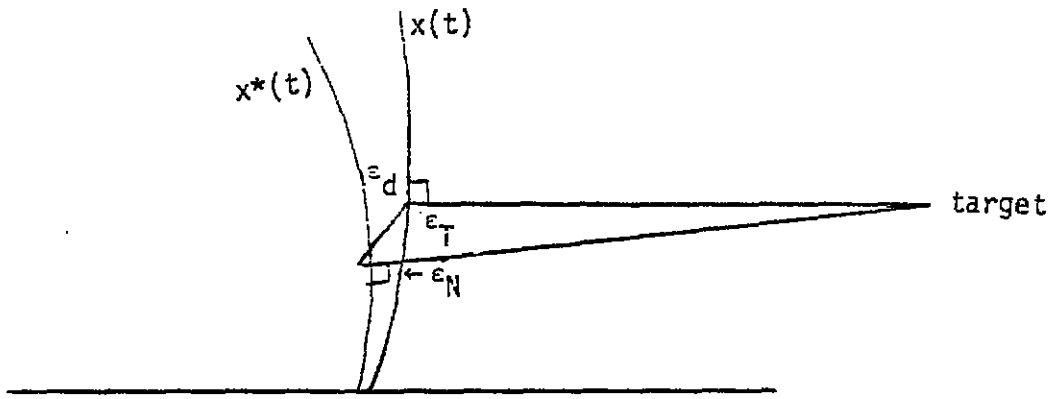

Figure 2.2-2 The error components (tangential and normal) at the miss-distance error ε_d.

The error, ε_T, derives its source from the fact that the direction in which d is measured is in error. However, this direction is orthogonal to the direction of ε_T, and since the quantity, d, which we are measuring, is a length, the error, ε_T, does not affect the results. Thus, the error in du must come from ε_N. To estimate the variance due to this error, the following lemma is needed: If X(t) is a least-squares fit polynomial of degree of n, then for a given t, the variance of X due to noise in the input data is:

$$\text{var } X(t)=\sum_{m=0}^{2^n} b_m t^m$$

where:

$$b_m=\sum_{k=0}^{m} \tilde{\sigma}_k,\ m-k,\ \sigma_{ij}=0 \text{ if } i>n \text{ or } j>n$$

$$\tilde{\sigma}=A\sigma A^T$$

$$A=(A_{ij})=\left(\sum_k \tilde{u}_{ik} w_j t_j{}^k\right)$$

$$U^{-1}=(\tilde{u}_{ij})$$

$$U=(u_{ij})=\left(\sum_k w_k t_k{}^{i+j-2}\right)$$

and

$$\sigma=(\sigma_{ij})=\left(E\ ((x_i-\bar{x}_i)\ (x_j-\bar{x}_j))\right)$$

The lemma will not be proven here. The computations necessary to show its validity are lengthy, but elementary at all times. The lemma may be applied for a value of t outside the domain in which the data are given. The lemma requires that the matrix for x, for y and for z be obtained.

$$\sigma_{ij}=\frac{1}{p}\sum_{p=1}\left(x_i{}^{(p)}-\bar{x}_i\right)\left(x_j{}^{(p)}-\bar{x}_j\right)$$

Here $\bar{x}_i$ is the average of $x_i{}^{(p)}$ for fixed is as p varies. $\bar{x}_i$ is an estimate of the true value of x_i, and $x_i{}^{(p)}-x_i$ is the noise at the i, the point on the pth realization. For example, $\sigma_{7,24}$ is the covariance between the noises at point 7 and point 24, i.e.,

$$\sigma_{7,24}=\frac{1}{p}\sum_{p=1} n^{(p)}(7)n^{(p)}(24).$$

These quantities are independent, and E (noise(i))=0 for any i. Therefore, if $i\neq j$ then $\sigma_{ij}=0$. If i=j, σ_{ij}=ave $(x_i-\bar{x}_i)^2$; i.e., it is the average of the square noise at the ith point. This is assumed to be independent of the particular point, and written simply var $x=\sigma_x{}^2$, a constant. The matrix, σ, which was previously required for the x coordinate, is $\sigma_x{}^2 I$ where I is the identity matrix whose dimension equals the number of raw data points. $\sigma_x{}^2$ is found from the usual equation

$$\sigma_c{}^2=B\sigma_R{}^2 B^T,$$

then

$$\sigma_{ij}=0$$

where σ_R^2 is the matrix of errors of precision of the particular radar used, and B is the matrix of the transformation of coordinates of the radar and the set of Cartesian coordinates of this problem based at the radar, and averaged over the region where data is acquired. Then var $x=\sigma_x^2$ is the first diagonal element of σ_c^2, and this provides σ for the x coordinate which enables the calculation of var X(t); the x component of the variance in d due to ε_N. Similiarly, the second diagonal element of σ^2 will give a matrix $\sigma=\sigma_y^2 I$ for the y coordinate and the third will give a matrix $\sigma=\sigma_x^2 I$ for the z coordinate permitting the calculation of var Y(t) and var Z(t) due to ε_N.

Finally,

$$\sigma_d^2 < \left(\sigma_{x0}^2+\sigma_{y0}^2+\sigma_{z0}^2\right)+\left(\sigma_{XR}^2+\sigma_{YR}^2+\sigma_{ZR}^2\right),$$

where the quantitiy in the last parentheses is the quantity just calculated, and the quantity in the first parentheses is the error in the surveyed impact point.

2.3 SURVEY TECHNIQUES

2.3.1 General

Survey techniques involve the use of angle measuring and distance measuring devices to determine position. A complete description of survey techniques, accuracies and methods is found in the Geodetic Survey and Field Computations Manual, M96-2, published by the 1st Geodetic Survey Squadron (1GSSQ) at Francis E. Warren Air Force Base, Wyoming. Typically, a Wild T2 or T3 theodolite is used to measure angles. A first-order survey rejects all readings that are greater than ±4 s away from the mean reading.

2.3.2 Advanced Techniques

Several advanced techniques are available for measuring distances. These include:

a. Subtense Bar Traverse

1. A 2-m bar is placed horizontally at the impact point. A known station then measures the angle between the ends of the bar. The distance to the impact can now be determined.

2. A typical accuracy at 100 m with ±1 second-angle error is one part in 5000 error.

b. Geodimeter Model 8

1. This device uses laser waves to measure distance.

2. 1σ accuracy=5 mm ±1 p/M of the distance.

3. Range is 15 m to 60 km.

c. Tellurometer

1. This device uses a microwave transmitter to measure distance.

2. 1σ accuracy=±1.5 cm, ±4 p/M of the distance.

3. Range is 200 m to 50 km.

d. Electrotape

1. This device is a radio wave transmitter for measuring distances.

2. 1σ=±1.0 cm, ±3 p/M of the distance.

3. Range is 50 m to 50 km.

2.3.3 First-Order Class-I Survey Technique

a. General Description

This technique can be used when extremely accurate position data are required. The impact point of the ordnance is marked and a first-order class-I survey is conducted. This survey requires the service of a qualified geodetic survey team. Basic surveying techniques are outlined in IGSSQ TM5-237, *Surveying Computers Manual*. Detailed techniques are given in IGSSQ M96-2, *Geodetic Survey and Field Computations Manual*.

b. Math Model

The math model for a first-order class-I survey is given in the above referenced documents.

c. Accuracy

A first-order class-I survey is accurate to 10 p/M. This is accurate to within 0.5 in/mi.

2.3.4 Tower Scoring System

a. Method

Azimuth angles are measured from two or more sighting towers to the impact point of a tested munition. Using this information and the coordinates of the towers, the impact point can be calculated using a geometric method of data reduction.

b. Math Model

See figure 2.3-1.

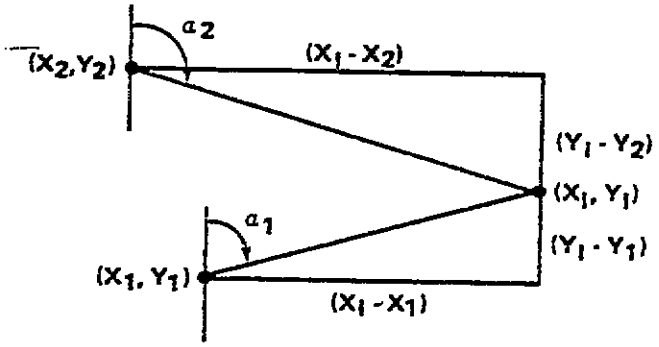

Figure 2.3-1 Math model.

where:

X_I, Y_I=Impact coordinates

X_1, Y_1=Coordinates of tower 1

X_2, Y_2=Coordinates of tower 2

α_1, α_2=Azimuth angles from towers 1 and 2, respectively, measured from north

$$Y_I = \frac{X_1 - X_2 + Y_2 \tan \alpha_2 - Y_1 \tan \alpha_1}{\tan \alpha_2 - \tan \alpha_1}$$

$$X_I = \frac{\tan \alpha_1 \left(Y_2 \tan \alpha_2 - X_2\right) - \tan \alpha_2 \left(Y_1 \tan \alpha_1 - X_1\right)}{\tan \alpha_2 - \tan \alpha_1}$$

Similar models are used when more than two scoring towers are used. The intersection of each pair of lines is determined as in a two-station solution, and a geometric mean taken to obtain the impact point. The Davis, Bodwell, Odel, etc., solutions could also be used to compute the impact point. However, these methods do not significantly improve the solution and require more computation time.

c. Accuracy

The approximate accuracy of a three-tower system located 2500 ft from a target is ±20 ft and is dependent upon the geometric configuration.

d. Advantage

The system is simple and inexpensive to operate.

e. Disadvantage

The system is subject to human error.

2.3.5 Range and Azimuth Techniques

a. Method

Place a theodolite on the target, sight a known reference azimuth, and swing to the impact point to determine the azimuth angle. Using a distance-measuring device, measure the distance from the target to the impact point.

b. Accuracy

The accuracy depends on the measuring device used. These accuracies are given in subparagraph 2.3.4 c. and are generally most satisfactory.

c. Advantages

This technique is simple and has a high degree of accuracy.

d. Disadvantages

This system is time consuming because the scoring theodolite has to be set up after each mission and the distances to the impact points physically measured.

2.3.6 Resection and Theodolite Technique

a. Method

Place a theodolite over the impact point. Measure the angles between three known references. From this information, the impact point can be determined.

b. Math Model

A math model of this technique is given in IGSSQ M96-2, Chapter 33, "Special Angle Computations."

c. Accuracy

The accuracy of this method is dependent on the survey techniques used. However, using a Wild T2 and first-order survey of the target boards, accuracies of 1 ft are common.

d. Advantages

The advantages of this technique are its simplicity and accuracy.

e. Disadvantages

The equipment has to be set up and measurements made after each mission.

2.3.7 Bomblet Scoring System

a. General Description

This system is used to determine the impact location of bomblets against a target area. Assume that the target area is covered with a marked grid of 100-ft squares.

1. The grid is lettered horizontally and numbered vertically. Each grid is identified by the intersection of lines in the lower left-hand corner. Therefore, the first grid is A1. An enlargement of a typical grid is shown in figure 2.3-2.

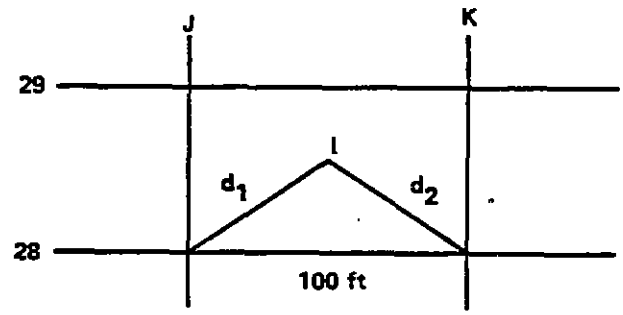

Figure 2.3-2 Typical grid.

This grid would be identified as J28. Shown in the grid at point I is the impact of a bomblet. A team would then measure the distances d_1 and d_2 to the lower left- and right-hand corners of the grid, using a tape measure. This would be recorded as:

J28 73.2 ft (d_1)

K28 51.7 ft (d_2)

2. Then teams of two would systematically walk the entire grid complex, marking and measuring each bomblet impact. This data is then reduced to indicate the XY position of each bomblet within the grid.

b. Math Model

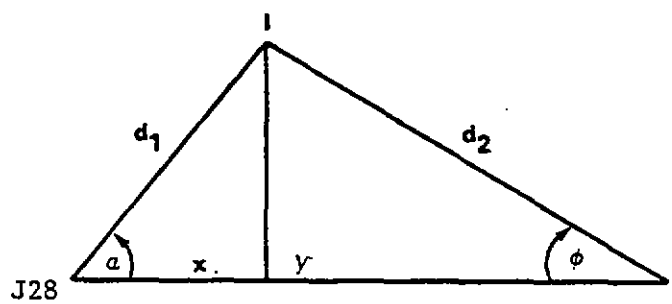

Figure 2.3-3 Isolated view of triangle shown in figure 2.3-2.

Determine the distances X and Y which will give the impact point with reference to the intersection point J28 as shown in figure 2.3-3 above.

$$\alpha=\cos^{-1}\left(\frac{d_1^2+r100^2-d_2^2}{200\ d_1}\right)$$

$$\phi=\cos^{-1}\left(\frac{d_2^2+r100^2-d_1^2}{200\ d_2}\right)$$

$$Y=d_1 \sin \alpha=d_2 \sin \phi$$

$$X=(d_1^2-Y^2)^{\frac{1}{2}}$$

This gives the location of I within grid J28. Appropriate transformations can now be made to reference this point to a target on the grid.

c. Accuracy

Each bomb can be located within the 100 sq ft grid to an accuracy of ±5 ft. The accuracy, with reference to the center of the grid, is a function of how accurately the grid is surveyed.

d. Advantages

1. A simple method of scoring.

2. Does not require highly trained personnel.

e. Disadvantages

1. Layout of a grid on the target is required.

2. Scoring grid must be cleaned after each mission.

3. Scoring technique is time consuming.

4. Normally, only one mission can be run per day.

f. Cost

The only equipment cost is for measuring tapes. All other costs are manpower related.

g. Reliability

This scoring system is highly reliable.

2.4 GROUND IMPACT SCORING UTILIZING THEODOLITE CAMERAS

2.4.1 General

One of the most regularly used systems in determining ground impact points is composed of a set of theodolite cameras judiciously located within a tracking area. These cameras are mounted on gimbals so that they can rotate in two orthogonal planes. The azimuth plane is tangent to the earth's surface at the station. The elevation plane is perpendicular to the azimuth plane. Each camera is free to rotate a full 360° in azimuth and approximately 92° in elevation, so that slightly more than a full hemisphere of coverage is obtained. The use of these cameras for tracking requires that an operator follow the object being tracked. The rotations in azimuth and elevation are recorded on magnetic tape as a function of time during the tracking. When the azimuth and elevation are recorded from at least two theodolite stations and the positions of these stations are known, the space position of the object can be calculated. Normally, more than two stations are used in this tracking; it is desirable to use three or more stations in obtaining a solution.

2.4.2 Math Model

a. The basic problem to be solved is the determination of the space position of an object when the angular position with respect to two or more known fixed coordinate systems is given. However, the measured angles must have a number of corrections applied before they can be used to calculate the space position. The following are definitions of the terms used in this calculation. The i subscript refers to data pertaining to the ith theodolite station.

A_i=Measured azimuth angle

E_i=Measured elevation angle

ε_{io}=Collimation Error - because the line of sight to a fixed object is not exactly parallel to the original when rotated through 360°

A_{io}=Zero correction for azimuth

E_{io}=Zero correction for elevation

ξ_i=Tracking error in azimuth

η_i=Tracking error in elevation

The tracking errors result from the fact that the camera line of sight is not always exactly on the object being tracked. Figures 2.4-1 and 2.4-2 illustrate the geometry as seen from the ith theodolite station with point, P, the point in space being tracked.

SOLUTION OF THEODOLITE DATA

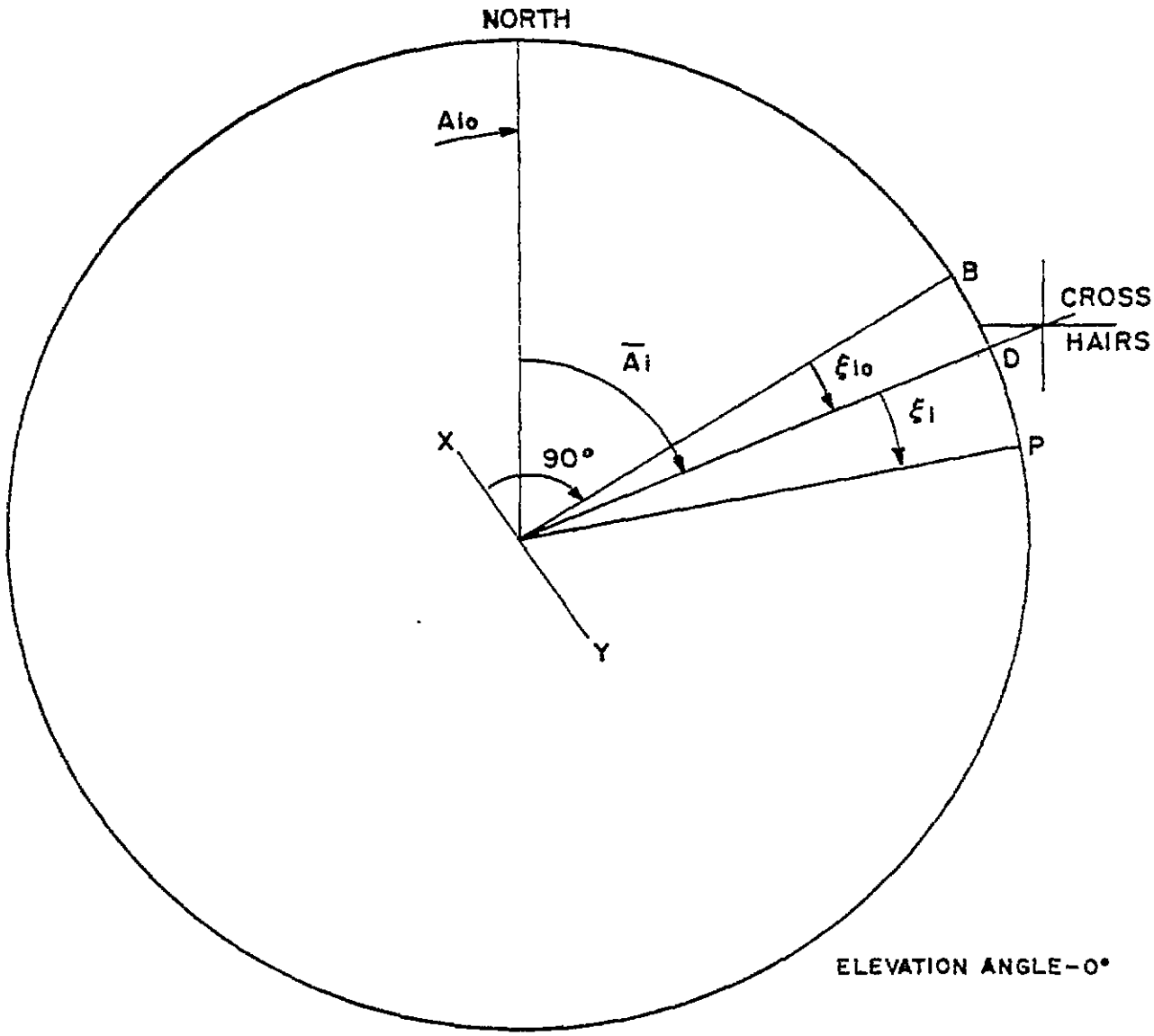

$\overline{XY}$ IS THE TRUNION AXIS
$\bar{A}_i$ IS THE AZIMUTH OF THE CROSS HAIRS MEASURED CLOCKWISE FROM NORTH
e_{io} IS THE COLLIMATION ERROR

ξ_i IS THE TRACKING ERROR
P IS THE LINE OF SIGHT TO POINT READ ON FILM
THE SUBSCRIPT "i" REFERS TO ITH THEODOLITE STATION

Figure 2.4-1 ith theodolite station.

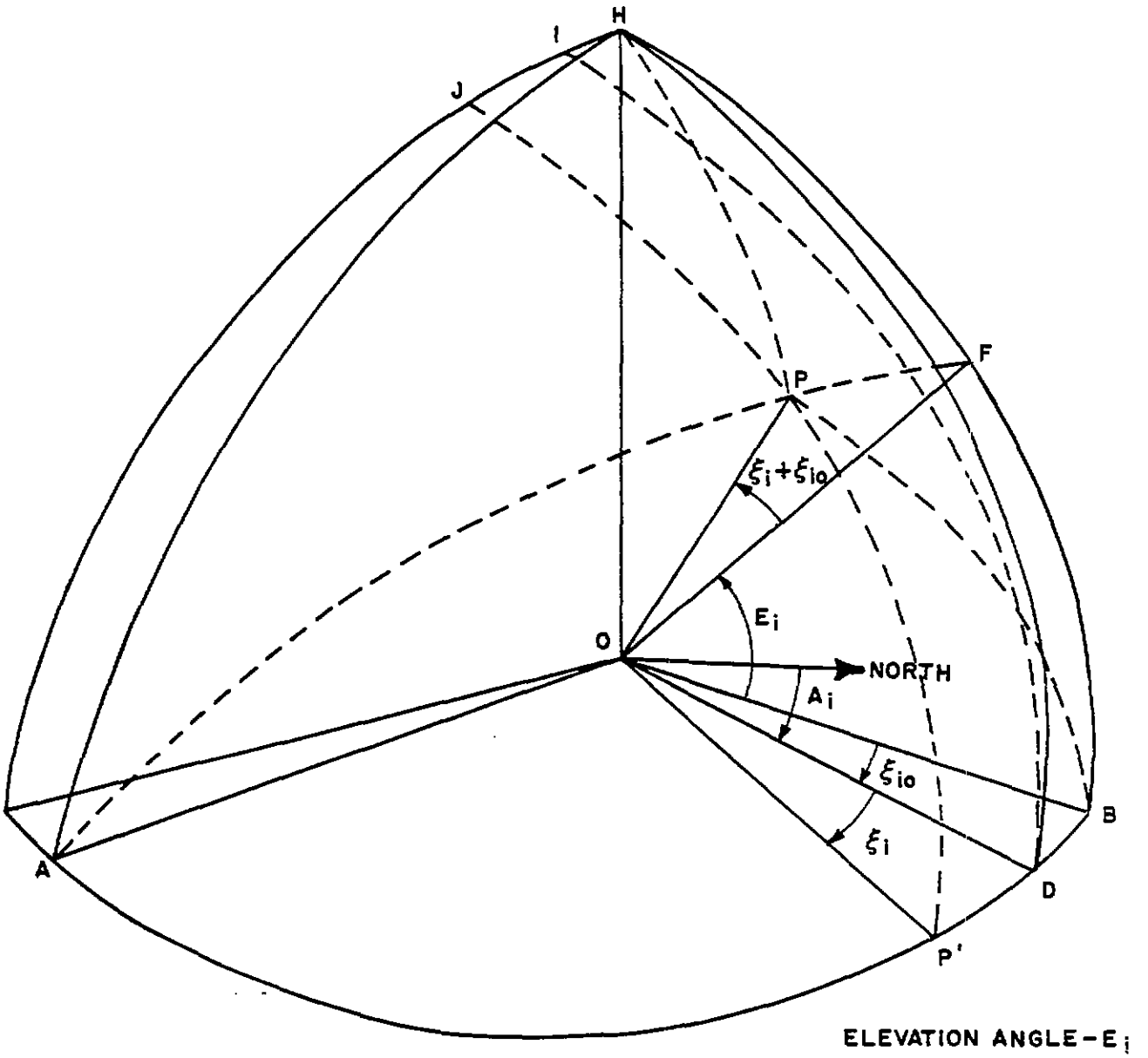

$\overline{OB}$ IS PERPENDICULAR TO THE TRUNION AXIS.
AXES OA, OB AND OH ARE ORTHOGONAL AND UNIT LENGTH.
AXES OC, OD AND OH ARE ORTHOGONAL.
AXIS OH IS PERPENDICULAR TO A HORIZONTAL PLANE.
$\overline{OP}$ IS THE LINE OF SIGHT TO POINT READ ON FILM.

Figure 2.4-2 ABH coordinate system.

b. The following steps must be accomplished before the space position computation is made:

1. The azimuth and elevation are corrected for zero effect.

2. The elevation angle is corrected for tracking error.

3. The direction cosines with respect to a coordinate system located at the theodolite station are calculated (azimuth tracking error corrections and collimation error corrections are included in this step).

4. The direction cosines for each station are computed with respect to the coordinate system of interest.

c. The zero offsets and the collimation error are determined from reference shots taken before the beginning of the mission. The corrections for zero offset are applied as follows:

$$\bar{E}_i=\bar{\bar{E}}_i-E_{io} \tag{1}$$

$$\bar{A}_i=\bar{\bar{A}}_i-A_{io} \tag{2}$$

d. The tracking errors, ξ_i and η_i, are obtained by reading film to determine the angular offset of a set of crosshairs on the camera lens from a point on the object being tracked. The elevation tracking error is applied directly.

$$E_i=\bar{E}_i+\eta_i \tag{3}$$

e. In the ABH coordinate system shown in figure 2.4-2 (the system in which the elevation angle is measured), the direction cosines of the line of sight to the point, P, are calculated as follows:

$$\cos(\alpha_i)=\sin(\xi_i+\varepsilon_{io}) \tag{4}$$

$$\cos(\beta_i)=\cos(\xi_i+\varepsilon_{io})\cos E_i \tag{5}$$

$$\cos(\gamma_i)=\cos(\xi_i+\varepsilon_{io})\sin E_i \tag{6}$$

where:

α=AOP

β=BOP

γ=HOP

To get the direction cosines in the CDH coordinate system (the reference from which the azimuth is measured), equations (4), (5) and (6) are rotated through the angle ε_{io} as follows:

$$\cos \alpha'_i = \cos \alpha_i \cos \varepsilon_{io} - \cos \beta_i \sin \varepsilon_{io} \quad (7)$$

$$\cos \beta'_i = \cos \alpha_i \sin \varepsilon_{io} + \cos \beta_i \cos \varepsilon_{io} \quad (8)$$

$$\cos \gamma'_i = \cos \gamma_i \quad (9)$$

where:

α'=COP

β'=DOP

γ'=HOP

And finally, the direction cosines with respect to a local East, North, Vertical coordinate system are given as follows:

$$\lambda'_{i1} = \cos \alpha'_i \cos \bar{A}_i + \cos \beta'_i \sin \bar{A}_i \quad (10)$$

$$\lambda'_{i2} = -\cos \alpha'_i \sin \bar{A}_i + \cos \beta'_i \cos \bar{A}_i \quad (11)$$

$$\lambda'_{i3} = \cos \gamma'_i \quad (12)$$

f. Once these local direction cosines are calculated for each station, they must be rotated to the same E-N-H coordinate system. This rotation is accomplished through the following set of equations:

$$\lambda_{i1} = \lambda'_{i1} - \lambda'_{i2} K_3 T_{i1} + \lambda'_{i3} + K_1 T_{i1} \quad (13)$$

$$\lambda_{i2} = \lambda'_{i1} K_3 T_{i1} + \lambda'_{i2} + \lambda'_{i3} K_1 T_{i2} \quad (14)$$

$$\lambda_{i3} = -\lambda'_{i1} K_2 T_{i1} - \lambda'_{i2} K_1 T_{i2} + \lambda'_{i3} \quad (15)$$

where:

K_1=Radians of latitude per foot northward at the origin

K_2=Radians longitude per foot westward at the origin times cosine latitude of the origin

K_3=K_2 times the tangent of the latitude of the origin

T_{ij}, j=1,2,3 represent the X, Y, and Z positions of the ith station relative to the origin

g. The space postion is computed by finding X_1, X_2, X_3 which minimizes the following functional:

$$J=\sum_{i=1}^{n} W_i \vec{e}_i \cdot \vec{e}_i \qquad (15)$$

where:

i=ith station

N=Number of stations

$\vec{e}_i$=ith error vector

W_i=Weight associated with the ith station

h. The error vector, $\vec{e}_i$, is determined as a function of X_1, X_2, X_3 with reference to figure 2.4-3.

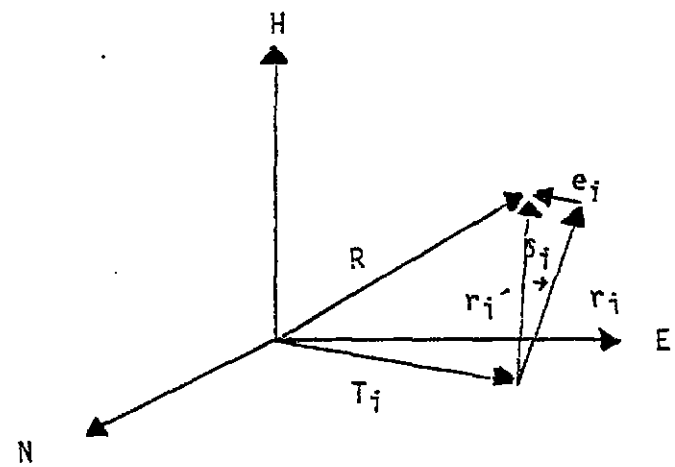

Figure 2.4-3 Error vector $\vec{e}_i$.

i. $\vec{R}$ is the vector from the origin to the solution point, T_i is the vector from the origin to the ith station, r_i is the vector from the ith station along the measured line of sight from that station, $\vec{r}_i'$ is the vector from the ith to the solution point, and $\vec{e}_i$, the error vector, is a perpendicular from the solution point to $\vec{r}_i \cdot e_i$ and is calculated as follows:

$$\vec{e}_i=\vec{r}_i'-\vec{r}_i \tag{17}$$

$$r_i'=\vec{R}-\vec{T} \tag{18}$$

$|r_i|=\vec{r}_i'\cdot\vec{\lambda}_i$, where $\vec{\lambda}_i$ is the unit vector along $\vec{r}_i$ (19)

Since $\vec{R}=(X_1,X_2,X_3)$ and the vectors $\vec{T}=(T_{i1},T_{i2},T_{i3})$ and $\vec{\lambda}_i=(\lambda_{i1},\lambda_{i2},\lambda_{i3})$ are known, $\vec{e}_i$ can be determined as a function of X_1, X_2, X_3 only. When the indicated operations are performed, $\vec{e}_i\cdot\vec{e}_i$ is easily obtained.

$$\vec{e}_i\cdot\vec{e}_i=(X_1-T_{i1})^2+(X_2-T_{i2})^2+(X_3-T_{i3})^2 - \left[(X_1-T_{i1})\lambda_{i1}+(X_2-T_{i2})\lambda_{i2}+(X_3-T_{i3})\lambda_{i3}\right]^2 \tag{20}$$

2. When equation (20) is substituted into equation (18), J is obtained as a function of (X_1,X_2,X_3) only. The solution to the minimization problem is obtained by finding the (X_1,X_2,X_3) which satisfies the following equation:

$$\frac{\partial j}{\partial X_i}=0 \qquad i=1,\ 2,\ 3 \tag{21}$$

The (X_1,X_2,X_3) which satisfies the three equations generated by equation (21) is the desired solution.

3. The weight, W_i, is usually taken to be the inverse of the distance from the station to the solution point.

$$W_i=\left[(X_1-T_{i1})^2+(X_2-T_{i2})^2+(X_3-T_{i3})^2\right]^{-\frac{1}{2}} \tag{22}$$

4. The solution is accomplished in two iterations; on the first, W_i is set equal to 1 and on the second, W_i is computed from equation (22) using the (X_1,X_2,X_3) obtained on the first iteration.

5. On the second iteration, a refraction correction is made to the elevation angle. This correction is given by

$$\Delta E_i = f(H, E_i, X_1, X_2, X_3) \tag{23}$$

where the indicated function is empirical in nature and may be found in item 1 in the Bibliography.

6. The solution (X_1, X_2, X_3) represents the best space position solution based on measurements recorded from N theodolite stations; however, the measurements obtained from one of these stations may be in error. Accordingly, the solution is not accurate with the inclusion of these measurements in the computation. As a result, a rejection criterion is used to eliminate bad measurements from the solution.

i. The first step in this rejection scheme is the calculation of the error angle, δ_i, for each station. Again referring to figure 2.4-3, δ_i would be the angle between r_i' and r_i and is given by

$$\delta_i = \sin^{-1} \frac{\left|\vec{e}_i\right|}{\left|\vec{r}_i'\right|} \tag{24}$$

which for small angles reduces to

$$\delta_i = \frac{\left|\vec{e}_i\right|}{\left|r_i'\right|} \tag{25}$$

$$= \frac{\left(\vec{e}_i \cdot \vec{e}_i\right)^{1/2}}{\left(\vec{r}_i' \cdot \vec{r}_i'\right)^{1/2}} \quad \text{in radius}$$

1. This computation is easily effected using equations (18) and (20). The criteria for an acceptable solution is as follows:

$\delta_i \leq 3'$ for 4- or more station solution

$\delta_i \leq 2'$ for a 3-station solution

$\delta_i \leq 1'$ for a 2-station solution

2. If this error criterion is not satisfied, the rejection criterion is used to determine which station is to be eliminated from the solution. This is determined with reference to figure 2.4-4.

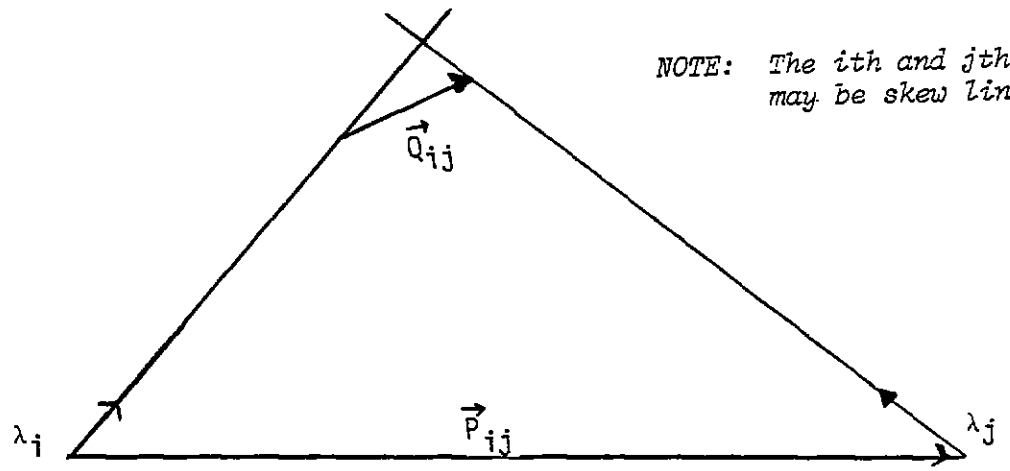

Figure 2.4-4 Station eliminator determinant.

Let $\vec{P}_{ij}$ be the vector from station i to station j

$$\vec{P}_{ij}=(T_{1j}-T_{1i},\ T_{2j}-T_{2i},\ T_{3j}-T_{3i}).$$

Let Q_{ij} be the vector which is the common perpendicular to the ith and jth rays, $\vec{\lambda}_i$ and $\vec{\lambda}_j$ from the ith and jth stations ($\vec{\lambda}_i$ and $\vec{\lambda}_j$ are unit vectors). The unit vector along $\vec{P}_{ij}$ is given by

$$Q_{ij}=\frac{\vec{\lambda}_i X \vec{\lambda}_j}{|\vec{\lambda}_i X \vec{\lambda}_j|}$$

The sums

$$S(k)=\sum_{i=1}^{N}\sum_{j=1}^{N}|p_{ij}|,\ i\neq k,\ j\neq k,\ i<j$$

are calculated.

3. The value of k, from which S(k) is a minimum, is the station number to be rejected. The computation is then performed without the measurements from the kth station.

j. When a theodolite system is used in computing miss distance, the missile, bomb or projectile is simply tracked from launch, or release, to impact. The position of the target is known with respect to the origin. Hence, the miss distance is computed from the distance between the coordinates of the impact point and the target. The position data along the trajectory are usually smoothed to take out random errors before this computation is made.

2.4.3 Accuracy

For a typical theodolite solution using at least three stations, good geometry accuracies in the order of 1 to 5 ft can be expected.

2.4.4 Advantage

The advantage of a good theodolite system is its accuracy. Because of this accuracy, theodolites are often used to calibrate other space position measuring systems.

2.4.5 Disadvantage

The main disadvantage is the amount of work required in setting up the data as input to a theodolite reduction program. When tracking corrections are to be applied, the tracking errors must be read from film at each time slice for which a space position is to be computed.

BIBLIOGRAPHY

1. Criss, R. F. and Jehn, L. A. *A FORTRAN IV Computer Program for the Maximum Likelihood Solution to Theodolite Data.* Dayton, Ohio: University of Dayton Research Institute, March 1965.

2. McAnelly, L. J. *Computation of Constants Used in the Solution of Theodolite Data.* Dayton, Ohio: University of Dayton Research Institute, January 1966.

2.5 AN IMPACT LOCATION SYSTEM USING SEISMIC DETECTION TECHNIQUES

2.5.1 General

A seismic detection system for locating the impact points of 8-in and 155-mm projectiles has been developed by Sandia Laboratories and installed at Tonopah Test Range (TTR). The system uses an array of 33 geophones, with each geophone reporting via an RF link to a central location where the shock signature time-of-arrival information from the impacting projectile is displayed. The time-of-arrival differences are used to plot the impact location relative to the geophone array. A simple mechanical computer has been designed to assist in plotting the data. With geophones spaced 2500 ft apart, operations at TTR indicate a system accuracy of around 12 percent, or approximately 300 ft.

2.5.2 Scope

a. A considerable number of test rounds has been fired at TTR to develop telemetry packages which can measure component performance under actual firing conditions and to test the components themselves. A parachute recovery system was developed so that the projectiles can be recovered without damage. The rounds are fired at an elevation angle of 87.5°, with muzzle velocities around 2700 ft/s. Apogees have ranged up to 70,000 ft, with ground ranges between 6,000 and 10,000 ft for unretarded rounds. If a soft landing is required, a parachute is deployed at apogee and impact velocity is around 100 ft/s with a downtime of about 400 s.

b. Radar tracks the projectile and provides trajectory data, acquisition and refocussing information for tracking cameras, and an impact location. An unretarded round drills a hole about 6-ft deep with very little cratering. Although the impact area at TTR is desert terrain with sparse vegetation, a hole made by a projectile is surprisingly hard to find unless its location is precisely known.

c. Radar can normally guide a recovery party to within about 30 ft of an impact so that locating the hole is easy. Unfortunately, because of ground clutter, the TTR radars must acquire a round as it passes through a "window" which may be as much as 13,000 ft above the muzzle. As the round passes through the window, the radar operator has less than a second to acquire and begin automatic tracking. If the projectile does not follow its predicted trajectory, because of structural failure for example, it may not be acquired by radar and its impact location will not be precisely known. If structural failure disturbs the projectile aerodynamics enough so that it misses the radar window, its impact point is very difficult for ground parties to find. Classified components and/or radioactive material inside certain units make their recovery mandatory, regardless of the time and personnel required for the search.

d. Although, statistically, the radar tracking record was excellent, a decision was made to develop and install a backup impact locating system which would be independent of radar and provide reasonably accurate, quick-look data over a target area large enough to handle trajectory anomalies. The system was to use available hardware wherever possible and was to be capable of operation and maintenance by as few people as possible.

e. A portable impact locating system using seismic detectors or geophones was developed in 1969 to determine the location of 81-mm mortar shell impacts. Although designed to cover a much smaller target area than that required at TTR, the portable system has demonstrated the practicality of using geophones. It also provided some very useful experience in data reduction techniques. It was used in New Mexico, Texas and the Panamanian jungle and turned out to be quite useful for zeroing in the weapon on the target in addition to enabling the location and recovery of every unit fired. The system presently installed at TTR is based directly on this prototype, although the hardware is more sophisticated and the area of coverage considerably larger.

2.5.3 Theory

a. In the system described in this section, the time of arrival of the shock wave at each detector location is recorded and the differences in time of arrival are measured. If the wave propogation velocity through the medium is known, the source of the disturbance can be located using hyperbolic positioning techniques similar to loran.

b. In figure 2.5-1, point P is a noise source, such as an impact. Points A, B and C represent the locations of seismic detectors or geophones. Let the time of arrival of the shock wave at the detectors be T_A, T_B and T_C. The differences in arrival times, using T_A as the initial reference, are T_B-T_A and T_C-T_A. If the wave progagation velocity, V, in the medium is known, the time differences may be converted to distance differences between point P and points A, B and C.

$$PB-PA=V(T_B-T_A)$$

and

$$PC-PA=V(T_C-T_A)$$

An infinite number of possible points P corresponds to a given value of PB-PA. A hyperbola can be defined as the locus of a point which moves so that the difference of its distances (PB-PA) from two fixed points (A and B) is a constant. Hence, all points having the same value of PB-PA must lie on a hyperbola having foci A and B. Further, a family of hyperbolas having common foci A and B can be constructed, each hyperbola representing a different value of PB-PA. Thus, a measurement of the time difference of arrival of a shock pulse at two geophones does not determine a source location, but defines a hyperbola, any point on which will satisfy the measured conditions.

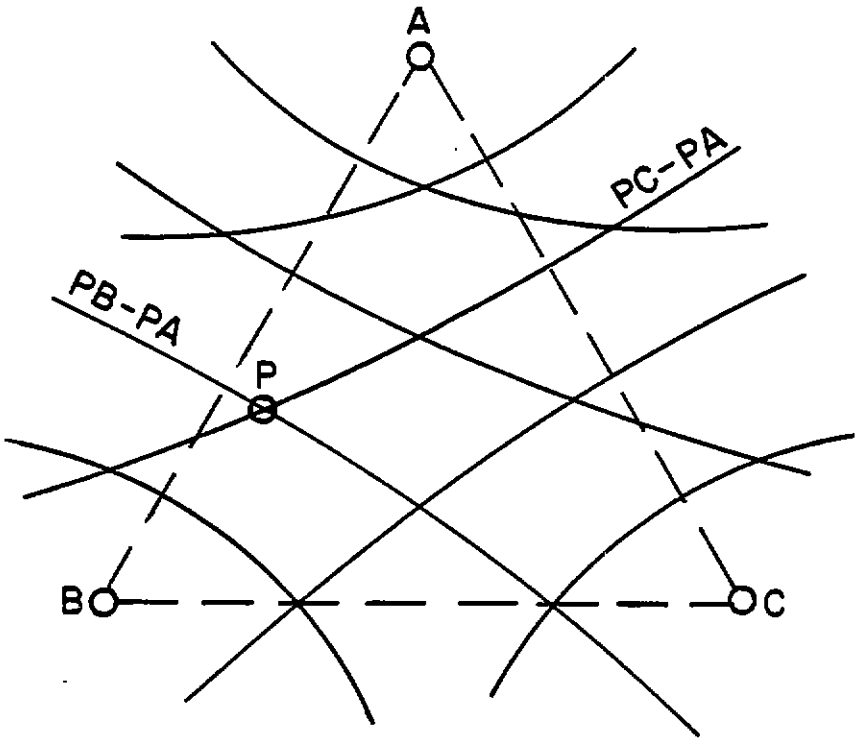

Figure 2.5-1 Noise source, geophone locations, and hyperbolas determining source location.

c. A second pair of geophones, A and C for example, may be used to define a second set of hyperbolas with their corresponding values of PC-PA. The actual location of a noise source relative to A, B and C is determined by the intersection of the hyperbolas representing measured values of PB-PA and PC-PA. A value of PC-PB may be calculated which defines a third hyperbola intersecting the others at the common point P. The accuracy is highest where the hyperbolas cross at right angles and decreases as the crossing angle becomes smaller. Hence, a point in the center of a three-geophone triangle may, in general, be located to a higher degree of accuracy than a point which falls outside the triangle. More detailed information is contained in subparagraph 2.5.7.

2.5.4 Hardware

a. The TTR system consists of a number of seismic detectors or geophones, each transmitting data via its own RF link to a central receiving site for processing and display. The geophones, transmitters and receivers had been developed for applications in Southeast Asia and were modified for use at TTR.

b. The geophones are emplaced in a 33-element array as shown in figure 2.5-2. They are arranged in equilateral triangles with 2500-ft sides. A projectile following a nominal, nonretarded trajectory will impact near the firing azimuth about 10,000 ft from the gun. Projectiles which have failed structurally may follow a perturbed trajectory but should still impact within the array area.

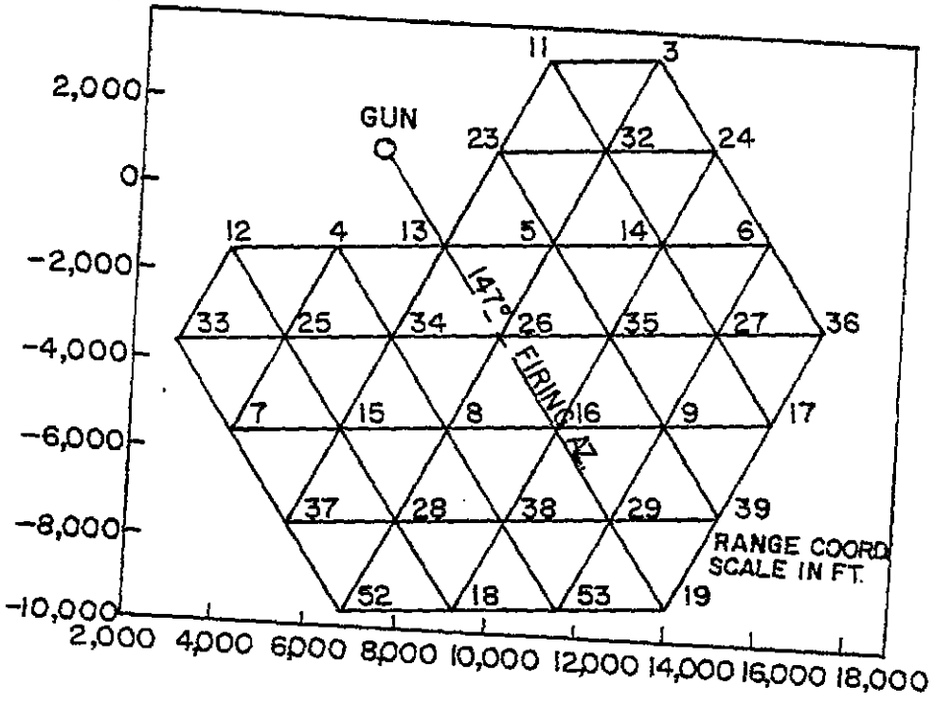

Figure 2.5-2 Impact location system sensor array - TTR.

c. The geophones are small, inexpensive, self-generating, seismic detectors with a natural frequency of around 14 Hz. An electrical impulse corresponding to a seismic shock wave is generated by the geophone and applied to a threshold detector which is set to discriminate against background noise produced by wind, etc. The detected signal is then amplified and used to trigger a 2-W VHF-FM transmitter. The geophone is buried 30 ft below the surface and connected by cable with the transmitter, which is buried so that only the antenna protrudes above the surface. Power is supplied by a 13-A hour nonrechargeable battery. When actuated by a signal from the geophone, the transmitter sends a digitally coded burst of RF about 8 ms in duration. After sending its RF burst, the transmitter is inhibited for 10 s. Under conditions of continuous siesmic excitation, the maximum data rate is one data point every 10 s. The inhibit circuit reduces battery drain to the point that the transmitters can operate unattended on an around-the-clock basis.

The TTR array has been in operation since it was installed in 1972. The 33 transmitters operate on 4 RF frequencies in the 164-174 MHz region. Each transmitter is identified by a combination of digital code and RF frequency.

d. At the receiving site, which is the Range Operations Center, an RF preamplifier feeds four receivers (figure 2.5-3). Each reciever in turn feeds a set of decoder/display units. Each decoder is tuned to its own geophone by a combination of RF frequency and digital code. An internal 1-kHz clock is counted by a counter which resets itself every 9999 ms. It can also be manually reset by a front panel switch at any time. When a geophone detects a seismic shock wave, it transmits its coded RF signal to the Range Control Center where it is received and decoded. The decoder strobes the accumulated count into its corresponding display which holds it until manually cleared. The counter continues to count and its contents are strobed into the other displays by their decoders as the wave is detected by their geophones. The relative time of arrival of the shock wave at the various geophones in the array is thus represented by the counter readings on the displays.

2.5.5 Operating Procedure

The system is operated as follows:

a. Apply power to the receiver-decoder/display unit. As previously stated, the transmitters are always on.

b. Clear all displays and reset the counter a few seconds before firing time.

NOTE

The acoustic wave generated by the firing of the gun activates each display in sequency as it ripples across the array. This provides a good check on the perfomance of each sensor in the array.

c. Again reset the displays and counter after the muzzle blast has activated the farthest sensor.

NOTE

When the projectile impacts, the shock wave activates the geophones in the immediate area. A nonretarded projectile may activate six or eight geophones versus three or four for a parachute retarded unit.

d. After the impact, which can be recognized by a sudden sequential activation of a number of displays, use an inhibit switch to block further incoming signals and prevent spurious noise from activating other displays and confusing the issue.

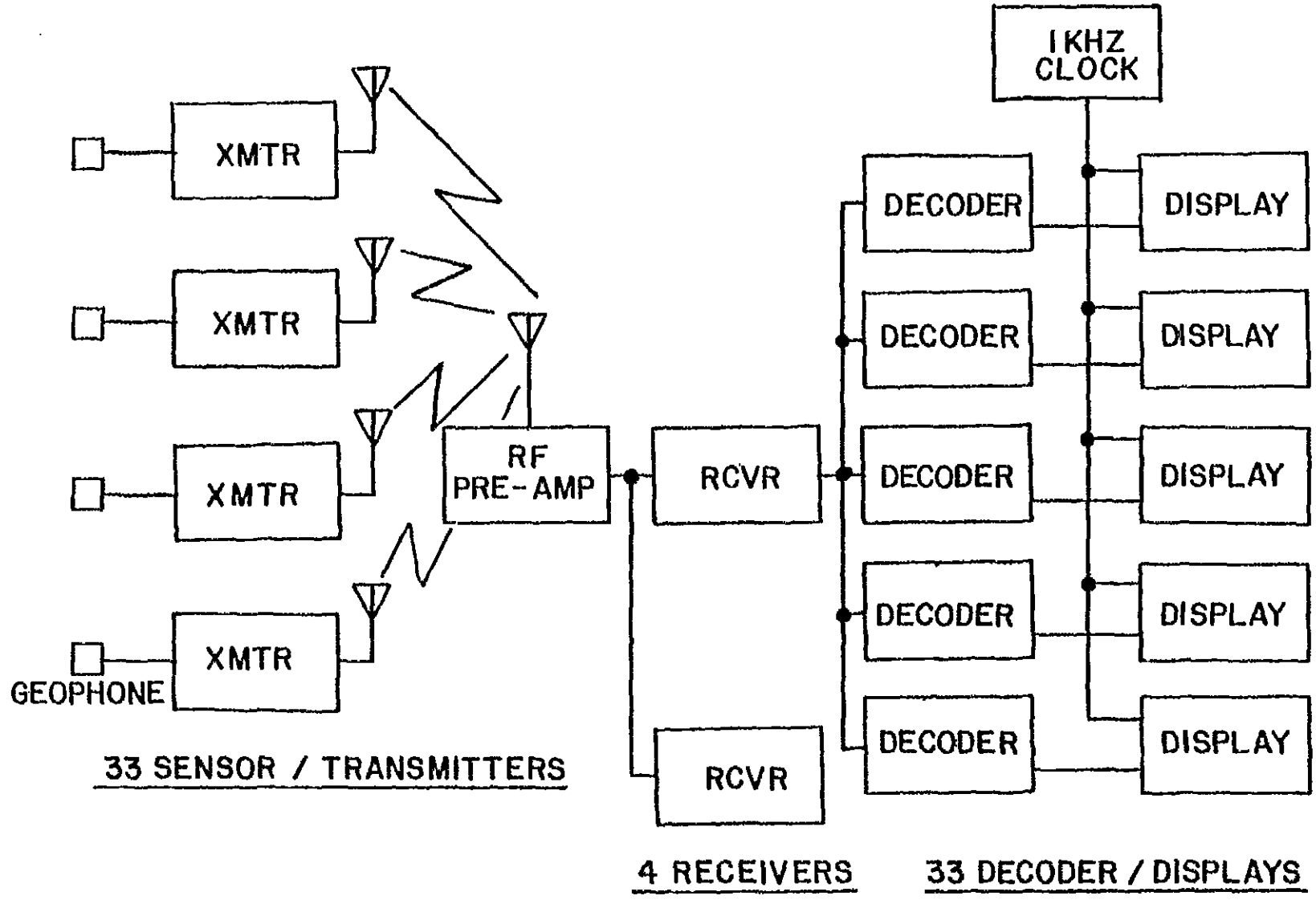

Figure 2.5-3 Range Control Center.

e. Record the times of arrival and use them to plot the impact location as described in subparagraph 2.5.6.

2.5.6 Data Reduction and Plotting

a. A mechanical plotter has been devised which enables rapid plotting of an impact location without elaborate computation. The plotter uses lengths of string to represent the time-distance variables. It was first used to predict bottom locations of water entry test vehicles with a hydrophone array providing the impact data.

b. The plotting board for the system is a piece of plexiglass upon which the geophone array is laid out using a scale factor of 250 ft/in. This scale factor is used because it makes the layout a convenient size. To plot impact location:

1. Drill a small hole through the board at each geophone location.

2. Tie together three pieces of cord at one end, p, and cut the other ends (a, b and c) so that the lengths ap, bp and cp are equal (figure 2.5-4).

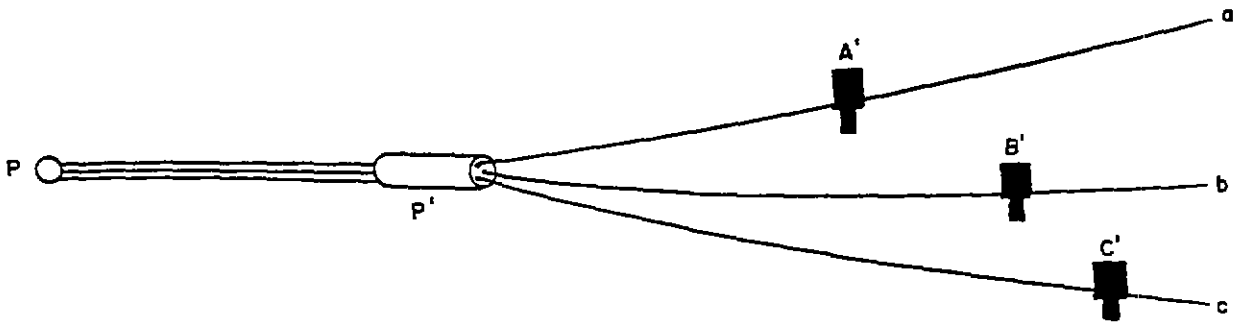

Figure 2.5-4 String computer.

3. Pass the free ends of the strings through a small collar, P', whose inside diameter is just large enough to allow it to slide easily along the strings. (Ordinary binding posts A', B' and C' are placed on the strings so that the lengths A'p, B'p and C'p can be easily varied.)

NOTE

The method using the string computer is best illustrated by an example. Assume that an impact has occurred and the displays show the times of arrival, T, at the various geophones. Further assume that the signal was received by geophones A, B and C, in that order, with typical values as follows:

A=3375 ms
B=3390 ms
C=3430 ms

therefore:

$T_B - T_A = 15$ *ms*

$T_C - T_A = 55$ *ms*

From a previous calibration, the shock wave velocity, V, is known to be 6000 ft/s.

Then

$$PB-PA=V(T_B-T_A)=6000x0.015=90ft$$

and

$$PC-PA-V(T_C-T_A)=6000x0.055=330ft$$

4. When converted to the scale of the plotting board, PB-PA= 0.36 inch and PC-PA=1.32 inches. Position the binding posts along the strings so that PB'-PA'=0.36 inch and PC'-PA'=1.32 inches. It can be seen that P'B'-P'A'=PB'-PA' and P'C'-P'A'=PC'-PA' for any position of the collar P', as long as there is no slack in the string.

5. Insert binding posts A', B' and C' into the corresponding holes in the plotting boards at the locations of geophones A, B and C. While tension is kept on point p, the collar P' is moved along the strings until it reaches the one position where all the strings are taut. This point is the impact location P. (See figure 2.5-5)

c. Consider only strings from points A' and B'. The collar P', as it slides along the two strings, traces a hyperbola, each point P of which satisfies the condition that PB-PA=0.36 inch on the plotting board scale. The actual impact point lies somewhere on this curve. If strings from A and C are taken by themselves, the collar P' traces another hyperbolic curve, each point P of which satisfies the condition that PC-PA=1.32 inch. Strings from B and C define the hyperbola corresponding to PC-PB. The use of three strings automatically plots the intersection of all three hyperbolas.

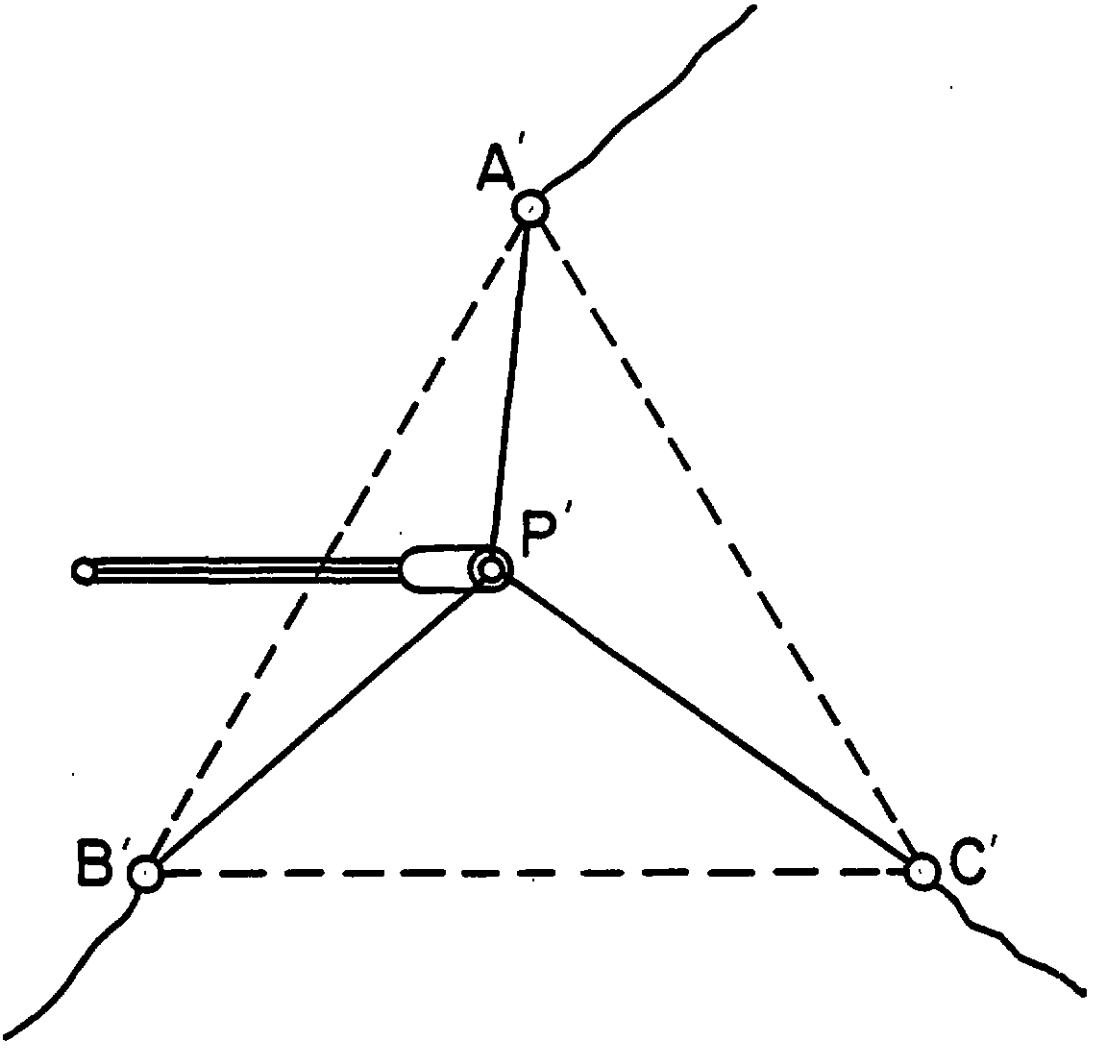

Figure 2.5-5 Impact location using string computer.

d. In practice, it has been convenient to set up a scale on the plotting board to convert time differences in milliseconds to distance differences in inches so that adjustments of string lengths may be made without computations. Since pa=pb=pc, the segment A'a may be held constant and the segments B'p and C'p lengthened relative to A'p by shortening B'b and C'c (figure 2.5-4).

e. Data from more than three geophones at a time can be used to plot an impact location, but working with more than three strings on the plotting board is not convenient. It is easier to plot successive locations using different combinations of three geophones.

2.5.7 Accuracy

a. The system accuracy depends on the measurement of the shock wave arrival time, geophone survey accuracy, the location of the impact relative to the array, and the determination of the wave propagation velocity in the target area. The accuracy obtainable also varies with terrain, unit size, impact velocity, and background noise. The arrival-time measurement depends on the rise time of the shock pulse, which has a basic frequency of around 20 Hz.

b. The threshold detector in the detector circuitry is adjusted to discriminate between low-level background noise and the shock wave made by an impacting object. Since both the amplitude and the frequency of a seismic wave decrease with distance from the source, the time error due to the threshold detector increases with distance. The time error, as shown in the note following subparagraph 2.5.6 b.(3), is less of a problem than the seismic wave propagation velocity, which must be accurately determined if consistent data are to be expected. In theory, to measure seismic wave velocity in the target area, a shock wave is generated at a known location within the geophone array and the times of arrival recorded. The distance between the source and the various geophones is accurately measured, the difference in distances calculated, and the shock wave velocity computed. In practice, however, it has been difficult to generate a high amplitude shock wave without dropping an object a considerable distance, such as from an airplane. Even then, only the closest geophones will be activated.

c. Calibration of a small mortar array was more practically accomplished by measuring the actual impact location of the first one or two rounds of a series. An approximation of the impact location was made using an estimated shock wave velocity for the first few rounds, until a physical location and measurement could be obtained.

d. Alternatively, one can start with an estimated velocity. By performing a number of plots using a different set of geophones each time and varying this estimated velocity, a shock wave velocity which produces the smallest dispersion of plotted locations can be obtained.

e. Unfortunately, the seismic wave propagation velocity over the array area is not a constant. The layers of dirt, sand, gravel, and other discontinuities cause the wave velocity to vary over a wide range of values. A wave front may propagate almost twice as fast in one direction as in another and its velocity in a given direction may vary with distance from the source. Experience has shown that the most accurate impact location is obtained by using data from five or six geophones and using several trial velocities. An impact point is plotted for each set of three geophones and each velocity. By using this iterative process, an average velocity can be found which will give the smallest grouping. The actual impact location is assumed to be at the centroid of the group. Obviously-erratic data points can be recognized and eliminated. Although this seems like a complicated procedure, an operator can plot a location in less than 20 min.

f. The error factors due to station configuration are shown in figures 2.5-6 through 2.5-13 for three- and four-station solutions. The error factor is defined as the ratio of the probable error in impact-position determination to the probable error in the range-difference measurements. The error in range-difference measurements is the vector sum of the station location error, time error multiplied by the propagation velocity, and the propagation velocity error multiplied by the difference in arrival times at the various geophones. The probable error for an impact location is then calculated by multiplying the error factor, read from the appropriate plot, by the aforementioned errors. Rather than a long derivation, the following typical example is given:

1. Assume station configuration as shown in figure 2.5-7.

2. Object impacts halfway between the top station and the middle station (error factor equals 1.8).

3. Velocity of shock wave propagation equals 6000 ft/s.

4. Emplacement error equals 2 ft.

5. Arrival-time error equals 0.010 s (approximately 1/4-cycle error assuming a 20-Hz basic frequency).

6. Propagation velocity error equals 10 percent.

7. Average time difference equals approximately 250 ms.

The probable error, E_i, of the impact location is then:

$$E_i=(e.f.)\sqrt{(S_e)^2+\left[(\Delta t_e)(C)\right]^2+\left[(C_e)(C)(\overline{\Delta t})\right]^2}$$

e.f.=Error factor S

S_e=Emplacement error

ΔT_e=Arrival time error

C=Propagation velocity

C_e=Propagation velocity error

$\overline{\Delta T}$=Average time difference between arrival of shock wave at the various stations

$$E_i=1.8\sqrt{2^2+[(.010)(6000)]^2+[(.10)(6000)(.250)]^2}$$

$$E_i=1.8\sqrt{4+3600+22500}$$

$$E_i=(1.8)(162)=291 \text{ ft}$$

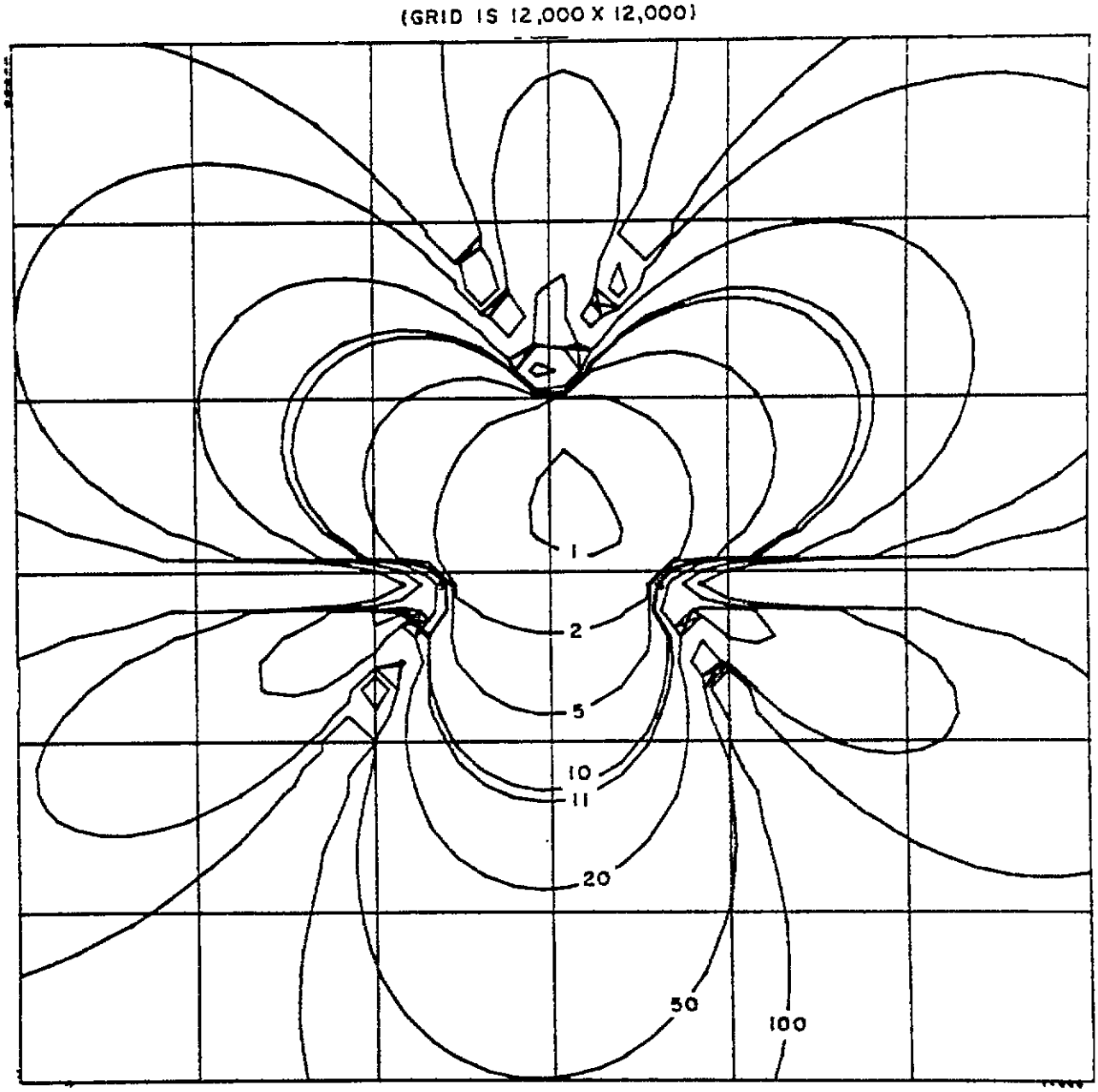

Figure 2.5-6 Error factor contour plot.

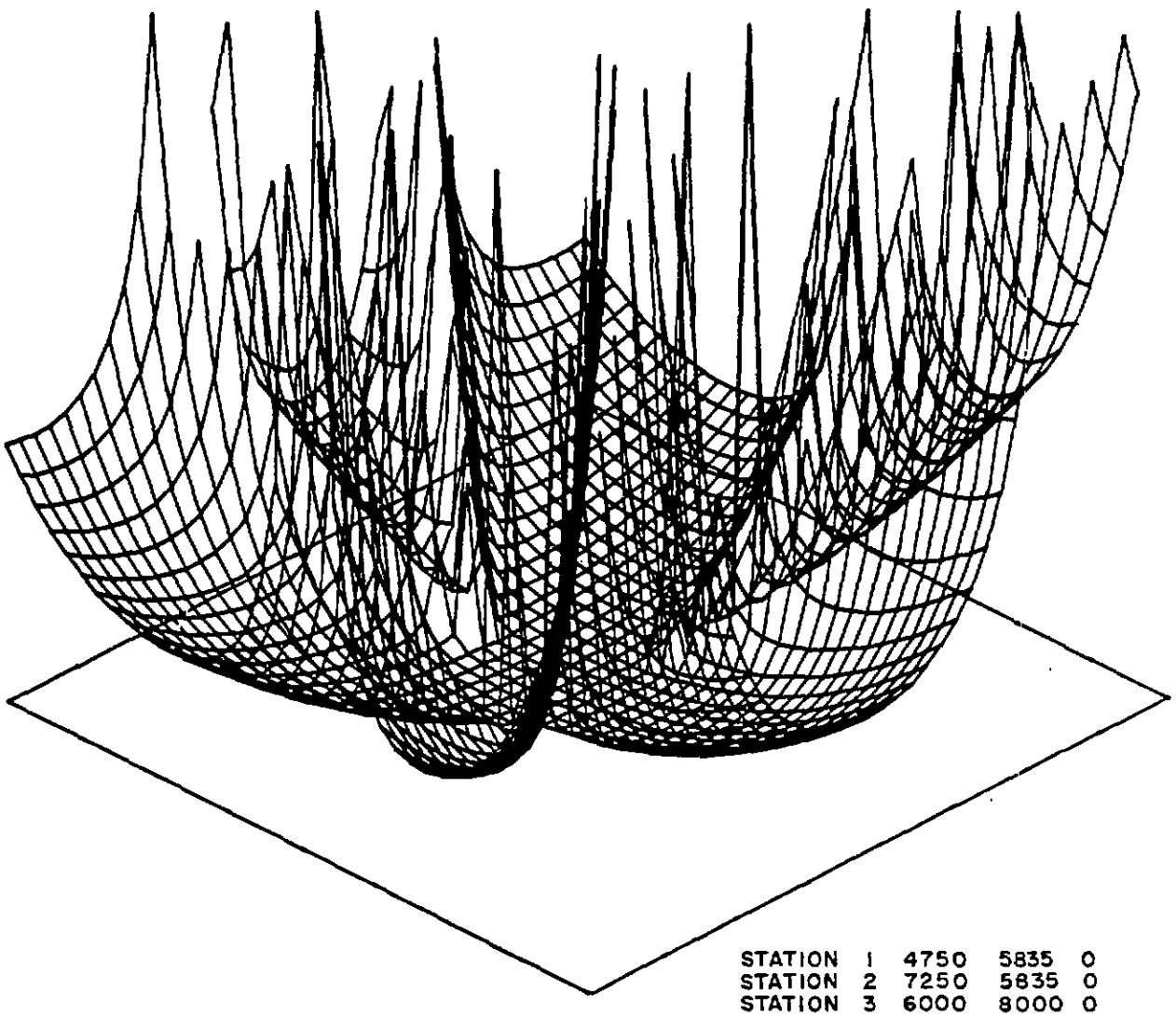

Figure 2.5-7 3-D error factor plot.

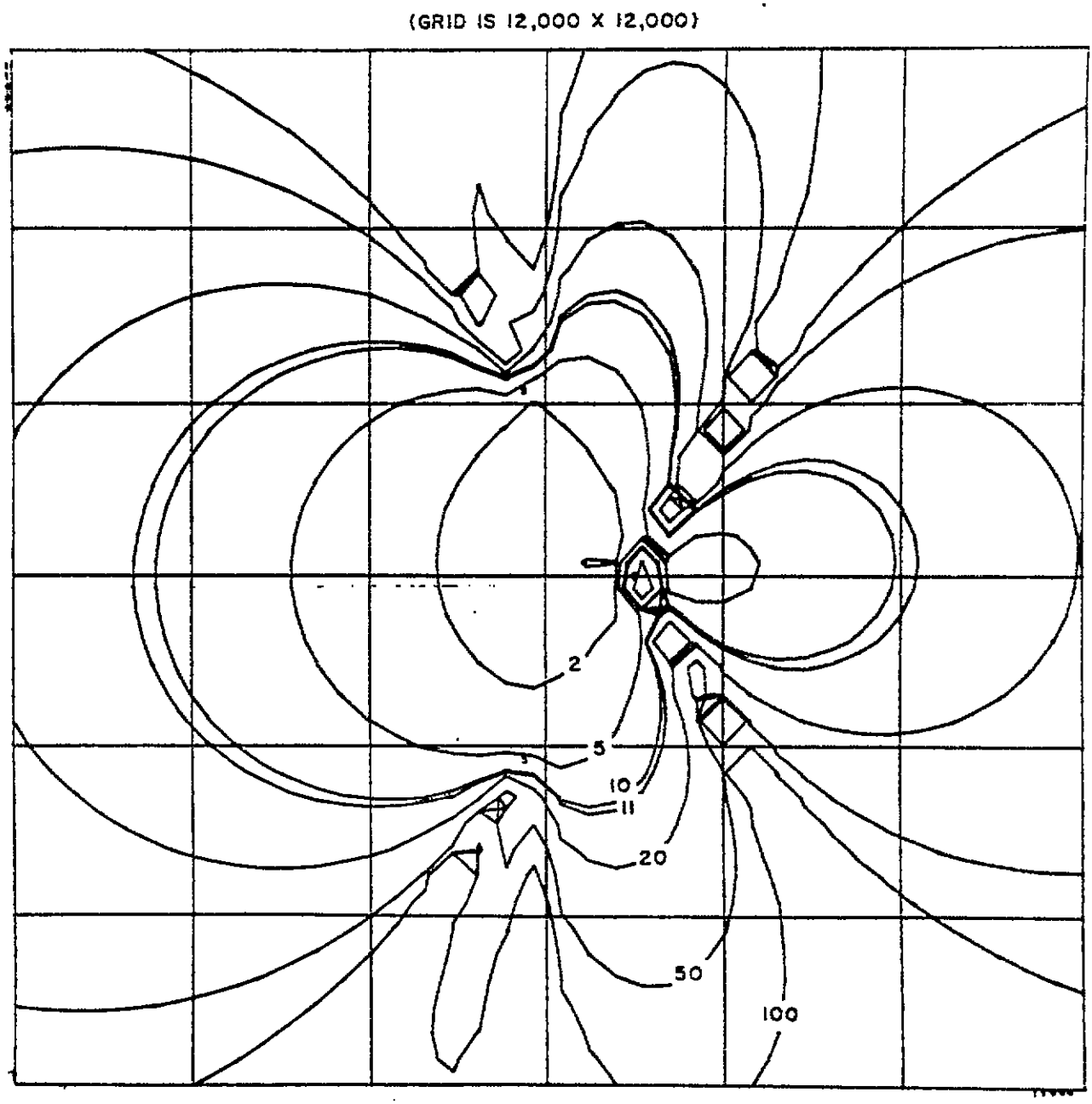

Figure 2.5-8 Error factor contour plot.

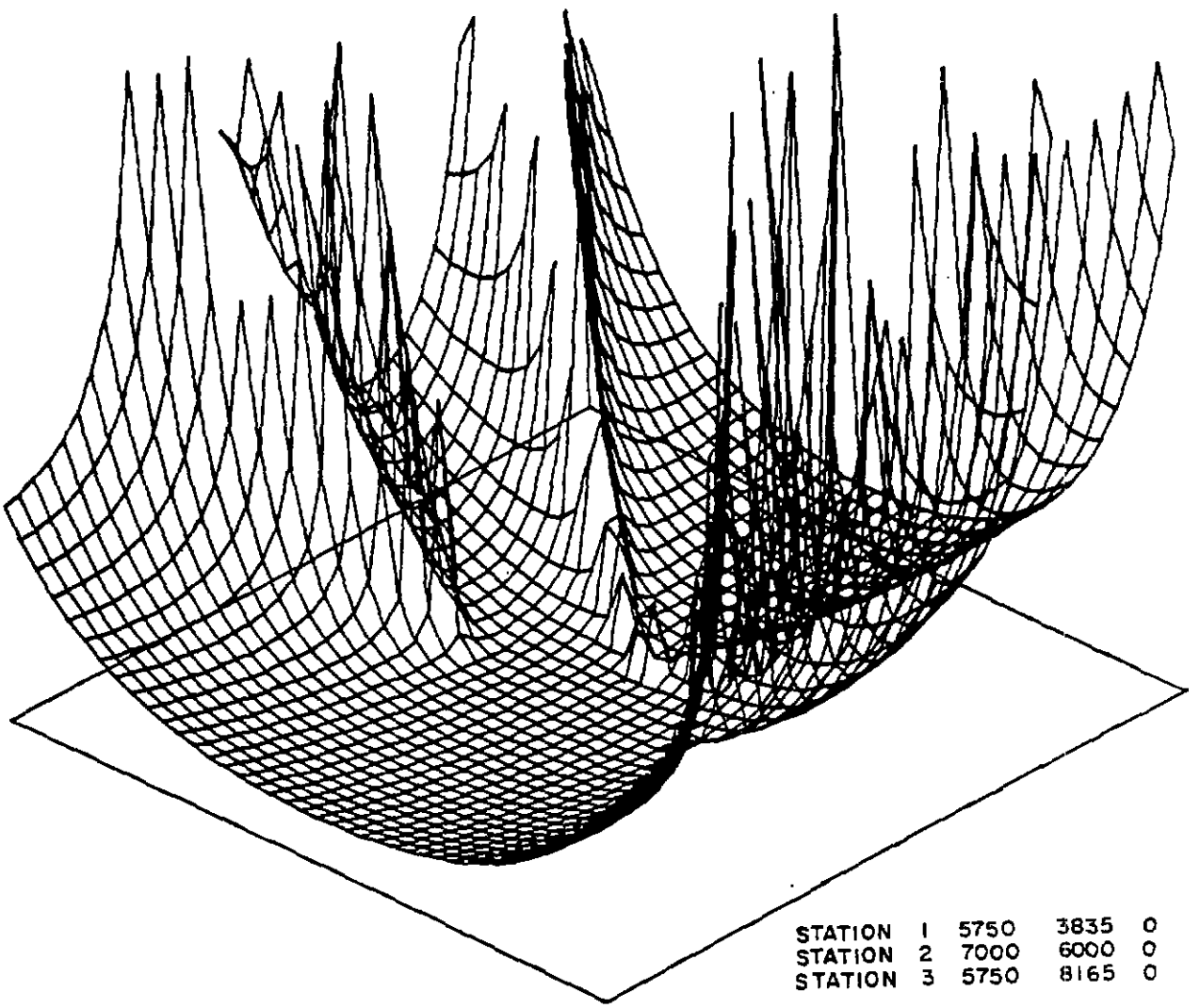

Figure 2.5-9 3-D error factor plot.

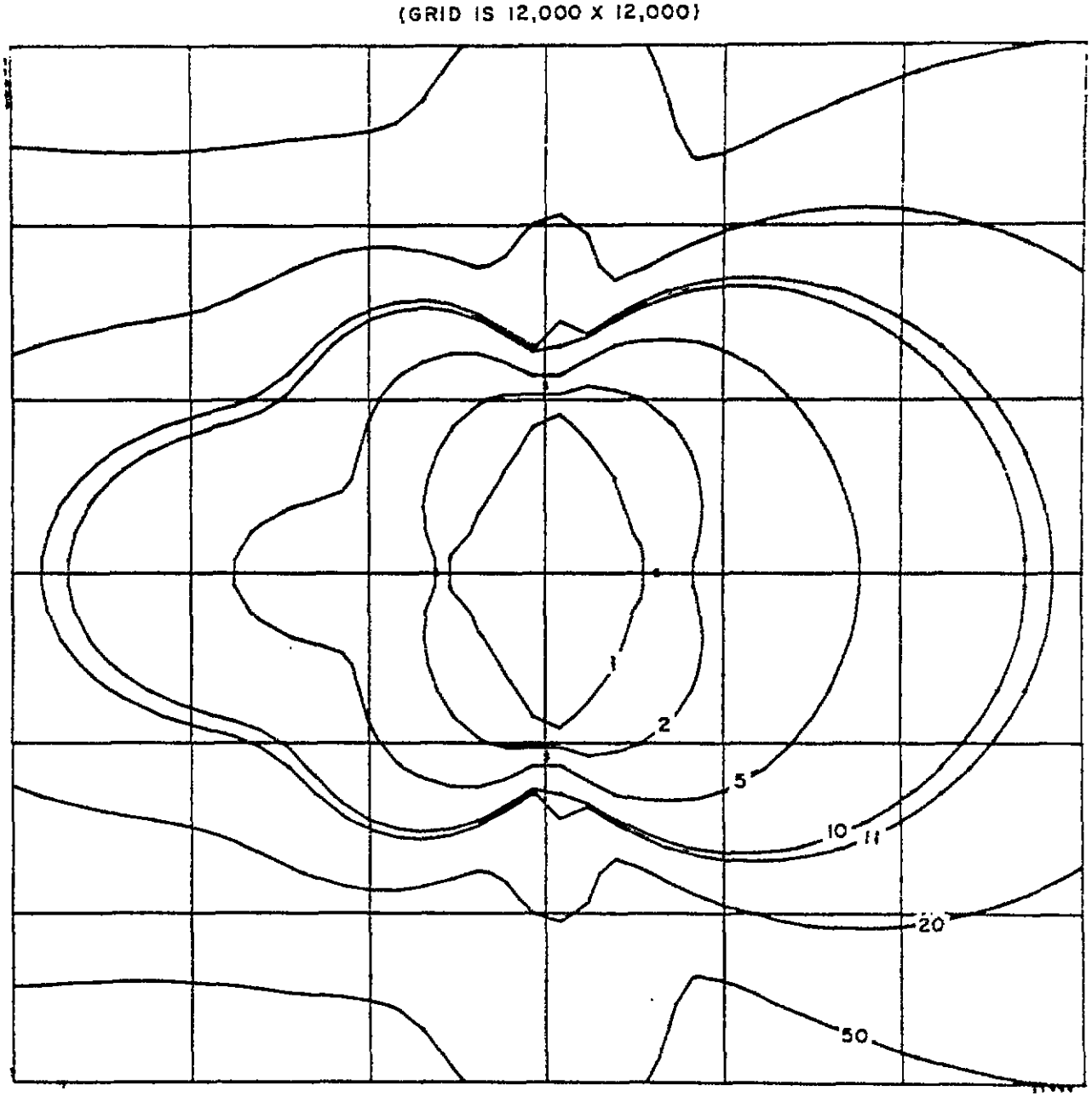

Figure 2.5-10 Error factor contour plot.

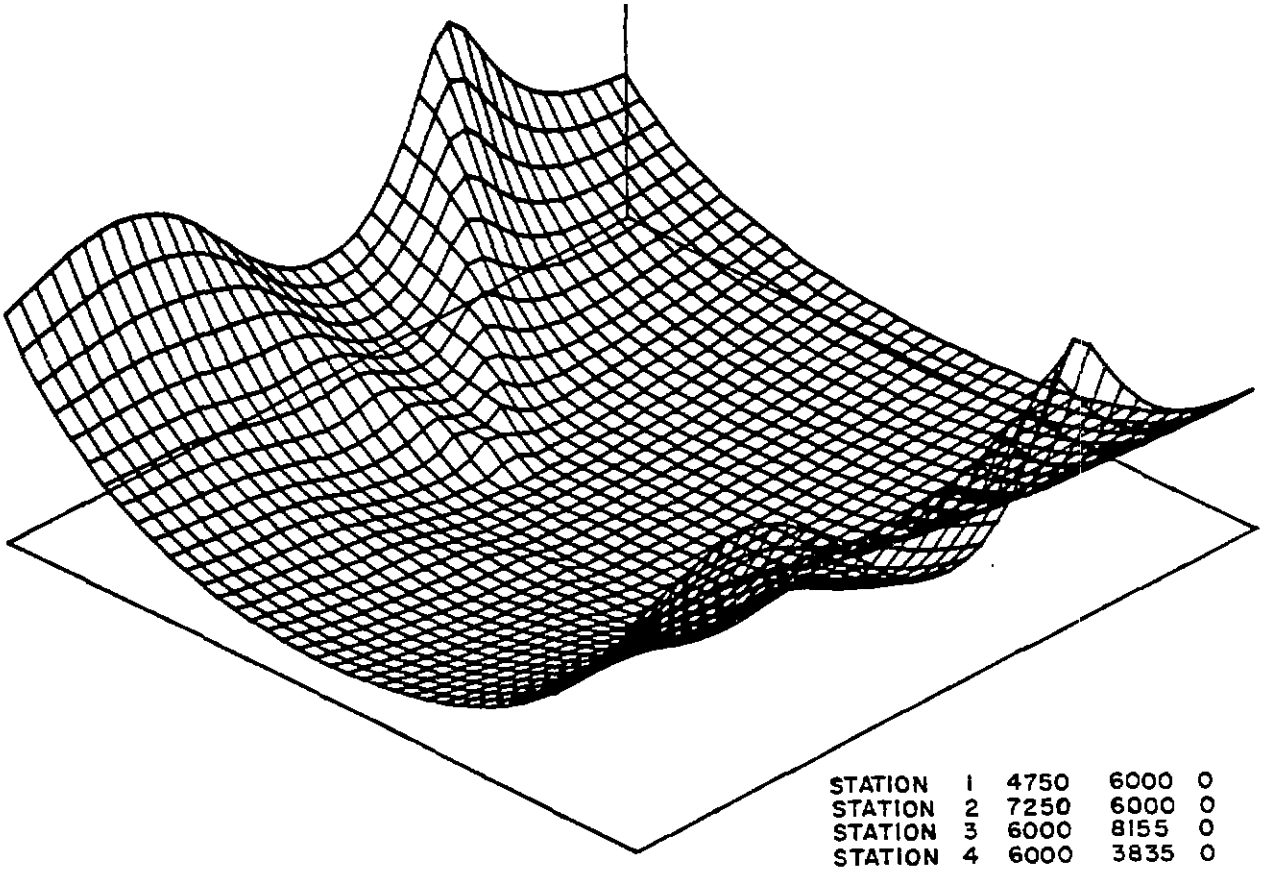

Figure 2.5-11 3-D error factor plot.

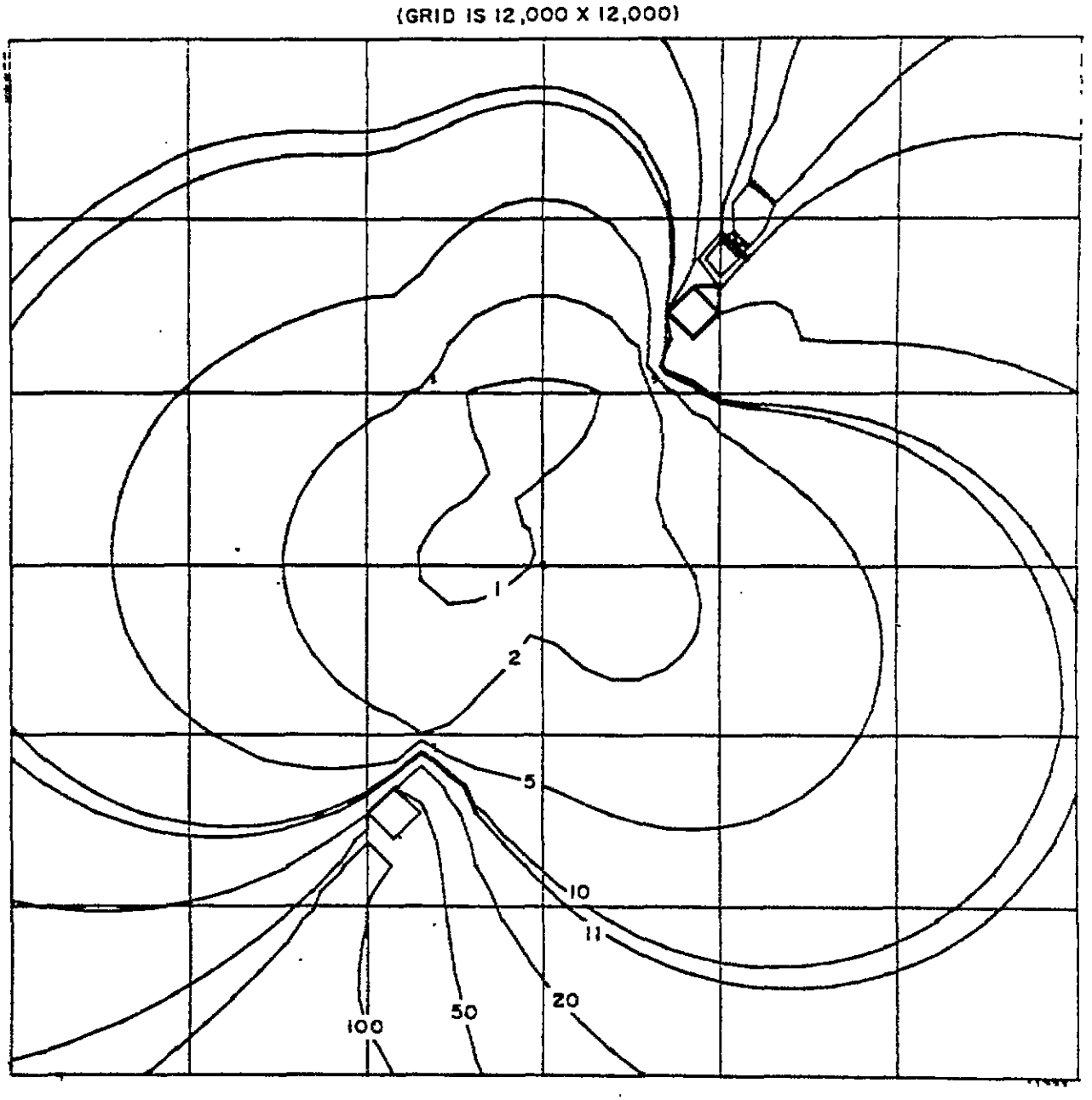

Figure 2.5-12 Error factor contour plot.

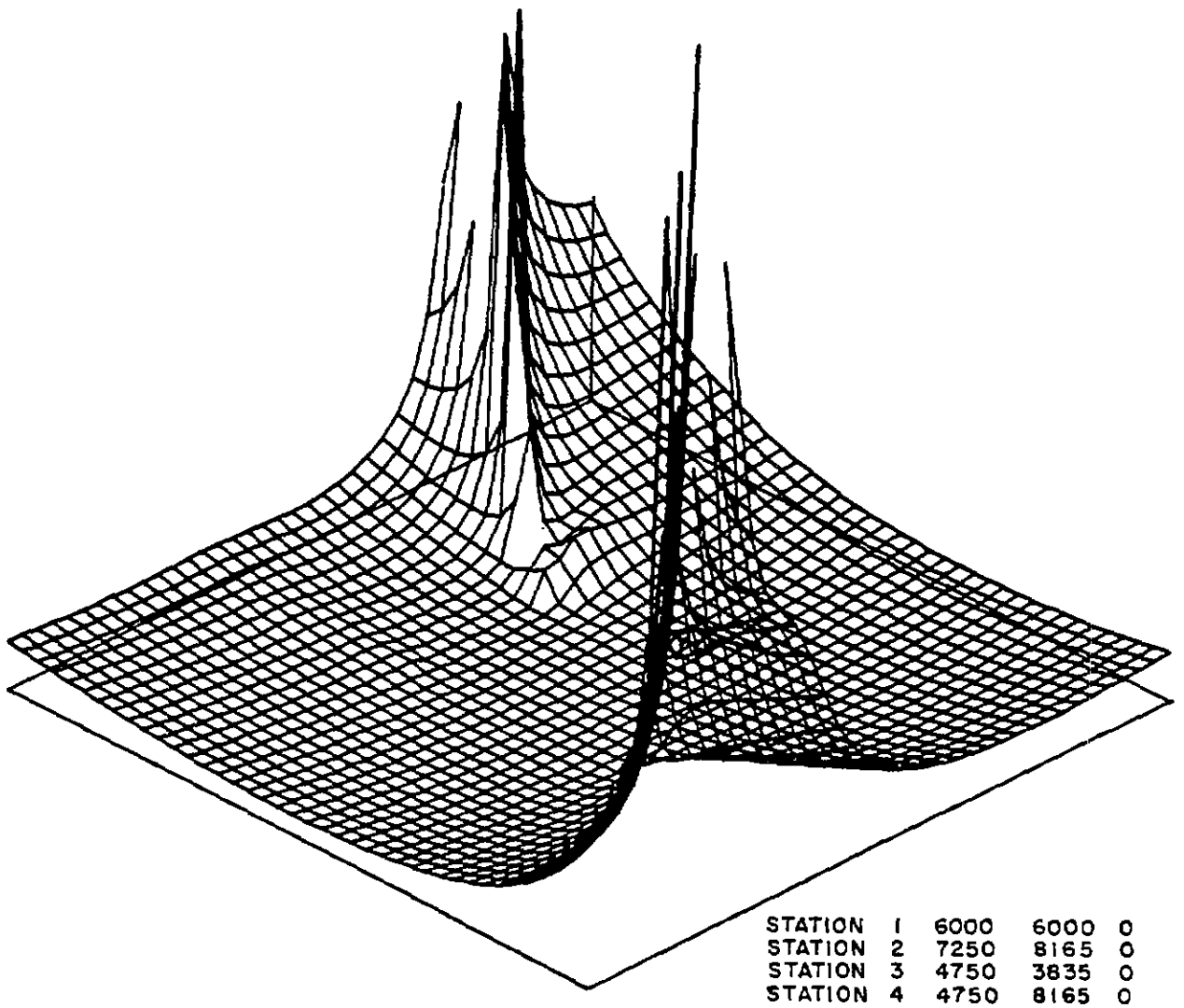

Figure 2.5-13 3-D error factor plot.

g. The difference between the plotted location and the actual impact point as it is measured by radar is generally within 300 ft. This accuracy is quite acceptable for recovery purposes when the primary consideration is the guidance of a ground party to the general impact vicinity.

2.5.8 Point of Contact

Code 9424
Sandia Laboratories
Albuquerque, NM 87115
Phone: (505) 264-8982
AUTOVON: 964-8982

2.6 ACCURACY TRANSDUCER SYSTEM (ATS)

2.6.1 General Description

a. The Accuracy Transducer System (ATS) is an automatic target scoring system designed for long-range, outdoor use employing large targets. Patented rod sensors completely enclose the target area and detect the shock wave created by the passage of a supersonic bullet. Electrical pulses generated by the rod sensors are processed, and the position of the bullet relative to the target center (of the sensor area) is automatically computed. The X-Y coordinate data generated by the ATS is automatically referenced to the center of the sensor area. By accurately positioning a paper target within the sensor area, the hit position of the bullet on a target is determined.

b. The ATS-432 is designed as a general-purpose scoring system for a variety of scoring applications. The system provides outputs to interface with a computer and has built-in displays (LED and printer) for use as a stand-alone system. The ATS-432 is capable of scoring single shots or high-rate bursts (6,000 shots per minute) and has built-in storage for as many as 512 shots. Equally important, the ATS-432 is able to score four sensor rods simultaneously or to select any pair of rods as the scoring rods. The four-rod scoring capability allows either redundant data to be collected (four-rod target: 2X, 2Y) or two independent targets (two-rod target: 1X, 1Y) to be scored through a single main control unit (MCU).

c. The basic Accubar ATS-432 components are shown in figure 2.6-1.

2.6.2 Objectives

Weapons' accuracy is a subobjective of the critical issue of effectiveness for operational testing. All operational tests, including Force Development Test Experimentation (FDTE), Operational Field Test (OFT), and innovative testing of small arms and automatic weapons firing a supersonic projectile, require an evaluation of the accuracy of the system. An MDI system employed during Operational Testing (OT) provides accurate test results and reduces the time and labor costs for the test. The instrumentation provides exact data of the accuracy performance of the weapons system, to include data from which the mean or average miss distance can be analyzed. It provides the data immediately after completion of the firing exercises, which reduces the time required for collection and analysis of test data. This results in a reduction in the time required for supporting-soldier labor to be present at the test site and the time required to prepare test reports.

2.6.3 Instrumentation Description

a. General. The basic Accubar ATS-432 consists of an MCU, a Secondary Control Unit (SCU), a Rod Sensor Assembly (RSA), a Transducer Signal Conditioner Unit (TSCU), a folding steel frame, and the necessary

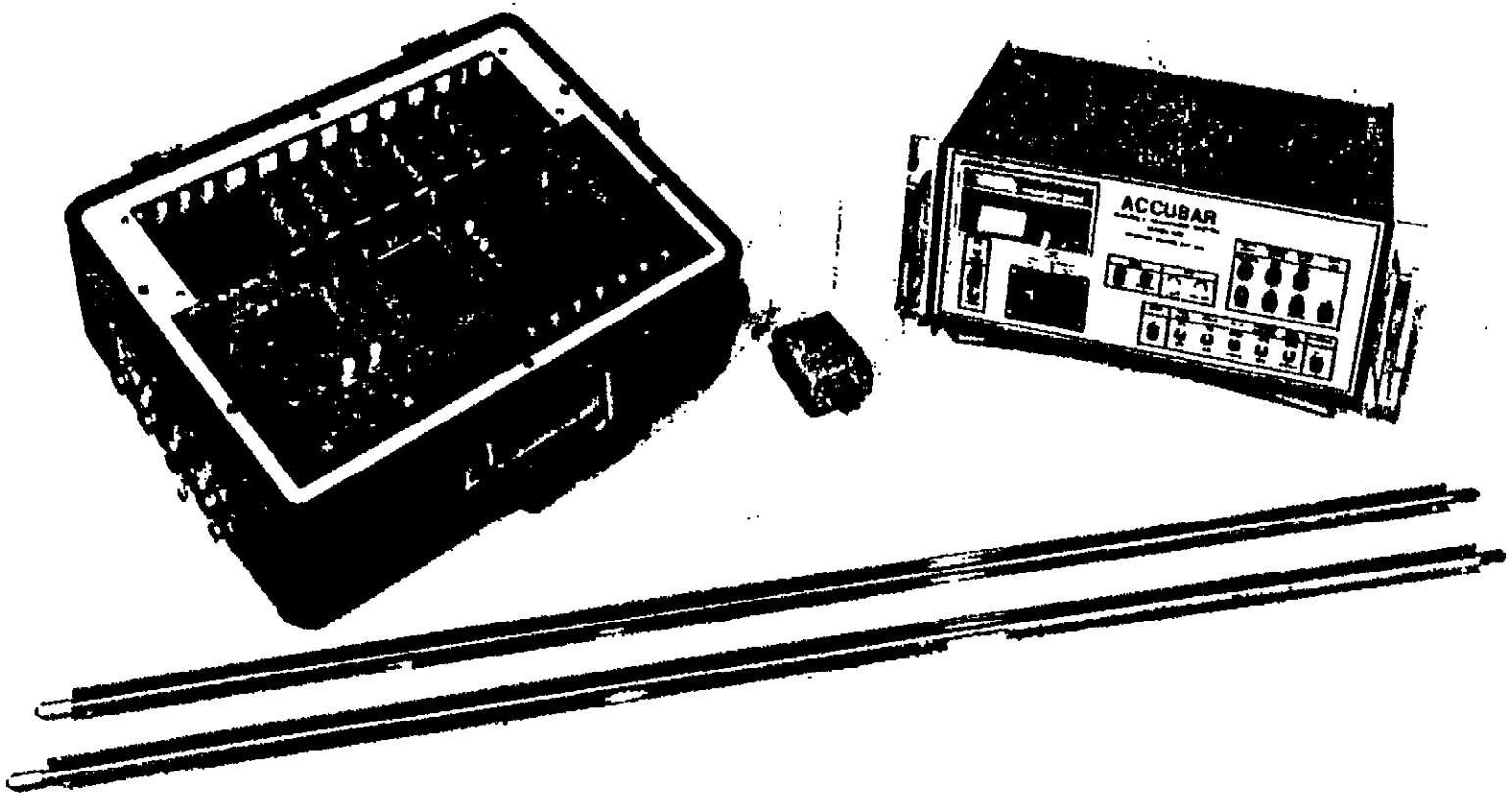

Figure 2.6-1 Basic Accubar system components.

interconnecting cables. The ATS-432 is designed for use as either a two-rod or four-rod sensing system and has the capability of scoring all four rods for each shot. Each rod sensor is modular in construction and can be as short as 4 ft or as long as 20 ft.

b. Description of Major Components

1. Main Control Unit (MCU)

(a) The MCU (figure 2.6-2) is an environmentally sealed package, ruggedized for field use and located downrange within 1,000 ft of the sensors. The MCU contains the signal processing, scoring and storage circuits for the ATS-432 and is operated either under its own panel controls or under control by the SCU. The MCU is connected to the SCU via a built-in modem by a telephone line or any two-wire field line. The MCU is powered by 115-V a.c., 50- or 60-Hz power, and contains d.c. power supplies for its own d.c. requirements and for the transducers at the target. The connector panel (figure 2.6-3) provides the two target inputs, the modem data output, and an a.c. power connector.

(b) The control panel of the MCU provides a complete set of controls allowing the ATS-432 to be operated without the SCU. The MCU controls are used for short-distance tests (1,000 ft) and for system setup and alignment. The MCU provides a front panel LED display and serial and parallel outputs for optional displays or for interfacing to a computer.

2. Secondary Control Unit (SCU)

(a) The SCU (figure 2.6-4) cabinet is designed for either rack-mounting or bench-top use. The SCU contains a modem and circuits for receiving, processing and displaying the score data from the MCU and for transmitting control signals to the MCU. A thermal printer in the SCU provides a paper record and serial and parallel data outputs coupled to auxiliary displays or a computer (figure 2.6-5). The SCU operates from 115-V a.c., 50- or 60-Hz power.

(b) The front panel of the SCU duplicates the controls of the MCU panel; however, the SCU cannot operate without the MCU. The SCU is truly a remote control panel for the ATS-432.

3. Rod Sensor Assembly (RSA)

(a) Each of the four sensors used by the ATS-432 consists of 3/8-in diameter aluminum rods and two ceramic piezoelectric transducers. Each aluminum rod is 4 or 8 ft long and has a tapped hole on each end that will accept a setscrew or a transducer. Rods of 20 ft are formed by joining two 8-ft rods and a 4-ft rod section with setscrews. The transducers are then screwed into the rod to form the rod sensor.

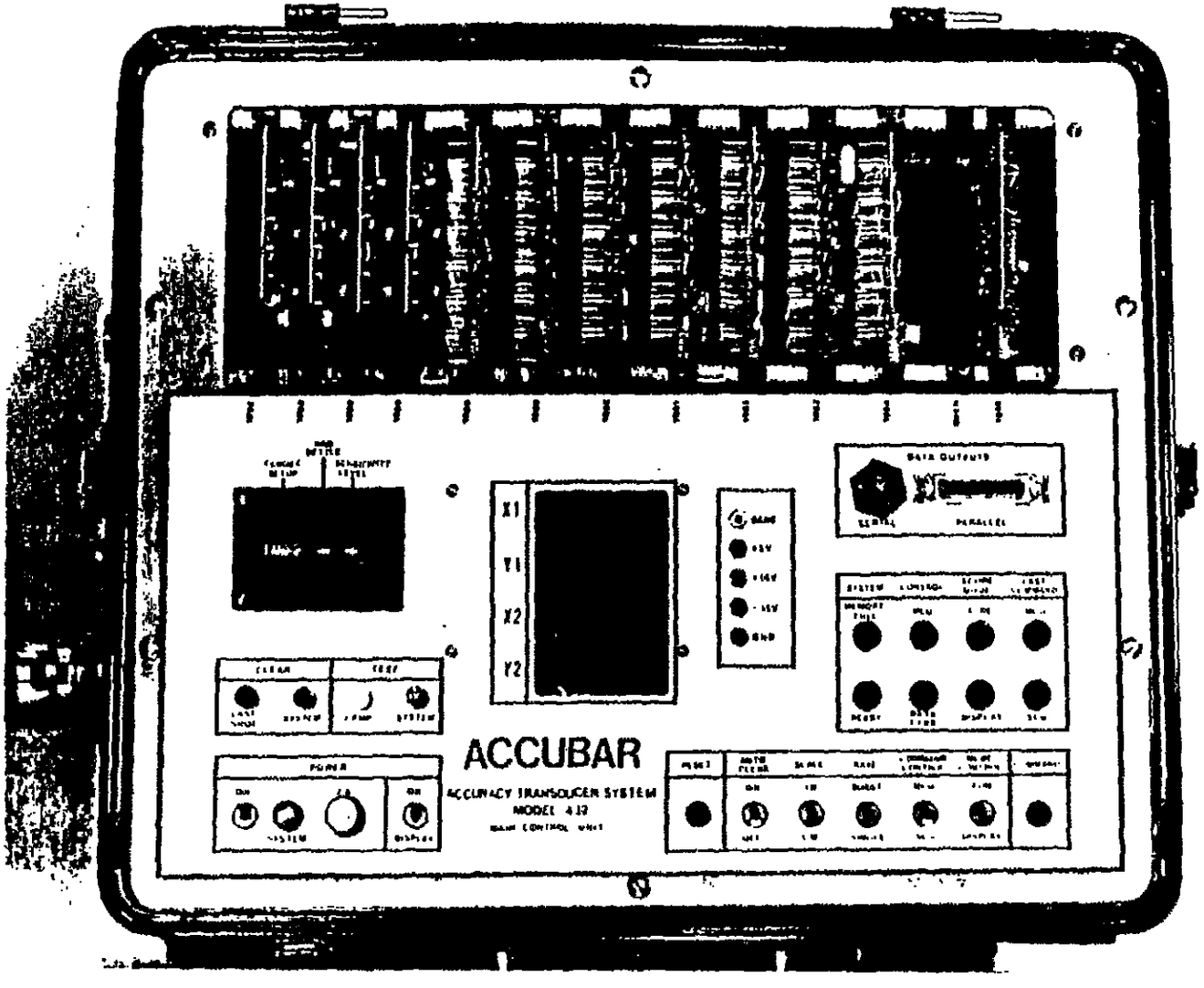

Figure 2.6-2 Main Control Unit (MCU).

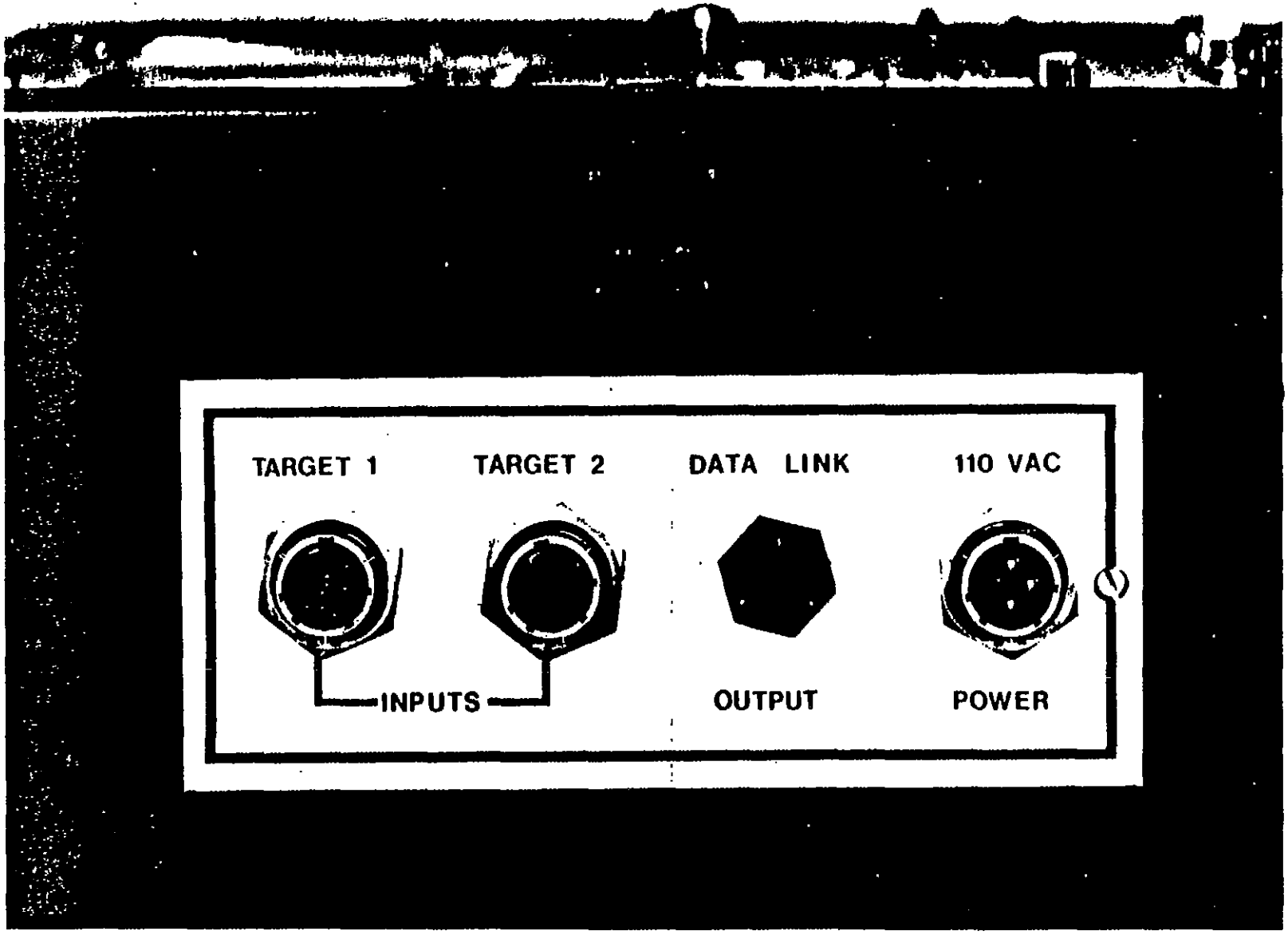

Figure 2.6-3 MCU connector panel.

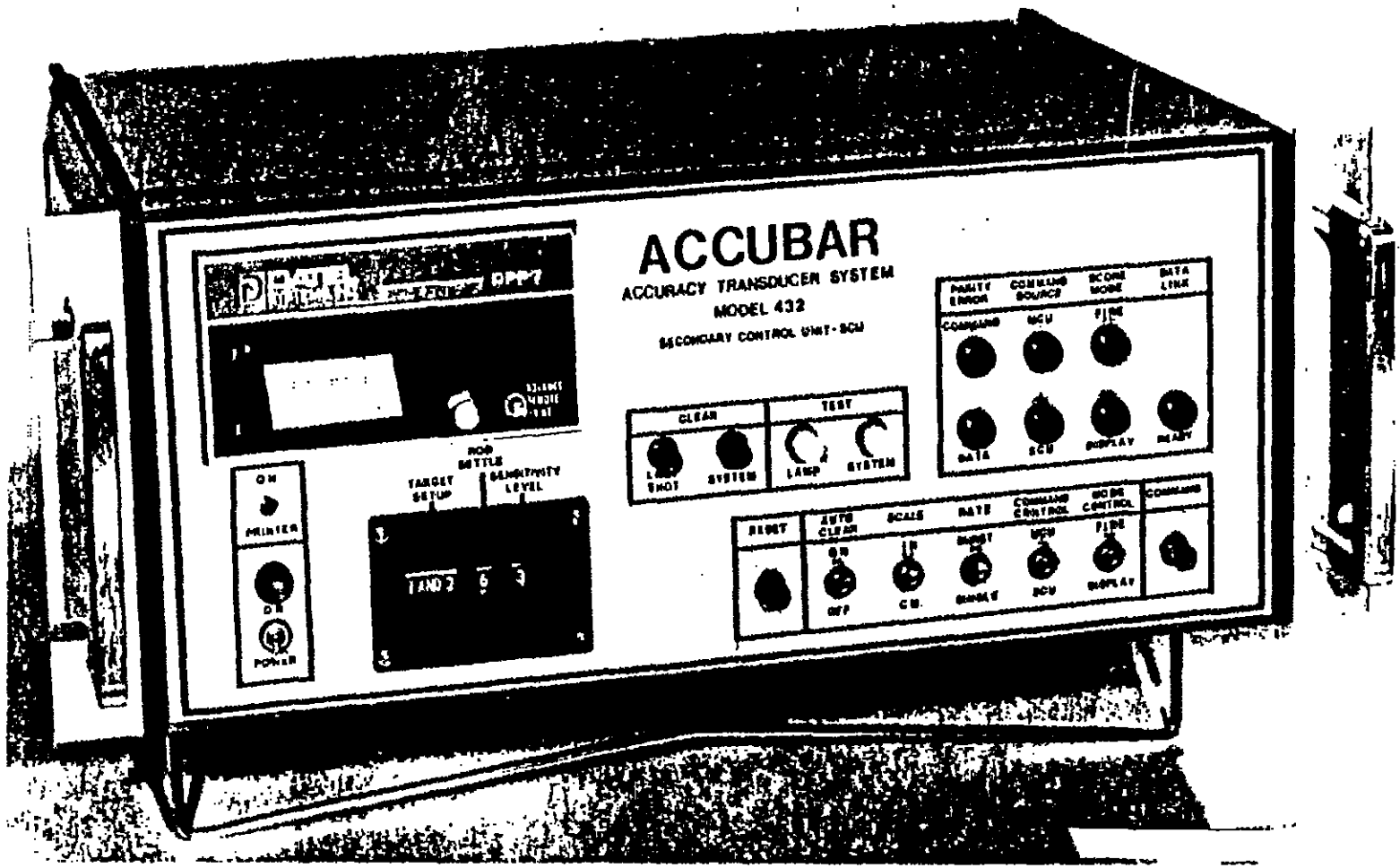

Figure 2.6-4 Secondary Control Unit (SCU).

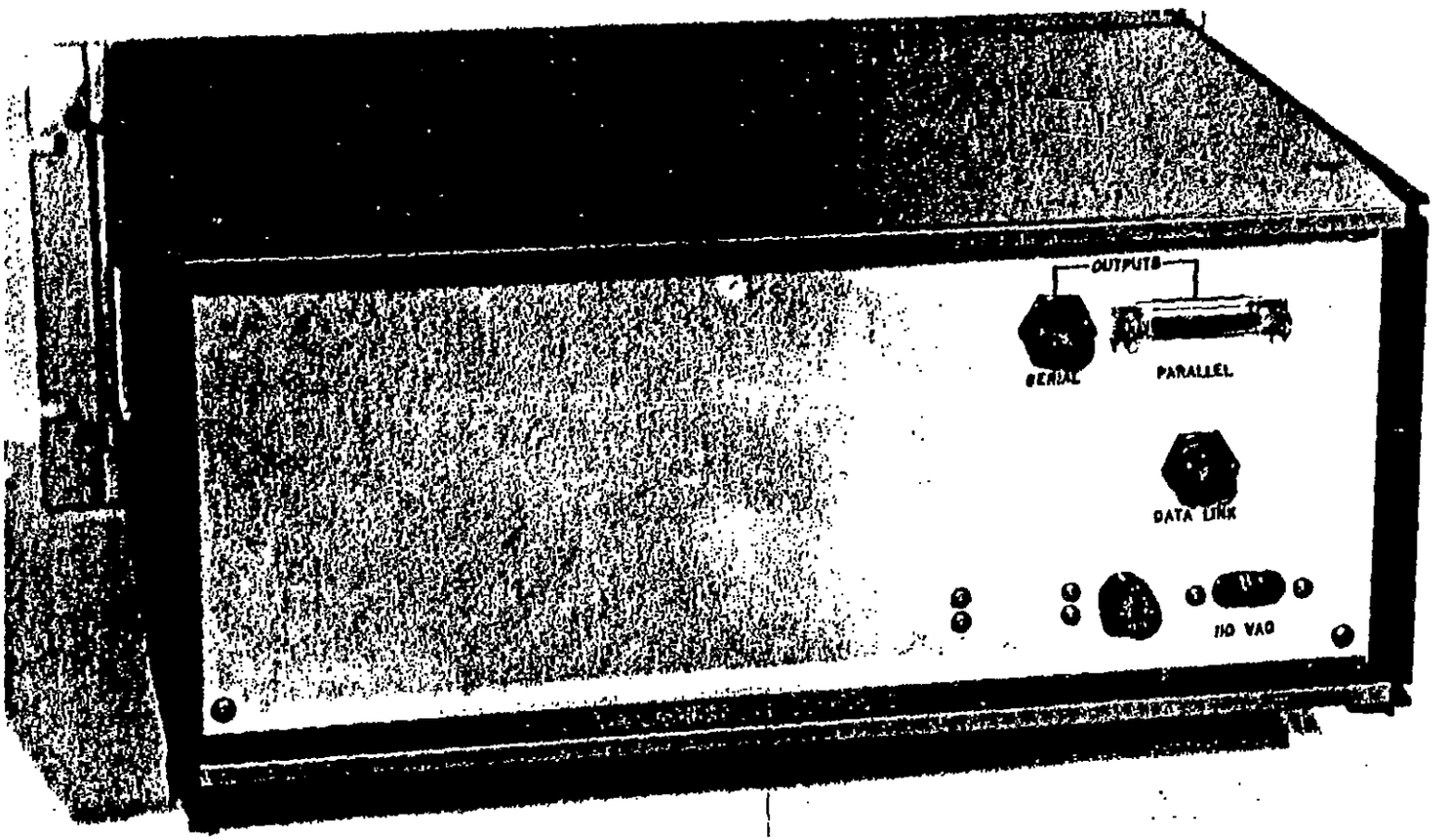

Figure 2.6-5 SCU rear panel.

(b) Each rod has a corresponding mounting subassembly with extruded rubber grippers bonded to a 4-ft-long support.

4. Transducer Signal Conditioner Unit (TSCU). A TSCU (figure 2.6-6) connects the RSA to the MCU of the ATS-432. The conditioner consists of four high-impedance amplifiers and four emitter-follower cable drivers. In addition, the conditioner unit, which is mounted on the frame and derives power from the MCU, contains the built-in test (BIT) circuits for energizing the transducers during a test sequence. The conditioner unit has four coaxial input connectors and a multipin main cable output connector.

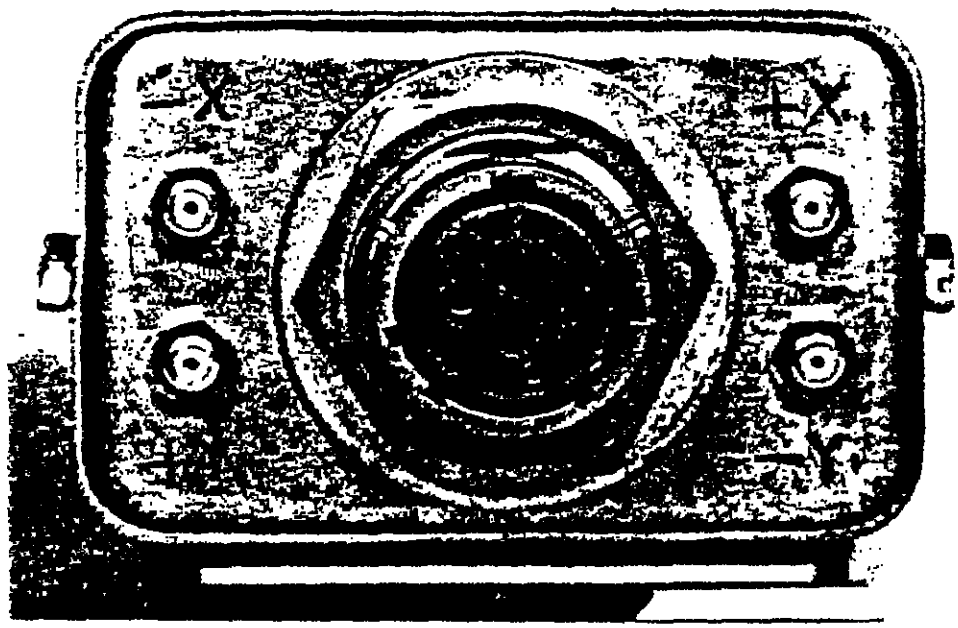

Figure 2.6-6 Transducer Signal Conditioner Unit (TSCU).

5. Frame. A self-supporting steel frame is provided to hold the RSA. A frame (2-in-by-2-in square) is constructed using Telespar tubing and is hinged to allow the vertical members (Y-rods) to be lowered for servicing. The frame is designed to mount two 20-ft rod sensors or smaller sections if desired. The modular frame can be set up as an 8-ft-by-8-ft unit as well as the 20-ft-by-20-ft unit.

6. Interconnecting cables. Each ATS-432 is provided with four coaxial cables to connect between the rod sensors and the signal conditioner mounted on the frame. In addition, a main cable (10 conductor) is provided to connect from the signal conditioner to the MCU. The main cable supplied is 200 ft long, but can vary in length from several feet to 1,000 feet, depending on customer requirements. The two-wire modem data link from the MCU to the SCU is not supplied.

2.6.4 Test Procedures

a. The basic principle of operation of the ATS-432 is relatively simple: the system senses the shock wave created by a supersonic bullet and computes the bullet's position relative to the system sensors. Bullet-position data is supplied in binary form as a pair of X-Y coordinates referenced to the center of each coordinate axis. The sign of the score indicates relative position with respect to the target center.

b. The sensors used by the ATS-432 are aluminum rods with ceramic piezoelectric transducers mounted at each end. The ballistic shock wave appears as an expanding cone with the bullet at the apex. Assuming that the bullet path is normal to the target plane, the shock wave will appear as an expanding circle concentric with the bullet path.

c. The bullet path shown in figure 2.6-7 passes through the sensor area in quadrant 1 and generates a shock wave that strikes rod X2 a distance, H, from the rod center. Secondary wave fronts are generated in the rod that moves away from the impact point at the speed of sound in aluminum. For the example shown, a secondary wave first reaches transducer +X2, then transducer -X2. The distance, H, from the rod center equals the time difference of arrival of the shock waves at the transducers, times one-half the speed of sound in aluminum. This is expressed as

$$H=\frac{|T_1-T_2|}{2} \quad V$$

The sign of H is determined by the first transducer pulsed.

d. Another part of the airborne shock wave strikes rod Y2 a distance, L, from the rod cener. The effect produced in rod Y2 is identical to that described above for rod X2. Rods X1 and Y1 also detect the shock wave and react the same as rods X2 and Y2. In this example, the X1 and X2 scores should be the same as the Y1 and Y2 scores. If rod-select logic is employed, only scores from X2 and Y2 would be retained while the other two scores would be inhibited.

e. The electrical pulses generated by the eight transducers are cabled to the MCU and applied to separate preamplifier circuits. All transducers and preamplifier circuits are identical to preserve the relative time of arrival of the transducer pulses. The outputs from the eight preamplifier circuits are digital voltage pulses indicating the time relationship of each transducer to the other transducers.

f. Input circuits in the MCU accept and measure the relative time of arrival of pulses from transducers on the same rod. When an input is received from a transducer on rod X2 and rod-select logic is used, the digital logic automatically inhibits the X1 rod circuitry and starts measuring time until the other X2 transducer signal arrives. The same

process occurs for rods Y1 and Y2. Distance from rod center is computed for both X and Y rods and stored as binary coded decimal (BCD) data with appropriate sign. If dual targets are employed, all four scores are retained.

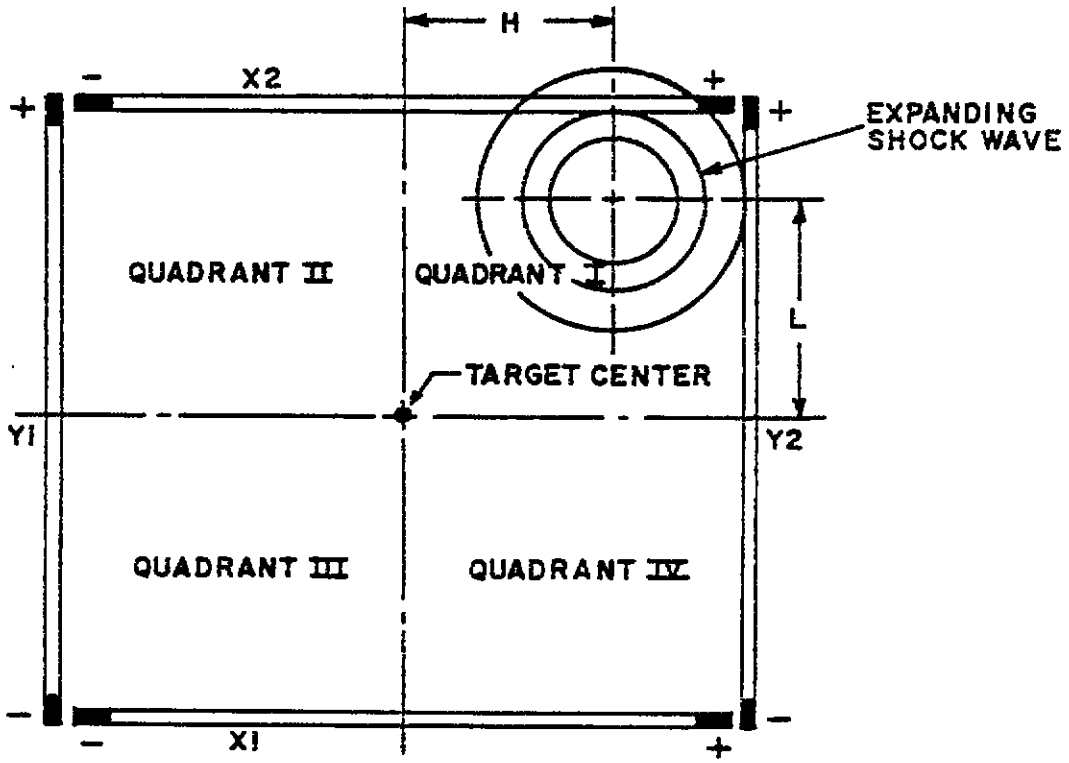

Figure 2.6-7 ATS-432 sensor operation.

g. For rapid-fire scoring, the MCU is reset automatically after a preselected time interval. The time interval is selected to allow all acoustic signals to clear the target area and for the rods to dampen to the quiet state. In single-shot scoring, the MCU can be reset manually or automatically.

2.6.5 General Application

a. Data Requirements

1. Round-to-round distribution about a point of aim

2. Identification of first round

3. Distribution of near misses

b. Data collection. Data is collected from X and Y coordinates about a point of aim; zero being the point of aim.

c. Data reduction. Data can be reduced by hand or the data can be fed directly into a computer for reduction to provide:

1. Mean radius for a shot group

2. Mean offset

3. Mean extreme spread

4. Mean drop

2.6.6 General Solution

Various techniques may be employed to analyze the data, depending upon what information is required. The techniques used most are multivariate analysis and analysis of variance.

2.6.7 Impact Scoring Indicators

Bullet position data are supplied in binary form as a pair of X-Y coordinates referenced to the center of each coordinate axis.

2.6.8 Accuracy

Accuracy of the displayed scores show hit position to the nearest 0.1 in for each axis for a 4-ft target and 0.5 in for a 20-ft target.

2.6.9 Advantages

a. Time saved in data collection.

b. Time saved in data reduction when interfaced with an automatic data processing system

2.6.10 Disadvantages

a. Projectiles must be supersonic when they pass through the rod sensor assembly.

b. Considerable test facility preparation is required.

2.6.11 Reliability/Availability/Maintainability

No such data is available on this new equipment.

2.6.12 Cost

Original cost of the system was $34,600.

2.7 LIGHT ATTACK RANGE OPTICAL SCORING SYSTEM (LAROSS)

2.7.1 General

The Light Attack Range Optical Scoring System (LAROSS) consists of two video cameras installed at known postions relative to an air-to-ground bombing target. The image of the target area is transmitted to a monitor in an observation post. The operator, using a light pen, feeds azimuth data to a computer which provides impact coordinates.

2.7.2 Objective

The LAROSS is designed to meet the requirement for a semiautomatic, single-operator system. Such a system improves scoring accuracy and the logistics associated with manning a bombing range.

2.7.3 Instrumentation Description

a. The LAROSS includes a precision video system, a data storage system and a computation and control system (CCS). The LAROSS is composed of the following major components (see figure 2.7-1):

1. Video System

   Cameras, lenses and mounts
   Screen splitter
   Video cable
   Line driver/receiver
   Precision monitor
   Video equalization amplifier/line drivers and receivers
   Scan converter
   Video tape recorder

2. Computation and Control System (CCS)

   Light pen unit
   Interface unit (I/U)
   Computer/display unit (with printer) (CDU)
   Time code generator with numeric inserter
   Plotter
   Remote display
   Console

b. The LAROSS contains the hardware and software necessary to perform the following functions:

1. Calibrate and precondition the system

2. Compute impact location in X and Y or range and clock position

3. Coordinate score to aircraft identification and run number

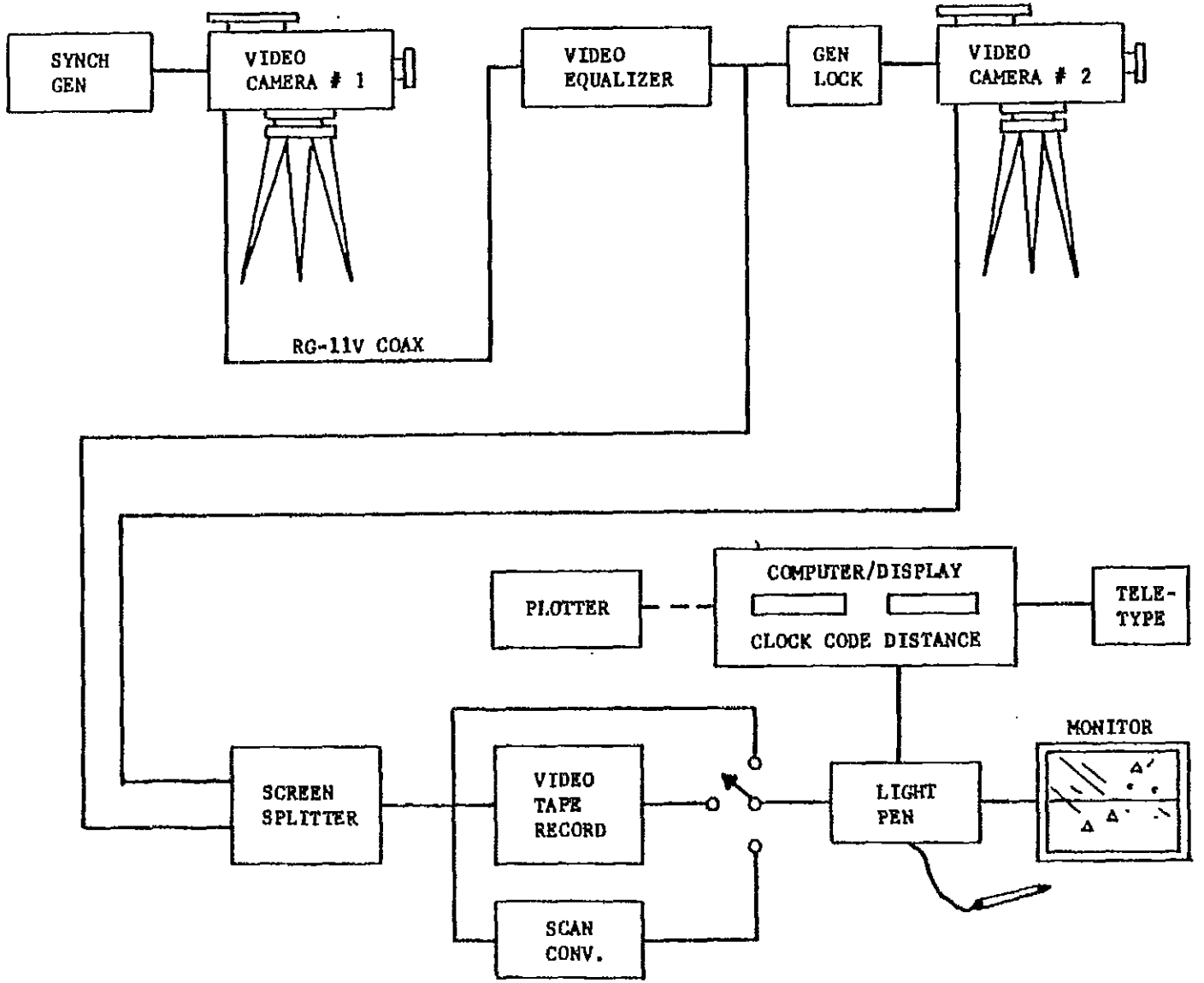

Figure 2.7-1 LAROSS components diagram.

4. Identify special conditons relating to target scoring (off target, no drop, missed score, etc.)

5. Format and present data in printed form

6. Present data on individual or composite plots

7. Format and display run scores on a remote readout

8. Generate and print out test score summaries

9. Generate and plot test score results

2.7.4 Test Procedures

a. Operational Overview

1. The LAROSS cameras are installed at a known distance from a target center with the lines of sight orthogonal to each other. The image of the target area is transmitted to a monitor at the observation post via video cable. When the operator observes a weapon impact on the monitor, the light pen is used to position the cursor over the strike as it appears on the camera. Pressing the tip of the light pen transfers the horizontal position of the cursor to the scoring computer. This procedure is repeated for the impact image on camera 2. The computer translates cursor position on the monitor to viewing angle and, subsequently, calculates position from target center in Cartesian or polar coordinates. The resultant values are displayed in real time.

2. Once the weapon impact has been spotted on TV, the observer has the option of immediately activating the scan converter to freeze the action by pressing a foot pedal. The strike may then be scored on the frozen image, reducing the effects of wind drift and smoke-charge offset angle.

3. If the observer is unable to spot the weapon impact initially, the video tape may be backed up and the scene replayed to examine the screen for telltale movements of the smoke plume. If the bomb impact is subsequently located, it may be scored from the tape recorder output in real time or stop action.

b. Technical Detail

1. Obviously, the operator has an important role in this system. The operator must be relied upon to visually identify the impact and to accurately illuminate the point of impact with the light pen. To perform this procedure, the following is required (See figure 2.7-2):

(a) A video monitor to provide the operator with a picture of the target area

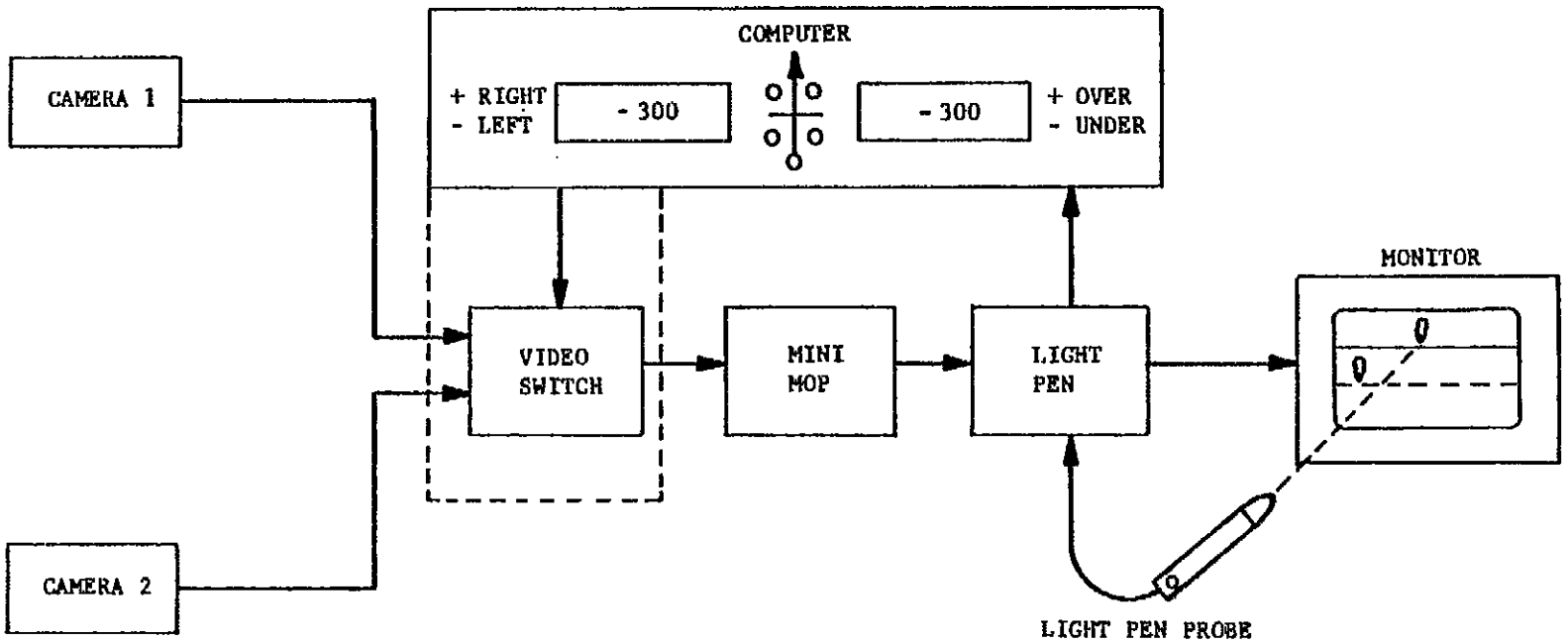

Figure 2.7-2 LAROSS data flow diagram.

(b) A light pen unit to provide a visual cursor and probe to identify the hit

(c) A CDU to provide visual indication of hit location in right/left or distance/clock positions.

2. The light pen is moved so that the cursor is aligned with the hit indication. The probe is then pushed in and the following takes place:

(a) The CDU accepts light pen data from camera 1.

(b) The CDU sends a signal to the video switch to switch to camera 2. The camera-2 image is now presented in the monitor, and the process is repeated.

(c) The CDU calculates the hit coordinates and displays the information in a format selected by the operator. After the operator records the hit information, the probe reset switch is depressed readying the system for the next event. The operator activity in probing both cameras requires approximately 2 s.

2.7.5 General Application

a. Data Requirements

To adequately install LAROSS, a first-order Class-II survey will be required to determine accurate positioning for the target center, camera positions, target markers, and prepositioned test shots. The included angles and the distances between each camera and from each camera to the target center will be measured.

b. Data Collection

1. After the operator has illuminated the burst, with the light pen "Get Data" on the console, the system samples the time which was stored in the interface when the first point was illuminated and also the upper and lower camera readings and saves these data in memory.

2. The camera readings are unpacked and used in conjunction with the target constants and calibration constants to compute the X, Y coordinates relative to the run-in line of target (see figure 2.7-3). The range is then computed. If the range is less than 100 ft, the program determines if the zoom mode is enabled, and if true, sets the zoom pass flag and "Get Data" operations. The program now converts X and Y to the appropriate units and packs them into a single data word and stores this word in the memory.

c. Data Reduction

The CPU performs the the basic geometric calculation necessary to generate the hit location and to display the answers relative to range coordinates. The computations follow this order:

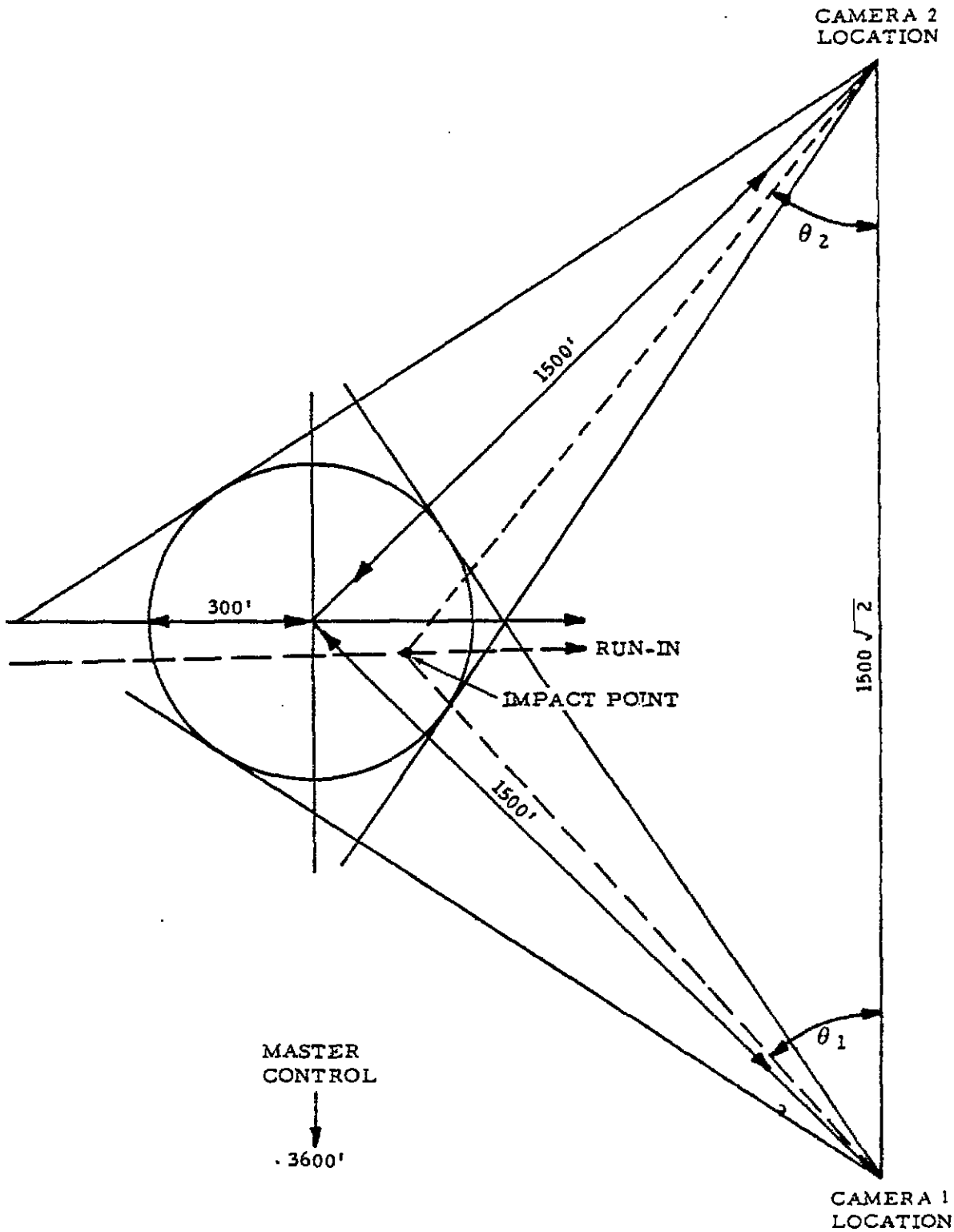

Figure 2.7-3 Camera locations.

1. Load and hold ϕ_1 and ϕ_2 (azimuths from cameras 1 and 2, respectively)

2. Apply calibration correction to ϕ_1 and ϕ_2

3. Calculate right-left/over-under in camera coordinates

4. Rotate coordinates to aircraft run-in coordinates, if necessary

5. Display answer in right-left/over-under, or calculate distance/clock code and display answer.

2.7.6 General Solution

a. Analysis Techniques. The computation portion of the system obtains data directly from the video monitor via a light pen. The data obtained are then automatically processed by the CDU which calculates and displays the desired answers.

b. Math Model. The solution is performed with the trigonometric relationships which exist between the cameras and the target, or impact (see figure 2.7-3). By determining the location of the impact with respect to one of the two cameras, the location relative to the target can be calculated.

c. Computer Program. The LAROSS software consists of 12 modules as shown in figure 2.7-4. The modules are divided into two categories: primary function routines and support routines. The primary function routines are:

1. Idle. This routine, as the name implies, is the idle or default mode of the system. Most of the other primary function modules exit to this routine. This routine provides the vectoring necessary to load and execute primary function modules.

2. Init I. This routine supports the initial setup of the overall system. Upon entry, this program generates an overall system reset and then begins an interaction with the operator to ensure that the system is operational.

3. Cal. This routine is entered from either Init I or Idle. Upon entry, this module determines which target has been selected and loads the appropriate target constants.

4. Init II. This routine requests the operator to select the unit of measurement (feet, yards, meters) and sets the appropriate flags in the interface and the software.

5. Run. This routine has several paths dependent upon the system status and the operator-selected action.

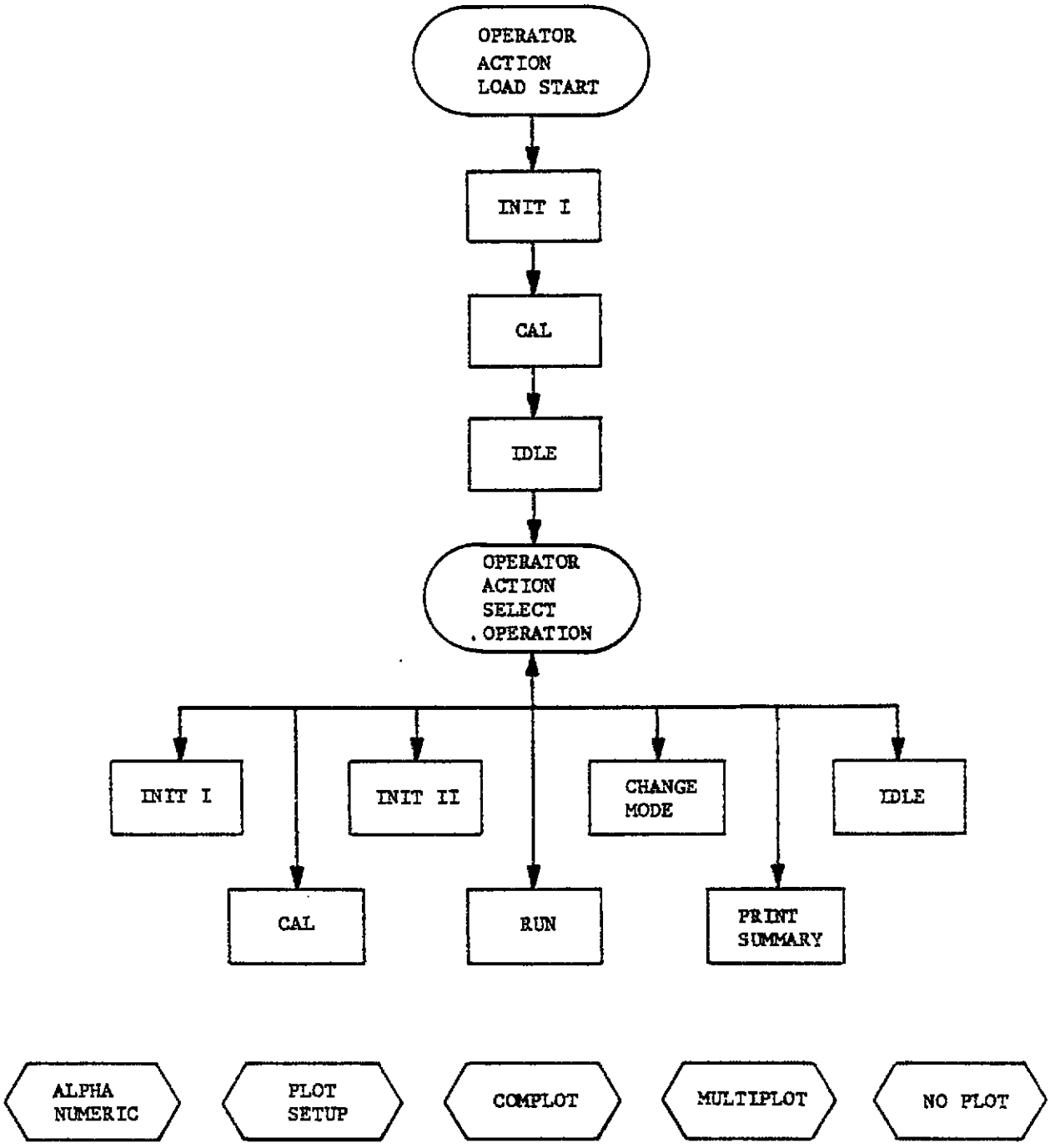

Figure 2.7-4 Functional block diagram.

6. Change mode. This routine is a short program which enables the operator to enter or exit the playback mode of operation. This routine sets the appropriate software flags and conditions the interface to operate in playback.

7. Print summary. This routine enables the operator to receive a total listing of the scores obtained during the mission.

The support routines are: Alpha Numeric, Plot Setup, Complot, Multiplot, and No Plot.

2.7.7 Accuracy

a. Controlled accuracy tests indicate an average error of 3 to 5 percent out to a 300-ft radius. A precision monitor with a linearity of 2 percent or better and 800 lines of resolution at the center presents the video picture of the target area. Current projections indicate a maximum error of 8 ft exists.

b. The accuracy of scoring bomb drops using the LAROSS is dependent on aligning a light pen cursor with some point of a scene observed on a video monitor. Since the actual impact point can only be estimated by the resulting smoke and dust cloud, the limiting accuracy of the system will seldom be achieved in practice.

2.7.8 Advantages

a. Scores at night when spotting charges are utilized. Addition of stop action and special camera vidicons ensure that impacts are not missed at night.

b. Scores both conventional (600-ft diameter) and special (4,000-ft diameter) weapons

c. Provides readouts in azimuth (clock code) and distance or over-under and left-right scores.

d. Scores duds on conventional and special weapons targets.

e. Features expanded capability to score moving targets.

f. Uses tape recorder to verify scoring accuracies, mission assessment, and safety of flight procedures.

2.7.9 Disadvantages

a. Excessive degradation of the cables transmitting the video data due to the hazardous range activities.

b. Maintenance difficult

c. Accuracy of system is dependent on the estimation of the impact point by the operator.

d. Impacts outside the view of both cameras cannot be scored.

2.7.10 Reliability/Availability/Maintainability

a. The LAROSS has been designed to achieve a goal of 1,100 h of mean time between failures.

b. With the necessary technical documentation, an electronic technician is supposed to adequately maintain the system. The equipment has to be periodically inspected and preventive maintenance has to be performed on an as-available basis. Each time the equipment is used, it must be calibrated.

c. Inspection routines are performed periodically and before operations.

2.7.11 Cost

The cost of LAROSS installed, checked out, and fully operational is approximately $500,000.

2.7.12 Point of Contact

Atlantic Fleet Weapons Training Facility
Code 71211
Telephone (804) 863-2000, ext 4842
AUTOVON: 894-3920, ext 4842

2.8 TV ORDNANCE SCORING SYSTEM (TOSS)

2.8.1 General

The TV Ordnance Scoring System (TOSS) is a weapons impact position measurement device employed by the Tactical Air Command. The system uses TV images, transmitted to a central site, to determine impact azimuth from two different TV sensors. The impact is located through triangulation and then translated into a score (position relative to target). This score is then relayed to the pilot.

2.8.2 Objectives

The U. S. Air Force tactical forces require accurate scoring of air-to-ground weapons delivery of single and multiple drops on multiple targets. The TOSS is designed to provide this capability on both controlled and tactics ranges.

2.8.3 Instrumentation Description

a. Each TOSS has a control room (scoring van) and two or three camera site locations.

b. A complete system consists of the following components:

1. A TOSS console assembly containing:

(a) VHF control panel for selection of discrete functions

(b) Audio amplifier/recorder for air-to-ground communications control

(c) Rate stick panel for controlling and positioning the azimuth cursor

(d) Scoring cursor panel for readout of score, time and selected discrete functions

(e) Passive video switcher panel for selection of video display and recording

(f) Calculator with CRT display screen and keyboard

(g) Hard copy unit for printout of data displayed on calculator CRT

(h) Video cassette recorder

2. A camera site installation consisting of:

(a) TV camera assembly

(b) Solar panels for powering the installation and charging batteries.

(c) Microwave relay system for transmitting/receiving camera positioning information

(d) Batteries (12-volt)

(e) Command and control encoder/decoder for deciphering pan, tilt, zoom, and focus commands and actuating the proper site mechanisms

2.8.4 Test Procedures

a. To produce accurate results, the cameras must be calibrated and aligned before each mission. For calibration, a field of view (FOV) is selected for the particular mission. A resolution target is viewed, and various known elevation angles are selected. The elevation angles are entered into the calculator along with the selected FOV. The calculator then determines the digital counts-to-degrees conversion for that particular setup. Next, the camera is aligned on a surveyed aimpoint and a zero reference angle is entered into the calculator. This procedure is repeated for each camera.

b. Scoring is accomplished by the operator observing the impact on the TV screen, positioning the cursor over the point of impact, and depressing the SCORE (input) switch. This sequence of operations enters the angle into the calculator. The TV display automatically steps to the other camera, and the procedure is repeated.

c. After receiving both input angles, the calculator computes impact location and relative position to the selected target. This information is then displayed to the operator.

2.8.5 General Application

a. Data requirements. The positions of the cameras, calibration points, and aimpoints must be known accurately. If relative score is desired, the aircraft heading is needed; otherwise the reference heading is true north.

b. Data collection. The data entry into the system may be automatic by means of the cursor or manual by use of the keyboard. The video display is recorded and may be played back to rescore an impact if it was initially missed by the operator. The calculator unit stores all calibration, alignment and survey information for use in triangulation.

2.8.6 General Solution

a. Analysis techniques. No analyst intervention is required. Should the scores seem unreasonable, the system can be entirely recalibrated and realigned, and the mission can be rescored from video tape.

b. Math model. Standard triangulation procedures are used.

2.8.7 Accuracy

The accuracy specification for this sytem is ±20 ft within 2,000 ft of the desired aimpoint. This accuracy requires a baseline between the cameras of 10,000 to 12,000 ft and nominal camera lines of sight orthogonal to each other.

2.8.8 Advantages

The TOSS can be used on tactics ranges to provide scores under simulated combat situations.

2.8.9 Disadvantages

The system, although reasonably simple, does require sophisticated electronics for operation.

2.8.10 Reliability/Availability/Maintainability

During operational test and evaluation, the system exhibited a mean-time-between-critical-failure of 15 h and a mean-time-to-repair of approximately 4 h; both considered outside the limits of acceptability. The vendor is improving reliability/maintainability.

2.8.11 Cost

The TOSS costs approximately $500,000 installed.

2.8.12 Point of Contact

USAFTFWC
Nellis AFB, NV 89191
Telephone: (702) 643-4030
AUTOVON: 682-4030

2.9 AIRBORNE RANGE INSTRUMENTATION SYSTEM (ARIS)

2.9.1 General

The Airborne Range Instrumentation System (ARIS) is a proven high-precision bomb scoring system employing simulated weapon delivery against any desired range area. ARIS, tested by Eglin AFB, evolved from the Close Air Support System (CLASS) blind-bombing system successfully demonstrated in 1972 at Holloman AFB. The ARIS consists of three basic components (see figure 2.9-1): an airborne pod assembly, a ground data terminal located in shop facilities at the airfield, and an array of transponders in the vicinity of the target. Printed reports and a magnetic tape recording of the results are produced. Post-flight analysis data has been used to study the causes for bombing error.

2.9.2 Objective

The objective of ARIS is to provide a realistic, flexible and cost effective means of testing tactical bombing systems. The ARIS places no restrictions on aircraft maneuvers. The system accurately predicts the impact of a simulated bomb drop, enhancing realism. Since target areas can be easily moved, equipment reused, and minimal personnel are required to conduct a test, ARIS is economical.

2.9.3 Instrumentation Description

ARIS consists of a pod carried by the aircraft, typically a set of four transponders on the ground in the target area, and a minimum of ground-based processing equipment. Minor modifications to equipment in production for other programs are required for ARIS application. No aircraft modifications are required to use ARIS pods.

a. Pod assembly. The pod contains an inertial navigation system, a range/range-rate interrogator, an air data subsystem, and a tape recording subsystem (see figure 2.9-2). Software for the integration of sensor data contains a highly effective Kalman filter for optimum system accuracy.

b. Transponders. The ground-based transponders are highly portable and allow flexibility in target location. Typical range configurations for transponders are illustrated in figures 2.9-3 and 2.9-4.

c. Ground-based processing equipment. This equipment is typically located in a shop or at an airfield. Since scoring results are available shortly after the simulated release, they can be sent to the ground before the aircraft returns to base. The interrogator contains data link capability which is used for this purpose. Thus, if a major target miss is measured, the aircraft could be directed from the ground to make another pass at the target. Post-flight reduction of data is also performed on the ground-based processing equipment.

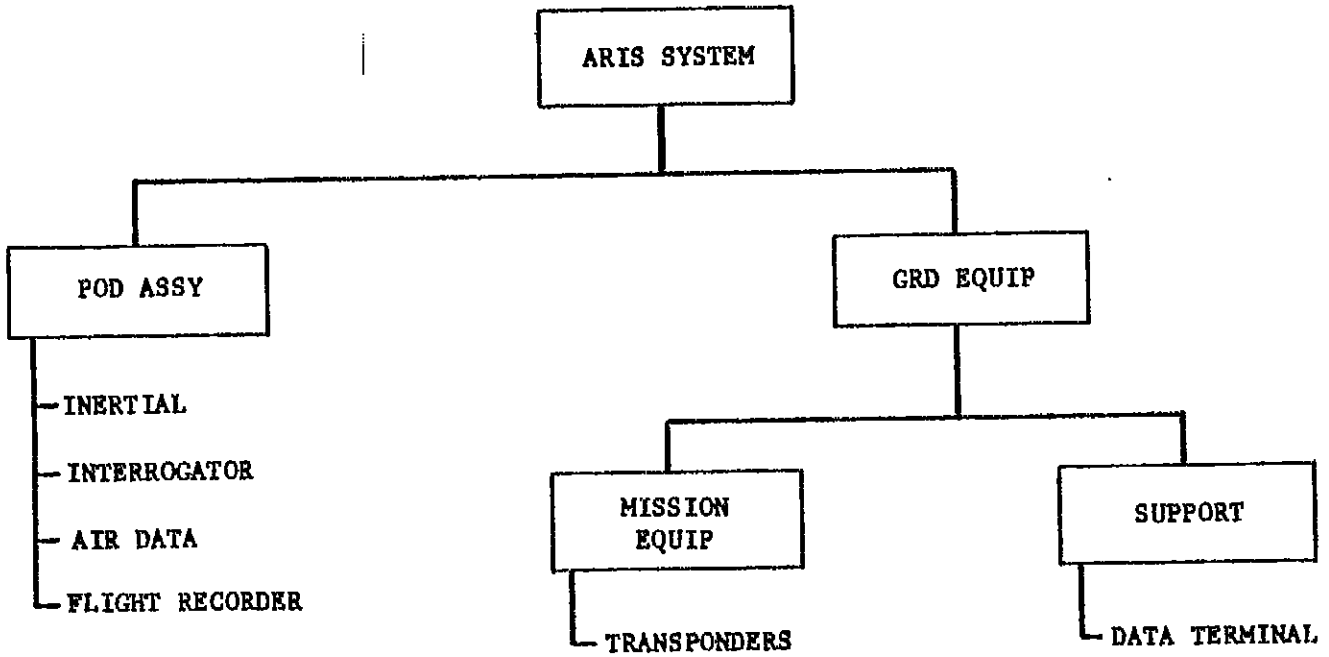

Figure 2.9-1 ARIS system configuration.

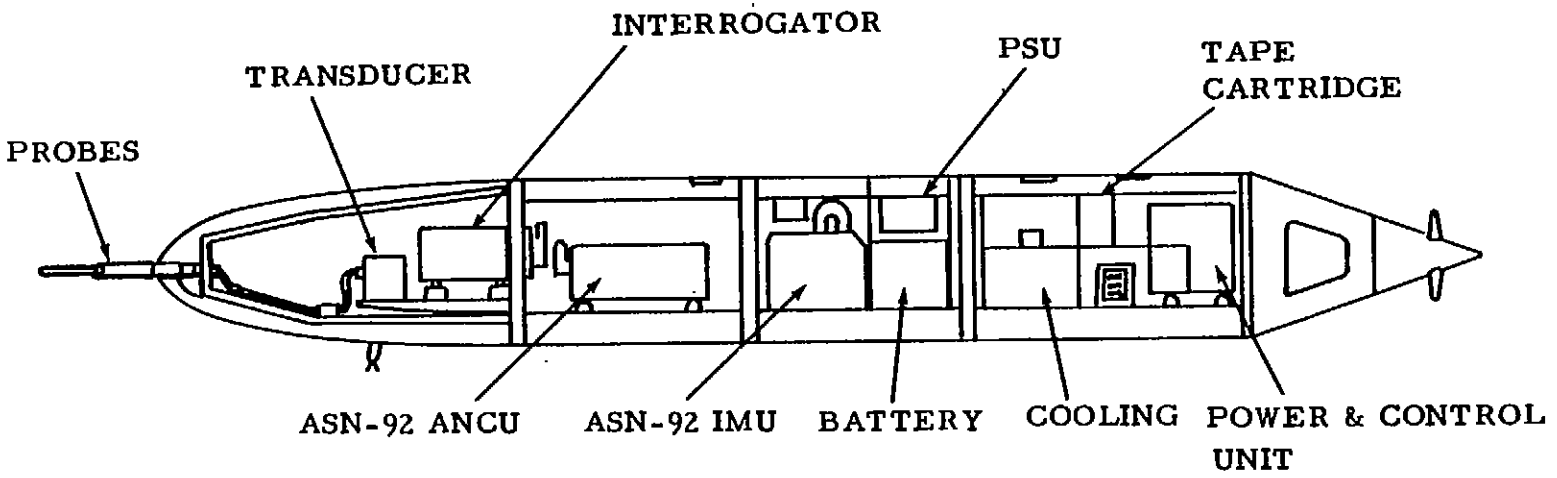

Figure 2.9-2 Airborne pod assembly.

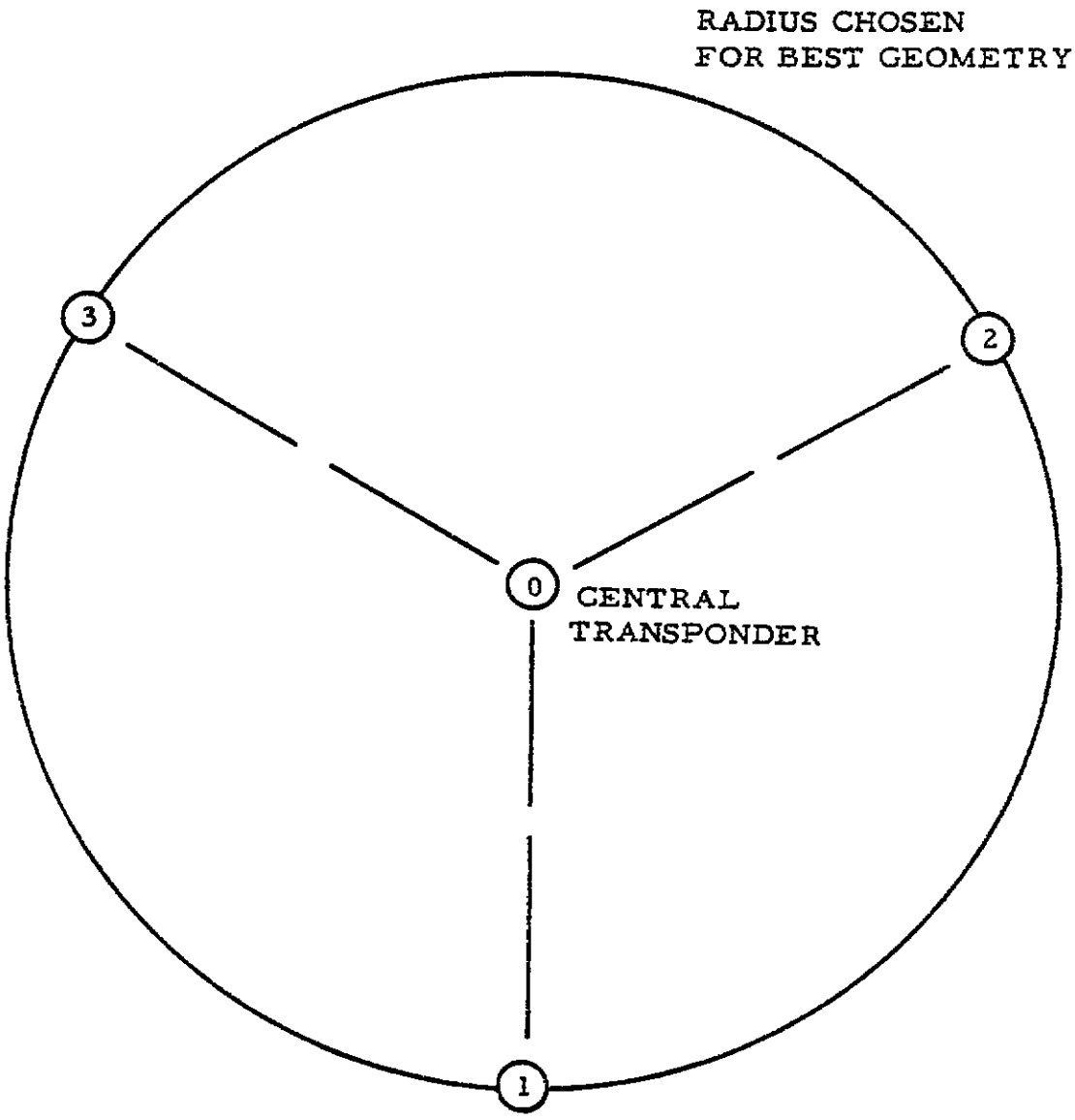

Figure 2.9-3 Transponder array (best geometry).

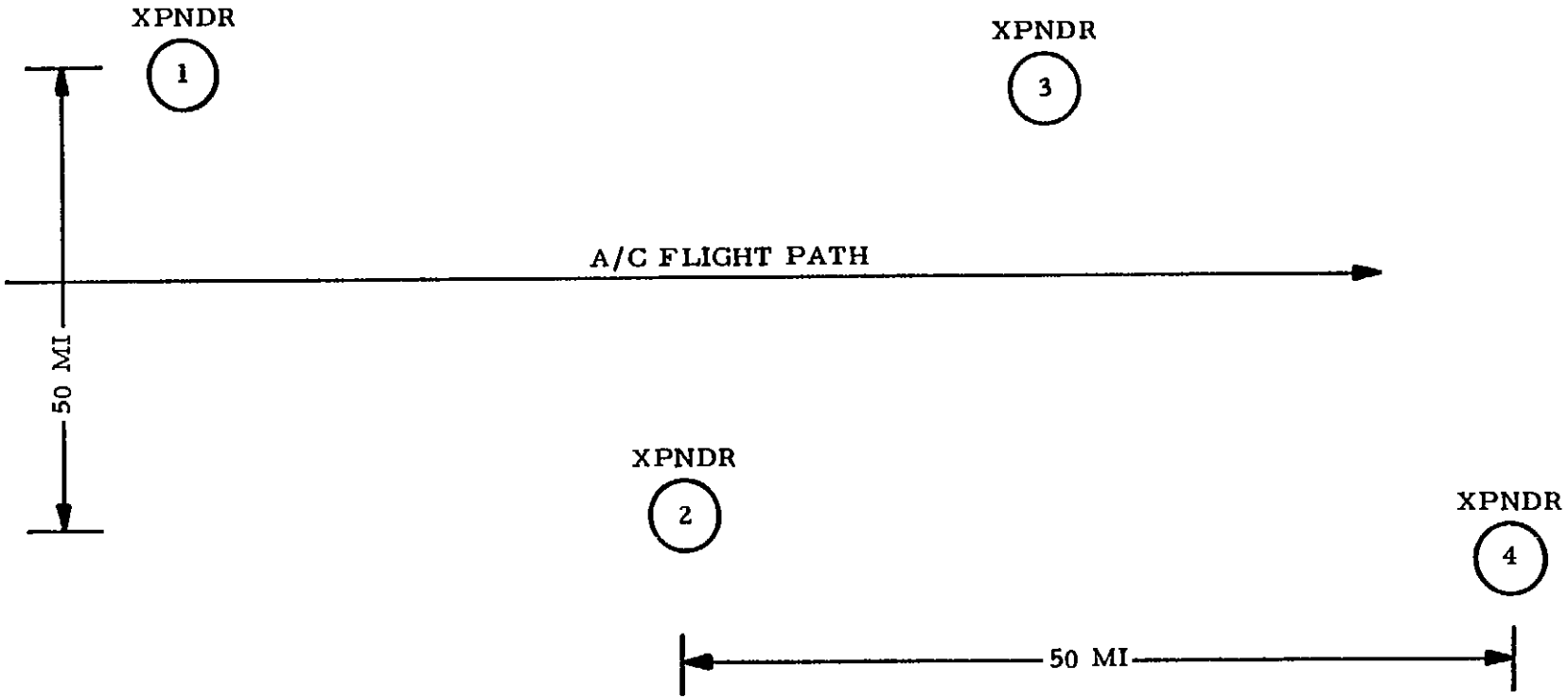

Figure 2.9-4 Range configuration for aircraft flight testing.

2.9.4 Test Procedures

The sequence of events in the use of ARIS is as follows:

a. The instrumentation pod is mounted on the aircraft to be tested. Either the right- or left-outboard pylon may be used. The left station is preferred because it allows better access to pod controls. A ground power cable is plugged into the pod and another into the aircraft, and the pod electronics is activated a minimum of 15 min before the flight.

b. At this time, initialization data are read into the pod computer by means of a tape cartridge installed in the pod. Initialization data consist of the coordinates of the target and of the transponders in the target vicinity, airfield coordinates, and weapon parameters to be used on the mission. Tape cartridges are prepared in the shop with a unit called the ground-data terminal.

c. After the aircraft engine starts, ground power is disconnected, and the aircraft proceeds on its mission. When the aircraft is at a predetermined range from the target, a radio reference system contained in the pod automatically transmits interrogations. The equipment in the vicinity of the target, typically a set of four transponders, responds to these interrogations.

d. The aircraft then makes a target approach and simulated attack. The pod receives the aircraft weapon release signal. It computes the impact point of the simulated weapon, based on pre- and post-release data from the interrogator, an inertial navigation system, and air data measurements all made from within the pod. The impact coordinates are compared with target coordinates, and scoring results are stored on the magnetic tape cartridge.

2.9.5 General Application

The ARIS information flow diagram (figure 2.9-5) illustrates a typical application and explains the flow of data between the three basic components of the system.

a. Data Requirements

1. ARIS has the capability of entry of target coordinates, offset from any of the tranponders. The scoring results are then directly printed out by the ground data terminal. However, the offset is often left at zero so that printouts can remain unclassified.

2. ARIS also has the capability of using up to three separate transponder arrays (target areas). Thus, a single aircraft mission can include attacks on three widely separated targets. The only limitations are the availability of a sufficient quantity of transponders and the number used per array. The characteristics of the bombs being simulated can be selected to meet test requirements. Several different high- and low-drag bombs have been simulated by ARIS.

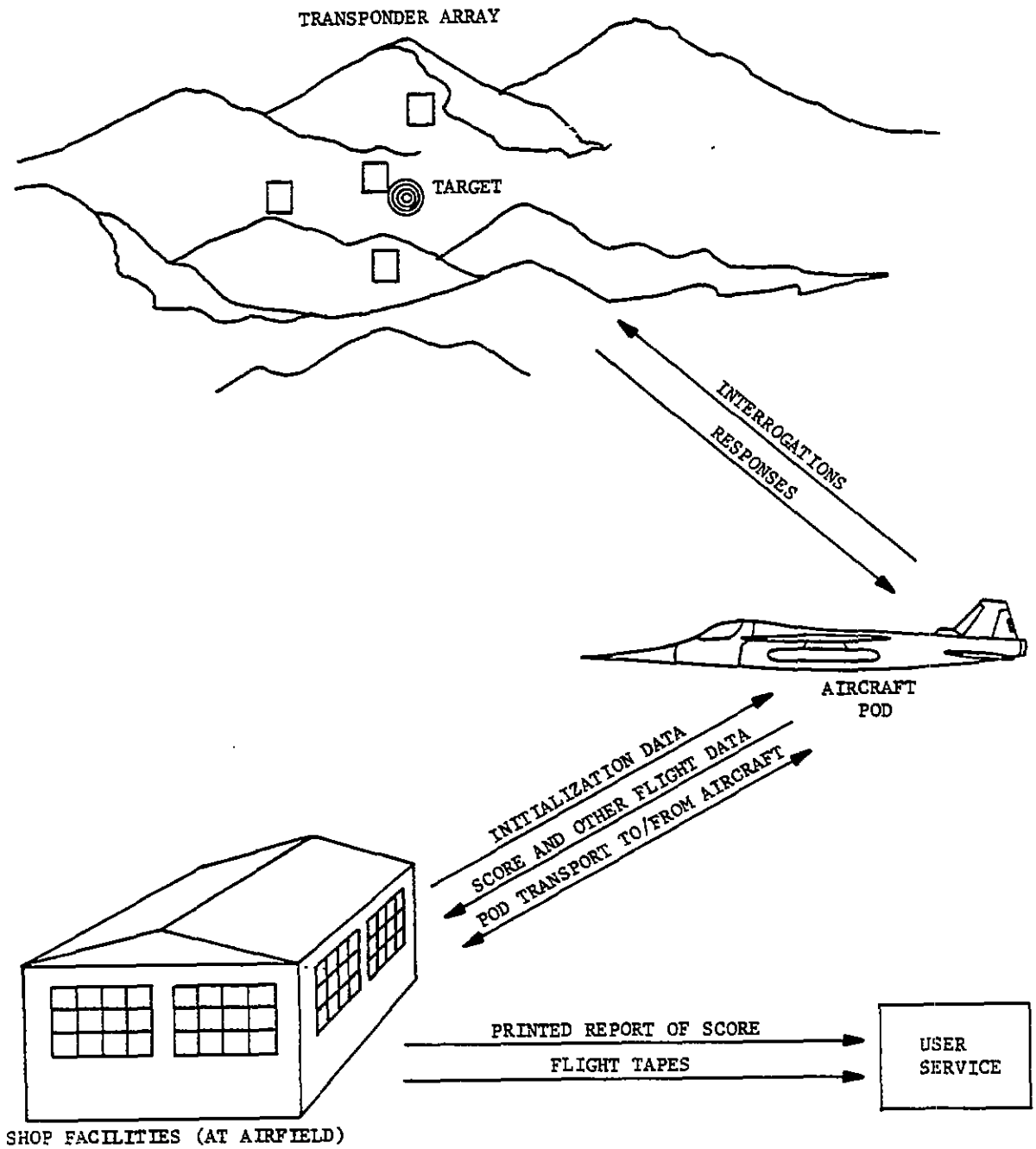

Figure 2.9-5 ARIS information flow diagram.

b. Data Collection and Reduction

1. After the aircraft returns to base, one panel of the pod is removed, power is shut down, and the magnetic tape cartridge containing the flight data is removed from the pod. The pod may then be reflown or down-loaded and returned to the shop, or loaded onto another aircraft. Another tape cartridge containing the new initial conditions would then be installed prior to system reactuation.

2. The tape cartridge containing the flight data is then taken to the shop area and plugged into the ground-data terminal. The scoring results are automatically printed out (a one-page report for each bomb dropped). After printout of the scoring results, the data are transferred to a reel of 9-track tape for review by maintenance personnel and for storage.

3. At the conclusion of a scoring flight, a report is printed by the ground terminal giving some general information related to that flight plus two copies of data for each simulated bomb drop.

2.9.6 General Solution

The ARIS principle of operation is illustrated in figure 2.9-6.

2.9.7 Advantages/Disadvantages/Accuracy

a. To make the tests as realistic as possible, the AIRS affords maximum flexibility in the assignment of target areas. ARIS allows the rapid set up of equipment in a new target location so as not to impose range down-time constraints on operations-planning personnel. The system is mechanized to provide maximum in-flight reliability to avoid costly flights that yield no useable data. Since minimal support personnel are required in the target area and at the air base, flight tests costs per operating hour are reduced.

b. The relative accuracy and the comparative advantages and disadvantages of the ARIS are summarized in table 2.9-I ARIS is not restricted to operation on any specified aircraft, since it has a minimal and standard aircraft interface.

2.9.8 Point of Contact

6585th Test Group/GDOC
Holloman AFB, NM 88330
AUTOVON: 349-2303

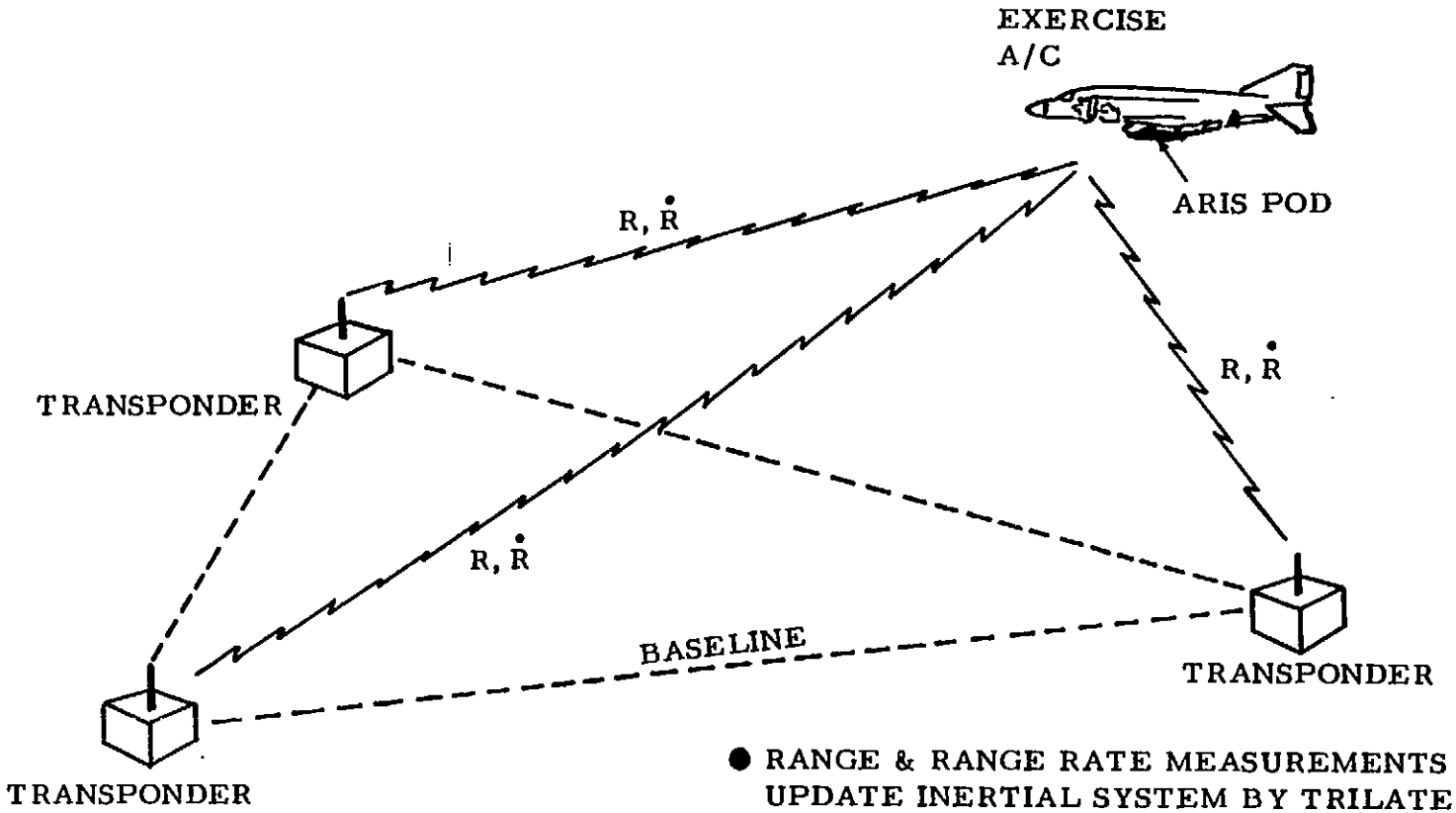

- RANGE & RANGE RATE MEASUREMENTS UPDATE INERTIAL SYSTEM BY TRILATERATION
- ARIS CALCULATES POSITION, VELOCITY ATTITUDE AND STORES INFORMATION ON MAGNETIC TAPE IRIG TIME CORRELATED

FIGURE 2.9.6 ARIS PRINCIPLE OF OPERATION

Table 2.9-I ARIS COMPARISON TO OTHER INSTRUMENTATION SYSTEMS

	ARIS	LASER	CINE	RADAR
POSITION	5 FT	1 FT	4 FT	50 - 150 FT
VELOCITY	0.25 FT/SEC	.50	0.7 FT/SEC	5 FT/SEC
ATTITUDE	5 MIN	NO	POOR	NO
DATA TURNAROUND	PRINTOUT DATA TAPE	COMPUTER SMOOTHING	PHOTO ANALYSIS +	COMPUTER SMOOTHING
NIGHT	YES	VISUAL ACQUISITION	VISUAL ACQUISITION	YES
ALL WEATHER	YES	NO	NO	NO
MOBILITY	SUITCASE UNITS (1 HOUR SETUP)	TRUCK/VAN SURVEYED SITE	FIXED INSTALLATION	FIXED INSTALLATION
SUPPORT PERSONNEL (ON RANGE)	NONE	2 - 3/SITE	2 - 3/SITE MULTI-SITES	6 - 8
MULTIPLE A/C	YES	NO	NO	NO
MANEUVER/ALTITUDE	ALL	REFLECTOR SHADOWING	ATTITUDE & VISIBILITY SENSITIVE	DEGRADED ACCURACY
AIRCRAFT MODS	NONE	RETROFLECTOR	NONE	BEACON

CHAPTER 3

3.1 OCEAN MISS-DISTANCE DETERMINATION/MISS-DISTANCE INDICATOR (MDD/MDI)/ SCORING SYSTEMS

a. The scoring of missile impacts in the ocean area is accomplished by using underwater acoustic sensors called hydrophones. The hydrophone is an underwater microphone which senses acoustic energies and converts these into frequency equivalent electrical energies which are transmitted via wire or atmosphere to a recording and display station. The acoustic energy generated by an impacting missile may be due to the splash created at impact or the acoustic energy generated by a pinger or explosive device carried onboard the missile.

b. For splash detection, the hydrophone net is usually mounted near the ocean floor directly under the impact location area. The net usually forms a quadralateral, pentagon, or hexagon. In the case of an explosive charge or sound fixing and ranging (SOFAR) bomb, the hydrophone array can be far from the impact area. The hydrophones are usually suspended on cables 2,700 to 3,000 ft below the surface of the ocean near the depth of the SOFAR axis. This is the depth where minimum sound velocity occurs. Above the minimum, rays are refracted downward; below the minimum, rays are refracted upward. Thus, the largest amount of sound energy is transmitted along the axis.

3.2 SPLASH DETECTION RADAR (SDR)

3.2.1 General

a. The Splash Detection Radar (SDR) is a scanning X-band radar system specifically designed to detect the splash of an RV as it impacts the water surface. The radar has a clear-weather capability of detecting a splash of 9-m minimum height and 3-s minimum duration at ranges of up to 37 km with a detection probability of at least 95 percent. The SDRs are located at Gellinam and Legan Islands as shown in figure 3.2-1.

b. The radar system, excluding the antenna, is housed in two 2.4-m by 3.1-m shelters. The data processor shelter contains the radar's control, recording and data processing equipment. The transmitter shelter houses the transmitter, receiver and the antenna-control equipment. The antenna is mounted atop a 30-m tower, providing an unobstructed view for a 360° radar scan pattern.

c. The SDR has a B-scan presentation, a plan position indicator (PPI) display for 360° of azimuth coverage with range sweep radii, plus a flicker-free synthetic B-scope display mode. To produce the synthetic display, radar video from 48 pulse-repetition intervals is digitized into 48, 9-m range cells and stored in a core memory. The stored data are then used to refresh the B-scope display to produce a continuous display of the target data which permits accurate positioning of the range and azimuth strobes. In this mode, the strobes are interpolated to a least-significant bit of 4.5 m and 0.19 mrad.

d. Corrections for range and azimuth zero sets are determined from the mid-lagoon calibration target. These corrections are applied to the raw synthetic score for quick-look results. The Honolulu Data Reduction Facility reduces the synthetic score (target and calibration sweeps) and provides a final impact report.

3.2.2 Math Model

a. Impact position. The SDR records range and azimuth data to the leading edge of the water plume referenced from the SDR antenna. This location is measured on the XY Cartesian plane where:

$$X_{plume} = R \cos (\text{azimuth angle})$$

$$Y_{plume} = R \sin (\text{azimuth angle})$$

Miss distance from the planned target is obtained by rotating the XY impact values into a coordinate system with origin at the planned target and new X-axis, positive downrange, aligned along the nominal flight azimuth. The radial miss distance is:

$$\sqrt{X^2+Y^2}$$

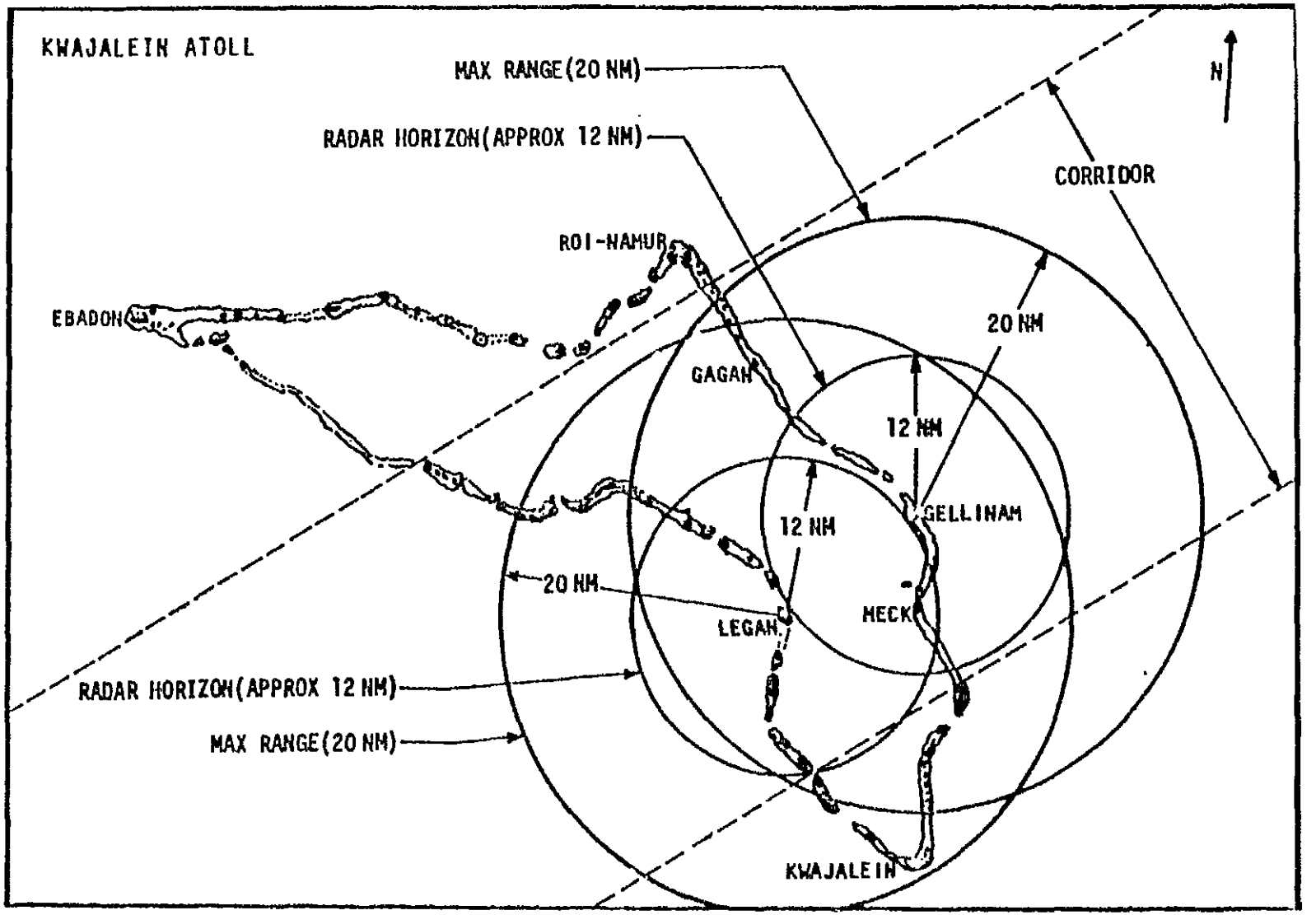

Figure 3.2-1 Splash detection radar coverage.

Present post-mission data processing techniques account for target dependent errors such as tide level, wind velocity, and impact time versus sweep time.

b. Impact time. The SDR does not measure the impact time (the time at which the constantly rotating antenna swept over the target) to the second in real time. However, Kwajalein Missile Range (KMR) personnel are able to read this time to the millisecond after the mission with the aid of a high-speed oscillograph.

3.2.3 Accuracy

The KMR SDRs have undergone extensive testing to measure the range and azimuth standard deviation values.[1,2,3] These 1σ values for instrumental accuracy on static point targets are:

Range sigma=6.7 m
Azimuth sigma=0.6 mrad

3.2.4 Data

Data are not presented here because of security constraints. However, KMR SDRs have been reporting RV impacts within the Kwajalein Lagoon since the installation of the original Ka-band SDR in 1966.

3.2.5 Advantages

The primary advantage of the SDR is that it provides the user with an accurate impact position within a few hours after impact. In addition, it can be employed extensively to position ships within its radar range and as a surface surveillance radar during local missile firings.

3.2.6 Disadvantages

a. Adverse weather limits the scoring capability of the SDR; rain is the major obstacle.

b. The radar range limitations are at 37 km for each radar. Encoder granularity is 4.5 m in range and 0.19 mrad in azimuth.

c. The SDR does not measure impact time.

3.2.7 Reliability

Reliability of the system has been very high.

3.2.8 Point of Contact

Code: BMDSC-RD
Ballistic Missile Defense Systems Command
P. O. Box 1500
Huntsville, AL 35807
Phone: (205) 895-4530
AUTOVON: 742-4530

REFERENCES

1. *SDR Performance Evaluation Interim Report*, RISA 71-001 (Huntsville, Alabama: Kentron Hawaii, Ltd.), November 1, 1971.

2. *Performance Evaluation Test of Splash Detection Radar No. 2 at KMR (Gagan Island)*, RISA 73-008 (Huntsville, Alabama: Kentron Hawaii, Ltd.), December 29, 1972.

3. *Correction of Data from Splash Plume Sensors for the Effects of Splash Plume Characteristics*, RISA 73-008 (Huntsville, Alabama: Kentron Hawaii, Ltd.), August 10, 1973.

3.3 MISSILE IMPACT LOCATION SYSTEM (MILS) HYDROPHONE NET

3.3.1 General

a. A Missile Impact Location System (MILS) consists of a hydrophone array (used to detect hydroacoustic signals generated as a result of missile impacts) and the associated shore facilities which record the detected signals. The hydrophones are connected to the shore facilities by underwater cables.

b. The acoustic signals detected and scored by a MILS array fall into two general types. The first type of signal is that generated by the actual impact of an RV on the ocean's surface. Such a "splash" signal is a comparatively low-energy signal having a relatively short range. The second general type of acoustic signal scored by MILS arrays is one generated by a special explosive device carried by the RV. The special explosive device is known as a sound fixing and ranging (SOFAR) signal. The SOFAR signals are detonated by pressure-sensitive fuses set for the hydrostatic pressure of the deep sound or SOFAR channel. This channel acts as a sort of wave guide providing a minimum-loss, maximum-range propagation path for signals originating within it. The SOFAR channel is at a depth of 2,500 to 4,000 ft, and its axis is the point of minimum sound velocity in the water column.

c. Accordingly, MILS hydrophone arrays may be classified by the principal signal type they were designed to detect. Thus, splash detection arrays, commonly called "target arrays" (TAs), were designed to score "splash" signals generated by actual RV impacts. Due to their geometry, TAs are also called "pentagons." They generally consist of five hydrophones arranged circularly around a sixth central hydrophone. All the units in a target array are bottom mounted allowing their locations to be considered as fixed points and to be precisely surveyed. During the survey, the representative sound velocity profile of the array area is determined as accurately as possible. The diameter of a TA is restricted to approximately 25 nmi by the range limit of the direct ray path followed by a sound ray going from the ocean surface to the ocean bottom. The hydrophone arrays designed to detect SOFAR signals do not suffer this range limitation. All the hydrophones in such arrays are suspended upward from the ocean bottom into the SOFAR channel.

d. The most common type of SOFAR scoring array is the Broad Ocean Area (BOA) array. A BOA array is composed of several independent elements; i.e., individual shore station connected to single hydrophones or to groups of hydrophones, separated by up to a few thousand miles. The data from this array are brought together at a single location for processing. Since the area of coverage is extremely large, the effective velocity of sound for each sound source hydrophone pair must be empirically determined. The Miniature Impact Scoring System (MISS) at Midway is a special case of the SOFAR-type array. Its hydrophones are arranged in a crossed-dipole pattern and are separated by only 30 to 60 nmi. A special survey and calibration of the array were performed during which a single effective sound velocity was determined for the entire array.

3.3.2 Math Model

The following is an outline of the least-squares approach to the determination of the acoustic source location.

Let

n=Number of hydrophones

t_i=Theoretical time of arrival of the sound wave at the ith hydrophone

tm_i=Measured time of arrival of the sound wave at the ith hydrophone

t_s=Time of origin of the sound wave

Ve_i=Effective velocity of propagation of sound from the source to the ith hydrophone

W_i=Weighting factor assigned to the ith hydrophone.

X_i, Y_i, Z_i=Geocentric coordinates of the ith hydrophone

X_s, Y_s, Z_s=Geocentric coordinates of the sound source,

then the least-squares regression model is:

$$Ve_i(t_i-t_s)=\left[(X_i-X_s)^2+(Y_i-Y_s)^2+(Z_i-Z_s)^2\right]^{\frac{1}{2}},$$

which may be rewritten as:

$$t_i=t_s+\frac{\left[(X_i-X_s)^2+(Y_i-Y_s)^2+(Z_i-Z_s)^2\right]^{\frac{1}{2}}}{Ve_i}=t_i(X_s,Y_s,Z_s,t_s).$$

The problem is then to minimize

$$\sum_{i=1}^{n} W_i\left[t_i(X_s,Y_s,Z_s,t_s)-tm_i\right]^2=G(X_s,Y_s,Z_s,t_s).$$

Thus, considering X_s,Y_s,Z_s, and t_s as the regression coefficients for the model, the normal equations are:

$$\frac{\partial G}{\partial X_s}=\sum_{i=1}^{n} W_i\frac{\partial t_i}{\partial X_s}(t_i-tm_i)=0$$

$$\frac{\partial G}{\partial Y_s}=\sum_{i=1}^{n} W_i\frac{\partial t_i}{\partial Y_s}(t_i-tm_i)=0$$

$$\frac{\partial G}{\partial Z_s} = \sum_{i=1}^{n} W_i \frac{\partial t_i}{\partial Z_s}(t_i - tm_i) = 0$$

$$\frac{\partial G}{\partial t_s} = \sum_{i=1}^{n} W_i \frac{\partial t_i}{\partial t_s}(t_i - tm_i) = 0$$

Although this is a nonlinear least-squares problem, it can be linearized by using the Gauss-Newton Method and by assuming an initial approximation given by a truncated first-order Taylor Series expansion.

The Taylor Series is:

$$t_i(X_s, Y_s, Z_s, t_s) \doteq t_{i_o}(X_{s_o}, Y_{s_o}, Z_{s_o}, t_{s_o}) + \left[\frac{\partial t_i}{\partial X_s}\right]_o (X_s - X_{s_o}) + \left[\frac{\partial t_i}{\partial Y_s}\right]_o (Y_s - Y_{s_o}) + \left[\frac{\partial t_i}{\partial Z_s}\right]_o (Z_s - Z_{s_o}) + \left[\frac{\partial t_i}{\partial t_s}\right]_o (t_s - t_{s_o})$$

where:

$X_{s_o}, Y_{s_o}, Z_{s_o}, t_{s_o}$ = Initial estimates of X_s, Y_s, Z_s, and t_s

and required partial derivatives are then:

$$\frac{\partial t_i}{\partial X_s} = \frac{-(X_i - X_s)}{Ve_i R_i}$$

$$\frac{t_i}{\partial Y_s} = \frac{-(Y_i - Y_s)}{Ve_i R_i}$$

$$\frac{\partial t_i}{\partial Z_s} = \frac{-(Z_i - Z_s)}{Ve_i R_i}$$

$$\frac{\partial t_i}{\partial t_s} = 1$$

where:

$$R_i = \left[(X_i - X_S)^2 + (Y_i - Y_S)^2 + (Z_i - Z_S)^2\right]^{\frac{1}{2}}$$

3.3.3 Error Analysis

As X_S, Y_S, Z_S, and t_S are the regression coefficients, the errors in them may be estimated by application of standard regression error propagation techniques. See IRIG Document 119-71, *Error Analysis and Methods for Estimating Errors in Position, Velocity, and Acceleration Data,* pages 51-52.*

3.3.4 Point of Contact

Code 3442
Pacific Missile Test Center
Point Mugu, CA 93042
Phone: (805) 982-7931
AUTOVON: 351-7931

Effective March 1984, document number changed to IRIG Document 153-71.

3.4 SONOBUOY MISSILE IMPACT LOCATION SYSTEM (SMILS)

3.4.1 General

a. The Sonobuoy Missile Impact Location System (SMILS) is an operational scoring system. It has successfully supported POSEIDON missile operations for approximately 10 years and more recently has provided support for TRIDENT missile operations. The SMILS was designed to detect and to score the hydroacoustic signals generated by the actual impact of a missile reentry body (REB) upon the ocean surface. The SMILS has fully met its design goals of operation in the BOA entirely independent of the existence of nearby shore facilities and of detection and scoring of multiple impact signals occurring over an interval of just a few seconds. While the SMILS was implemented using the well established deep ocean transponder (DOT) and airborne antisubmarine warfare (ASW) technologies, it has remained evolutionary in nature with improvements and innovations being incorporated only after thorough testing and demonstration.

b. Airborne ASW technology contributes two of the three major data gathering subsystems of the SMILS. The first of these is the Lockheed P-3 Orion ASW aircraft. The air-deployable sensor carrying sonobuoys form the second. Arrays of DOT units, mounted on the ocean bottom, provide the third major data acquisition subsystem. In a given impact area, the DOT array provides geodetic control for the free-floating sonobuoy pattern. This pattern was sown onto the ocean surface by the P-3. Each sonobuoy in the pattern is an independent collection point for hydroacoustic data. Each sonobuoy transmits its data over an individual RF link to the support aircraft where it is recorded for subsequent analysis on magnetic tape along with timing signals.

3.4.2 The SMILS Support Aircraft

a. Currently, SMILS missions are normally flown by a dedicated P-3C aircraft and crew from Navy Squadron VX-1. However, development of a modularized SMILS instrumentation package has made possible the use of any available fleet P-3C or P-3B as the support aircraft. Several operations have been supported in this manner. The support aircraft provides the sonobuoy receivers and antennas, the sonobuoy dispensing system, internal communications, external radio communications, basic navigation, and the electric power for the SMILS instrumentation package. The navigation capability of the SMILS aircraft is critical. For adequate achievement of a required support station after a flight of 3- to 4-hrs duration and a range of up to 1,200 nmi, the maximum deviation from the true position must be less than 10 nmi. The VX-1 aircraft keeps the navigational errors within this bound through utilization of both OMEGA and a dual airborne inertial navigation system which has a very low gyro drift rate.

b. The SMILS instrumentation system is composed of a timing group, a magnetic tape recorder group, a recording oscillograph group, an environmental data support group, and a DOT navigator unit. Cross

connection between various elements in the SMILS instrumentation package is achievable through a master patch panel. The output of each channel of the aircraft's sonobuoy receiver is paralleled to the SMILS master patch panel and to the aircraft's ASW systems. The magnetic tape recorder group is the primary data recording medium and has the capacity to simultaneously record each of the 31 different sonobuoy channels together with appropriate timing signals. These signals are provided by the timing group which consists of a WWV receiver, a time code generator, and a time code reader. Timing signals are also provided to the recording oscillograph group and to the environmental data support group. The recording oscillograph group displays acoustic data from selected sonobuoys. These records are used to verify proper operation of a sonobuoy and for quick-look data reduction of the impact signals. The environmental data support group is used to determine the velocity of sound at the depth of the sonobuoy hydrophones. The DOT navigator provides an interval timing capability for various acoustic signal pairs. These signal pairs are principally those associated with the interrogation of the units in the DOT array on the ocean bottom beneath the target point.

3.4.3 DOT Arrays

a. A DOT array provides the SMILS with a geodetic control for the free-floating sonobuoy pattern sown in the target area by the support aircraft. The DOT array is composed of a group of acoustic transponder units mounted on the ocean bottom surrounding the nominal target point. The DOT arrays are planted and precisely surveyed by ship, well before a target area is used. A discussion of implant and survey techniques is found in AFETR Report No. 81-SR-75-2 Revision 3, *AFETR Sonar Transponder Arrays*, Vol 1 (Sonar Survey Techniques), 1 November 1977. Upon receipt and recognition of an interrogation pulse, the DOT unit will respond by transmitting a reply pulse of a preselected frequency. The interrogation frequency for all of the DOT units used in support of SMILS is 16.0 kHz, while the reply frequency is selected from a set of 10 possible response frequencies. The possible DOT response frequencies are 7.5, 8.0, 8.5, 9.0, 9.5, 10.0, 10.5, 11.0, 11.5, and 12.0 kHz.

b. The configuration of the standard target area DOT array is presented in figure 3.4-1. The standard target area array consists of 10 DOT units arranged in 2 concentric circles. The inner circle of 4 DOT units is at a radius of 2.5 nmi from the array center, while those in the outer circle are at a radius of 5.5 nmi. All units are placed at regular intervals within their respective ring. To minimize attenuation due to frequency, the low frequency units (7.5 to 10.0 kHz) are normally placed in the outer ring, while the high frequency units (10.5 to 12.0 kHz) are placed in the inner ring. The minimal array useful for SMILS is the inner 4-DOT ring.

c. The nominal DOT locations are designated by the letters A through J, with A through F in the outer ring and G through J in the inner ring. The A location is approximately due east of the array center, while location G is at a nominal bearing of 315° True.

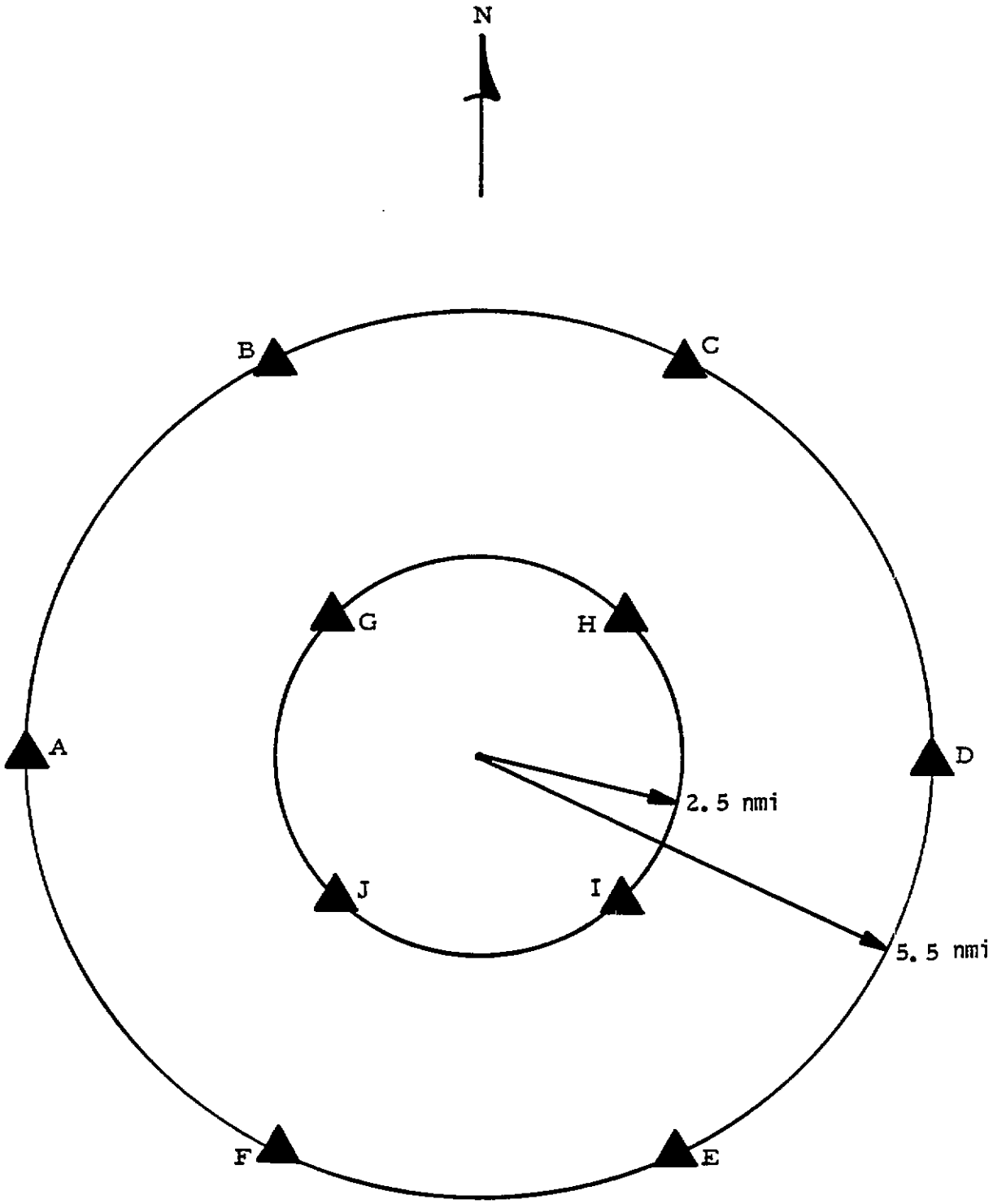

Figure 3.4-1 Standard SMILS dot array.

A particular DOT in the array is labeled by both reply frequency and its location letter, e.g., 7.5A or 9.0F.

3.4.4 SMILS Sonobuoys

a. The sonobuoys used for SMILS are drawn from the standard Navy inventory and modified for the SMILS application. The sonobuoys are ejected from the support aircraft through a launching tube. They are stabilized to a vertical position during descent by either a rotochute or a parachute. Upon impact with the ocean surface, the descent mechanism is jettisoned, the unit's saltwater batteries are activated, and its sensors are deployed. Data are then collected and transmitted to the support aircraft over an RF link. Some of the general characteristics of the sonobuoys used for SMILS are presented in table 3.4-I below.

Table 3.4-I

Summary of Sonobuoy General Characteristics

Transmitter	31 channels at an interval of 0.375 MHz over the frequency range 163.25 to 173.50 MHz
RF Power	1 W
Max FM Modulation Deviation	±0.75 MHz
Activation Time After Splash	1 to 3 min
Power Source	Seawater batteries
Operating Life	7 h*
Sensor	
Acoustic Frequency Range	10 to 20 kHz*
Operating Depth	30 ft*
Weight	16 to 21 lb (depending on sonobuoy type)

**Indicates standard SMILS modification*

b. For SMILS usage, the sonobuoys fall into two broad categories according to the type of data they acquire. The first category is the collection of the desired acoustic data, while the second category is the gathering of the supporting environmental data.

1. Acoustic Sonobuoys

(a) Three distinct types of acoustic signals must be detected by the sonobuoys in a SMILS pattern. The first type is the DOT unit interrogation and response pair. These are used to track the sonobuoy pattern across the ocean surface. The second type of signal is a low-frequency pulse used to determine the range between the individual sonobuoys in the pattern, thus calibrating the pattern. Finally, the third signal type is the splash signals generated by REB impacts.

(b) The units used to communicate with the DOT arrays are air deployable interrogators (ADIs) which are modified SSQ-57A sonobuoys built by Sparton Electronics. They receive the standard SMILS modifications to extend battery life to 7 h and to restrict sensor deployment to a depth of 30 ft. A 16.0-kHz pinger together with the associated electronic circuits and battery power supply are added.

(c) The units used to tie the pattern together through near-surface transmission of acoustic pulses are designated low-frequency pingers (LFPs). Since the Hermes SSQ-41A sonobuoys have a line array of hydrophones which produce a 6-dB greater gain in the horizontal direction than in the vertical at the ping frequency, they are suited for this function.

(d) Besides the standard SMILS modifications, the upper limit of the unit's frequency response was raised to 20 kHz and a 2.33-kHz crystal-controlled pinger with supporting circuitry and power supply were added. Identification of transmissions from individual LFPs is aided by bench-setting their pulse repetition rates to one of several different possible values during unit modification. Under ideal conditions, the pings emitted by the LFPs may be detected up to a range of 50 nmi.

(e) "High frequency (HF) sonobuoy" is the designation given to those units whose primary task is the collection of impact signals. The Hermes SSQ-41A used for the HFs receives the standard SMILS alterations and has the gain of the audio amplifier lowered 6 dB to reduce overload during receipt of a splash signal and its reverberations.

2. Environmental Sonobuoys

(a) There are two kinds of environmental data-gathering sonobuoys. One is the air-deployable velocimeter (ADV). This is an SSQ-41A sonobuoy in which the hydrophone assembly and electronics have been replaced by a "sing-around" velocimeter and its electronics. The

velocimeter directly measures the velocity of sound in water by transmitting sound pulses around a fixed length path with receipt of a pulse triggering the transmission of the next pulse. The pulse repetition frequency (PRF) is proportional to the sound velocity over the water path between the projector and the receiver. The PRF is then transmitted over the sonobuoy radio link. The velocimeter is deployed at a depth of 30 ft and measures the velocity of sound to within ±0.5 m/s. The transmitting life of the ADV is 7 h.

(b) The other kind of environmental data sonobuoy is the standard Navy SSQ-36 Airborne Bathythermograph (BT). Its thermistor probe is specially calibrated in the laboratory to attain a temperature measurement precision of ±0.5° over the range of -2.22°C to 35°C (28°F to 95°F). Upon the BT's entry into the ocean, its probe is allowed to stabilize to the surface temperature before being released. It then sinks at a fixed rate of approximately 5 ft/s to a depth of 1,000 ft. Once that depth is reached, RF transmission is terminated and the BT begins to sink. The probe is connected to its electronic package in the sonobuoy by means of a fine wire contained on reels in both units. As the probe sinks, both reels unwind simultaneously, leaving the wire at rest in the water with little or no tension placed on it. The resistance of the thermistor varies with changing temperature and is converted by the electronics package in the floating sonobuoy to a function of frequency which is then transmitted over the RF link. The vertical temperature profile is closely related to the sound velocity profile and is used to determine the presence and quality of a surface sound duct. A high-quality duct will allow near surface sound transmissions to reach maximum ranges.

3.4.5 SMILS Operations

a. SMILS impact scoring operations are possible once a DOT array has been established around a selected target point and surveyed. The SMILS support aircraft is deployed from the nearest suitable airfield to its target area support station. There must be sufficient time alloted between aircraft deployment and missile launch to allow the underwater acoustic conditions of the impact area to be determined and the sonobuoy pattern to be laid.

b. As noted previously, the navigational capability of the support aircraft must assure arrival within 15 nmi of the center of the target area DOT array. When the aircraft's navigation systems indicate it is passing over the datum point (or array center), an ADI is launched. This ADI is used to confirm that the datum point has been attained. Its position is determined by acoustic data from the DOT array. If it is outside the array or if it is too far from the datum point, navigation corrections are computed, the aircraft flies to the new location, another ADI is dropped, and the confirmation procedure is repeated. As soon as attainment of the datum point is confirmed, drift calculations are made from rough acoustic tracks of the ADI. Simultaneously, ADV and

BT sonobuoys are launched to determine the ambient acoustic characteristics of the ocean in the target area. Knowledge of the acoustic conditions and of the drift rate and direction to the sonobuoys will allow appropriate changes to be made to the standard SMILS sonobuoy pattern before it is laid. The absence of a surface sound duct requires shrinking the sonobuoy pattern or adding more units to maintain coverage area, while the presence of a good duct allows expansion of the coverage area or reduction of the number of units deployed. Once the required pattern modifications are decided upon by the SMILS Test Director, the support aircraft proceeds to deploy the sonobuoys. Units which fail either during or after deployment are replaced, as necessary, prior to the aircraft taking up its final test support position.

c. Currently, only minimal quick-look data reduction is performed on the aircraft during near real time. Oscillograph recordings of the acoustic signals from selected sonobuoys versus time are made for the period of REB impact. From these records, the number of impacts and locations in or out of the target area are determined and reported to range control.

3.4.6 SMILS Sonobuoy Patterns

A diagram of the standard SMILS pattern is presented in figure 3.4-2. The standard SMILS pattern consists of 14 free-floating sonobuoys. This configuration includes 3 ADIs, 8 LFPs and 3 HFs. Actual operational patterns may be modified to suit ambient conditions of wave, wind and acoustic propagation. The standard sonobuoy pattern provides an internal area of 154 square miles. Use of multiple DOT arrays, each with a sonobuoy pattern, allows effective impact coverage over much larger areas. The only real limitations on SMILS are that the number of sonobuoy RF channels used may not exceed 31 and that the individual target points must be located so they can be simultaneously supported by a single support aircraft. The second requirement is that all sonobuoys in the multiple patterns be within radius range of a common aircraft test support point.

3.4.7 SMILS Data Processing

a. All data collected during a SMILS operation are returned to the laboratory for processing. Only the data from the interval or intervals containing the splash signals are reduced. During the data reduction, two basic problems must be solved. The position of each of the free-floating sonobuoys must be established versus time, and the location of each of the splash signals must be determined.

b. The determination of track for each sonobuoy is essentially a problem in signal identification and sorting. Figure 3.4-3 shows the standard SMILS sonobuoy pattern superimposed over the DOT array. To the maximum extent possible, the time of arrival of all acoustic signals received by each sonobuoy is determined automatically by special processing equipment. The emission time of each ping from either an ADI or

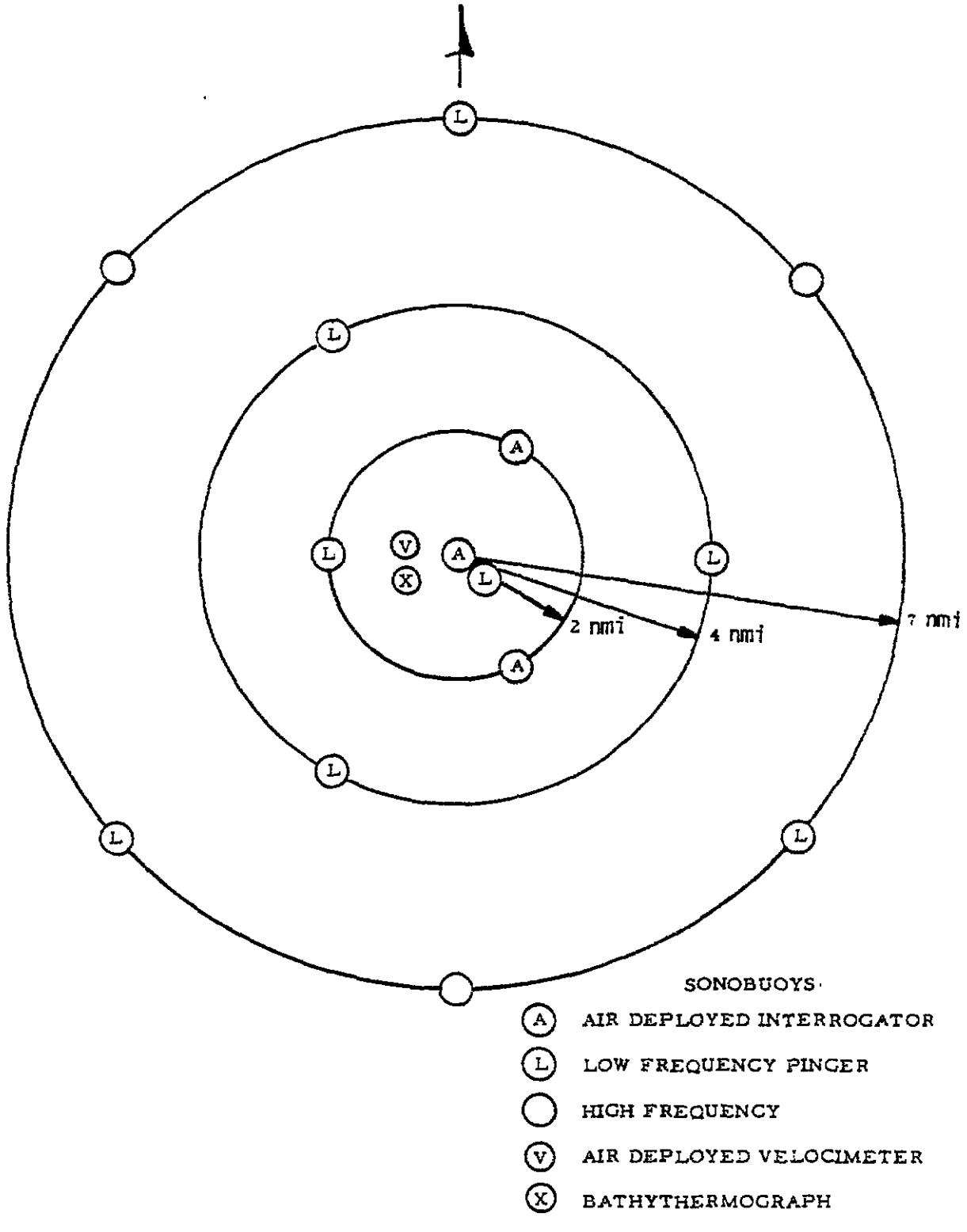

Figure 3.4-2 Standard SMILS sonobuoy pattern.

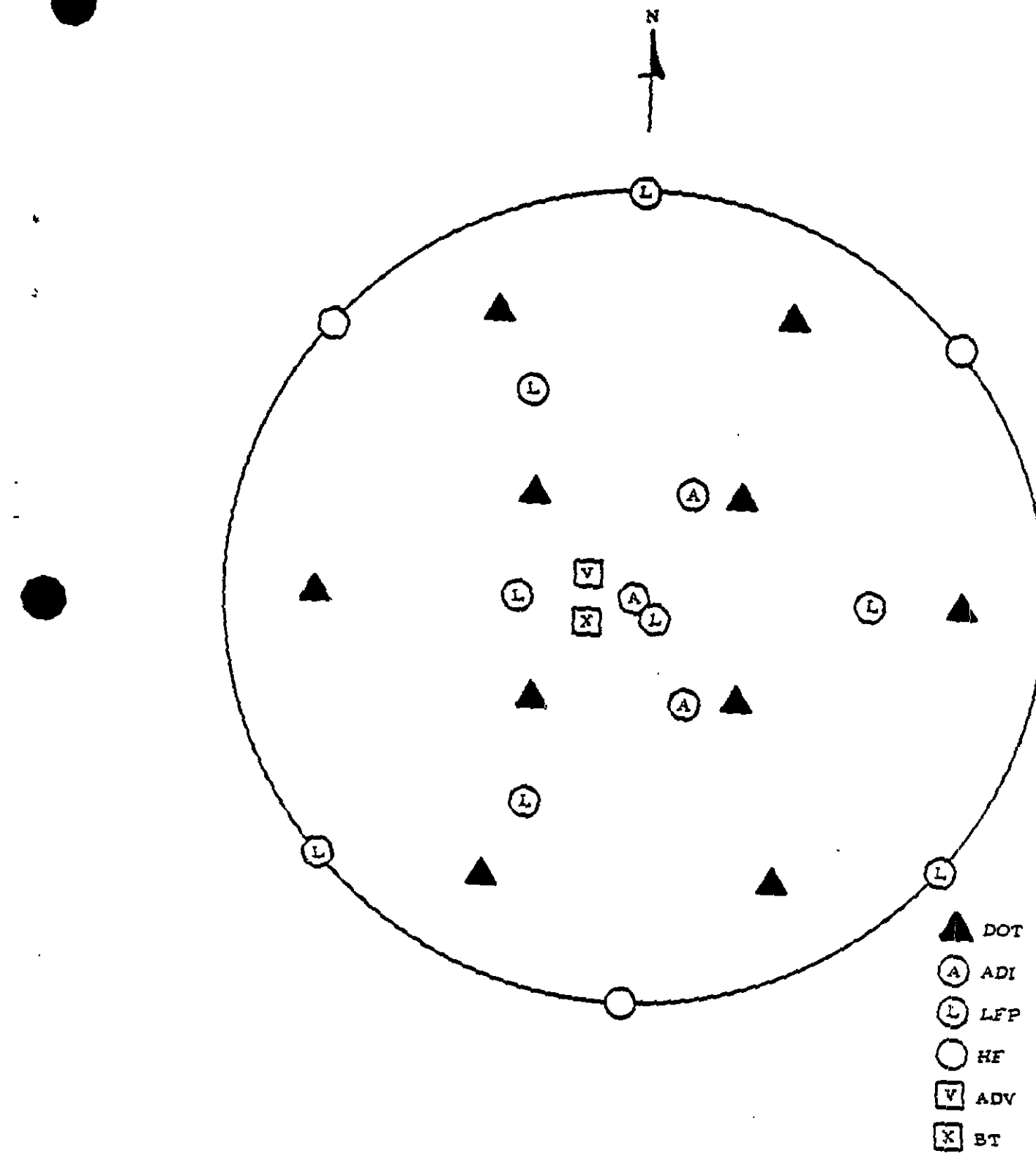

Figure 3.4-3 Composite SMILS sensor pattern.

an LFP is readily determined by monitoring the units own hydrophone output signal. There is no delay between ping transmission and reception because the pulse is picked up within the sonobuoy electronics package without its traveling the approximate 1-ft water path between the pinger and the hydrophone. It remains for each DOT unit response signal to be associated with a given ADI interrogation signal and for each low-frequency pulse received to be identified with a given LFP ping. Time gates based on the velocity of sound, knowledge of each ADI's and LFP's PRF and knowledge of the nominal deployment coordinates greatly aid in the signal identification and sorting process. The nominal deployment coordinates are obtained from the support aircraft navigator. In addition to using them in the signal sorting process, nominal deployment coordinates are used as initial estimates for computing the actual sonobuoy coordinates. (Figure 3.4-3 is a composite of figures 3.4-1 and 3.4-2 and shows the nominal location of all SMILS sensors, DOTs and sonobuoys.)

c. With the sonobuoy positions determined, computation of the splash signal locations is essentially a standard acoustic source location problem and is handled accordingly. Identification of individual REBs within a group of multiple impacts cannot be accomplished solely by the use of acoustic data. Predicted impact time and point for each REB is required to solve this problem.

3.4.8 Utilization of the SMILS

The SMILS was designed, developed and operated by the Bermuda Division of the Palisades Geophysical Institute (PGI) under funding from the Navy's Strategic Systems Projects Office (SSPO). Applications should be made to SSPO, Code SP-25. Phone (202) 697-0600 (AUTOVON: 227-0600) for information regarding use of the SMILS including costs, scheduling PGI services, and VX-1 aircraft support.

3.5 HYDROACOUSTICAL IMPACT TIMING SYSTEM (HITS)

3.5.1 General

The KMR Hydroacoustical Impact Timing System (HITS) is an underwater sound detection system used to detect and record the impact of an RV on the water surface. The system records and time tags impacts, determines the sound velocity in the water, and calibrates the sensors prior to each operation. Quick-look and post-mission data reduction provide the RV impact position and time.

3.5.2 System Description

a. The HITS consists of four underwater hydrophones, three velocimeters, and a pinger located on the lagoon floor (figure 3.5-1). All hydrophones are connected to a station located on Gellinam. The shore-station equipment consists of signal amplifiers, filters, a VR3700 data recorder, CEC-5-133 recording oscillograph, and an audio-visual monitoring system. Figure 3.5-2 presents a functional block diagram of the shore equipment for H1 and H2. The shore equipment for H3 and H4 are similar and each has a velocimeter.

b. The sound velocity measurement can be made adjacent to each hydropone using a self-contained velocimeter (figure 3.5-3). A pinger located at H1 allows measurement of sound velocity over a broader area and provides a means of system calibration. Figure 3.5-4 shows the HITS sensor locations.

c. An Environmental Profiling System (EPS), located aboard the marine vessel *Neptune*, is used to provide a means of determining sound velocity, temperature and salinity profiles of areas of interest in the lagoon or BOA. The EPS gives direct readouts of sound velocity as function of depth.

3.5.3 Accuracy

The system impact timing accuracy is ±1.3 ms which corresponds to an impact location accuracy of ±2 m to ±4 m for the distribution of lagoon targets presently scored by the HITS.

3.5.4 Actual Data and Case Example

a. The hydrophone senses the impact energy and transmits a signal via submarine cable to the shore station where it is recorded on video tape concurrently with IRIG B timing. The recorded event is played back through selectable high-pass filters to a recording oscillograph. The operator examines the oscillograph to determine the exact time at which the impact signal was received at each hydrophone.

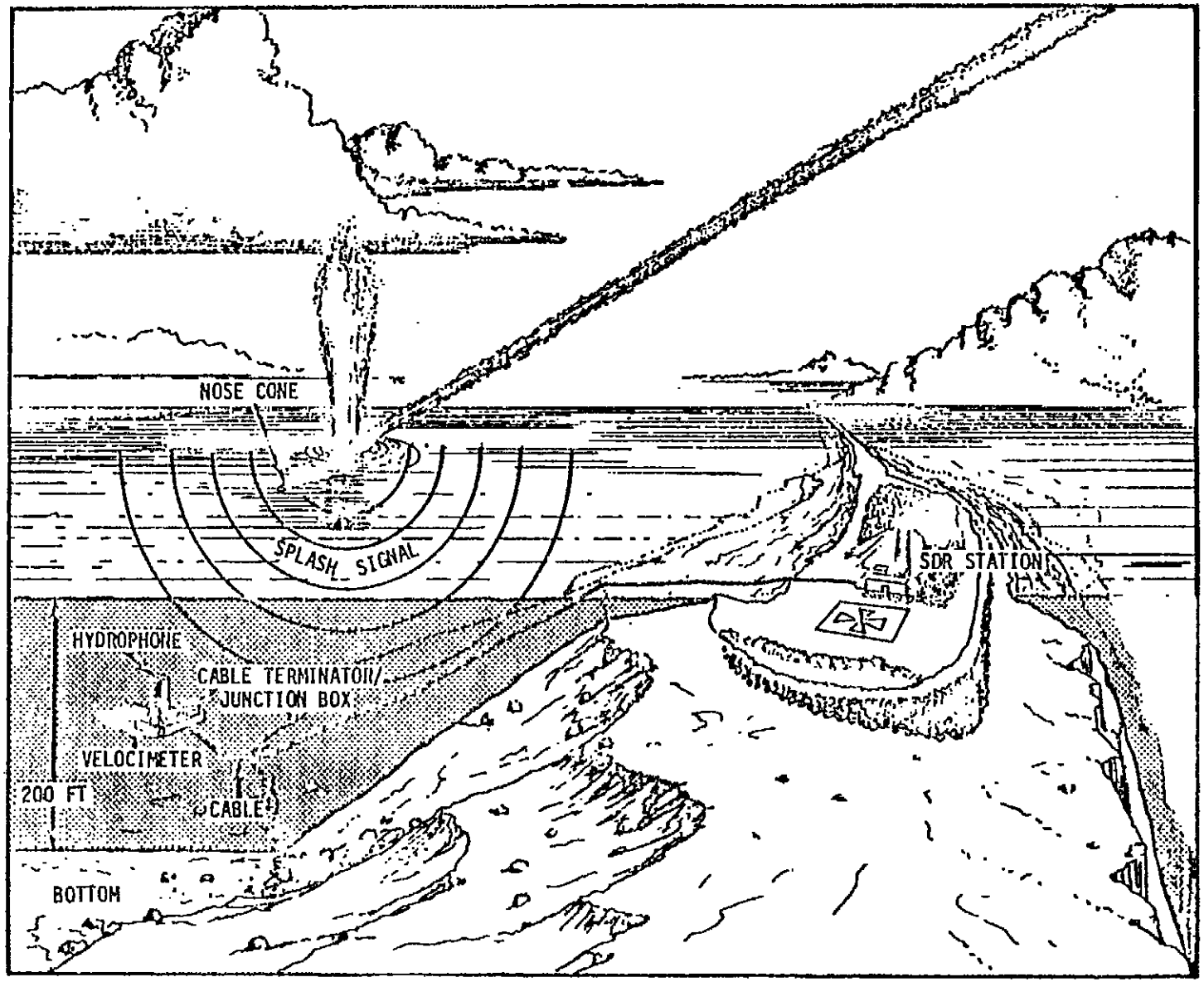

Figure 3.5-1 HITS shore station.

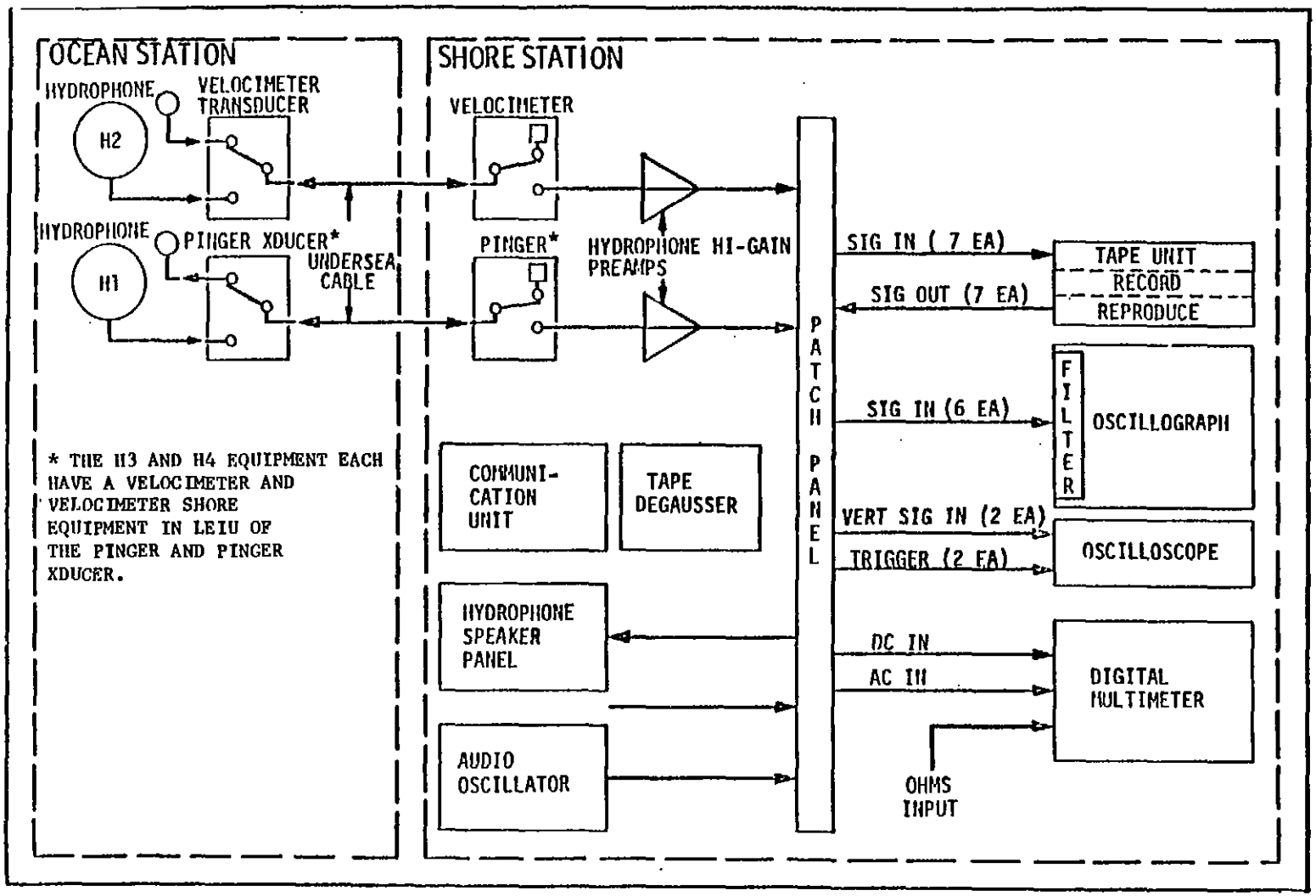

Figure 3.5-2 HITS functional block diagram.

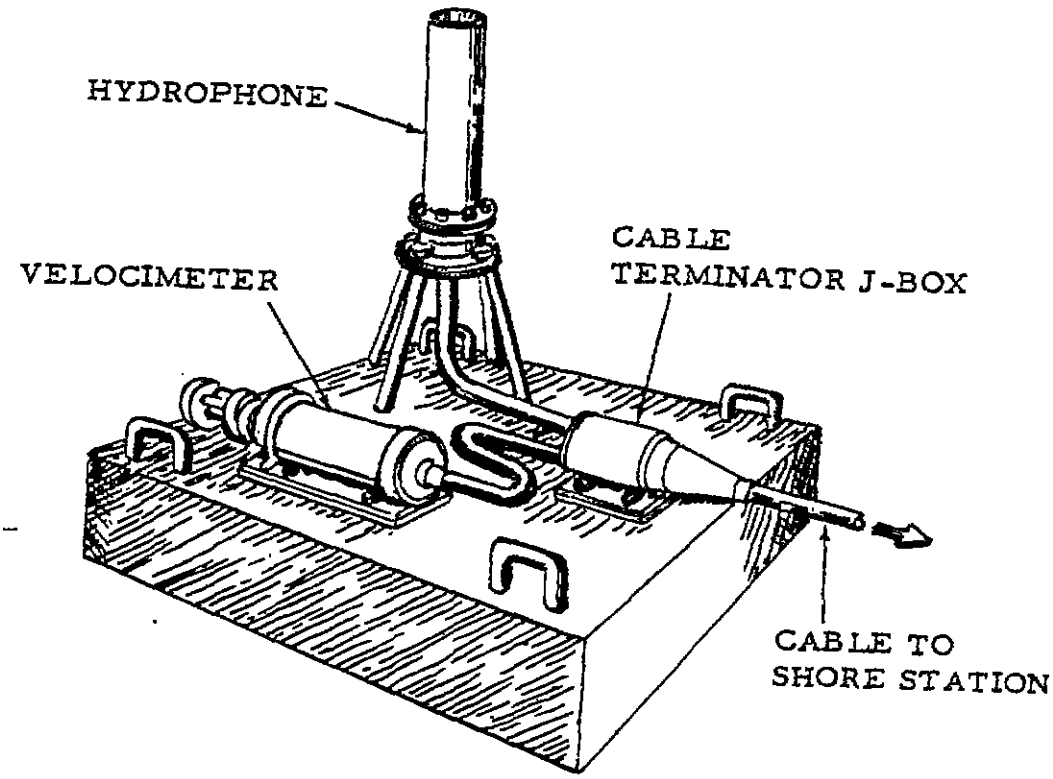

Figure 3.5-3 Artist concept of anchor block, hydrophone, velocimeter and cable terminator box (H2, H3, H4).

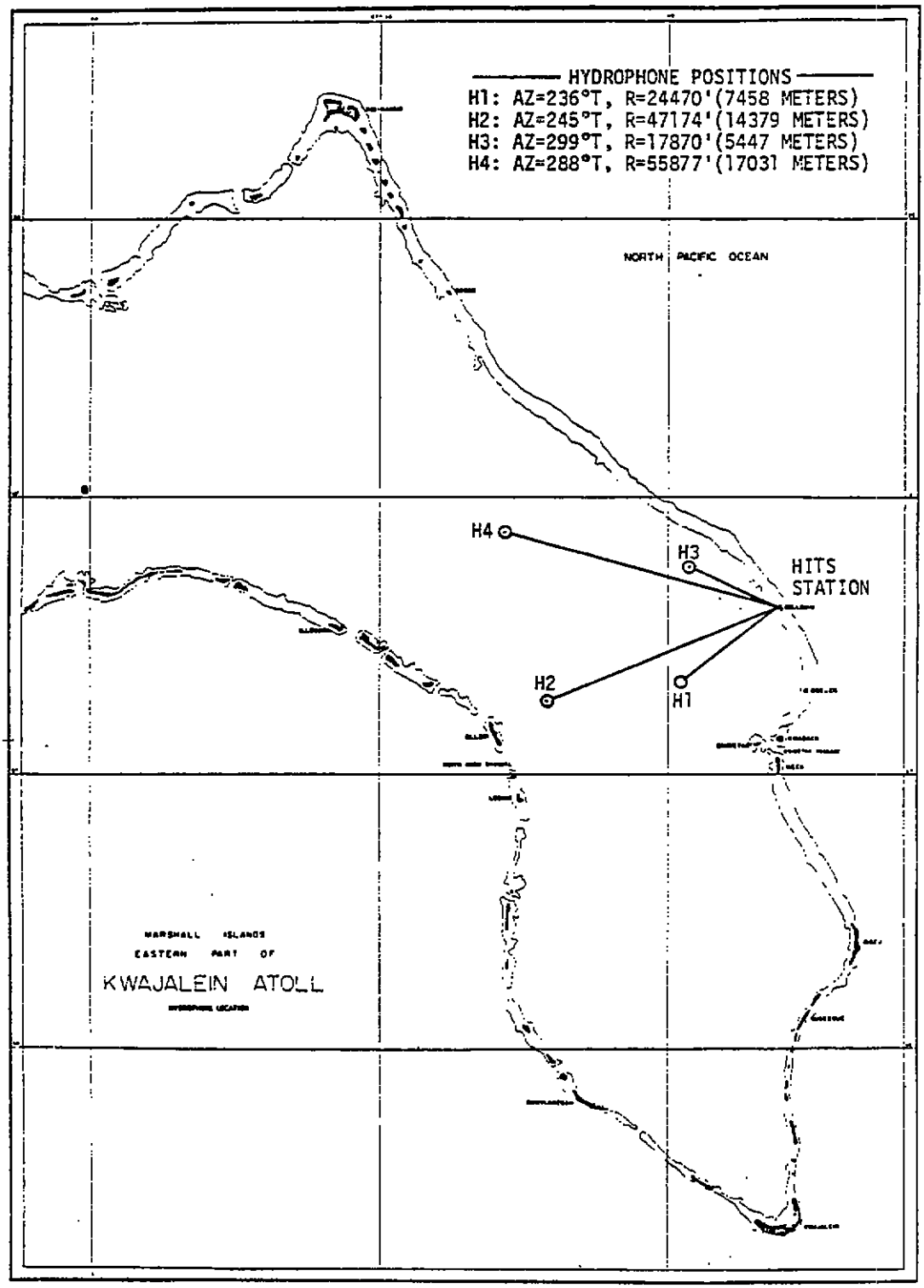

Figure 3.5-4 Underwater sensor locations.

b. For impact scores produced at the Honolulu Data Reduction Facility, the HITS data are utilized in an optimal multisensor estimate which includes extrapolations of the optics-radar best estimate of trajectory (BET) and also corrected splash detection radar (SDR) data. This method provides the best estimate of impact using data from all KMR sensors.

c. For quick-look impact scores produced at Kwajalein, the HITS data are utilized in a computer program called ZSCORE which also simultaneously includes SDR data. This method provides an optimal multisensor estimate, using data from the KMR quick-look sensors (HITS and SDR).

3.5.5 Advantages

This system gives KMR the capability of providing the users with an accurate time of impact within a few hours after launch that is independent of weather constraints.

3.5.6 Disadvantages

This system is only capable of scoring vehicles which impact within the southeastern portion of the KMR Lagoon.

3.5.7 Cost

Data reduction time is very minimal; however, actual data cost figures are not available.

3.5.8 Reliability

The system is very reliable but requires periodic cleaning because of algae in the water.

3.5.9 Applicable Programs

HITS is available for any program requiring impact time within the KMR Lagoon.

3.5.10 Point of Contact

Code, BMDSC-RD
Ballistic Missile Defense System Command
P. O. Box 1500
Huntsville, AL 35807
Phone: (205) 895-4530
AUTOVON: 742-4530

BIBLIOGRAPHY

1. *Kwajalein Missile Range Instrumentation Handbook.* Huntsville, Alabama: Kwajalein Missile Range Directorate, 15 December 1972.

2. Urick, R. I. *Principles of Underwater Sound for Engineers.* New York: McGraw Hill, Inc., 1967.